SCUOLA NORMALE SUPERIORE

Ph.D. thesis in

UNDERSTANDING THE LONG-LASTING ANALGESIC EFFECT OF ANTI-NGF AND ANTI-TRKA ANTIBODIES IN A MOUSE MODEL OF NEUROPATHIC PAIN

RENATA CERNA

Pisa, 2020

Supervisor: ANTONINO CATTANEO

ACKNOWLEDGEMENTS

My sincere thanks to

Dr. Antonino Cattaneo, my supervisor, for support and interest in my work,

Dr. Mara D'Onofrio, Dr. Ivan Arisi, Dr. Rossella Brandi and Dr. Marco Mainardi for introducing me to science, inspiring discussions and scientific encouragement,

all my friends and colleagues at the SNS, EBRI and the CNR institute for creating a pleasant working atmosphere,

and my family for understanding and patience.

ABSTRACT

Neuropathic pain (NP), caused by nerve injury in the somatosensory nervous system, is among the most common forms of chronic pain. Current treatment for neuropathic pain is largely unsatisfactory, causing adverse side effects. The NGF system, as a key player in the onset and progression of pain signals in sensory neurons and of inflammation at lesion sites, has emerged as a promising target for the treatment of neuropathic pain and chronic pain. The laboratory in which I worked for my thesis had previously demonstrated that anti-NGF (mAb αD11) and anti-TrkA (mAb MNAC13) monoclonal antibodies induce an effective analgesic effect in NP murine models, that remains up to 21 days after the last dosage (Ugolini et al 2007; Covaceuszach et al 2012).

To understand the role of the NGF system in NP, both as a crucial regulator and a potential therapeutic target, I evaluated in a mouse model of NP:

a. the time course and the duration of the analgesic effect following the anti-NGF and anti-TrkA antibody treatment;
b. the gene expression changes during and after the anti-NGF and anti-TrkA treatments in dorsal root ganglia(DRG), spinal cord (SC) and anterior cingulate cortex (ACC);
c. the bioinformatic comparative study of the pain-specific and antibody-specific gene expression fingerprinting in the DRG.

The behavioural and transcriptomic data indicate that anti-NGF and anti-TrkA antibodies counteract NP in the chronic constriction injury (CCI) model, showing a very long-lasting analgesic effect and induction of regenerative processes. Both anti-NGF and anti-TrkA antibodies induce analgesia, but with different dose and time-dependent effects: some differences are evident shortly after the CCI induction, while on a longer time scale they converge into a similarly effective analgesic phenotype. This suggests that they follow partially different pharmacological mechanisms.

This data is supported more clearly by the transcriptomic profile: both antibodies modulate a large set of genes in the peripheral nervous system (DRG). In the central nervous system (spinal cord and cortex), the anti-NGF induces a large transcriptional modulation, while the anti-TrkA affects only a very small number of mRNAs in the same tissues. The two antibodies modulate largely different genes peripherally in DRGs, although acting on the same signalling system. Indeed, the differentially expressed genes (DEGs) modulated by the two antibodies in DRGs show only a partial overlap. Gene categories affected by the two treatments include synaptic components, immune system, inflammation, ionic channels, synaptic signalling. A minimal set of thirty mRNAs whose expression was reverted in common by the two antibodies, across all times, was identified. The DEGs regulated in common by the anti-TrkA and anti-NGF mAbs in DRGs reveal a number of potential new targets that might be linked to long lasting analgesia. Among these, the attention was focused on N6amt1.

The results presented in this thesis identify a remarkably long-lasting analgesic effect of anti-NGF and anti-TrkA mAbs, that is likely due to the onset of a new analgesic transcriptional program, or to the reconstitution of a pre-lesion expression profile. This study is the first direct transcriptomic comparison of the analgesic effects of anti-NGF and anti-TrkA antibodies in a well characterized neuropathic pain model. The results strongly support the importance of NGF and TrkA for the pharmacological control of NP and the characterization of new and more specific molecular targets.

Contents

0 ABBREVIATIONS

ACC	anterior cingulate cortex
AMPA	α-amino-3-hydroxy-5-methyl-4-isoxazolepropionic acid
ATP	adenosine triphosphate
BBB	blood-brain barrier
BDNF	brain-derived neurotrophic factor
BNB	blood-nerve barrier
cAMP	cyclic adenosine monophosphate
CCI	chronic constriction injury
cGMP	cyclic guanosine monophosphate
CGRP	calcitonin-gene related peptide
ChIP-seq	chromatin immunoprecipitation with parallel DNA sequencing
CNS	central nervous system
DAVID	Database for Annotation, Visualization and Integrated Discovery
DEGs	differentially expressed genes
DNA	deoxyribonucleic acid
DRG	dorsal root ganglion
ECM	extracellular matrix
ELISA	enzyme-linked immunosorbent assay
eRF1	eukaryotic translation termination factor 1
FDA	Food and Drug Administration
GABA	gamma-aminobutyric acid
GDNF	glial-derived neurotrophic factor
GluRs	glutamate receptors
GO	Gene Ontology
GPCR	G-protein-coupled receptors
GTP	guanosine-5'-triphosphate
IP	immunoprecipitation
KEGG	Kyoto Encyclopaedia of Genes and Genomes
LTP	long-term potentiation
mAb	monoclonal antibody
MAPK	mitogen-activated protein kinase

MTase	methyltransferase
MWT	mechanical withdrawal threshold
N6AMT1	N-6 Adenine-Specific DNA Methyltransferase 1
NGF	nerve growth factor
NMDA	N-methyl-D-aspartate
NP	neuropathic pain
NSAIDs	nonsteroidal anti-inflammatory drugs
OA	osteoarthritis
PKA	protein kinase A
PKC	protein kinase C
PLC	phospholipase C
PNS	peripheral nervous system
PPIA	peptidylprolyl isomerase A
qRT-PCR	quantitative reverse transcription polymerase chain reaction
RNA	ribonucleic acid
SC	spinal cord
SLC	solute carrier
TGF-β	transforming growth factor beta
TNF-α	tumor necrosis factor alpha
TrkA	tropomyosin-related kinase A
Trmt112	tRNA Methyltransferase Subunit 11-2
VEGF	vascular endothelial growth factor
WB	Western blot

1 INTRODUCTION

1.1 Neurobiology of pain

Pain is produced by the activation of the nociceptive system, the part of the nervous system which is specialized for the detection and processing of noxious stimuli, usually intense mechanical (noxious pressure, torque, sheer, or stretch), chemical or thermal stimuli (noxious heat and cold) (Schaible 2015). The sensation of pain contributes to providing to the brain information about the occurrence or threat of injury (Wall, McMahon et al. 2006). The ability to detect noxious stimuli is essential to an organism´s survival and wellbeing. Individuals who suffer from congenital abnormalities that render them incapable of detecting painful stimuli, such as HSAN IV or HSAN V, do not engage in appropriate protective behaviours, which may result in life threatening situations (Basbaum, Bautista et al. 2009). Thus, pain is an important, evolutionarily conserved physiological phenomenon that is necessary for survival. Contrarily, it represents a major clinical challenge as one of the most frequent symptoms of a variety of pathological conditions (Gangadharan and Kuner 2013).

There are three basic categories of pain: physiological pain, which protects the body from being damaged, pathophysiological pain, which prevents the tissue from further damage and supports healing processes, and pathological pain, which results from damage or disease of neurons of the nociceptive system (Gangadharan and Kuner 2013, Schaible 2015). Under suitable conditions, pathophysiologic nociceptive pain disappears after successful healing. Neuropathic pain, which belongs to the third category, is considered abnormal, often aberrant, and it is usually combined with loss of the normal nerve fibre function. As it becomes chronic and debilitating, it may have a major negative impact on quality of life (Schaible 2015). Persistent pain associated with injury (damage to nerve fibres) or diseases (diabetes, arthritis, or tumour growth) can result from alterations in the properties of peripheral nerves, such as changes in their conduction, increased spontaneous firing, generation of ectopic discharges or alterations in neurotransmitter properties. Chronic pain may even persist long after an acute injury, perhaps most commonly experienced as lower back pain or sciatica (Basbaum, Bautista et al. 2009). Chronic pain can be described as the persistence of a pain sensation and perception, long after the causes that initially triggered pain have been removed.

In the pathophysiologic pain condition, the nociceptive system undergoes significant changes leading to enhanced responsiveness of nociceptors, called hypersensitivity (Wall, McMahon et al. 2006, Schaible 2015). Normally innocuous stimuli, such as light touch or warmth, are perceived as painful (a phenomenon referred to as allodynia), or normally painful stimuli elicit enhanced pain responses (referred to as hyperalgesia) (Basbaum, Bautista et al. 2009). Following a tissue injury or during inflammation, hyperalgesia develops at the site of injury (primary hyperalgesia) and in the surrounding uninjured skin (secondary hyperalgesia). Primary hyperalgesia is a sensitization caused by the local release of inflammatory mediators. Secondary hyperalgesia is due to sensitization of neurons in the central nervous system (Wall, McMahon et al. 2006).

1.1.1 Peripheral sensitization

Peripheral neural apparatus responds to noxious (injurious or potentially injurious) stimuli and thus provides a signal to alert the organism to potential injury (Wall, McMahon et al. 2006). Peripheral sensitization is one of the hallmarks that characterizes pathophysiologic nociceptive pain at the peripheral level. During peripheral sensitization, sensory nerve fibers exhibit a reduction in the excitation threshold and/or an increase in magnitude of responsiveness. The threshold for elicitation of pain response at the peripheral ends is lowered into the normally innocuous range (Gangadharan and Kuner 2013, Schaible 2015). At the site of nerve damage or inflammation, spontaneous activity and ectopic mechanical, thermal, and chemical sensitivity develop in the injured nociceptors. The properties of nearby, uninjured nociceptors are also changed (Wall, McMahon et al. 2006). The sensitization of nociceptive and non-nociceptive sensory afferents results from the release of chemical mediators produced by nociceptors and non-neuronal cells (e.g. mast cells, basophils, platelets, macrophages, neutrophils, endothelial cells, keratinocytes and fibroblasts) (Gangadharan and Kuner 2013).

1.1.2 Central sensitization

Peripheral nociceptive processes often trigger changes in the spinal cord which are called central sensitization. Central sensitization refers to the process through which a state of hyperexcitability is established in the central nervous system, leading to enhanced processing of nociceptive signals (Basbaum, Bautista et al. 2009). In the sensitized state, nociceptive spinal cord neurons receive increased sensory input from inflammated regions due to the sensitization of peripheral nociceptors. They undergo significant changes, such as increased responses to innocuous and noxious stimuli, an expansion of the receptive fields, and the suprathreshold activation of synapses. These events result in an increase of the synaptic processing and in many aspects resemble the long-term potentiation (Schaible 2015). Numerous mechanisms have been implicated in central sensitization, including the NMDA receptor-mediated hypersensitivity of postsynaptic CNS neurons, the involvement of glial cells in pain states (activation of glial cells and subsequent production of cytokines and other mediators which facilitate the spinal processing) and loss or decrease in the activity of GABAergic and glycinergic inhibitory interneurons (Basbaum, Bautista et al. 2009, Schaible 2015). In sum, the nociceptive system undergoes significant changes at the peripheral as well as the central level in many chronic pain states (Schaible 2015).

1.2 Mechanisms of pain transduction pathways

1.2.1 The role of peripheral sensory afferent neurons

The peripheral afferents are composed of the nociceptive nerve fibres (peripheral nociceptors: unmyelinated C-fibres and myelinated Aδ-fibres) and non-nociceptive afferents (myelinated Aβ-fibres). Nociceptive sensory fibres are a specialized subpopulation of primary afferents that respond to intense, noxious stimuli. Noxious stimuli are sensed by peripheral nociceptive neurons (nociceptors) in the process known as nociception. The excitation threshold of these nociceptors is near or at the noxious (tissue damaging) range. There are two major classes of nociceptors based on properties of the nerve fibre (Wall, McMahon et al. 2006, Gangadharan and Kuner 2013, Schaible 2015).

The first class of nociceptors includes medium diameter myelinated Aδ nociceptive afferents that signal acute, well-localized "first" or fast pain. Aδ nociceptors are further subdivided into two main types. Type I Aδ-fibres include a population that is both heat and mechanically sensitive although having relatively high heat thresholds. They convey signals mostly from the sharp pain provoked by pinprick and other intense mechanical stimuli. Type II Aδ afferents are most likely heat-sensitive due to their much lower heat threshold, but a very high mechanical threshold. They certainly mediate the "first" acute pain response to noxious heat stimuli (Basbaum, Bautista et al. 2009).

The second class of nociceptors comprises small diameter unmyelinated "C" fibres that mediate poorly localized, "second" or slow pain. These unmyelinated nociceptors signal the burning pain from intense heat stimuli, as well as the pain from sustained pressure. Most unmyelinated C-fibres are heterogeneous and polymodal, that is, they respond to noxious mechanical and thermal stimuli as well as to a variety of chemical stimuli (Wall, McMahon et al. 2006, Basbaum, Bautista et al. 2009, Schaible 2015). The so-called "peptidergic" population of C nociceptive sensory neurons synthesizes and releases neuropeptides, such as substance P, and calcitonin-gene related peptide (CGRP). They also express the TrkA neurotrophin receptor, to which nerve growth factor (NGF) binds (Basbaum, Bautista et al. 2009). The nonpeptidergic population of C-nociceptors expresses the c-Ret receptor, whose ligand is glial-derived neurotrophic factor (GDNF), as well as artemin and neurturin (Basbaum, Bautista et al. 2009).

A third type of peripheral afferents, larger diameter unmyelinated Aβ fibres, respond to non-nociceptive stimuli. They represent low threshold afferents involved in the rapid conduction of innocuous mechanical stimuli, such as light touch, movement or vibration, under normal physiological conditions (Basbaum, Bautista et al. 2009, Gangadharan and Kuner 2013).

The cell bodies or somata of both nociceptive and non-nociceptive sensory afferents are localised in the dorsal root ganglia (DRG) and the trigeminal ganglion. Primary afferent fibres have a unique pseudo-unipolar morphology: they possess both a peripheral and central axonal branch emanating from a common axonal stalk. The peripheral terminals innervate their target organ and their central terminals synapse in the superficial spinal dorsal horn (Basbaum, Bautista et al. 2009, Gangadharan and Kuner 2013). The primary afferent nerve terminals sense noxious stimuli (of a thermal, mechanical, or chemical nature) and transmit this information into the changes in membrane potential and propagation of action potential along the nerve fibre, leading to synaptic activation of nociceptive neurons in the spinal cord. The transduction of these thermal and mechanical signals is mediated by a diverse range of voltage-gated ion channels that are present on sensory nerve endings (Wall, McMahon et al. 2006, Basbaum, Bautista et al. 2009, Schaible 2015). Activation of voltage-gated sodium and potassium channels generates action potentials that transmit nociceptor signals from the peripheral nervous system into the central nervous system (CNS) (Basbaum, Bautista et al. 2009, Gangadharan and Kuner 2013). Voltage-gated calcium channels are involved in the generation of pain or neurogenic inflammation, caused by neurotransmitter release from central or peripheral nociceptor terminals, respectively (Basbaum, Bautista et al. 2009).

1.2.2 Ascending tracts

Nociceptive neurons in the spinal cord are either local interneurons which activate neurons within the same or adjacent segments, or projection neurons which carry the nociceptive information to the thalamus and the brain stem along ascending tracts (Schaible 2015) (Figure 1a). Primary afferent nerve fibers convey nociceptive inputs to projection neurons within the dorsal horn of the spinal cord. Neurons within lamina I of the spinal cord generally process noxious information (via Aδ- and C-fibers). Most peptidergic C nociceptors project to lamina I and the most dorsal part of lamina II. By contrast, the nonpeptidergic afferent fibers terminate in the mid-region of lamina II. Spinal cord neurons in laminae III and IV respond primarily to innocuous stimulation (via Aβ afferents), and neurons in deeper lamina V of the dorsal horn receive a convergent non-noxious and noxious signals via direct (monosynaptic) Aδ- and Aβ-fiber inputs and indirect (polysynaptic) C-fiber inputs (Basbaum, Bautista et al. 2009). Spinal projection neurons within laminae I and V further process sensory inputs and relay them to brain centres via diverse ascending pathways, including the spinothalamic and spinoreticulothalamic tracts, which carry pain messages to the thalamus and brainstem, respectively (Basbaum, Bautista et al. 2009, Gangadharan and Kuner 2013). The spinothalamic tract is crucial for the sensory-discriminative aspects of the pain experience, whereas the spinoreticulothalamic tract is generally considered to process information relevant to poorly localized pain (Basbaum, Bautista et al. 2009).

The spinothalamic tract ascends to the ventrobasal complex of the thalamus which in turn transmits the information to the sensory cortex, where the perception of pain together with its emotional and aversive components is generated. Hence, the thalamocortical nociceptive system generates the conscious pain experience (Gangadharan and Kuner 2013, Schaible 2015). The lateral component of the thalamocortical system consists of neurons in the ventrobasal nucleus of the thalamus and somatosensory cortex. The activation of these neurons likely generates the sensory discriminative component of pain, providing information about the location and intensity of the painful stimulus (Basbaum, Bautista et al. 2009, Schaible 2015). The medial system consists of neurons in the medial part of the thalamus and projections to the insular cortex, the anterior cingulate gyrus, and the forebrain. These pathways are relevant to the emotional aspects and generate the affective component of the pain, the unpleasant feelings and the suffering. They also play an important role in the generation of behavioural responses to pain (Schaible 2015).

Other spinal cord projection neurons belonging to the spinoreticulothalamic tract connect to the brainstem, e.g., to the parabrachial region of the dorsolateral pons which forms a very rapid connection to the amygdala, a major site for the generation of fear and aversive properties of the pain experience (Basbaum, Bautista et al. 2009, Schaible 2015). One of the consequences of such interactions is the occurrence of depression during pain states.

1.2.3 Descending tracts

Branches of the ascending neurons also form connections to brain stem nuclei, which make a part of the descending inhibitory and excitatory systems (Figure 1b). The descending inhibition originates in the midbrain periaqueductal gray which projects to the rostroventral medulla (Schaible 2015). These nuclei are involved in descending feedback systems that

regulate the output from the spinal cord. The descending inhibitory system serves as an endogenous pain control system which keeps the spinal nociceptive processing under control and can be activated from the brain (Basbaum, Bautista et al. 2009, Schaible 2015).

Figure 1. Pain processing pathways.

a) Different types of primary afferent sensory neurons play a role in transmitting noxious (C and Aδ fibers) and non-noxious (Aα and Aβ fibers) stimuli from the periphery to second-order neurons in the dorsal horn of the spinal cord or dorsal column nuclei. The second-order neurons ascend to higher centers of the brain, including the thalamus. The thalamus, in turn, projects to cortical areas in the brain, such as the somatosensory, anterior cingulate and insular cortices that are important for the conscious perception of pain.

b) Higher pathways in cortical areas, such as the amygdala, hypothalamus and anterior cingulate cortex are involved in modulating the transmission and perception of pain. Neurons in these regions of the brain project to regions in the hindbrain, including the periaqueductal grey, which, in turn, projects to the rostral ventromedial medulla in the brainstem. Neurons located in this area project to and modulate neurons in the dorsal spinal cord and thus, neurons from higher regions of the brain can inhibit or facilitate the transmission of pain information through the spine (Mantyh 2006).

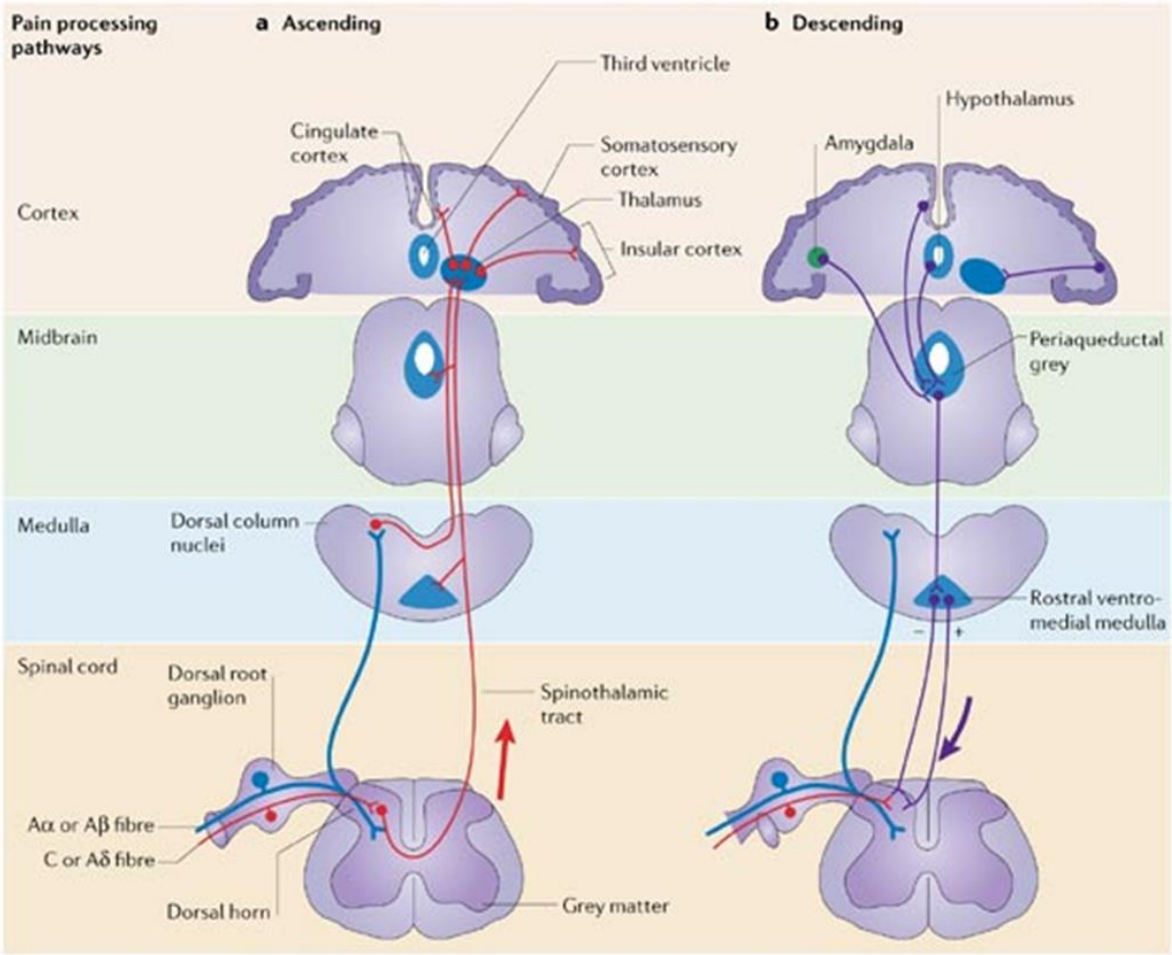

Copyright © 2006 Nature Publishing Group
Nature Reviews | Neuroscience

1.3 NGF involvement in pain transduction mechanisms

NGF is a 13kDa polypeptide initially discovered in the 1950s as a tumour tissue-produced soluble factor, firstly described in tumours grafted onto chick embryos where an increased production of nerve fibers was observed. NGF serves in regulating the function of sensory and sympathetic neurons in the developing nervous system. During embryonic development, NGF is synthesized and released by target tissues, thereby promoting the growth and differentiation of neuronal crest primary sensory and sympathetic neurons and contacts with their targets (Levi-Montalcini 1987). It also plays an important role in survival of these neurons since NGF inhibition during development, by antibody injection, leads to a marked loss of sensory and sympathetic neurons due to apoptosis (Levi-Montalcini and Booker 1960, Gorin and Johnson 1979). In adults, in addition to actions in the central nervous system (where it regulates the maintenance and survival of basal forebrain cholinergic neurons (Hefti 1986), NGF also regulates pain perception and regeneration after peripheral nerve injury (Seidel, Wise et al. 2013). It is involved in the modulation of nociception and is found to be elevated in chronic pain conditions leading to pain hypersensitivity (Mantyh, Koltzenburg et al. 2011, Patel, Kaye et al. 2018).

NGF is a neurotrophin which belongs to a family of neurotrophic factors consisting of brain-derived neurotrophic factor (BDNF) (Leibrock, Lottspeich et al. 1989), neurotrophin-3 (NT-3) (Ernfors, Ibanez et al. 1990, Maisonpierre, Belluscio et al. 1990), and neurotrophin-4/5 (NT-4/5) (Berkemeier, Winslow et al. 1991, Hallbook, Ibanez et al. 1991). Neurotrophins act by binding to two types of cell surface receptors: neurotrophin receptor (NGFR or p75NTR) and a family of tyrosine kinase receptors, tropomyosin-related kinase A (trkA), B (trkB), and C (trkC). All neurotrophins bind NGFR/p75 with similar affinity, but each neurotrophin binds to a specific trk receptor with higher affinity (Chao 2003). NGF forms tightly bound homodimer proteins which preferentially bind to the tropomyosin-related kinase A (trkA) with high affinity and to the p75 receptor with lower affinity (Mendell 2002, Mantyh, Koltzenburg et al. 2011). The former activates MAP kinases, Ras and phosphatidyl inositol-3 (PI3)-kinase. p75 signalling includes activation of Jun kinase, nuclear factor-kappaB (NF-kappaB) and others (Seidel, Wise et al. 2013). Binding of NGF to p75NTR increases the affinity of NGF for TrkA and enhances its specificity against other neurotrophins (Chao 2003). The formation of a simultaneous trimolecular signalling complex between NGF, TrkA and p75NTR at the plasma membrane has been proposed, based on co-immunoprecipitation experiments, but its structural demonstration has been elusive and is currently debated (Marchetti et al. 2019, Chao 2019). Perhaps one of the principal receptors for pain modulation is trkA, which is expressed on the cell membrane of peripheral nociceptors. TrkA downstream signalling regulates the expression and activity of ion channels and molecules that play a key role in the modulation of pain signalling (Patel, Kaye et al. 2018). TrkA is found in high quantities in nerve fibers of the sensory neurons in the dorsal root ganglia (DRG) during embryogenesis (Mendell 2002); however, by the postnatal period, trkA expression together with NGF sensitivity decline, and NGF signalling shifts its role from promoting neuron growth and survival to regulating the sensitivity of the peripheral nervous system to noxious stimuli (Bennett 2001). Thus, in the adult, NGF is no longer required for survival of primary sensory or sympathetic neurons, it serves instead in pain signalling through the binding of NGF to its receptors, trkA and p75 (Mantyh, Koltzenburg et al. 2011), which are expressed on the peripheral terminals of

myelinated Aδ- and unmyelinated C-fibers (Bennett, Koltzenburg et al. 1998, Hefti, Rosenthal et al. 2006, Belanger, West et al. 2018).

1.3.1 The role of NGF in central and peripheral sensitization and inflammation

NGF is produced and released by peripheral tissues following noxious stimuli (eg, injury and inflammation) secondary to the production of inflammatory cytokines, such as interleukin-1 and TNFα. NGF binds to trkA receptors, that are selectively expressed on the peripheral terminals of A-delta and peptidergic unmyelinated C-fibers, with multiple modulating effects on pain signalling (Mantyh, Koltzenburg et al. 2011, Chang, Hsu et al. 2016). Upon binding of NGF to TrkA in the peripheral fibers, the NGF-trkA complex is internalized peripherally and transported retrogradely to the cell soma in dorsal root ganglia, where it activates transcription factors responsible for regulating the gene expression of a variety of pronociceptive pain transducers (Patel, Kaye et al. 2018). These modulators comprise a number of peripheral nociceptive receptors and ion channels at the membrane surface, including transient receptor potential vanilloid 1 (TRPV1), acid-sensing ion channels 2 and 3 (ASIC 2/3), endothelin receptors, bradykinin receptors, voltage-gated sodium and calcium channels, putative mechanotransducers, as well as delayed rectifier potassium currents and TRPV1 receptor-mediated currents (Kendall, Brar-Rai et al. 1995, Woolf 1996, Miller and Kaplan 2001, Delcroix, Valletta et al. 2003). The increase in activity of these channels result in peripheral sensitization and pain hypersensitivity.

NGF–trkA signalling also leads to transcriptional changes that result in the increased synthesis of several peptides and neurotransmitters involved in nociception, such as substance P (SP), calcitonin gene-related peptide (CGRP), and BDNF, thereby leading to central sensitization (Lindsay and Harmar 1989, Mantyh, Koltzenburg et al. 2011, McKelvey, Shorten et al. 2013). These pain signalling molecules show a dual mechanism of action consisting of action potential neurotransmission to the central nervous system (CNS) and, at the same time, induction or perpetuation of peripheral inflammation. They are able to induce peripheral inflammation at the site of peripheral nociceptors after antidromal axoplasmatic transport (Seidel, Wise et al. 2013). Activation of trkA receptors located on mast cells is a proinflammatory process, which elicits the release of inflammatory mediators such as histamine, serotonin or 5-hydroxytryptamine (5-HT), protons, as well as NGF itself, resulting in a positive feedback loop (Mantyh, Koltzenburg et al. 2011, McKelvey, Shorten et al. 2013).

In conclusion, NGF signalling is involved in both peripheral sensitization of nociceptors in the DRGs and central sensitization of dorsal horn neurons in the spinal cord in response to noxious stimuli. In addition, NGF also plays an important role in inflammatory responses, by activating chemotaxis in polymorphonuclear leukocytes (Gee, Boyle et al. 1983), by increasing vascular permeability (Otten, Baumann et al. 1984) and, by recruiting mast cells to the injured site (Sawada, Itakura et al. 2000, Skaper 2001). Conversely, proinflammatory mediators released by recruited mast cells induce NGF-upregulation which can result in a chronic self-perpetuating pain sensation mechanism (Sofroniew, Howe et al. 2001). Moreover, the expression of TrkA was found to be stimulated by NGF itself (Kojima, Ikeuchi et al. 1995) suggesting that upregulation of NGF may result in amplification of pain sensation with hyperesthesia and allodynia.

1.3.2 NGF status in pain states

As mentioned previously, NGF concentration is generally elevated in chronic neuropathic pain states, such as diabetic neuropathy, and cancer pain, in particular, invasive nerve cancers (McMahon 1996, Ugolini, Marinelli et al. 2007, Wild, Bian et al. 2007). Similarly, NGF overexpression was observed in human rheumatic diseases (Seidel, Herguijuela et al. 2010) and in animal models with experimentally induced arthritis (Garry and Hargreaves 1992) and OA in dogs (Ferrell and Russell 1986). Increased levels of NGF in inflammatory pain conditions, such as interstitial cystitis, prostatitis, arthritis, pancreatitis, are due to its release by mast cells, macrophages, and lymphocytes (Patel, Kaye et al. 2018).

NGF also mediates mechanical and thermal hyperesthesia upon systemic application in animals (Lewin, Ritter et al. 1993) and humans (Petty, Cornblath et al. 1994). Intradermal injection of NGF into the forearm and masseter muscle of healthy individuals induces allodynia and increases pain sensitivity in the surrounding skin (Dyck, Peroutka et al. 1997, Svensson, Cairns et al. 2003, Ugolini, Marinelli et al. 2007). Both in rodents and humans, direct subcutaneous administration of NGF leads to activation and sensitization of nociceptors, causing behavioural hyperalgesia within 1-3 hours after administration in rats and long-lasting pain sensitivity in humans (Lewin, Rueff et al. 1994, Andreev, Dimitrieva et al. 1995, Dyck, Peroutka et al. 1997, Svensson, Cairns et al. 2003). The rapid and long-lasting nociceptor sensitization of cutaneous receptors indicates that NGF plays a crucial role in both acute and chronic pain (Mendell, Albers et al. 1999, Pezet and McMahon 2006). Clinical studies (Apfel, Kessler et al. 1998, Apfel, Schwartz et al. 2000, McArthur, Yiannoutsos et al. 2000, Schifitto, Yiannoutsos et al. 2001) have demonstrated a significant dose-dependent hyperalgesia at the site of NGF injection.

NGF-upregulation was observed in preclinical models of both inflammation and peripheral nerve injury. But the relationship between NGF signalling and neuropathic pain states appears to be more complex than previously thought, and in some patients with diabetic neuropathy, NGF levels are actually decreased (Wild, Bian et al. 2007). Thus, the role of NGF-mediated signalling in chronic nociceptive and neuropathic pain states remains controversial (Hefti, Rosenthal et al. 2006, Watson, Allen et al. 2008, Mantyh, Koltzenburg et al. 2011, McKelvey, Shorten et al. 2013). On one hand, NGF induces hyperalgesia and neuropathic pain conditions are in most cases correlated with elevated NGF levels. On the other hand, NGF exerts neuroprotective and trophic action on peptidergic small-diameter dorsal root ganglia cells after nerve injury (Gold, Mobley et al. 1991, Frade and Barde 1998, Ugolini, Marinelli et al. 2007).

Conversely, NGF sequestration via systemic injection of neutralizing antibodies, NGF-sequestering antibody or TrkA immunoglobulin G (IgG) fusion protein, or blockade of TrkA receptor activation by neutralizing anti TrkA antibodies, appears to decrease allodynia and hyperalgesia in animal models of neuropathic pain, such as chronic constriction injury and partial sciatic nerve transection (Zahn, Subieta et al. 2004, Ugolini, Marinelli et al. 2007, Wild, Bian et al. 2007, Mantyh, Koltzenburg et al. 2011, Belanger, West et al. 2018). In models of bone cancer, NGF blockade has shown to be efficient not only at the decrease of ectopic discharges and a reduction of cancer pain but also in the inhibition of neuroma formation (Mantyh, Jimenez-Andrade et al. 2010).

1.4 Current pain therapies

Many local and systemic immunopathologies characterized by proinflammatory events might be preceded by, or coincide with, increasing pain sensation. Persistent peripheral nociceptor stimulation leads to a self-perpetuating activation of neurogenic inflammation with typical characteristics such as swelling, reddening and oedema (Seidel, Wise et al. 2013). In rheumatology, painful disorders predominate in bone diseases and arthropathies, such as rheumatoid arthritis and OA. Neuropathic pain, on the other hand, results from damage to the neurons of the somatosensory system, secondary to either direct injury or disease-related dysfunction, and results in the generation of ectopic discharges that occur independently of somatic stimuli (Cohen and Mao 2014, Chang, Hsu et al. 2016).

While acute pain has been successfully treated in many patients, a considerable proportion of chronic pain states remain challenging to treat. There are still about 20% of the people in the population suffering from chronic pain. Thus, chronic pain is a clinical situation of huge medical need and there is a growing interest in pain research, which would enable to identify the mechanisms involved in the generation and maintenance of different pain states and, based on this knowledge, develop new analgesic drugs for pain treatment (Schaible 2015).

Persistent chronic pain is a long-term condition which impairs the quality of life of the affected individuals, among which neuropathic pain, osteoarthritis and non-specific low back pain (LBP) are the leading causes of disability and reduced quality of life worldwide (Turk, Wilson et al. 2011, Kalso, Aldington et al. 2013, Chou, Deyo et al. 2017). Besides, patients suffering from chronic inflammatory and neuropathic pain have decreased productivity and increased health-care costs, thus having significant societal consequences and contributing to the overall economic burden on society (Patel, Kaye et al. 2018). Existing analgesic drugs induce several unwanted side effects or do not provide desirable outcomes in a significant proportion of patients suffering from chronic pain (Turk, Wilson et al. 2011, Kalso, Aldington et al. 2013, Chou, Deyo et al. 2017), hence there are several pharmacological drugs being developed in order to reduce suffering in patients, thereby decreasing health care costs. The clinical practice involves multimodal analgesic therapy, consisting of both pharmacologic and non-pharmacologic modalities, to optimize patient outcomes and to minimize adverse effects (Patel, Kaye et al. 2018).

Current pain medications include nonsteroidal anti-inflammatory drugs (NSAIDs), neuropathic agents, antidepressants, opioids, anticonvulsants and targeted spinal injections (Bhangare, Kaye et al. 2017, Patel, Kaye et al. 2018). Therapeutic medications commonly used in the management of chronic pain disorders have limited effectiveness and may have very significant side effects, associated with issues of dependence and poor tolerance by many patients (Bjordal, Ljunggren et al. 2004). Therefore, the long-term use of mild analgesics, anti-inflammatory agents that block the cyclooxygenase pathways or more potent central acting narcotics are generally inadequate (Turk, Wilson et al. 2011, Kalso, Aldington et al. 2013, Seidel, Wise et al. 2013, Chou, Deyo et al. 2017). In case of NSAIDs use, the adverse effects include gastrointestinal, renal, cardiovascular toxicity which makes its use in patients limited (Chou, Huffman et al. 2007, Vadivelu, Gowda et al. 2015). The long-term treatment with opioids increases the risk of cognitive dysfunction, accompanied by respiratory depression, and addiction or CNS toxicity with potentially lethal outcomes (Seidel, Wise et al. 2013, Patel,

Kaye et al. 2018). Targeted spinal injections do not represent the first-choice therapy either, due to their potential risks and complications. Accordingly, there is an imminent need for the development of new and better tolerated painkillers that are both safe and effective and do not share side effects that are observed with NSAIDs or opioids (Belanger, West et al. 2018).

Fortunately, a substantial progress has been made in recent decades to better understand the molecular and cellular mechanisms underlying pain in physiological, as well as pathophysiological contexts. Numerous potentially interesting targets for developing novel analgesic drugs have emerged from the studies using a mechanism-based approach which consists in identification of intracellular signals involved in the pain transduction pathway (Norman and McDermott 2017, Patel, Kaye et al. 2018). Some current areas of research have investigated compounds that attenuate glial activation (e.g., minocycline and methylxanthine derivatives); drugs that inhibit proinflammatory cytokine production (e.g., cytokine inhibitors and antagonists to toll-like receptor 4 activation); anti-inflammatory agents that reduce inflammation and other compounds that target protein kinases, CGRP, Nav1.7 and other molecules involved in pain transduction signalling pathway (Bowler, Worsley et al. 2011, Lee, Park et al. 2014, Chang, Hsu et al. 2016). However, despite continuous drug development efforts, only cytokine- and NGF-directed monoclonal antibodies have reached clinical trials (Kissin 2015, Chang, Hsu et al. 2016). Thus, the development of NGF and TrkA monoclonal antibodies represents a novel approach to the treatment of chronic pain (Woolf and Max 2001, Hefti, Rosenthal et al. 2006).

1.5 Anti-NGF directed therapies

The nerve growth factor (NGF) and its receptors, important key mediators in pain signalling pathway, are one of the most promising specific targets that have evolved from basic and applied research. Efforts of the researchers have been focused on several approaches that target the NGF-TrkA pathway and its effect on pain initiation and maintenance: prevention of NGF binding to its receptors; inhibition of TrkA function and activation; sequestration of free NGF, to name the most important ones (Hefti, Rosenthal et al. 2006, Mantyh, Koltzenburg et al. 2011, Chang, Hsu et al. 2016).

1.5.1 Compounds targeting TrkA receptor

The nonpeptide small molecule ALE-0540 is a TrkA antagonist that inhibits the binding of NGF to both TrkA and p75, as well as signal transduction and biological responses mediated by TrkA receptors. Pain behaviour was significantly reduced following intraperitoneal or spinal intrathecal administration of ALE-0540 in rat models of neuropathic pain and thermally-induced inflammatory pain (Owolabi, Rizkalla et al. 1999). However, when tested with other receptors *in vitro*, ALE-0540 showed a lack of specificity. Thus, despite its demonstrated antiallodynic effect, it has not been moved onward into clinical trials (Chang, Hsu et al. 2016).

k252a is a small-molecule protein kinase inhibitor that inhibits the activation of the entire tropomyosin receptor kinase family, PKC and PKA. Systemic treatment with k252a alleviated pain in a rat model of acute necrotizing pancreatitis, suppressed the phosphorylation of TrkA in the pancreas and reversed the increase in neuropeptide CGRP expression associated with pancreatitis. Similarly to ALE-0540, due to its lack of specificity, no human trials have

ever been initiated and this kinase inhibitor will most likely not make it through human clinical trials (Winston, Toma et al. 2003, Chang, Hsu et al. 2016).

Syntaxin 8 (STX8), a Q-SNARE protein, is a TrkA-binding protein that facilitates TrkA receptor transport from the Golgi apparatus to the plasma membrane and regulates TrkA cell surface levels. Furthermore, knockdown of STX8 in rat DRG resulted in analgesia in models of formalin-induced inflammatory pain and could eventually lead to the development of specific agents for the treatment of pain (Chen, Zhao et al. 2014). It is however not yet clear how to turn this interaction into a therapeutic target.

The most promising approach targeting TrkA is based on the monoclonal antibody mAb MNAC13. MNAC13 is a well characterized anti-TrkA monoclonal antibody with remarkable function neutralizing properties (Cattaneo, Capsoni et al. 1999, Covaceuszach, Cattaneo et al. 2005). This antibody was raised against native human TrkA to block the NGF–TrkA interaction (see below).

1.5.2 Compounds targeting NGF ligand

NGF-sequestering agents and inhibitors have been developed and studied in both preclinical models and clinical studies of painful conditions (Seidel, Wise et al. 2013).

The domain 5 of the TrkA receptor, TrkAd5, is a soluble receptor involved in the binding of NGF. The recombinant TrkAd5 binds NGF with picomolar affinity (Dawbarn, Fahey et al. 2006). In a murine OA model induced by destabilisation of the medial meniscus, TrkAd5 was highly effective at suppressing pain (McNamee, Burleigh et al. 2010). In addition, the analgesic efficacy of the TrkAd5 has been demonstrated in preclinical models of inflammatory pain and asthma by the sequestration of excess levels of endogenous NGF. These studies therefore indicate that TrkAd5 represents a potent novel analgesic agent in OA and inflammatory pain (Dawbarn, Fahey et al. 2006).

The therapeutic use of antibodies, when compared to small compounds, represents significant advantages. Antibodies possess a generally higher specificity and a reduced number of off-targets (Watson, Allen et al. 2008, Chang, Hsu et al. 2016). Moreover, small molecule NGF-TrkA antagonists are more likely than larger antibody molecules to cross the blood-brain barrier, leading to unwanted neurological side effects (Covaceuszach, Marinelli et al. 2012). Finally, anti NGF antibodies have a significant success track record in the research literature of NGF, as a way to neutralize NGF *in vivo*, ever since the original immunosympathectomy experiment by Rita Levi-Montalcini (Levi-Montalcini and Booker 1960, Cattaneo 2013).

Overall, the research on monoclonal antibodies has led to significant results in the treatment of cancer and immunological disorders. The studies regarding their potential use in the treatment of pain are still in progress, with a special attention being focused on NGF and TrkA antagonism.

Anti-NGF therapy is among the prospective new analgesic therapies with favourable results in preclinical and clinical studies. Monoclonal antibodies targeting NGF are characterized by their anti-hyperalgesic (normalizing a decreased nociceptive threshold) as well as analgesic (increasing normal and sensitized nociceptive thresholds) effects (Patel, Kaye et al. 2018). Anti-NGF agents, including tanezumab, fulranumab and fasinumab, have been

developed as a novel approach in pain therapy management. In preclinical models, they have been proved to be efficacious in the treatment of certain pain conditions that are currently poorly treated, such as knee and hip pain, bone cancer pain and autoimmune arthritis (Seidel, Wise et al. 2013, Belanger, West et al. 2018). Other potential indications include treatment of prostatitis, pancreatitis, and interstitial cystitis (Patel, Kaye et al. 2018). Thus, blockade of NGF represents a promising strategy to develop new pain therapeutics (Hefti, Rosenthal et al. 2006, Watson, Allen et al. 2008, Covaceuszach, Marinelli et al. 2012).

1.5.3 Tanezumab

Tanezumab is a recombinant humanized monoclonal antibody (IgG) with high sensitivity and specificity for NGF that was developed by Pfizer (New York, NY, USA) to target NGF (Patel, Kaye et al. 2018). This protein is currently in clinical development for the treatment of several pain conditions (Hefti, Rosenthal et al. 2006). The Fc mutation limits antibody dependent cell mediated toxicity and complement activation (Patel, Kaye et al. 2018). It binds both circulating and local tissue NGF, thereby preventing interaction of NGF with its receptors (Abdiche, Malashock et al. 2008, Mantyh, Koltzenburg et al. 2011). Tanezumab is a large molecule and, hence, does not cross the blood-brain barrier, its plasma half-life is 22-25 days (Tanga, Nutile-McMenemy et al. 2005, Friedly, Standaert et al. 2010). Tanezumab was investigated in 26 studies, including long-term open-label extension safety studies, which enrolled over 11,000 patients in total (Miller, Guermazi et al. 2015).

Beside tanezumab, two other monoclonal antibodies targeting NGF, namely fulranumab and fasinumab, have been involved in clinical studies conducted by the manufacturers Janssen (Beerse, Belgium) and Regeneron (Tarrytown, NY, USA), respectively. Fulranumab and fasinumab are recombinant, fully human, NGF monoclonal antibodies that bind to NGF and have also been investigated for the treatment of chronic pain conditions (Lane, Schnitzer et al. 2010, Katz, Borenstein et al. 2011, Brown, Murphy et al. 2012, Kivitz, Gimbel et al. 2013, Sanga, Katz et al. 2013, Balanescu, Feist et al. 2014, Ekman, Gimbel et al. 2014, Gimbel, Kivitz et al. 2014, Tiseo, Kivitz et al. 2014, Mayorga, Wang et al. 2016). This class of drugs was primarily investigated in patients with symptomatic osteoarthritis and chronic non-specific LBP (Miller, Guermazi et al. 2015).

Due to unexpected joint adverse events in clinical studies and concerns about sympathetic nervous system toxicity in animals, these agents were placed on 2 separate partial clinical holds, which were subsequently lifted after rigorous evaluations were conducted to understand how inhibition of NGF impacts safety (Belanger, West et al. 2018). At the time of the first clinical hold, tanezumab was the only anti-NGF mAb at an advanced stage of clinical development (Bannwarth and Kostine 2014).

FDA hold on Tanezumab

The Biological Investigational New Drug application for tanezumab was submitted to the US Food and Drug Administration (FDA) in April 2004 for indications related to the treatment of moderate to severe chronic pain (Vadivelu, Gowda et al. 2015, Patel, Kaye et al. 2018). Clinical trials (Phase I and II) demonstrated the efficacy of tanezumab in treating the osteoarthritic pain of the hip and knee joint as well as chronic low back pain (Hefti, Rosenthal et al. 2006, Lane, Schnitzer et al. 2010, Katz, Borenstein et al. 2011). However, in 2010, the

US Food and Drug Administration (FDA) suspended all clinical trials involving anti-NGF antibodies for all indications except for terminal cancer pain, due to reports of rapidly destructive arthropathies and osteonecrosis leading to joint replacement. Reported cases were observed in patients using NGF-antagonists alone or with NSAIDs and involved extensive bone damage and joint destruction (Janssen research and development LLC, 2012, Pfizer, 2012, Regeneron pharmaceuticals, and arthritis advisory committee meeting, 2012). These events were investigated by an independent, multidisciplinary adjudication committee, comprising bone pathologists, orthopaedic surgeons, and rheumatologists, charged with reviewing all reports of osteonecrosis leading to joint replacement (Hochberg 2015). Review of all available case reports diagnosed osteonecrosis and rapid OA progression in 2.3% and 66.7% subjects, respectively. No evidence was found indicating that tanezumab treatment was associated with an increase in osteonecrosis (Hochberg, Tive et al. 2016, Patel, Kaye et al. 2018). Increased risk for rapidly progressive OA (RPOA) was noted in patients who received concomitant therapy with anti-NGF agents and NSAIDs (Nickel, Atkinson et al. 2012, Hochberg, Tive et al. 2016). Based on these findings and the apparent low incidence of osteonecrosis, the FDA voted in favour of continued development of anti-NGF drugs due to their potential benefit for a multitude of pain conditions and lifted the joint safety partial clinical hold on tanezumab in March 2012 (Seidel, Wise et al. 2013, Patel, Kaye et al. 2018). Shortly after reinitiating clinical studies, a second class-wide partial clinical hold was implemented by the FDA in December 2012, owing to sympathetic nervous system safety concerns raised by animal toxicology studies (Norman and McDermott 2017). As additional preclinical investigations showed no sympathetic neuronal loss, and only small alterations in neuronal size, which were reversible upon treatment cessation, FDA lifted the partial clinical hold on tanezumab in March 2015 (Norman and McDermott 2017). Tanezumab clinical trials conducted by Pfizer resumed in July 2015 and include clinical risk mitigation measures, related to joint safety and sympathetic nervous system safety that were agreed to with FDA, such as limiting trials to the use of the lowest effective doses, restriction of NSAID use, and the development of a screening radiologic protocol (Belanger, West et al. 2018).

Safety issues related to Tanezumab therapy

Adverse events of anti-NGF therapy related to abnormalities in peripheral sensation have been reported by patients receiving tanezumab (Kivitz, Gimbel et al. 2013, Gimbel, Kivitz et al. 2014). The most common neurosensory symptoms included paresthesia (pins and needles sensation), followed by hypoesthesia (numbness) and burning sensation (Lane, Schnitzer et al. 2010, Katz, Borenstein et al. 2011, Brown, Murphy et al. 2012, Brown, Murphy et al. 2013, Kivitz, Gimbel et al. 2013, Sanga, Katz et al. 2013, Spierings, Fidelholtz et al. 2013, Balanescu, Feist et al. 2014, Ekman, Gimbel et al. 2014, Gimbel, Kivitz et al. 2014, Tiseo, Kivitz et al. 2014, Mayorga, Wang et al. 2016). Among other treatment-related side effects of anti-NGF therapy were peripheral oedema, transient arthralgias, extremity pain, and rarely, osteonecrosis (Bannwarth and Kostine 2014). The side effects related to abnormal peripheral sensation were generally mild to moderate in severity and were usually transient.

A small number of patients suffered from a rapidly progressive OA (RPOA) and underwent joint replacement. However, these adverse events were more common in patients who received tanezumab treatment in combination with NSAIDs than either treatment alone. in the tanezumab–plus-NSAID group compared to the group on mono-NGF therapy (Seidel,

Wise et al. 2013, Schnitzer, Ekman et al. 2015). The adverse events in the group on mono-NGF therapy were fewer compared to patients receiving opioids alone and mixed results were obtained when comparing to NSAID group (Lane, Schnitzer et al. 2010, Katz, Borenstein et al. 2011, Brown, Murphy et al. 2012, Brown, Murphy et al. 2013, Kivitz, Gimbel et al. 2013, Sanga, Katz et al. 2013, Spierings, Fidelholtz et al. 2013, Balanescu, Feist et al. 2014, Ekman, Gimbel et al. 2014, Gimbel, Kivitz et al. 2014, Tiseo, Kivitz et al. 2014, Mayorga, Wang et al. 2016). General safety at the lower doses appeared similar to placebo. The severe adverse effects that included osteonecrosis and earlier than expected joint replacement were investigated as noted above. Although a causal relationship was not seen, additional investigation on both efficacy and safety of these antibodies is needed in order to define the optimal dose and to maximize the benefit to risk ratio (Patel, Kaye et al. 2018). One may also speculate that inhibiting pain through anti-NGF treatment may result in increased cartilage degradation due to overuse of joints (Seidel, Wise et al. 2013).

In addition to evaluating pain-related behaviours, non-clinical studies have been conducted to determine the dependence of adult sympathetic neurons on NGF. Some of the previous studies indicated an apparent loss of neurons with NGF blockade, although no studies ever revealed images of dead or dying neurons. More recently, in-depth studies demonstrated that tanezumab was associated with smaller ganglion volume, smaller average neuron size/area, and lower estimated total neuron counts. Nevertheless, these changes did not progress over time or persist with continued exposure to tanezumab and were completely reversible (Butt, Evans et al. 2014, Belanger, Butler et al. 2017). Thus, no evidence of neuronal apoptosis or necrosis in clinical studies was demonstrated and no changes were observed in the sympathetic control of cardiovascular function in response to tanezumab (Belanger, Butler et al. 2017). Studies evaluating the bone morphology did not result in any changes in bone innervation, bone remodelling, or fracture healing.

Recent clinical studies with tanezumab in different patient populations, including patients suffering from osteoarthritis, low back pain, and diabetic peripheral neuropathy, demonstrated a clear efficacy. Even though the tanezumab monotherapy was generally well-tolerated with a low incidence of side effects (Schnitzer, Ekman et al. 2015, Chang, Hsu et al. 2016, Patel, Kaye et al. 2018), a clinical research should be conducted that would include additional large-scale comparative-effectiveness studies with long-term follow-up periods in human patients in order to overcome any safety concerns related to the use of this drug (Chang, Hsu et al. 2016).

To date, preclinical studies evaluating the effects of anti-NGF and anti-TrkA neutralizing antibodies exhibit a consistent benefit in the prevention of hyperalgesia and allodynia and the systematic study of the selective inhibition of NGF-TrkA system in humans has yielded promising efficacy and safety results (Chang, Hsu et al. 2016). Despite the fact that the selective inhibition of NGF and TrkA shows a promising outcome with potentially tolerable adverse effects, current and future studies will have to focus their efforts on understanding the molecular mechanisms that govern the NGF-TrkA signalling pathways. NGF is not only a key modulator of inflammatory and nociceptive responses in chronic and inflammatory pain conditions (Covaceuszach, Marinelli et al. 2012), this neurotrophin is also involved in other important biological processes. NGF is a pleiotropic molecule that plays a key role in neuronal development, function, survival, and growth. This molecule regulates a variety of metabolic

pathways, such as wound healing, neoplastic diseases, immunosuppression and organ functions in the CNS and the peripheral nervous system. NGF-antagonists may have an impact on all these organ systems although clinical trials thus far have not shown substantial signals (Seidel, Wise et al. 2013, Chang, Hsu et al. 2016). Pharmacotherapies targeting NGF-TrkA system need to take into careful consideration potential unwanted or undesirable side effects resulting from the pleiotropism of this pathway and take appropriate safety measures.

In any case, tanezumab completed Phase III clinical trials in osteoarthritis patients, showing effective analgesia only at the higher dose and no major safety concern, except for a higher incidence of RPOA in the 5 mg group (2.8%) versus the 2.5 mg group (1.4%) (Tive, Bello et al. 2019, Berenmbaum, Blanco et al. 2020). Based on these results, it is expected that tanezumab might receive market approval by FDA in the forthcoming months, but the trade-off between efficacy and risks will require to be carefully balanced in the choice of the group of patients recommended for tanezumab treatment.

1.5.4 Anti-NGF antibody αD11 and its humanized version hum-αD11

As mentioned before, the development of NGF antagonists (Hefti, Rosenthal et al. 2006) represents a key approach in the treatment of chronic and inflammatory pain conditions due to their potent analgesic effects which have been observed not only in a variety of animal pain models, but also in humans (Pezet and McMahon 2006, Covaceuszach, Marinelli et al. 2012). NGF antagonizing antibody αD11 has emerged as a new strategy for the development of an analgesic drug for human pathologies linked to chronic and inflammatory pain.

Firstly, the rat anti-NGF monoclonal antibody (mAb) αD11 (Cattaneo, Rapposelli et al. 1988) was produced with the following properties: it does not cross-react with closely related members of the neurotrophin superfamily (Molnar, Tongiorgi et al. 1998), it can bind mouse NGF (mNGF) with picomolar affinity (Paoletti, Covaceuszach et al. 2009), and antagonizes very effectively with biological function of NGF in a variety of *in vitro* and *in vivo* systems (Ruberti, Bradbury et al. 1993, Berardi, Cellerino et al. 1994, Molnar, Ruberti et al. 1997, Garaci, Aquaro et al. 2003, Capsoni, Tiveron et al. 2010, Covaceuszach, Marinelli et al. 2012).

Anti-NGF αD11 mAb, similarly to other antibodies of therapeutic interest being derived from murine monoclonal antibodies, must be humanized prior to its use in patients for therapeutic purposes. In order to advance its therapeutic development, variable regions of the αD11 antibody were humanized by applying a novel structure-based humanization strategy (Covaceuszach, Marinelli et al. 2012). This allowed to obtain a humanized version (hum-αD11) whose binding characteristics and NGF neutralizing biological activity, both *in vitro* and *in vivo*, were fully preserved with respect to the parental rat antibody. Surprisingly, not only was the NGF binding affinity of the humanized hum-αD11 maintained, it was even improved, by an order of magnitude, over that of the parental antibody (Covaceuszach, Marinelli et al. 2012).

αD11 mAb exhibited significant analgesic properties in two different murine models of persistent pain, with noteworthy and surprisingly long-lasting effects that might be clinically relevant (Covaceuszach, Marinelli et al. 2012). The analgesic effects of the hum-αD11 antibody were demonstrated in the formalin test and neuropathic pain tests *in vivo*. The treatment in the formalin-induced inflammatory pain model consisted in antibody injection performed 45 min before formalin injection and testing. Fab hum-αD11 was able to reduce

formalin-evoked pain both in the early and in the late phase of the formalin test, with a stronger effect in the later phase which is related to the inflammatory component of pain. Thus, it clearly retained the analgesic properties of the parental antibody (Ugolini, Marinelli et al. 2007, Covaceuszach, Marinelli et al. 2012).

The dose/response effect of Fab hum-αD11 was measured also in the neuropathic pain model induced by the CCI of the sciatic nerve (Bennett and Xie 1988) followed by two treatment protocols. Either four intraperitoneal injections of mAb αD11 at a dose of 50 mg/mouse each injection or eight intraperitoneal injections at a dose of 70 mg/mouse each of them were administered starting from the day 3 after surgery. The nerve injury-induced mechanical allodynia was assessed by a dynamic plantar aesthesiometer, measuring the sensitivity of both the ipsi- and contralateral hindpaws to normally non-noxious punctuate mechanical stimuli (Ugolini, Marinelli et al. 2007, Covaceuszach, Marinelli et al. 2012). The study confirmed a strong antiallodynic activity of the hum-αD11 in the persistent chronic pain model.

Although there are already several existing mAbs raised against NGF that entered into clinical trials, αD11 deserves a special attention thanks to its unique characteristics and properties: high affinity and specificity (Paoletti, Covaceuszach et al. 2009), which has been validated in many different experimental models, antagonistic potency (Ruberti, Bradbury et al. 1993, Berardi, Cellerino et al. 1994, Molnar, Ruberti et al. 1997, Garaci, Aquaro et al. 2003, Capsoni, Tiveron et al. 2010, Covaceuszach, Marinelli et al. 2012), and most importantly, its analgesic properties suggesting long-lasting effects, that have been explored and characterized in this thesis. It is also worth noting that αD11 is the only anti-NGF monoclonal antibody for which a 3D structure has been derived (Covaceuszach, Cassetta et al. 2004, Covaceuszach, Cassetta et al. 2008). Based on this, the anti-NGF hum-αD11 has been suggested as an effective therapeutic candidate for clinical applications in the therapeutic area of chronic pain states (Covaceuszach, Marinelli et al. 2012).

1.5.5 Anti-TrkA antibody MNAC13

MNAC13 is a well characterized anti-TrkA monoclonal antibody with remarkable function neutralizing properties (Cattaneo, Capsoni et al. 1999, Covaceuszach, Cattaneo et al. 2005). This antibody was raised against native human TrkA to block the NGF–TrkA interaction. Nevertheless, it also recognizes the rodent TrkA receptor. The mAb MNAC13 binds to the extracellular domain of TrkA and does not cross-react with the structurally related tyrosine kinase receptors TrkB and TrkC (Cattaneo, Capsoni et al. 1999).

By binding to TrkA receptors exposed at the cell surface and, also to soluble forms of its extracellular domain, mAb MNAC13 effectively prevents the interaction of NGF with the TrkA receptor on cells and the subsequent activation of TrkA in a variety of systems, including NGF-induced cell survival and differentiation, modulation of pain perception and regeneration from nerve injury (Cattaneo, Capsoni et al. 1999).

First study demonstrating TrkA-neutralizing properties of the MNAC13 was done in the rat basal forebrain *in vivo* by the implant of antibody-secreting cells. The authors explored the antagonistic role of the antibody in the maintenance of the cholinergic phenotype by blocking the NGF–TrkA interaction in the basal forebrain (Cattaneo, Capsoni et al. 1999). Thus, mAb MNAC13 was initially developed with the purpose of characterizing NGF-TrkA

signalling pathways in biological systems. Subsequently, the research has been focused on its striking capacity of inducing analgesia which may result in the development of new potent analgesic drugs in directed pain therapies. The anti-TrkA antibody exhibited impressive antiallodynic properties in models of both inflammatory (formalin injection) and neuropathic pain (sciatic nerve ligation) in mice (Ugolini, Marinelli et al. 2007).

The effects of MNAC13 administration were evaluated in a mouse model of inflammation-derived persistent pain (formalin-evoked pain) (Porro and Cavazzuti 1993) and in the chronic constriction injury (CCI) model of neuropathic pain (Bennett and Xie 1988). Treatment with the MNAC13 was able to induce analgesia in both inflammatory and neuropathic pain models, with a surprisingly long-lasting effect in the latter. In the neuropathic pain model, repeated intraperitoneal injections of MNAC13 induced a significant functional recovery in mice subjected to sciatic nerve ligation, with antiallodynic effects persisting after administration. In addition, when MNAC13 was administered in combination with low-dose opioids, the drug demonstrated a clear synergistic effect (Ugolini, Marinelli et al. 2007). Towards a clinical perspective, mAb MNAC13 has been humanised by a structure-based CDR grafting method (Covaceuszach, Lamba and Cattaneo (2005) "Methods for the humanization of antibodies and humanized antibodies thereby obtained". Patent WO/2005/061540).

In conclusion, the development of an antagonistic antibody directed against the TrkA receptor has allowed to further deepen the knowledge about the complexity of the NGF–TrkA interactions in several brain regions, such as the basal forebrain and the visual cortex (Cattaneo, Capsoni et al. 1999, Pesavento, Margotti et al. 2000). Besides that, blocking TrkA receptor represents a promising way of reducing both acute and chronic pain, which makes mAb MNAC13 a valuable tool for future applications in pharmacotherapy (Ugolini, Marinelli et al. 2007). This also has been one goal of my thesis.

1.5.6 Anti NGF (mAbαD11) and anti TrkA (mAb MNAC13) comparison

There is a growing interest in targeting NGF-TrkA system, known as a master control system for pain. Thus, antagonizing the NGF-TrkA signalling pathway via inhibition of the NGF ligand or its receptor represents an auspicious approach in the pharmacotherapy that might finally lead to the development of a new generation of analgesic therapeutic agents (Hefti, Rosenthal et al. 2006, Pezet and McMahon 2006, Watson, Allen et al. 2008, Covaceuszach, Marinelli et al. 2012).The availability, in our laboratory, of two neutralizing monoclonal antibodies against NGF and against TrkA provides the background to this thesis and a unique possibility to compare the effectiveness of the two approaches of inhibiting the NGF-TrkA signalling axis in chronic pain preclinical models: neutralizing the ligand or the receptor. No study has been published investigating such a comparison. Given the high interest of this target in chronic pain, the comparison would be very informative.

Anti-NGF and anti-TrkA directed treatments may differ in their effects due to several reasons. Indeed, anti-NGF binding by mAb αD11 blocks the interaction of NGF with both TrkA and p75NTR receptors. In the case of the anti-TrkA treatment, MNAC13 blocks only TrkA receptors without affecting p75 receptor-mediated signalling. Thus, any signalling via p75NTR in pain models would not be affected by MNAC13 treatment, because a secreted free form of NGF might still be allowed to interact with the p75 receptors. This would allow to dissect the role of p75NTR signalling in pain. Also, selective blocking of the TrkA exclusively,

might lead to cell death according to some authors based on the proposed role of the TrkA activation in counteracting cell death induced by activated p75 receptor (Van der Zee, Ross et al. 1996, Yoon, Casaccia-Bonnefil et al. 1998). However, results from many studies have failed to show an evidence for neuronal apoptosis (Cattaneo, Capsoni et al. 1999, Butt, Evans et al. 2014, Belanger, Butler et al. 2017, Norman and McDermott 2017).

Regarding anti-NGF treatment, the sequestration of NGF by the αD11 antibody does not impede the binding of other TrkA-specific ligands, such as the neurotrophin NT-3, which is known to interact with the TrkA receptor (Davies, Minichiello et al. 1995, Wyatt, Pinon et al. 1997). Thus, the activation of TrkA-mediated pathways is not completely abolished by the αD11 antibody which might, in turn, allow other putative TrkA ligands to substitute for NGF (Cattaneo, Capsoni et al. 1999).

The functional neutralization of the TrkA receptor by the MNAC13 is not obviously equivalent to the sequestration of NGF by the αD11, as a consequence of the complexity of the two-receptor system mediating NGF activity (Ugolini, Marinelli et al. 2007). NGF exerts its neuronal activity by binding to two types of membrane receptors, TrkA and p75, implying that the outcome of NGF action depends on the fine balance in the signalling from both receptors. The two receptors that mediate NGF signal transduction can function independently by interacting with NGF, each with a relatively low affinity. However, in the presence of both receptors, a ternary heterocomplex TrkA/NGF/p75NTR is formed with the so-called high-affinity NGF binding sites, which alter the signalling (Toni, Dua et al. 2014). Some authors have demonstrated that p75 increases NGF binding affinity and specificity to TrkA receptor (Hempstead, Martin-Zanca et al. 1991, Clary and Reichardt 1994, Toni, Dua et al. 2014). Moreover, in presence of p75 receptors, lower levels of NGF are needed to elicit TrkA-dependent responses in neurons (Lee, Davies et al. 1994, Horton, Laramee et al. 1997, Toni, Dua et al. 2014). However, the role of the p75 receptor in the modulation of the TrkA-mediated signalling has not been completely elucidated. The models for elucidating the p75–TrkA interaction mechanism have been studied computationally and experimentally and two different hypotheses have been proposed, consisting of the ligand-passing mechanism and the heterodimer mechanism (Chao and Hempstead 1995, Esposito, Patel et al. 2001). Nevertheless, the precise mechanism of the interaction between these two receptors remains a matter of debate (Toni, Dua et al. 2014). The character and intensity of NGF activity may vary depending on the actual interaction between NGF and its receptors. Thus, the use of αD11 and MNAC13 mAb might lead to very different outcomes depending on whether the NGF signalling pathway is interrupted either at the level of the ligand or its receptor.

αD11 and MNAC13, function-blocking monoclonal antibodies targeting the NGF ligand (Covaceuszach, Cassetta et al. 2008, Covaceuszach, Marinelli et al. 2012) or its TrkA receptor (Cattaneo, Capsoni et al. 1999, Ugolini, Marinelli et al. 2007) respectively, have shown promising anti-inflammatory and analgesic responses.

In summary, both antibodies directed either against NGF or TrkA might be used to explore the biological mechanisms involved in the initiation and maintenance of acute and chronic pain states. Comparing their performance in a well validated preclinical model is an objective of my thesis. There is also a high potential of these two antibodies with analgesic properties for using them successfully in the chronic pain therapy in near future.

2 AIMS

The overarching aim of my thesis was to compare the effect of an anti-NGF and an anti-TrkA neutralizing antibody in a well validated mouse model for neuropathic pain, the chronic constriction injury (CCI) model of the sciatic nerve. In making this head-to-head comparison, I further investigated the suggestion, coming from previous experiments from the lab (Ugolini, 2007 and Covaceuszach, 2012), that the analgesic effect of both anti-NGF and anti-TrkA antibodies in the CCI model might be long-lasting. This thesis represents the next logical step of those studies, also given the strong interest in understanding the role of anti-NGF and anti-TrkA antibody treatment in the long-lasting analgesia in mice that underwent chronic constriction injury (CCI) of the sciatic nerve. Since the previous studies did not examine the time course of late analgesia and mechanical allodynia in this animal model, the principal objective of this PhD work was the characterisation of the analgesic response at late time points after the treatment, in comparison to the pharmacokinetics of both antibodies.

In parallel to the pharmacological evaluation of the analgesic potency of the two antibodies at the behavioural level, my aim was to analyse transcriptomic changes occurring at various ascending stations of the pain processing pathways, in mice that underwent CCI of the sciatic nerve, after the treatment with either anti-NGF or anti-TrkA antibodies. The purpose of this analysis was to identify biological pathways involved in the pain phenotype caused by the CCI, that might be reversed by the antibody treatment. Finally, my aim was to perform an initial bioinformatic analysis of the differentially expressed genes in the CCI model, and of those mRNAs that have been reversed by the antibody treatment. A special attention of my analysis was given to the differentially expressed genes that were in common between anti-NGF and anti-TrkA. The aim of this analysis was to identify pathways and targets that might be involved in the long-lasting analgesia induced by each of the antibodies. Further validation of these targets, which is beyond the scope of my thesis, might provide the basis for developing a new generation of analgesic drugs targeting the NGF-TrkA signalling axis in pain, but not suffering from the identified liabilities of NGF or TrkA inhibitors and capable of inducing a long term modulation of pain.

3 MATERIALS AND METHODS

3.1 MNAC13 and αD11 antibody preparation, production and purification

Monoclonal antibody MNAC13 was derived as described by Cattaneo et al. (Cattaneo, Capsoni 1999), by a congenic immunization protocol injecting mouse 3T3-transfected cells, expressing human TrkA, into BALB/C mice. Briefly, female BALB/C mice were immunized with five injections at 2-week intervals, prefusion sera were tested for their ability to inhibit the binding of NGF to the TrkA receptor on TrkA-BALB/C 3T3 cells. Three days after a boost injection of TrkA-BALB/C 3T3 cells, mice were killed, the spleens were removed, and splenocytes were fused to NSO myeloma cells (10:1 ratio) with polyethylene glycol (PEG 1500), as described previously (Novak et al., 1991). The MNAC13 hybridoma growth and selection were performed according to standard methods (Cattaneo, Capsoni et al. 1999). Monoclonal antibody MNAC13 was purified from MNAC13 hybridoma supernatant by precipitation with 29% ammonium sulfate followed by affinity chromatography using a Protein G Sepharose column (Pharmacia) and eluted with low-pH buffer (10 mM HCl) (Covaceuszach, Cattaneo et al. 2001). MNAC13 IgG1 fractions were pooled and dialyzed across a Spectra-Por Membrane 12/14K (Spectrum). The purified protein was quantified using Lowry assay (Bio-Rad).

The anti-NGF αD11monoclonal antibody was derived from rats immunized long term with mouse NGF (Cattaneo et al 1988). The anti-NGF αD11 monoclonal antibody was purified from hybridoma cell supernatants by precipitation with 29% ammonium sulfate followed by affinity chromatography using a Protein G Sepharose column (Pharmacia) and eluted with low-pH buffer (10 mM HCl) (Covaceuszach, Cattaneo et al. 2001). MNAC13 IgG1 fractions were pooled and dialyzed across a Spectra-Por Membrane 12/14K (Spectrum). The purified protein was quantified using Lowry assay (Bio-Rad).

3.2 Chronic Constriction Injury (CCI) model

One of the most widely used animal models mimicking peripheral nerve injury (Austin, Wu et al. 2012), the unilateral sciatic nerve chronic constriction injury (CCI) was established in 1988 (Bennett and Xie 1988) to study chronic neuropathic pain. The pathological condition of this model is quite similar to human peripheral nerve injury and its consequent behavioural manifestations (Zhi, Liu et al. 2017). We used an adapted method, originally proposed by Bennett and Xie (1988) for producing the CCI model in rats, to induce neuropathic pain in mice (Luvisetto, Marinelli et al. 2006). Adult (250-350 g) male C57BL/6J mice (Charles River Laboratories, Como, Italy) at the age of 3 months were used in all experiments according to the guidelines of the International Association for the Study of Pain. In this adapted CCI pain model, mice develop mechanical allodynia and thermal hyperalgesia usually within 1 week or less (Luvisetto, Marinelli et al. 2006).

Surgical procedure was performed under sterile conditions. Mice were anesthetized with chloral hydrate (500 mg/kg, intraperitoneal injection). After shaving and sterilizing the right leg with iodophor, a 1.5 cm longitudinal skin incision was made cutting through the connective tissue between the gluteus superficialis and biceps femoris muscles and the right sciatic nerve was exposed at the level of the middle of the thigh. With the help of a lens,

proximal to the sciatic's trifurcation, about 7 mm of nerve was freed of adhering tissue and three ligatures (5-0 chromic gut, Ethicon) were tied loosely around the sciatic nerve with about 1 mm spacing, to just occlude but not arrest epineural blood flow. The incision was then carefully closed with 4-0 silk suture. After nerve ligation, the phenotypes of spontaneous pain (or dysesthesia) and mechanical hyperalgesia were present in mice, such as hindlimb discoordination, toes curling up, and limb lameness.

3.3 Behavioural pain testing

The nerve injury-induced mechanical allodynia was measured through a Dynamic Plantar Aesthesiometer (Model 37400; Ugo Basile, Varese, Italy), a mechanical stimulation apparatus designed to assess "touch sensitivity" on the plantar surface of the rodent foot and to quantify light touch in the laboratory animal automatically. This apparatus applies a reproducible light touch to the rodent foot with an ascending non-flexible tip (0.5 mm diameter) which exerts a mechanical force of gradually increasing intensity until the mouse withdraws its hind paw. Mechanical stimulus is delivered via the tip to the mid-plantar surface of the mice hind paw, which falls within the area innervated by the branches of the sciatic nerve. Mechanical pain thresholds are determined by mechanically stimulating both injured and uninjured hind paws until their withdrawal. Because the effective contact area between the hind paw and the tip is undetermined, the stimulus intensity is expressed as grams of force driving the tip. The nociceptive threshold is then defined as the force, in grams, which triggers paw withdrawal (Bennett and Xie 1988, Luvisetto, Marinelli et al. 2006, Austin, Wu et al. 2012).

The sample size (N=10 mice/group) for behavioural experiments was estimated by a power analysis, based on the effect size calculated from previous data obtained in the same lab (Ugolini et al, 2007). The generation of neuropathic pain in our model was assessed by measuring the sensitivity of both the ipsilateral and contralateral hind paws to normally non-noxious punctuate mechanical stimuli. Before pain assessment, mice were placed into the testing apparatus and were allowed to habituate to the testing procedure. Mechanical pain thresholds were separately tested preoperatively and on the post-operative days from D3 to D150 after surgery. After the measurement of postoperative day 3, different groups of mice were administered either with MNAC13 IgG (70 or 100 µg/mouse/day) or αD11 IgG (70 or 100 µg/mouse/day) from day 3 to day 10 (eight intraperitoneal injections) and tested for 3 months. At the end of the experiment mice were killed and the presence of the ligature was checked. Each testing day, the latency time to withdraw ipsilateral and contralateral hind paws was measured three times with at least 10 second intervals between each measurement and the three measured data were averaged. The mean of the three measurements per paw represented the mechanical threshold for each testing day. All values in behavioural plots were expressed as mean±SEM. Two-way ANOVA for repeated measures was used to analyse the effects of Time (within factor) X Treatment (between factor), across the whole experiment, from Day3 to Day90. The F-values for global ANOVA (all time points) were as follows: F-value (Treatment)=345.077, F-value (Time)=5.656, F-value (Time x Treatment)=7.589. Then, at each time point, a one-way ANOVA (Treatment factor) was used to assess the difference between antibody-treated mice and saline-treated mice. The F-values for one-way ANOVA for aD11 treatment at different time points were as follows: 5.510 at D7, 9.911 at D10, 8.060 at D11, 20.277 at D12, 27.616 at D13, 35.938 at D14, 55.866 at D17, 51.846 at D19, 141.272 at

D21, 63.707 at D24, 21.793 at D26, 95.191 at D28, 37.521 at D31, 70.073 at D34, 32.101 at D38, 73.115 at D42, 54.907 at D46, 60.810 at D49, 80.001 at D53, 88.308 at D56, 26.821 at D60, 79.875 at D63, 137.832 at D67, 27.442 at D70, 12.128 at D74, 30.807 at D77, 77.289 at D81, 35.236 at D84, 4.636 at D90. Differences were considered significant at $p<0.05$.

3.4 Tissue dissection from mice

Dorsal Root Ganglia (DRG) dissection protocol was performed according to Sleigh and Schiavo (Sleigh, Weir et al. 2016). The back fur of the deceased animal was sprayed with 70 % ethanol. A large transverse cut was made in the middle of back skin using iris scissors. The pelt was then removed from the head to the base of the tail, by careful tearing of the skin in the transverse plane, followed by pulling the pelt on the rostral and ventral side in opposite directions to remove all back skin and expose cervical, thoracic and lumbar spinal regions. The abdominal wall musculature was cut on the ventral side and continued laterally, until the spinal column was reached. With the help of the scissors, all ribs were detached close to the spinal column on both sides. The diaphragm, viscera, and rib cage were removed from the anterior side of the column. The femurs were then cut using bone scissors close to the column, and the whole spinal column removed by making a transverse cut at the level of the femurs.

Extraneous muscle, fat, spinal nerves and other soft tissue found on the exterior of the column were removed from the excised spinal column. The column was then cut in the transverse plane through the vertebrae between the discs delimiting the lumbar region of the spinal cord, with one cut just below the most caudal rib to orientate the spinal cord region. Thick forceps were used to hold the spinal column segment straight and steady, dorsal side facing up, while a sterile surgical scalpel blade was used to divide the spinal column in half down the midline. Using a dissection scope, the two halves of the spinal column were then pinned out in Sylguard-lined petri dish, medial side facing up, using insect pins through the exterior intervertebral discs. Sterile, ice cold PBS was then added to the petri dish to aid dissection and keep the sample from desiccation. To keep the dissection cold, PBS was regularly replaced.

The spinal cord was slowly detached in a rostral to caudal direction from the column, revealing the DRG below. The lumbar part of the spinal cord was transferred to 1.5 ml Eppendorf tubes containing RNAlater (Sigma-Aldrich). The meninges were carefully removed using fine forceps. With the help of fine forceps, the L5 DRG ipsilateral to the ligature was grasped and lifted out of the column taking care not to touch and damage the ganglion. The long and thin white axon bundles, easily distinguished from the round and darker DRG, were cut away using fine spring scissors and any connective tissue attached to DRGs was removed in order to reduce myelin debris and glial cell contamination. Once dissected and cleaned, ganglia were then collected in 1.5 ml Eppendorf tubes containing RNAlater (Sigma-Aldrich) and stored at 4°C for later use.

3.5 Immunohistochemistry of DRGs

For immunohistochemical analysis, dorsal root ganglia (DRG, L5 ipsilateral to the ligature) from saline- and MNAC13- (100mg/day/mouse) treated mice were collected at D90 and 25µm cryostat sections were taken from frozen DRGs. The sections were immunostained

with different antibodies: anti-GABA A receptor alpha 2 antibody (N399/19, Abcam) for GABRA2 staining, anti-Glutamate Receptor 3 antibody (Abcam) for GRIA3 staining, anti-NMDAR2B antibody (Abcam) for GRIN2B staining, anti-Grm5 antibody (EPR2425Y, Abcam, ab76316) for Grm5 staining. After immunostaining, images were acquired by laser scanning confocal microscopy using a TCS SP5 microscope (Leica Microsystem) connected to digital camera diagnostic instruments operated by I.A.S. software of Delta Systems Italia. Figures were assembled using Adobe Photoshop CS3 and Adobe Illustrator 10. The quantification was performed by the ImageJ software (version 1.41, National Institutes of Health, USA). High magnification (63X) images of DRG were acquired. The fluorescence of the different markers was quantified with the Fluorescence Index RGB (Red, Green and Blue) method (Inman CF, Rees LE, Barker E, Haverson K, Stokes CR, Bailey M. Validation of computer-assisted, pixel-based analysis of multiple-colour immunofluorescence histology. J Immunol Methods. 2005 Jul;302(1-2):156-67).

3.6 RNA isolation from DRG

DRG tissue samples were homogenized in 800 µl of TRIZOL® Reagent (Cat. No. 15596-018, Invitrogen) using a power homogenizer (ULTRA-Turrax T8 Homogenizer, IKA-werke). The homogenized samples were incubated for 5 minutes at room temperature to permit the complete dissociation of nucleoprotein complexes. Following sample lysis, 160 µl of chloroform was added and tubes were shaken vigorously by hand for 15 seconds and incubated at room temperature for 3 minutes. The samples were centrifuged. Following centrifugation at 12,000 × g for 15 minutes at 4°C, the mixture separated into three phases: a lower red, phenol-chloroform phase, an interphase, and a colourless upper aqueous phase. The aqueous phase containing RNA was transferred to a fresh tube and 5 µg RNase-free glycogen (Cat. No 10814, Invitrogen) was added as carrier to the aqueous phase prior to precipitating the RNA with isopropyl alcohol. The RNA was precipitated from the aqueous phase by mixing with 400 µL isopropyl alcohol. Samples were incubated at RT for 10 minutes and centrifuged at 12,000 × g for 10 minutes at 4°C. The RNA precipitate forming a gel-like pellet on the side and bottom of the tube was washed once by adding 800 µL 75% ethanol, the samples were mixed by vortexing and centrifuged at 7,500 × g for 5 minutes at 4°C. At the end of the procedure, the RNA pellet was air-dried for 10 minutes and dissolved in 10 µL RNase-free water by pipetting a few times and incubated for 10 minutes at 55°C and stored at -80°C for next use.

3.7 Quality assessment of the RNA

Prior to amplification or hybridization, the integrity and purity of the input RNA was determined. The quality of the RNA samples was assessed using the NanoDrop UV-VIS Spectrophotometer and the Agilent 2100 Bioanalyzer. To assess RNA concentration and purity, we used the NanoDrop ND-1000 UV-VIS Spectrophotometer. Only high-quality total RNA samples which had an A260/A280 ratio of 1.8 to 2.0 (which indicates the absence of contaminating proteins) and with an A260/A230 ratio of >1.8 (which indicates the absence of other organic compounds, such as guanidinium isothiocyanate, alcohol and phenol as well as cellular contaminants such as carbohydrates) were used in further experiments.

The quality and integrity of the RNA was assessed using the RNA 6000 Nano LabChip kit (RNA 6000 Nano KG, Agilent). Before starting to use the Agilent 2100 BioAnalyzer, the

RNase decontamination of the electrodes with RNase ZAP had to be performed. Following the electrodes cleaning, the gel Agilent RNA 6000 Nano Gel matrix was filtered and the gel-dye mix was prepared by adding 1 µL of RNA 6000 Nano dye concentrate to a 65 µL aliquot of filtered gel. The tube containing the gel-dye mix was vortexed thoroughly and spun for 10 minutes at room temperature at 13,000 x g. The RNA Nano chip was placed on the chip priming station. 9 µL of the gel-dye mix were loaded at the bottom of the well marked G, then the Chip Priming Station was closed for exactly 30 seconds and subsequently the plunger was released with the clip release mechanism and the Chip Priming Station was open. 5 µL of the RNA 6000 Nano marker were pipetted into the well marked with the ladder symbol and each of the 12 sample wells. 1 µL of the RNA ladder was loaded into the well marked with the ladder symbol and 1 µL of each sample into each of the 12 sample wells. The chip was vortexed in the IKA vortex mixer for 60 seconds at 2,400 rpm. Following the vortex, the chip was inserted carefully into the receptacle of the Agilent 2100 Bioanalyzer and the chip run was started using the Agilent 2100 Expert program. After the chip run was finished, the results of the run were checked. The resulting electropherogram contained two distinct peaks representing the 18S and 28S ribosomal RNA, and additional bands representing the lower marker, and the potentially 5S RNA. The software automatically provided the RNA Integrity Number (RIN), which provides a quantitative value for RNA integrity. RIN of 7 was defined as a minimum threshold RIN number, and only samples with the RIN number higher than 7 were considered for further experiments.

3.8 Microarray assay

Transcriptomics was performed by the Agilent One-Color Microarray platform, using 8x60K whole mouse genome chips (grid-ID 028005). The Low Input Quick Amp Labeling Kit, One-Color (Agilent) protocol was used to synthesize cDNA from total RNA. Sample 200 ng input of total RNA was added to a 1.5-mL microcentrifuge tube. The total RNA of concentrated samples was diluted just prior to use with nuclease-free water to obtain 200 ng of total RNA in a 1.5 µL volume. Using the RNA Spike-In Kit, One-Color (Agilent), serial dilutions of Spike Mix were prepared for Cyanine 3-labeling proportionally to the amount of total RNA input. 2 µL of diluted Spike Mix were added to 200 ng of sample total RNA. T7 Primer Mix was prepared by adding nuclease-free water. 1.8 µL of T7 Primer Mix per reaction was added into each tube containing 3.5 µL of total RNA and diluted RNA spike-in controls. The primer and the template were denatured by incubating the reaction at 65°C in the thermocycler (BIORAD iCycler iQ5) for 10 minutes. At the end of reaction, tubes were placed on ice and incubated for 5 minutes.

In the meantime, the 5x First Strand Buffer was prewarmed at 80°C for 4 minutes to ensure adequate resuspensions of the buffer components, briefly mixed on a vortex mixer and spun in a microcentrifuge. Immediately prior to use, the components for preparing cDNA Master Mix were added to a 1.5-mL microcentrifuge tube as following: 2 µL of 5x First Strand Buffer, 1 µL of 0.1 M DTT, 0.5 µL of 10 mM dNTP Mix and, 1.2 µL of Affinity Script RNase Block Mix per reaction. The components were gently mixed by pipetting and 4.7 µL of cDNA Master Mix was added to the individual assay tubes and mixed by pipetting up and down. Each sample tube was briefly spun in a microcentrifuge to drive down the contents from the tube walls. Samples were incubated at 40°C in a thermocycler (BIORAD iCycler iQ5) for 2 hours. Following the incubation, the Affinity Script enzyme was inactivated by heating at 70°C for

15 minutes. After that, samples were put on ice and incubated for 5 minutes, briefly spun in a microcentrifuge to drive down the contents from the tube walls and lid.

The components for the Transcription Master Mix were added immediately prior to use into a 1.5 mL microcentrifuge tube in the following order: 0.75 µL of nuclease-free water, 3.2 µL of 5x Transcription Buffer, 0.6 µL of 0.1 M DTT, 1 µL of NTP Mix, 0.21 µL of T7 RNA Polymerase Blend, 0.24 µL of Cyanine 3-CTP per reaction. They were gently mixed using a pipette. 6 µL of Transcription Master Mix were added to each sample tube and gently mixed by pipetting, each tube containing a total volume of 16 µl. Samples were incubated in a thermocycler at 40°C for 2 hours. The enzyme T7 RNA Polymerase Blend, which can simultaneously amplify target material and incorporate Cyanine 3-CTP, was used for the fluorescent cRNA synthesis *in vitro*. The amplified cRNA samples were purified using the RNeasy Mini Kit (Qiagen). The purified cRNA was quantified using the NanoDrop ND-1000 UV-VIS Spectrophotometer version 3.2.1. Based on the concentration of cRNA (ng/µl), the cRNA yield in µg was determined. The specific activity of each reaction was determined using both the concentrations of cRNA (ng/µl) and cyanine 3 (pmol/µl). Only samples with the yield higher than 0.825 µg and the specific activity of at least 6 pmol Cy3 per µg cRNA were used in the next steps.

The Fragmentation mix for 8-pack microarray format was prepared in a way that for each microarray, following components were added to a 1.5 mL nuclease-free microcentrifuge tube: 600 ng of Cyanine 3-labeled, linearly amplified cRNA and 5 µL of 10x Gene Expression Blocking Agent were brought to the total volume of 24 µL with nuclease-free water. Subsequently, 1 µL of 25x Fragmentation Buffer was added per each reaction. The tubes were mixed well but gently on a vortex mixer and incubated at 60°C in a water bath for exactly 30 minutes to fragment RNA. After 30 minutes, the tubes were immediately cooled on ice for 1 minute. To stop the fragmentation reaction, 25 µL of 2x Hi-RPM Hybridization Buffer was added and mixed well by careful pipetting part way up and down. Sample tubes were spun for 1 minute at RT at 13,000 x g in a microcentrifuge to drive the sample off the walls and lid and to aid in bubble reduction. Samples were placed immediately on ice and loaded onto the array as soon as possible. A clean gasket slide was loaded into the Agilent SureHyb chamber base with the label facing up and aligned with the rectangular section of the chamber base. 40 µL hybridization sample was slowly dispensed onto the gasket well in a “drag and dispense” manner. The slide was slowly put “active side” down, parallel to the SureHyb gasket slide, making sure that the sandwich-pair was properly aligned. The hybridization slide chamber was assembled and placed in a rotisserie in a hybridization oven set to 65°C, with the hybridization rotator set to rotate at 10 x g for 17 hours.

One day before proceeding with the microarray slides washing steps, the equipment was cleaned by washing it with Milli-Q water. 2 mL of Triton X-102 (10%) was added to the Gene Expression wash buffers (the final dilution of Triton X-102 is 0.005%) to reduce the possibility of array wash artifacts. Gene Expression Wash Buffer 2 was pre-warmed overnight at 37°C in a water bath. Next day after hybridization, the hybridization chamber was removed from the hybridization oven and disassembled. The array-gasket sandwich was removed with gloved fingers from the chamber base and transferred quickly to slide-staining dish number 1 containing Gene Expression Wash Buffer 1. The sandwich, completely submerged in Gene Expression Wash Buffer 1, was open from the barcode end only, by separating the slides with

the forceps. The microarray slide, grasped at the top corner, was then transferred quickly into the slide rack in the slide-staining dish n. 2 containing Gene Expression Wash Buffer 1 at room temperature. After stirring for 1 minute (setting 4), the slide rack was transferred to slide-staining dish n. 3 containing Gene Expression Wash Buffer 2 at elevated temperature. The wash buffer was stirred with a magnetic bar using setting 4 for 1 minute. After washing, the slide rack was slowly removed minimizing droplets on the slides. The slides were put in a slide holder with Agilent barcode (the active microarray surface) facing up. The slides were scanned immediately to minimize the impact of environmental oxidants on signal intensities.

3.9 Microarray scanning, feature extraction and transcriptomic data analysis

Agilent G2564B microarray scanner was used for scanning SurePrint G3 formats. The assembled slide holders were put into a scanner carousel. Before starting to scan slots, the scan settings for one-color scans were verified. Microarray scan images were extracted using Agilent Feature Extraction software for gene expression. After the extraction was successfully completed, the QC reports for each extraction set were reviewed.

The Agilent Feature Extraction Software (ver 10.7.3.1) was used to read out and process the microarray image files, to extract expression table for all mRNA probes (features). All the following data analysis and plotting were performed using R-Bioconductor packages: R-limma v3.36.5 (Ritchie et al, 2015), R-ggplot2 v3.0.0 (Wickhamm, 2016) and R-clusterProfiler v3.8.1 (Guangchuang et al, 2012).

All the features with the flag gIsWellAboveBG=0 (too close to background level) were filtered out and excluded from the following analysis. Filtered data were normalized by aligning samples to the 75th percentile. Differentially expressed genes were selected by a combination of fold change and moderated T-test thresholds (R-limma test p-value with the FDR-correction < 0.05; |Log2 fold change ratio| > 1.0). R-limma test is based on linear models, very similar to the Anova approach.

Functional analysis of gene lists was performed by on-line tools (DAVID Gene Ontology). Pathway analysis of differential gene lists and network plotting was performed by R-clusterProfiler using the ORA (Over-representation Analysis) approach, with the KEGG human pathway database (https://www.genome.jp/kegg/): ORA is based on the hypergeometric distribution (Fisher's exact test) to calculate the statistical significance of the overlap between input gene list and each pathway gene sets. A FDR-corrected p-value < 0.05 was considered statistically significant.

3.10 Two-step qRT-PCR

Before proceeding with the reverse transcription, the treatment with the DNase I (RNase free) (New England BioLabs) (cat. Number M0303S) was performed. 500 ng of total RNA from DRGs was resuspended in 1x DNase I Reaction Buffer, 0.2 units of DNase I (2000 U/mL) was added to each tube, mixed thoroughly and incubated at 37°C for 10 minutes. 1 µl of 0.05M EDTA (5 mM final concentration) was added to the reaction mix bringing it to the final volume of 10 µl. The reaction was heat inactivated at 75°C for 10 minutes.

For the first-strand cDNA synthesis, the SuperScript™ III Reverse Transcriptase (Invitrogen) was used. 20-µl reaction volume was prepared with the 500 ng of total RNA input

from DRG tissue (2ug of total RNA input from the visual cortex and hippocampus). The following components were added to a nuclease-free microcentrifuge tube: 10 µl of sample RNA input (after DNase I treatment), 1 µl of 250 ng Random Primers (Invitrogen, Cat. Number 48190-011), 1 µl of 10 mM dNTP Mix (10 mM each dATP, dGTP, dCTP and dTTP at neutral pH) and 1 µl sterile, distilled water, each tube containing 13 µl of total volume. The mixture was heated to 65°C for 5 minutes in a thermocycler (BIORAD) and incubated on ice for at least 1 minute. After a brief centrifugation, the Reverse Transcription Mix was prepared as follows: 4 µl 5X First-Strand Buffer, 1 µl 0.1 M DTT, 1 µl RNaseOUT™ Recombinant RNase Inhibitor (Cat. no. 10777-019, 40 units/µl), 1 µl of SuperScript™ III RT (200 units/µl) per reaction. 7 µl of the Mix were added to each sample tube already containing RNA, random primers and dNTP Mix reaching a total reaction volume of 20 µl. The tubes were mixed gently by pipetting up and down and incubated in the thermocycler (BIORAD) at 25°C for 5 minutes, followed by an incubation at 50°C for 60 minutes. The reaction was inactivated by heating at 70°C for 15 minutes. The cDNA was used as a template for amplification in the qRT-PCR.

PowerUp™ SYBR™ Green Master Mix Protocol was used for the qRT-PCR reaction. 1–10 ng of input single-stranded cDNA was used per reaction. Reaction mixes were prepared according to the number of reactions. Each PCR reaction was performed in three replicates in a reaction volume of 10 µL as recommended. The following components were added to a PCR reaction tube: 5 µL PowerUp™ SYBR™ Green Master Mix (2X), 1 µl Sense primer (6 µM), 1 µl Antisense primer (6 µM), 1 µl of DNA template (cDNA from first-strand reaction) and 2 µl nuclease-free water per reaction. The components were mixed gently and thoroughly and 10 µL volume of each reaction was transferred to each well of an optical plate. The plate was sealed with an optical adhesive cover, then centrifuged briefly to spin down the contents and eliminate any air bubbles.

Real-time quantitative PCR was performed on a real-time thermal cycler (Applied Biosystems). As a source for the design of primers and probes served a public PrimerBank (http://pga.mgh.harvard.edu/primerbank/index.html). Primers used were as following: N6amt1 (Mus musculus): forward 5′-GAAGGGGAAAGTAGACCTGCT-3′ and reverse 5′-TCTTCAGGCGGAGTCACTACA-3′ (Tm 64°C), Trmt112 (Mus musculus): forward 5′-CGTAAGCCTTTGCAGTCTCCC-3′ and reverse 5′-TTCATGTTGTCACAGCGGAGC-3′ (Tm 68°C).

PCR reaction conditions included: initial heat activation at 95°C for 3 minutes, followed by 35 cycles of PCR: denaturation at 95°C for 15 seconds, annealing at a temperature specific for each set of primers for 30 seconds, extension at 70°C for 30 seconds. The amplification products were verified by melting analysis. The relative concentration of templates in different samples was determined using a comparative C_T method ($\Delta\Delta C_T$). The data were obtained from at least 3 biological replicates and averaged. The measurements for individual target gene expression were normalized to the endogenous internal control PPIA. The statistical significance of the relative gene expression among different samples was evaluated using t-test.

3.11 Statistical analysis

The methods used for statistical analysis for the different experiments have been described in the relevant sections above.

4 RESULTS

4.1 Characterisation of analgesic response in the CCI neuropathic pain model after anti-TrkA and anti-NGF treatment

4.1.1 Behavioural analysis

The analgesic effects of either αD11 or MNAC13 monoclonal antibodies were assessed in the chronic constriction injury (CCI) neuropathic pain model. Firstly, CCI was induced by the sciatic nerve ligature of the right hind limb in 3 months old male C57BL/6J mice (Fig. 2). Subsequently, the mice were treated with either αD11 or MNAC13 at a single dose (100 µg/mouse) or two different doses (70 µg/day/mouse or 100 µg/day/mouse) administered repeatedly from day 3 (D3) to day 10 (D10) post-operatively. Finally, the mechanical pain sensitivity was measured, as shown in Figures 3 and 4. The control group was injected with saline.

The behavioural testing (Fig. 3 and 4) has demonstrated that the withdrawal mechanical threshold of the ipsilateral hind paw of mice that underwent the sciatic nerve ligation (Sal ipsi) was significantly lower in comparison to their contralateral non-operated hind paw (Sal contra), as measured by Dynamic plantar aesthesiometer. This increased pain sensitivity persisted up to the last day of observation at day 90 (D90), indicating that the operated mice still have not recovered from the injury, at this time point. The behavioural testing confirmed that the CCI procedure induced mechanical hypersensitivity.

Regarding the efficacy of treatment, a single dose (100µg/mouse) (Fig. 3) of either MNAC13 (purple circle) or αD11 (green triangle) proved not to be efficient in inducing anti-allodynia, since the paw withdrawal threshold of the ipsilateral hind paw of treated mice (MNAC13 ipsi and αD11 ipsi) was comparable to that of the control group injected with Saline (Sal ipsi) in all studied time points.

A repeatedly administered lower dose (70 µg/mouse/day, from D3 to D10) (Fig. 4) resulted in ineffective treatment of chronic neuropathic pain. Repeated administration of lower dose (70 µg/mouse/day) of MNAC13 (red circle) or αD11 (dark green triangle) effectively increased the mechanical pain threshold only during the early phase of neuropathic pain (from D12 to D31 for αD11 70 µg, from D10 to D19 for MNAC13 70 µg), while later in the chronic phase they ceased to induce anti-allodynic effect and the behavioural response to neuropathic pain was comparable to that of non-treated control mice injected with saline (Saline group). MNAC13-treated mice (MNAC13 70 µg ipsi) reached the peak of the mechanical allodynia threshold at around D14 with the mechanical withdrawal threshold (MWT) values returning back to those of saline-treated control mice (Sal ipsi) at D21, while the lower dose of αD11 (αD11 70 µg ipsi) presented a delayed analgesic response with respect to the same dose of MNAC13 (MNAC13 70 µg ipsi) with the MWT peak at D24, and lost its anti-allodynic potential at D34, when the MWT of both MNAC13- and Saline-treated animals (MNAC13 70 µg ipsi vs. Sal ipsi) approached the same values.

On the other hand, a repeated administration of a higher dose (100µg/mouse/day, from D3 to D10) (Fig. 4) of either MNAC13 (purple circle) or αD11 (light green triangle) exhibited a strong anti-allodynic effect, as shown by an increased paw withdrawal threshold (MNAC13

100µg ipsi vs. Sal ipsi, αD11 100µg ipsi vs. Sal ipsi). The significant changes in behavioural response were observed starting from D7 after surgery and lasting during the whole experimental protocol including the chronic phase, with MNAC13 100 µg closely approaching the mechanical withdrawal threshold of the contralateral (non-operated) hind paw at D90. Interestingly, the higher dose of MNAC13 (100µg/mouse/day) seemed to be less effective than that of antiNGF αD11 (100µg/mouse/day) at early experimental time points, until D42 post-CCI. At D42, the anti-allodynic effect of antiNGF αD11 (αD11 100 µg ipsi) was still comparably higher than that of MNAC13 (MNAC13 100 µg ipsi). Starting from D46 onwards, the analgesic effect induced by MNAC13 was continuously increasing until the end of the experiment, overcoming the effect of αD11. The effects of αD11 (100µg/mouse/day), instead, were more consistent from the beginning to the end of the behavioural testing, showing no prominent changes in the MWT values across the time.

Since the obtained data have not provided any information about the total duration of analgesia induced by each treatment, I decided to expand the originally proposed experiment and thus, continued with the nociceptive behavioural testing until no anti-allodynic effect was observed (Fig. 5). The continuation of behavioural studies has revealed that the drug-induced analgesic effect lasted until day 130 (D130) post-CCI. After this time, all tested animals presented a similar MWT, showing no statistically significant difference between MNAC13 100 µg ipsi and Sal ipsi groups.

Overall, the treatment with either αD11 or MNAC13 at a higher dosage (100 µg/mouse/day) significantly increased the mechanical pain threshold in the CCI mice making their ipsilateral hind paw less sensitive to mechanical pain stimuli. When comparing the higher doses of both antibodies, MNAC13 showed an inversion in the analgesic response with respect to αD11, observed at D46. At early tested time points, MNAC13 (100µg/mouse/day) seemed to be slightly less effective in reducing mechanical allodynia than αD11 (100µg/mouse/day), while demonstrating a stronger analgesic effect during later chronic phase of the neuropathic pain condition. Surprisingly, the analgesic effect of MNAC13 mAb lasted up to D130 after surgery.

The long-lasting analgesic effect of anti-TrkA and anti-NGF led me to speculate about the possible molecular mechanisms behind this observation, which might be a consequence of a shift to a new transcriptional program that activates an analgesic response, possibly involving epigenetic changes as well. Thus, for further experiments I decided to use the higher dosage of 100 µg of both antibodies administered repeatedly from D3 to D10, which resulted to be the most effective one.

Figure 2. The scheme of the experimental design.

Chronic constriction injury was induced in C57BL/6J mice by the sciatic nerve ligature of the right hind limb. The CCI-induced mice were then treated with either αD11 or MNAC13 (100 µg/day/mouse) administered repeatedly from D3 to D10 post-operatively. Samples were collected from ACC, SC and DRG at different time points (D3, D11, D24 and D90 after surgery). The sciatic nerve injury-induced mechanical allodynia was assessed using dynamic plantar aesthesiometer.

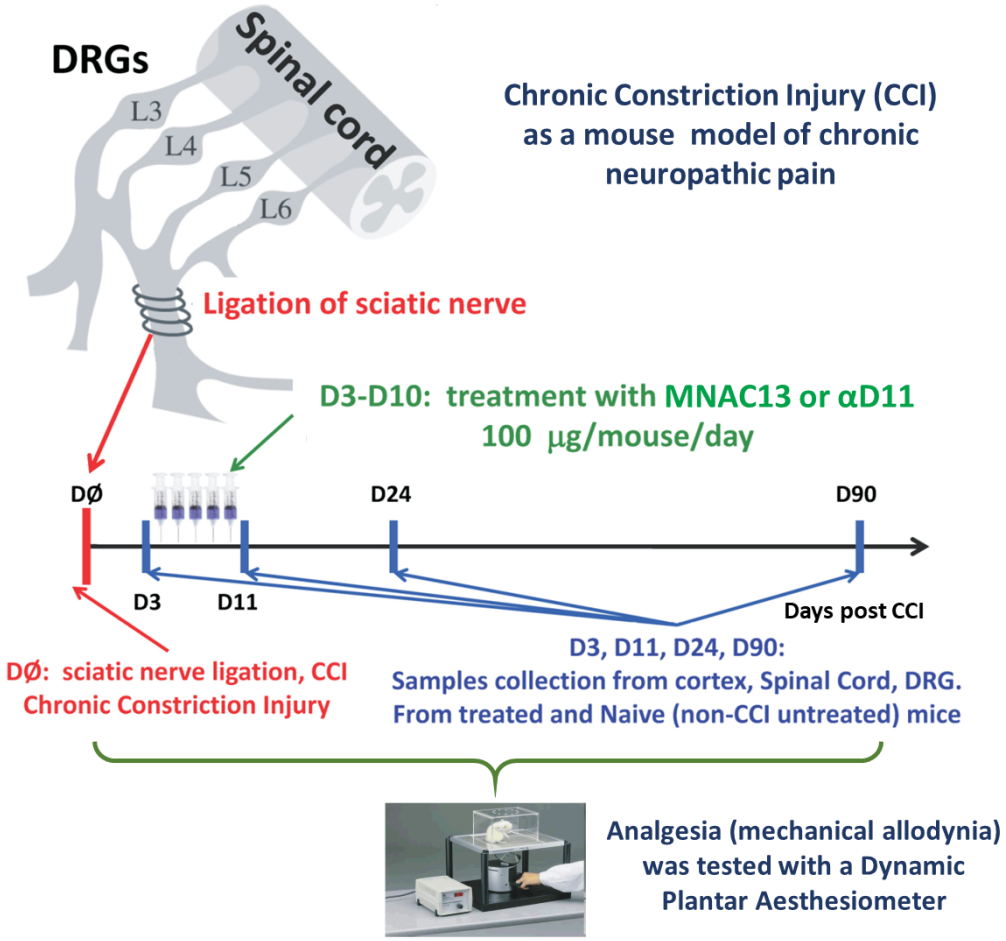

Figure 3. Behavioural testing after single administration of MNAC13 or αD11 (100µg/mouse)

The figure shows the time course of mechanical allodynia threshold in the CCI-mice treated either with Saline or with a single dose of either αD11 or MNAC13 mAbs (100µg/mouse) injected intraperitoneally at D3 post-surgery. The mechanical withdrawal threshold (MWT) of both ipsi- and contralateral hind paw of the mice was detected by dynamic plantar aesthesiometer from D3 to D31 post-CCI. MWT was measured by assessing hind paw sensitivity to innocuous mechanical stimulation. The maximum applied force (in grams) needed to withdraw the hind paw was recorded by the device. The MWT of each animal was represented by the mean values calculated from three different measurements. N=10 mice in each group. All data were expressed as means +/- SD. Statistical analysis consisted of repeated measures two-way ANOVA tests. * $p < 0.05$, ** $p < 0.01$, *** $p < 0.001$ (comparison between treated and non-treated ipsilateral hind paws).

Mice in the Saline group showed higher mechanical hypersensitivity on their ipsilateral (operated) hind paw when compared with their contralateral (non-operated) hind paw in all tested time points (Sal ipsi vs. Sal contra in blue square), corroborating a successful reproduction of the neuropathic pain model.

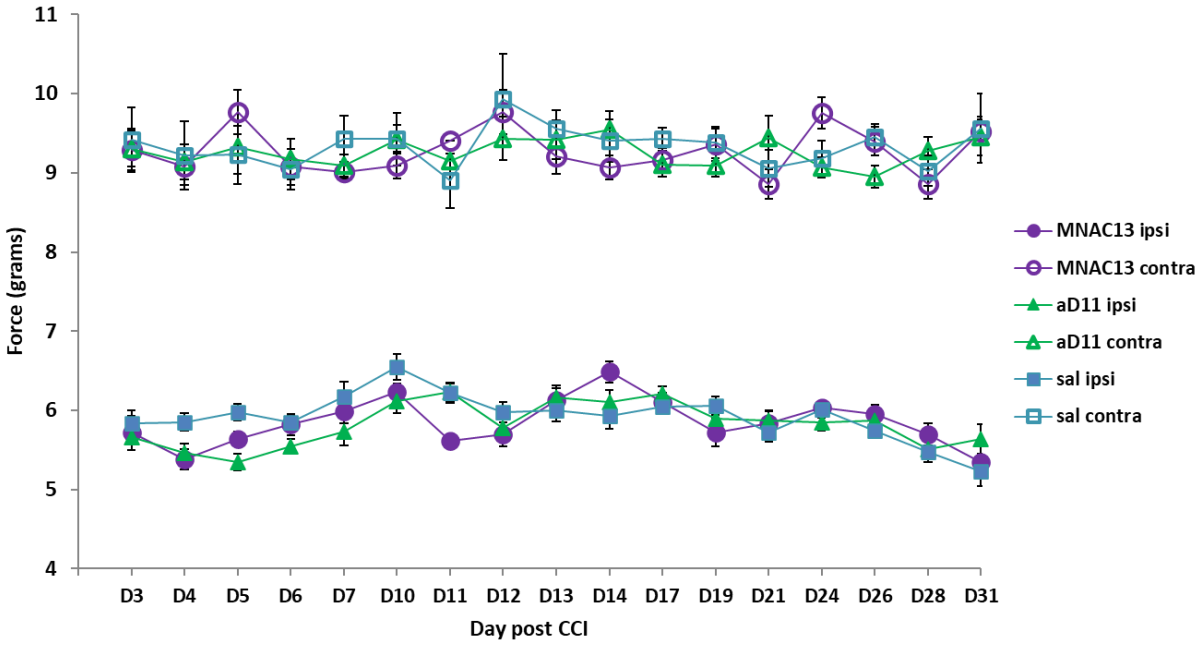

Figure 4. Behavioural testing after repeated administration of MNAC13 or αD11 (70µg/mouse/day or 100µg/mouse/day).

The figure represents the time course of mechanical allodynia threshold in the CCI-mice treated either with Saline or with two different doses of αD11 and MNAC13 mAbs (70µg/mouse/day and 100µg/mouse/day) administered intraperitoneally from D3 to D10. The mechanical withdrawal threshold (MWT) of both ipsi- and contralateral hind paws of the CCI-mice was determined by dynamic plantar aesthesiometer from D3 to D90 postoperative days. MWT was measured by assessing hind paw sensitivity to innocuous mechanical stimulation. The maximum applied force (in grams) needed to withdraw the hind paw was recorded by the device. The MWT of each animal was represented by the mean values calculated from three different measurements. N=10 mice in each group. All data were expressed as means +/- SD. Statistical analysis consisted of repeated measures two-way ANOVA tests. F values are reported in the Methods section.

* $p < 0.05$, ** $p < 0.01$, *** $p < 0.001$ (comparison between treated and non-treated ipsilateral hind paws).

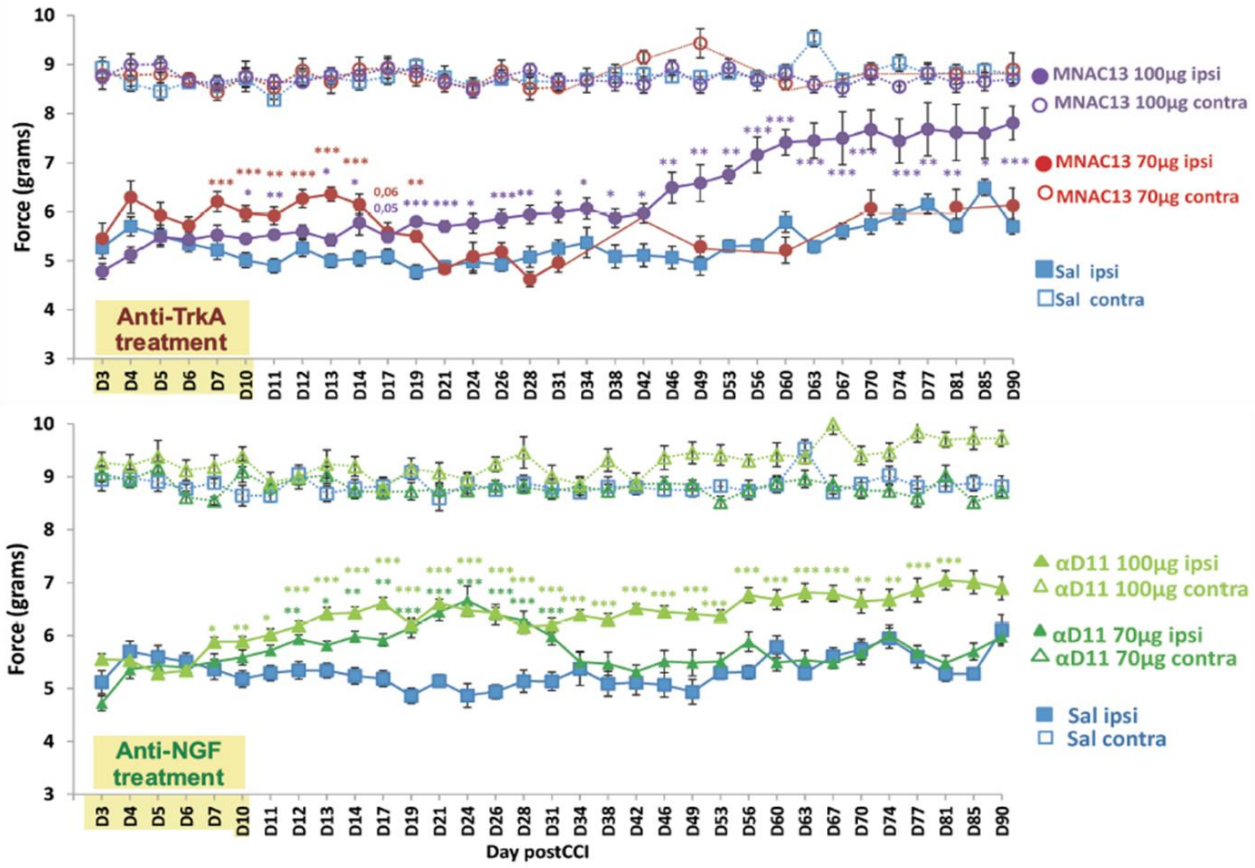

Figure 5. Behavioural testing aimed to evaluate the duration of analgesia induced by repeated administration of MNAC13 (100µg/mouse/day).

The figure represents the continuation of behavioural studies (shown in the Fig. 4) aimed to evaluate the duration of analgesia induced by repeated administration of MNAC13 mAb (100µg/mouse/day, from D3 to D10) in the CCI-mice. The mechanical withdrawal threshold (MWT) of both ipsi- and contralateral hind paws of the tested animals was determined by Dynamic plantar aesthesiometer from D90 to D150 post-CCI. MWT was measured by assessing hind paw sensitivity to innocuous mechanical stimulation. The maximum applied force (in grams) needed to withdraw the hind paw was recorded by the device. The MWT of each animal was represented by the mean values calculated from three different measurements. N=10 mice in each group. All data were expressed as means +/- SD. Statistical analysis consisted of repeated measures two-way ANOVA tests. * $p < 0.05$, ** $p < 0.01$, *** $p < 0.001$

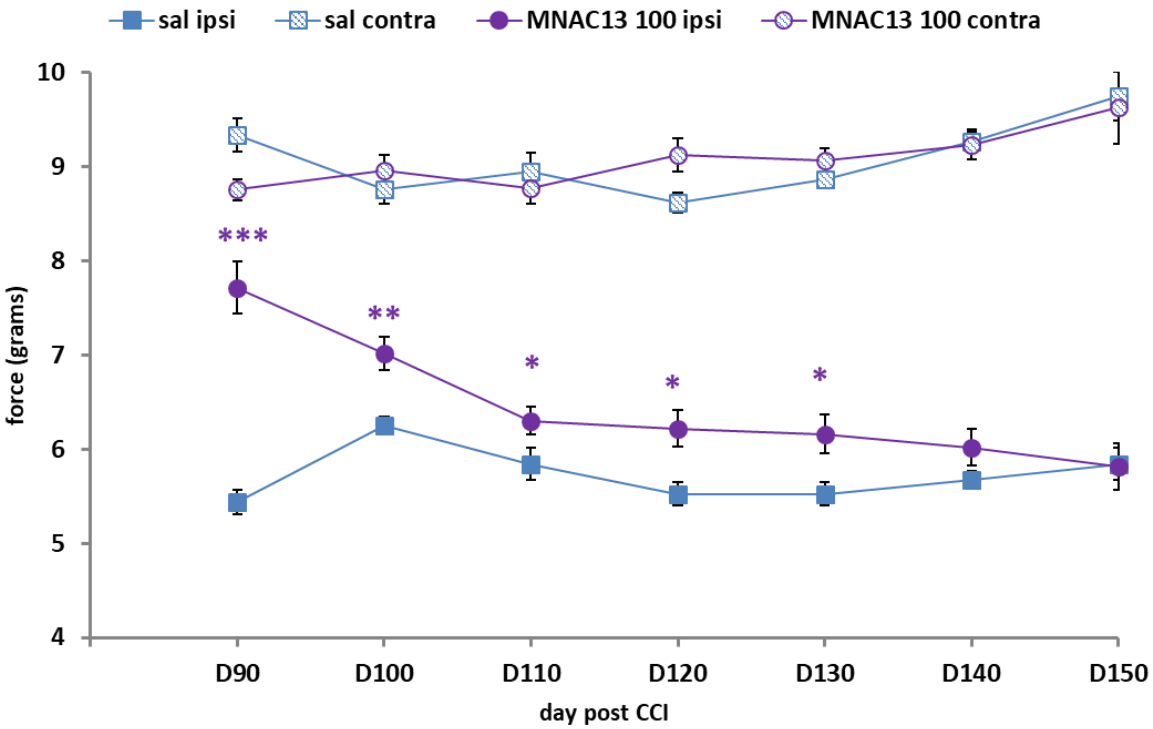

4.1.2 Pharmacokinetic data and the health status of DRGs

The long-lasting analgesic effect induced by anti-TrkA and anti-NGF led me to investigate whether the long time course of the behavioural effect might depend on an unusual long time persistence of the injected antibodies. To this aim, a pharmacokinetic analysis was performed, by measuring the levels of the injected antibodies in the serum, as a function of time.

Pharmacokinetic analysis showed, as expected, a gradual decrease of the antibody level in the blood of CCI-induced mice treated with either MNAC13 or αD11 monoclonal antibodies, as measured by ELISA from the serum of mice at different time points (D11, D24, D46, D72 and D90). A schematic illustration of the ELISA method used to detect the anti-NGF and anti-TrkA antibodies in the serum is shown in Fig. 6. Both ELISA assays are robust and well established. The results of the ELISA measurements for anti-TrkA MNAC13 and anti-NGF αD11 serum levels are shown in Figures 7 and 8, respectively.

Regarding MNAC13 pharmacokinetics (Fig. 7), the mice were repeatedly injected with two different doses (70µg/mouse/day or 100µg/mouse/day) of mAb MNAC13 or with saline, from D3 post-surgery to D10, as in the experiments above. Serum samples from both saline- and MNAC13-treated mice were collected at different time points (D11, D24, D46, D72, D90), and the amount of mAb MNAC13 was determined by the ELISA assay described in Fig 6a. The pharmacokinetics profile for serum MNAC13 showed that the amount of MNAC13 reached its peak at D11, reflecting the effective accumulation of the antibody after repeated intraperitoneal administration (Figures 7 and 8a). Starting from D11, the antibody levels in the serum gradually decreased, with the concentration at D46 being lower than the pharmacologically active dose. Indeed, the anti-TrkA antibody levels of the 100µg/mouse/day group (blue bars in the histogram of Fig. 7) at D46 (around 100µg) were comparable to the levels of the 70µg/mouse/day, at earlier time points (red bars in the histogram of Fig. 7). Note that the 70µg/mouse/day animals showed no analgesia at any time point. It is also worth to mention that the single administration at the dose of 100µg/mouse (the approximate level of MNAC13 at day D46) is ineffective (see above). Yet, even though the serum concentration of antibody in the 100µg/mouse/day group, from day D46 onwards was well below the efficacy threshold, the mice from this group showed a strong analgesic effect well after D90 (Fig. 4). I can conclude that from D46 onwards, analgesia is observed under conditions in which the serum concentration of mAb MNAC13 is below the efficacy threshold.

The results for the αD11 pharmacokinetics were less clear, being complicated by the fact that the presence of endogenous NGF in the serum interferes with the assay aiming to detect the presence of anti-NGF antibodies. Indeed, even though the anti-NGF ELISA assay is robust and well established, I have faced difficulties regarding the detection of αD11 levels in the serum of the CCI mice treated with αD11 antibody due to the inter-individual variability in the levels of endogenous NGF. It has been reported previously that NGF serum concentrations present a large variability between individuals (Lang, Gallinat et al. 2003). Due to this fact, the binding sites of αD11 antibody present in the mouse serum might have been occupied by a different amount of endogenous NGF, in different samples, making it unable to bind to the exogenous NGF ligand coated onto the ELISA plate (Figure 6b). Thus, the sequestration of αD11 by a variable amount of free NGF physiologically present in the blood resulted in the occurrence of putative “false negatives” and, consequently, in a higher intra-group variability,

making a proper statistical analysis unfeasible (Figure 8b). In any case, from the point of view of the aim of this experiment, the conclusion for the case of anti-NGF αD11 injection is that the systemic bioavailability of anti-NGF is virtually null from D24 onwards.

The implication is that the long-lasting phase of the analgesic effect, observed after anti-TrkA MNAC13 and anti-NGF αD11 injections, is an indirect "non-pharmacological" effect. We might postulate that it could involve the activation of a specific gene expression program that is maintained in time.

Next, I investigated the health status of DRG neurons, in order to exclude that the analgesic effect observed in the antibody-treated groups might be due to a neuronal disconnection or damage at the DRG level, that might be potentially caused by the action of either of the antibodies. Indeed, both antibodies target the NGF-TrkA signalling pathway, known to play a key role in the regulation of survival of sympathetic and sensory neurons of the peripheral nervous system during the development (Levi-Montalcini and Angeletti 1968, Thoenen and Barde 1980). In adult sensory neurons, however, the supply of NGF is no longer needed to sustain their survival (Lindsay 1988). Despite literature evidence ensuring that an effect of the antibodies on DRG neuronal survival should not be the case, I performed an immunostaining of DRGs of MNAC13-treated CCI mice in order to examine the health status of the DRG tissue (Fig. 9).

In the experiment shown in Figure 9, DRG sections were taken from Saline- and MNAC13-treated (100µg/mouse/day) CCI mice at D90 post-operatively and stained for the microglial marker IBA1 (red) and the neuronal cell marker NeuN (red). Moreover, the neuronal cells were immunostained in order to identify various neuronal subtypes, such as neurons expressing ionotropic glutamate receptor NMDA (blue), GABAergic inhibitory neurons expressing $GABA_A$ (green) and neurons expressing metabotropic glutamate receptors GluR3 (green) and GluR5 (green). The examination of immunostained DRGs under the confocal microscope, followed by the quantification, revealed that DRGs from MNAC13-treated group showed no difference in these marker immunostainings, compared to those from Saline-treated mice. Fluorescence intensity measurement of the most relevant cell-specific markers showed no statistically significant difference between MNAC13-treated mice and CCI-induced mice treated only with Saline. As shown in the graphs in the Figure 9, MNAC13 administration had no effect on the expression of any of the cell-specific markers at protein level. The proportion of each cell type represented by different cell-type specific markers remained unchanged after MNAC13 treatment. All these observations demonstrate that the antibody-induced analgesia did not alter the health status of DRGs, which presented no damage nor disconnection of neurons in the tissue. A similar result was obtained after the treatment with anti-NGF (data not shown).

In conclusion, from day 46 onwards (D46+), the concentration of residual antibodies detected in the blood was below the threshold of pharmacological activity, yet we observed a long-lasting analgesia in the late chronic phase of the neuropathic pain. This observation raised the question about the mechanism of late analgesia which could not be attributed to the presence of the residual antibodies in the blood, since their levels were below the effective dose, as mentioned above. Thus, I hypothesized that the activation of downstream signalling pathways by the two antibodies might induce the expression of genes responsible for the long-lasting anti-hyperalgesic effect, especially gene products involved in epigenetic modifications.

To start addressing this question, I conducted a transcriptome analysis from tissues relevant to the pain processing pathway.

Figure 6. The ELISA assay employed for measuring antibody levels in the mouse serum.

a) A simplified scheme of the ELISA assay used for measuring antibody levels in the serum of mice that underwent the treatment with MNAC13. The TrkA FC chimera coupled to the solid phase is a TrkA immunoadhesin, i.e. the extracellular domain of TrkA receptor fused to the Fc portion of an immunoglobulin G.

b) A simplified scheme of the ELISA assay used for measuring antibody levels in the serum of mice that underwent the treatment with αD11. In this assay, there is a confounding factor, namely the unknown and highly variable presence of endogenous NGF. Endogenous NGF (in red) is competing with the NGF ligand present in the ELISA assay (in blue) for binding the αD11 antibody. Since the levels of endogenous NGF in the mouse serum are variable among individuals, the αD11 antibody remains partly saturated by a variable amount of endogenous NGF, hence introducing heterogeneity into the assay. The measurement of the anti-NGF antibody bound to the solid phase-coupled NGF is therefore affected by the variable and not controlled presence of endogenous NGF.

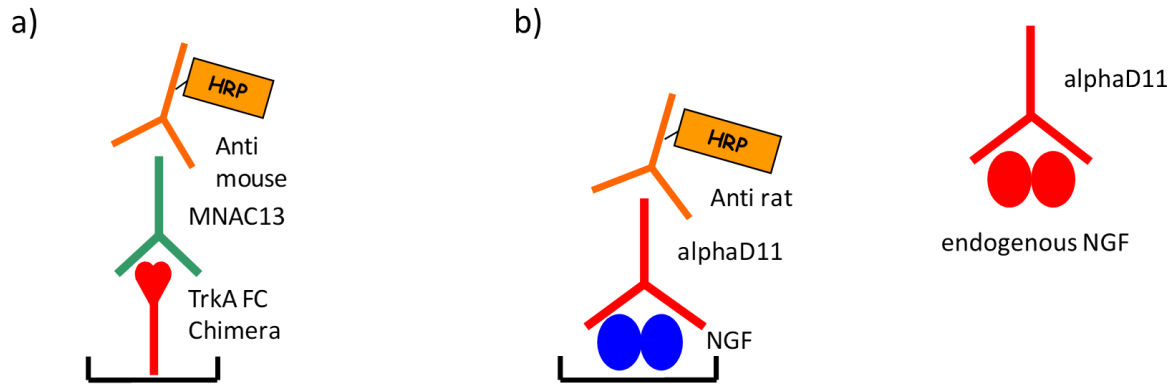

Figure 7. *In vivo* pharmacokinetics assays of repeated administration of MNAC13.

Serum samples from both saline- and MNAC13-treated mice (n=5/group), repeatedly injected with 70µg/mouse/day or with 100µg/mouse/day from D3 to D10 (as in experiments above) and collected at different time points (D11, D24, D46, D72, D90), were measured by an ELISA assay, *ad hoc* developed. The values of saline-injected mice were subtracted from the corresponding values obtained in the MNAC13 group. The assays were repeated three times and then, the averages and standard deviations were calculated. The data were tested by pairwise Student's t-test. In the histogram, the total amount of MNAC13 in µg for each time point is reported. These values were obtained multiplying the concentration values measured by ELISA (reported in the table embedded) by the volume of serum, supposed to be 1.46 ml for a mouse of about 25 g of weight.

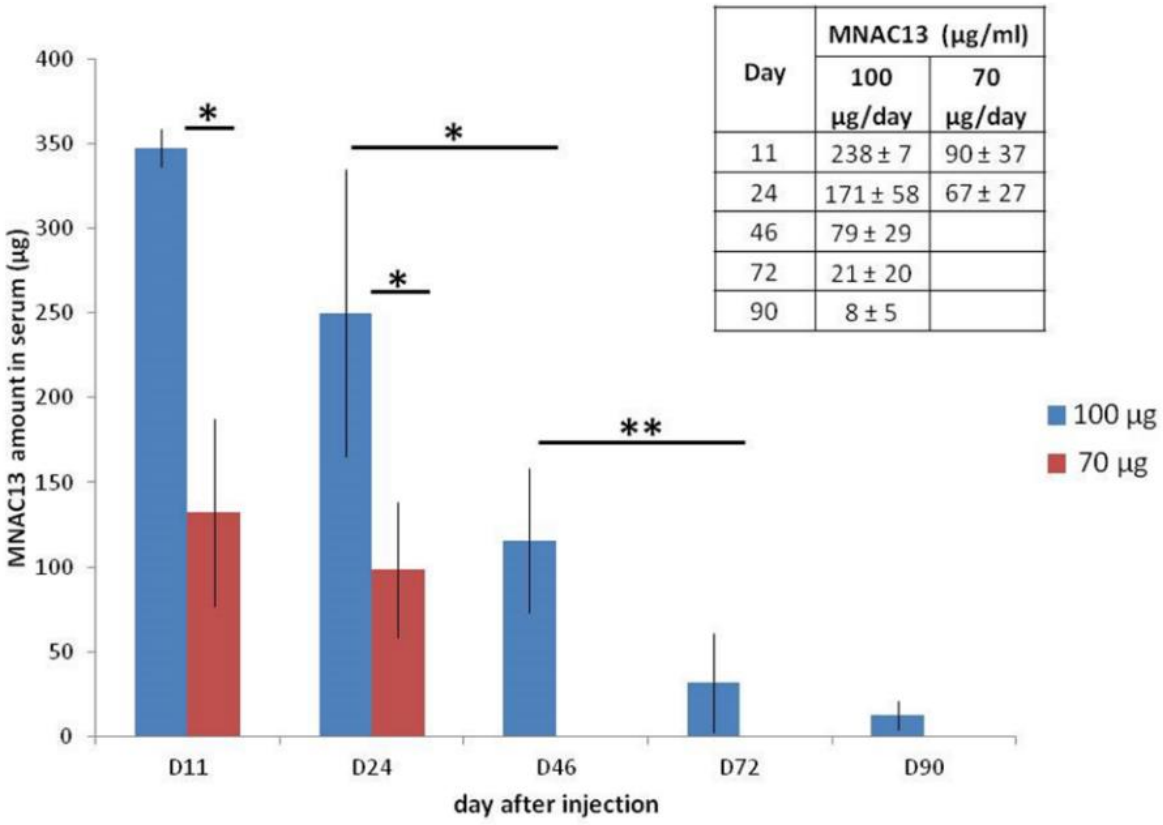

Day	MNAC13 (µg/ml)	
	100 µg/day	70 µg/day
11	238 ± 7	90 ± 37
24	171 ± 58	67 ± 27
46	79 ± 29	
72	21 ± 20	
90	8 ± 5	

Figure 8. *In vivo* pharmacokinetics assays of repeated administration of MNAC13 and αD11: measurements from individual mice

Serum samples from the CCI-mice treated repeatedly either with MNAC13 or αD11 (dosage 100µg/day/mouse) (from D3 to D10, as above) were collected in different time points (D11, D24, D46, D72, D90). The antibody concentration (µg/ml) in the mouse serum was measured by an ELISA assay. n=5 per group, * $p < 0.05$, ** $p < 0.01$. The values for the individual samples are shown. While the variability of the MNAC13 samples is very low, the variability of αD11-injected samples is extremely high. See text for explanation, discussion and interpretation of this data. A pairwise Student's t-test was used for MNAC13 ELISA statistical analysis.

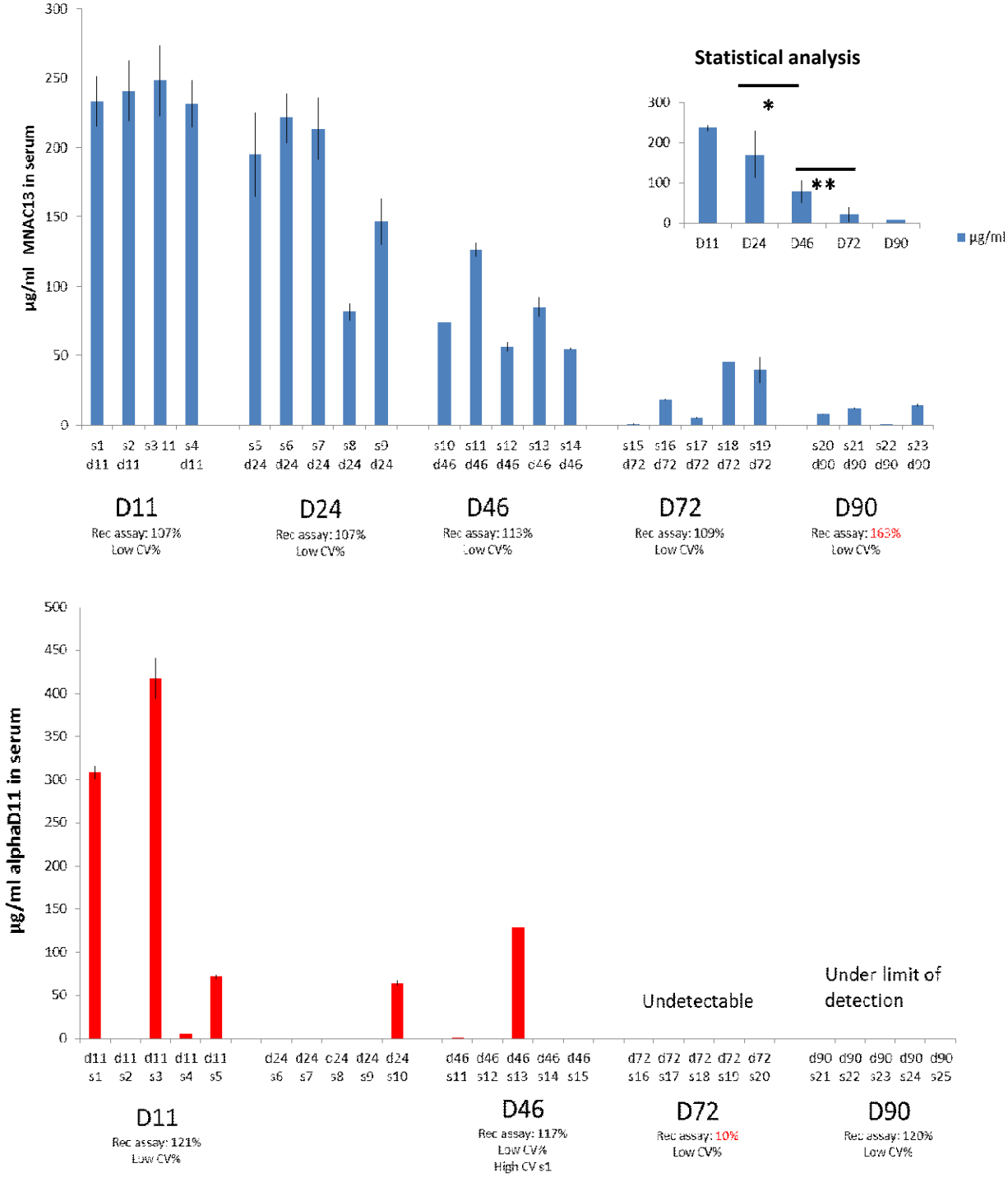

Figure 9. Immunofluorescence staining of DRGs from mice treated with MNAC13 sacrificed at D90 post-CCI.

The figure shows representative confocal microscopy images of immunostaining of markers specific for different cell types present in the mouse DRG. DRG sections were taken from Saline- and MNAC13-treated (100µg/mouse/day) CCI mice at D90 post-operatively and stained for the following markers: microglial marker IBA1 (red) and neuronal cell marker NeuN (red). The neuronal cells were immunostained in order to identify various neuronal subtypes, such as neurons expressing ionotropic glutamate receptor NMDA (blue), GABAergic inhibitory neurons expressing $GABA_A$ (green) and neurons expressing metabotropic glutamate receptors GluR3 (green) and GluR5 (green). The graphs represent the quantification of relative fluorescence intensity measured from the average signal intensity for each cell-specific marker in both conditions (Saline and MNAC13). RGB = Red, Green and Blue Fluorescence Index.

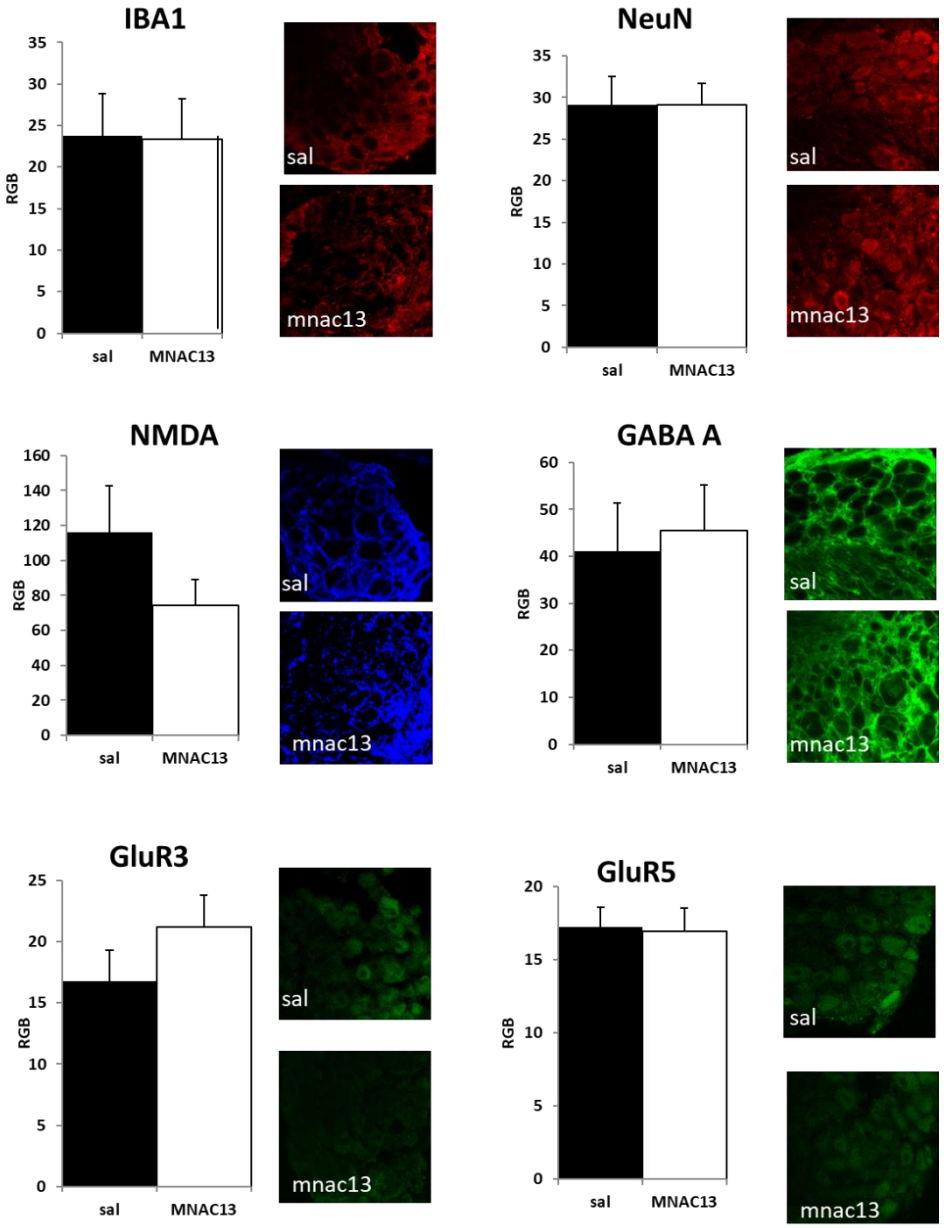

4.2 Transcriptomic changes in the neuropathic pain model after anti-TrkA and anti-NGF treatment

4.2.1 Overall transcriptome analysis in tissues related to pain processing pathways

To identify genes that are involved in different stages of the pathological process of neuropathic pain, as well as genes that are responsible for anti-hyperalgesia induced by either MNAC13 or αD11 treatment, I decided to analyse tissues involved in the pain processing pathways using Agilent Microarray technique. The tissue from the anterior cingulate cortex (ACC), lumbar section of the spinal cord (SC) and lumbar dorsal root ganglia (L3-L4 DRGs) were collected at different days following CCI surgery from the operated mice treated either with saline or antibodies. Differentially expressed genes (DEGs) were determined using 2 criteria: an expression level greater than ≥ 2-fold change, and p value ≤ 0.05 from ANOVA test.

The time points relevant to the experiment were carefully chosen, representing different phases of the neuropathic pain development: D3, right after surgery and before starting the treatment, reflecting the onset of acute pain state characterized by intensive immune response; D11, right after completing the antibody treatment, representing the peak of the antibody concentration in the blood and the highest antibody effect directly counteracting the establishment of neuropathic pain processes; D24, representing the transition from acute to chronic phase of the pain condition accompanied by a shift in the behavioural testing; D90, the last experimental time point representing chronic pain state (planned to be extended in the future experiments).

DEGs in the neuropathic pain condition

CCI involves a pathogenic mechanism associated with changes in gene expression. Through analysing the gene expression profile **in neuropathic pain condition**, I compared the group of CCI-induced mice (Saline-treated mice) with the naïve group at four time points (D3, D11, D24, D90) in the cortex ACC, spinal cord SC, and L4 DRG (Fig. 10).

In the **cortex**, I found 59 (7 downregulated, 52 upregulated), 5009 (4799 downregulated, 210 upregulated), 2762 (2155 downregulated and 607 upregulated) and 482 (421 downregulated and 61 upregulated) DEGs at D3, D11, D24 and D90, respectively.

In **the spinal cord**, the expression profile in the neuropathic pain has changed as following: there were 17 downregulated and 51 upregulated DEGs at D3, 2933 downregulated and 91 upregulated DEGs at D11, 1368 downregulated and 187 upregulated DEGs at D24 and 2124 downregulated and 1140 upregulated DEGs at D90.

The highest number of DEGs was found in the **DRG tissue** as shown in the Figure 10: 3833 downregulated and 4206 upregulated DEGs at D3, 3217 downregulated and 2441 upregulated DEGs at D11, 4534 downregulated and 1630 upregulated DEGs at D24 and 2591 downregulated and 495 upregulated DEGs at D90.

DEGs in the CCI-mice after the treatment with MNAC13 and αD11

In order to study the effect of each antibody on the changes in the transcriptome profile, I compared the expression levels of genes in the CCI mice treated either with αD11 or MNAC13 to the gene expression in the CCI-induced mice treated with Saline. Both antibodies induced massive gene expression changes in the PNS (in the DRGs), whereas MNAC13 mAb influenced the modulation of genes in the CNS (ACC and SC) to a lesser extent compared to αD11.

In the **cortex**, I identified a total of 6 (4 downregulated, 2 upregulated), 45 (32 downregulated, 13 upregulated) and 37 (25 downregulated, 12 upregulated) DEGs induced (probably indirectly) by MNAC13 in the mice that underwent the surgery at D11, D24 and D90 respectively. Similarly, few genes were found to be modulated in the **spinal cord** of the CCI-induced mice after the treatment with MNAC13: 257 (246 downregulated, 11 upregulated) at D11, 54 (46 downregulated, 8 upregulated) at D24 and 20 (14 downregulated, 6 upregulated) at D90. Among all types of tissues collected from the CCI-induced mice treated with MNAC13, **DRG tissue** appeared to undergo the most transcriptional changes with 2102 (807 downregulated, 1295 upregulated) DEGs at D11, 3526 (574 downregulated, 2952 upregulated) DEGs at D24 and 2648 (193 downregulated, 2455 upregulated) DEGs at D90.

Unlike MNAC13, the effect of αD11 could be observed also at the central level, with substantially greater number of genes being modulated in the **cortex**: 1767 (52 downregulated, 1715 upregulated) at D11, 1272 (749 downregulated, 523 upregulated) at D24 and 731 (487 downregulated, 244 upregulated) at D90; and in the **spinal cord**: 2228 (368 downregulated, 1860 upregulated) at D11, 1695 (962 downregulated, 733 upregulated) at D24 and 1956 (488 downregulated, 1468 upregulated) at D90. The most considerable changes in the gene expression induced by αD11 were detected in the **DRG** tissue with a total of 2841 (1045 downregulated, 1796 upregulated) DEGs at D11, 3318 (889 downregulated, 2429 upregulated) DEGs at D24 and 2211 (872 downregulated, 1339 upregulated) DEGs at D90.

Taken together, in the CNS (ACC and SC) the neuropathic pain condition led remarkably to the downregulation of genes when compared to naïve mice, while the treatment with αD11 resulted mostly in their upregulation; MNAC13 effect had lesser impact on the transcriptomic changes in the CNS. Not surprisingly, the highest number of DEGs was observed in the DRG tissue, due to the expression and direct availability of NGF receptors, TrkA and p75, in the DRGs.

The minimal effect of MNAC13 observed in the CNS could reflect the fact that the antibody is not allowed to penetrate the blood-brain barrier (BBB), as shown in Figure 11. Both naïve and CCI-mice that were injected repeatedly with a higher dose of MNAC13 (100 µg/mouse/day) (Fig. 11a, lane 6.-9.) did not show the presence of the antibody in the brain tissue at the time point (D11) when the antibody concentration in the serum reached its highest peak (see ELISA assay results in Figure 8). I repeated the same experiment with the anti-NGF αD11 and, likewise, observed no crossing of the BBB and no presence of the anti-NGF antibody in the brain (data not shown).

Since both analgesic drugs do not cross the BBB, they are not able to execute their function on the CNS directly, yet I observed, contrary to MNAC13, quite a remarkable impact of anti-NGF αD11 on cortical gene expression in the CNS. One of the reasons for this

difference might be a different mechanism of action of both analgesic drugs: while MNAC13 acts on NGF indirectly through blocking its receptor (TrkA), αD11 neutralizes NGF directly, reducing the amount of free NGF present in the blood by its sequestration. Peripheral sequestration of NGF by the circulating systemic antibody might limit its availability for the NGF-signalling in the brain, by a so-called "sink effect". Therefore, both antibodies probably act upon the CNS indirectly, most likely via altered DRG signalling and additionally, αD11 through the sequestration of free NGF present in the blood.

Next, I focused my further efforts on analysing the gene expression changes in the DRGs, among all analysed tissues, since this region is the first station in the ascending pain pathways and resulted to have the most affected transcriptome profiling by the antibody treatment. I postulated that the changes in the gene expression induced by the chronic pain state might be, in part, reversed upon the treatment. To answer the question whether the gene expression dysregulated in neuropathic pain might be reversed upon the treatment with both antibodies, I performed a bioinformatics analysis.

4.2.2 Differential gene expression in the DRGs

Transcriptome changes in the DRGs induced by chronic constriction injury (CCI) and the antibody treatment at key time points were determined by Agilent Microarray technique, as mentioned previously. The purpose of this gene expression profiling was to identify and evaluate neuropathic pain specific mRNA fingerprinting together with analgesia-related mRNA fingerprinting induced by both antibodies.

Volcano plots of transformed (log2) fold-change values vs. FDR of all probe sets of CCI-induced group relative to naïve group at D3, D11, D24 and D90 are represented in figures 12 and 13. More than 8.000 probe sets at D3, 5.000 at D11, 6.000 at D24 and 3.000 at D90 were listed as differential ($|FC| > 2.0$) between the CCI-induced mice and naïve mice. The differential expression of genes in the DRGs in the NP model after the treatment with MNAC13 or αD11 relative to CCI-induced mouse model are depicted by the volcano plots in Figures 12 and 13, respectively. In the MNAC13-treated group (Fig. 12), I found over 2.000 significantly dysregulated genes at D11, 3.000 at D24 and 2.000 at D90 after surgery. A similar behaviour was observed in the group of αD11-treated mice (Fig. 13).

Overall, the transcriptome analysis has shown that the treatment with either antibody induced a massive upregulation of genes in the CCI-mice at all studied time points, while in the neuropathic pain condition both downregulation and upregulation of genes was observed in the early phase with the tendency to downregulation in the late phase. Further bioinformatics analysis was led in order to identify the genes whose dysregulated expression in neuropathic pain was reversed by the antibody treatment.

Figure 10. Histograms of differential gene expression.

X axis indicates specific time points, the y axis indicates the total number of significantly up-regulated (red) and down-regulated (green) genes in different conditions (CCI+Sal, CCI+MNAC13, CCI+αD11) and in different tissues (DRG, SC, and ACC).

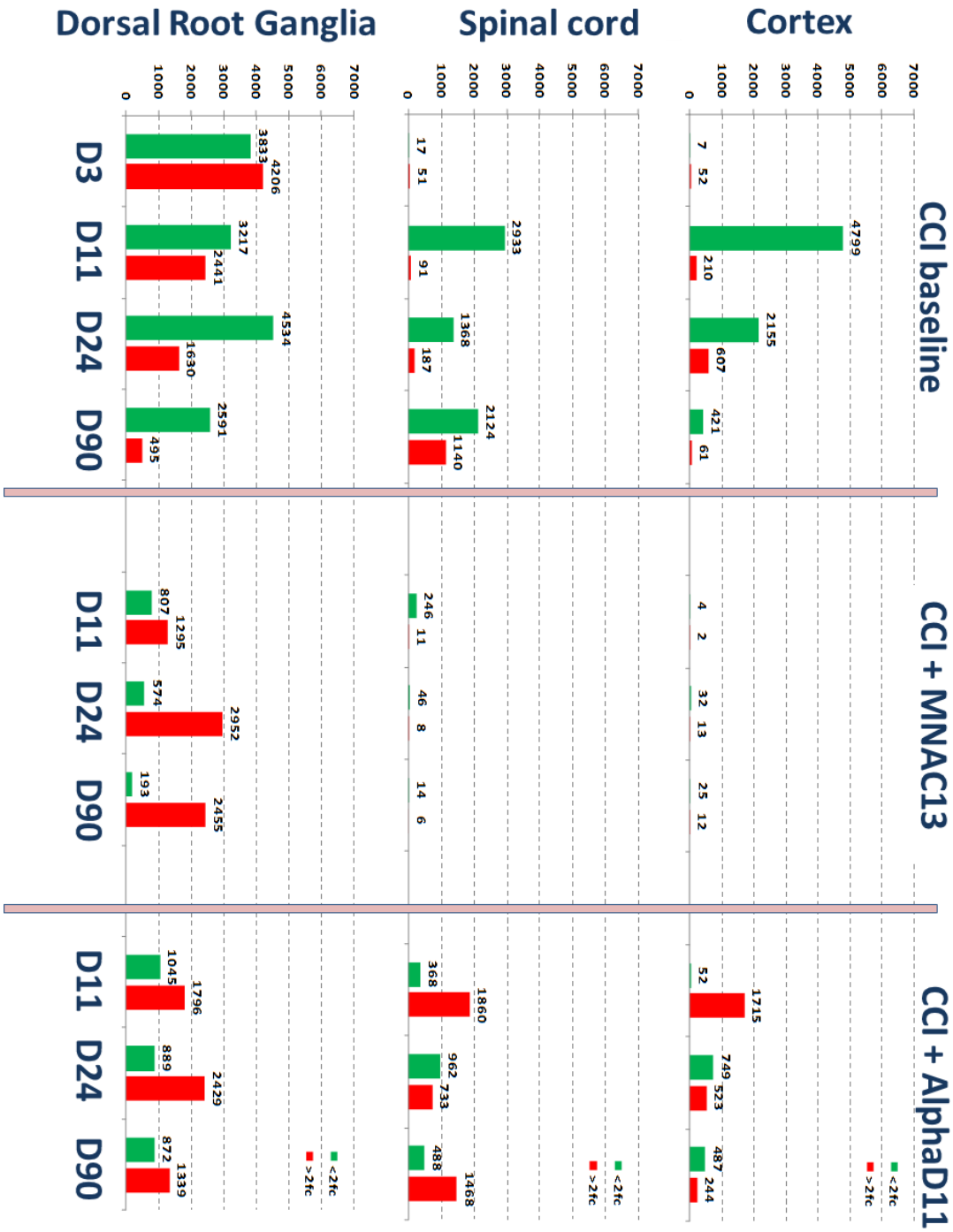

Figure 11. MNAC13 administered intraperitoneally does not cross the BBB.

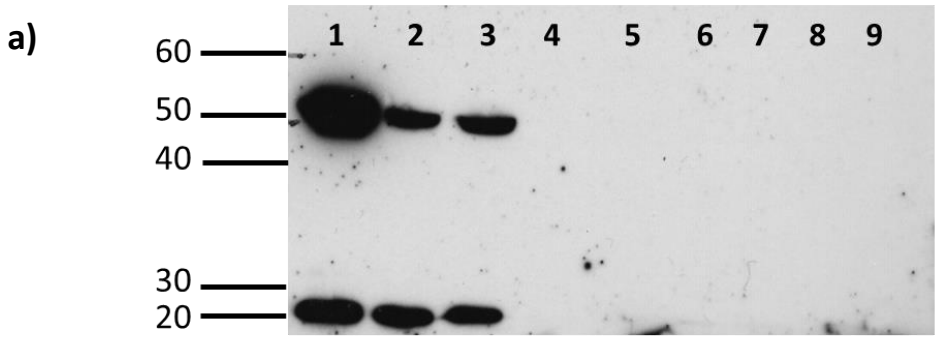

Representative WB after IP of brain tissues from naïve and CCI mice. Biotinylated MNAC13 or saline were administered to mice, both CCI and naïve. Immunoprecipitation on extracts of brains, isolated at D11, was performed with a streptavidin resin, followed by western blot (WB) with an anti-mouse IgG.

Samples order:
1. MNAC13 mAb 500 ng;
2. IP naïve saline-treated + MNAC13-spiked;
3. IP CCI saline-treated + MNAC13-spiked;
4. naïve saline-treated;
5. CCI saline-treated;
6. Naïve 1 MNAC13-treated;
7. Naïve 2 MNAC13-treated;
8. CCI 1 MNAC13-treated;
9. CCI 2 MNAC13-treated.

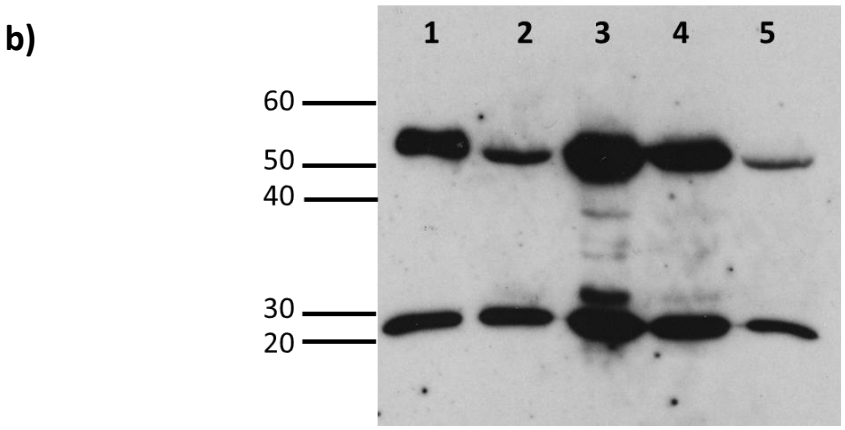

Control Experiment for IP and WB: A pool of 4 brains from naïve mice treated with saline was homogenized, divided into four samples and spiked with 4 different concentrations of biotinylated MNAC13 (333-110-37-4 ng). Immunoprecipitation followed by WB was then performed.

Samples order:
1. MNAC13 mAb 82 ng;
2. IP pool naïve brain + MNAC13 spiked 37 ng;
3. IP pool naïve brain + MNAC13 spiked 333 ng;
4. IP pool naïve brain + MNAC13 spiked 110 ng;
5. IP pool naïve brain + MNAC13 spiked 4 ng.

Figure 12. Volcano plots for the DEGs analysis by MNAC13 in DRG.

Distribution of up- and down-regulated genes in a) CCI-induced mice vs Naïve mice; b) CCI-mice treated with MNAC13 (100µg/day from D3-D10) vs untreated CCI-mice in different time points (D3, D11, D24 and D90). X axis indicates the Log2(Fold-Change) and Y axis indicates the –Log10(FDR), the Benjamini-Hochberg corrected p-value. Red and Green highlighted regions show 2-fold up- and down-regulated genes respectively, with FDR adjusted p-value ≤ 0.05, for different Dorsal Root Ganglia (DRG) contrasts. The horizontal dashed line indicates FDR threshold (0.05), while the vertical dashed line indicates Log2(Fold-Change) thresholds (<-1.0, >+1.0).

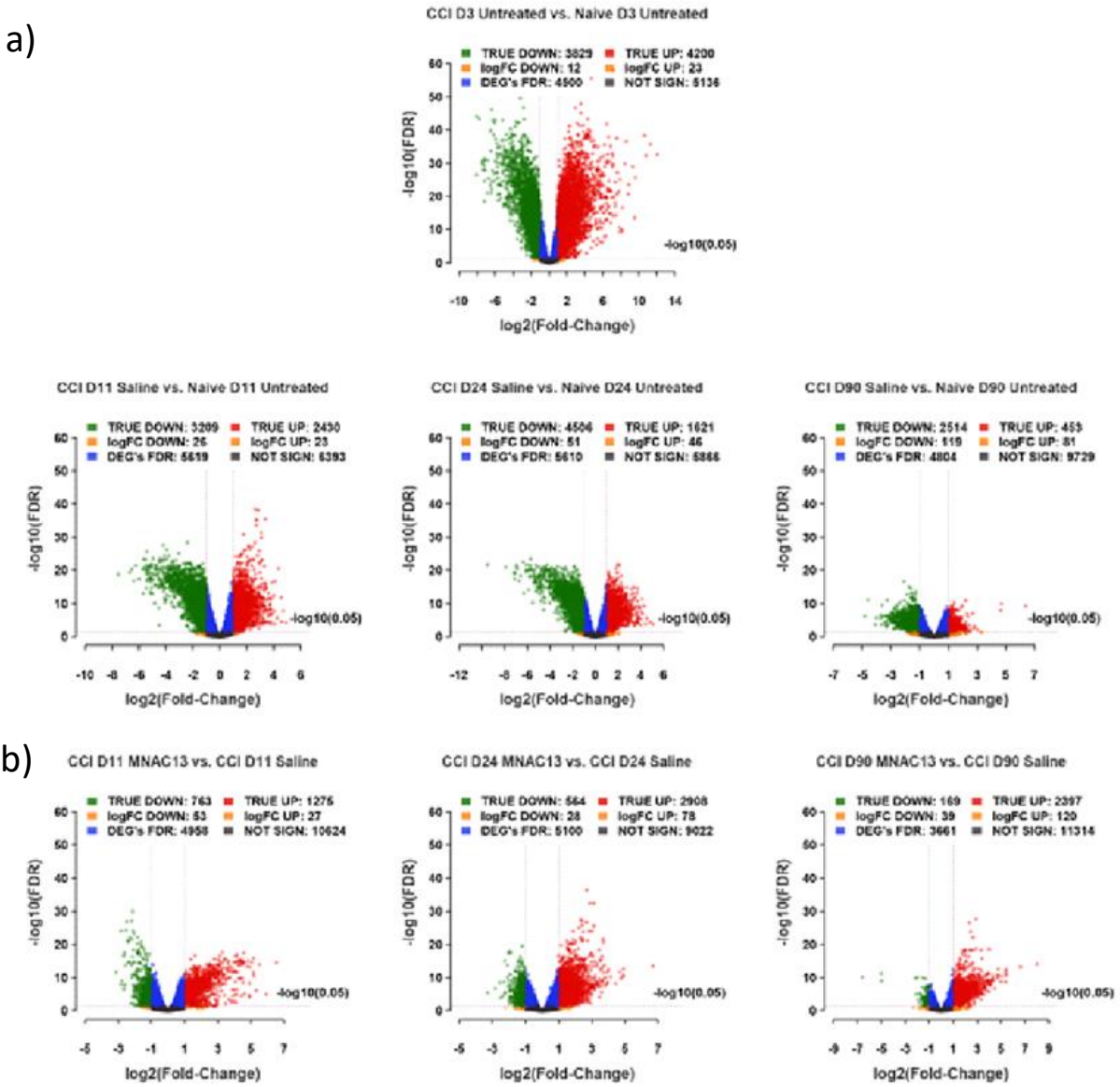

Figure 13. Volcano plots for the DEGs analysis by αD11 in DRG.

Distribution of up- and down-regulated genes in a) CCI-induced mice vs Naïve mice; b) CCI-mice treated with αD11 (100µg/day from D3-D10) vs untreated CCI-mice in different time points (D3, D11, D24 and D90), with X axis indicating the Log(2)-Fold-Change and Y axis indicating the −Log(10)(FDR) from the Benjamini-Hochberg test, as measures of differential expression. Red and Green highlighted regions show 2-fold up- and down-regulated genes respectively, with FDR adjusted p-value ≤ 0.05 throughout Dorsal Root Ganglia (DRG) contrasts.

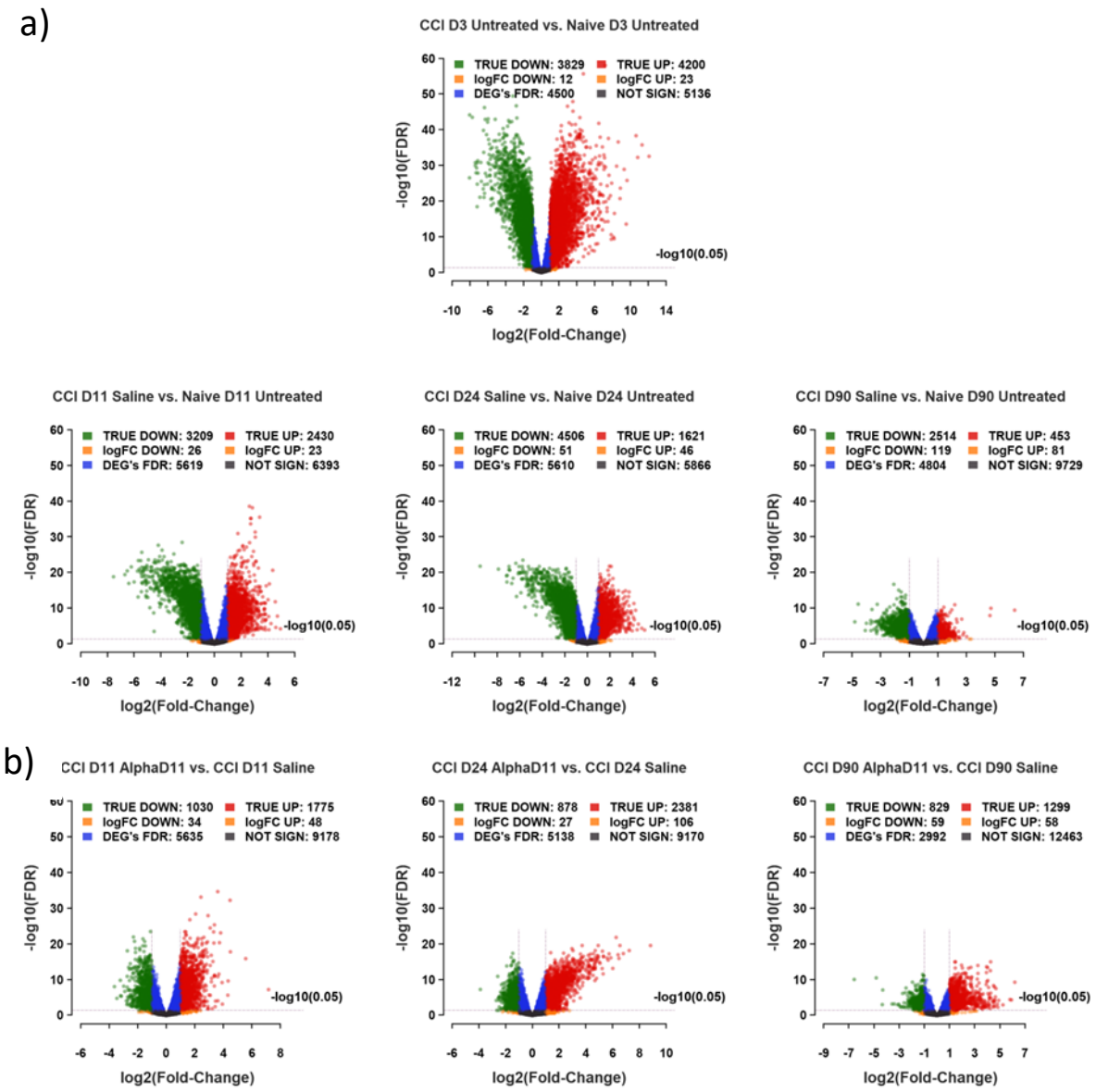

4.3 Bioinformatic analysis of the transcriptomic data in the DRGs

I conducted a detailed bioinformatic analysis of the transcriptomic data in the DRGs of the CCI-induced mice and after the treatment with either MNAC13 or αD11. I decided to analyse each time point separately in order to characterise both the initiation and the progression of the neuropathic pain and the effects that both antibodies exert at different stages of the disease development. The structure of this chapter is as following:

4.3.1 Bioinformatic analysis at D3
Genes modulated in the neuropathic pain model at D3
4.3.2 Bioinformatic analysis at D11
Genes modulated in the CCI-model at D11
Genes modulated in the CCI-model after MNAC13 treatment at D11
Genes modulated in the CCI-model after αD11 treatment at D11
4.3.3 Bioinformatic analysis at D24
Genes modulated in the CCI-model at D24
Genes modulated in the CCI-model after MNAC13 treatment at D24
Genes modulated in the CCI-model after αD11 treatment at D24
4.3.4 Bioinformatic analysis at D90
Genes modulated in the CCI-model at D90
Genes modulated in the CCI-model after MNAC13 treatment at D90
Genes modulated in the CCI-model after αD11 treatment at D90
4.3.5 Comparative bioinformatic analysis of anti-TrkA and anti-NGF transcriptomic data from the DRGs
Commonalities between MNAC13 and αD11 treatment in the neuropathic pain model

Bioinformatic analysis was performed using available online tools, including DAVID Gene Ontology, KEGG, REACTOME and g:Profiler in order to identify significantly enriched biological functions and interaction networks characterising different phases of neuropathic pain development and, more importantly, gene clusters modulated by either anti-TrkA or anti-NGF treatment in the CCI-induced mice. I used DAVID (**D**atabase for **A**nnotation, **V**isualization and **I**ntegrated **D**iscovery) bioinformatics database (https://david.ncifcrf.gov/) to identify and cluster significantly enriched biological terms, and g:Profiler toolset (https://biit.cs.ut.ee/gprofiler) to perform gene set enrichment analysis and to find enriched KEGG and REACTOME pathways and biological categories using Benjamini-Hochberg FDR method for multiple testing correction with a significance threshold 0.05 ($p < 0.05$). REACTOME (https://reactome.org/) is an open access, peer-reviewed pathway database that provides the visualization, interpretation and analysis of biological pathways. KEGG (**K**yoto **E**ncyclopaedia of **G**enes and **G**enomes) (https://www.genome.jp/kegg/) is a database resource for understanding high-level functions of the biological system at cellular and molecular level. Both serve as a useful bioinformatics tool in genome analysis of large-scale datasets generated by high-throughput microarray technologies. DAVID GO functional annotation clustering was done separately for upregulated and downregulated genes, while KEGG and REACTOME pathways were analysed for all modulated genes together.

4.3.1 Bioinformatic analysis at D3

Genes modulated in the neuropathic pain model at D3

A Gene Ontology (GO) enrichment analysis of genes differentially expressed in neuropathic pain state (CCI+Saline) compared to normal non-operated mice (Naïve group) was performed to identify significantly enriched GO terms. GO terms were assigned for downregulated and upregulated DEGs separately and these were ranked based on their enrichment score in the decreasing order. Only categories with FDR < 0.05 were considered significant. As shown in Table 1, I found that most downregulated genes induced by the CCI procedure were classified into the categories of synaptic transmission and its regulation, neurotransmitter secretion, ion channel activity and cation transport, neurogenesis and neuron development. On the other hand, the biological functions most significantly upregulated in DRGs 3 days after sciatic nerve injury were: regulation of immune response, extracellular matrix component and collagen alpha chain, blood vessel development and cholesterol metabolic process (Table 2).

Table 1. DAVID GO analysis of genes downregulated in neuropathic pain condition at D3.

GO-ID	GO term	Enrichment score	P value	FDR	Count of genes
GO:0030054	cell junction	18.78	1.08E-18	1.45E-15	115
GO:0007268	synaptic transmission	18.29	2.25E-19	3.71E-16	62
GO:0005216	ion channel activity	14.19	1.29E-13	1.71E-10	83
GO:0007269	neurotransmitter secretion	9.04	8.08E-10	1.36E-06	19
GO:0006812	cation transport	8.07	3.12E-08	5.25E-05	90
IPR001508	NMDA receptor	7.82	8.39E-09	1.43E-05	13
GO:0022008	neurogenesis	7.62	2.71E-08	4.58E-05	93

Table 2. DAVID GO analysis of genes upregulated in neuropathic pain condition at D3.

GO-ID	GO term	Enrichment score	P value	FDR	Count of genes
GO:0044420	extracellular matrix part	11.39	1.81E-14	2.42E-11	39
GO:0005783	endoplasmic reticulum	7.59	6.56E-09	9.03E-06	141
GO:0006695	cholesterol biosynthetic process	7.15	3.37E-09	5.82E-06	15
GO:0050778	positive regulation of immune response	6.32	1.16E-07	2.01E-04	36
GO:0001568	blood vessel development	6.29	4.14E-08	7.16E-05	54
PTHR10499	collagen alpha chain	5.17	6.67E-06	0.0105	23

When performing the pathway enrichment analysis, biological process terms in KEGG and REACTOME pathways satisfying the criteria of p-value < 0.05 and the minimum hits >4 were considered to be significantly enriched terms (Supplementary table 1). REACTOME enrichment analysis indicated that activation and trafficking of AMPAR, activation of NMDAR, GABAR and kainate receptors, glutamate neurotransmitter release, eph-ephrin

signalling, neurexins and neuroligins were significantly regulated biological processes in the neuropathic pain model at D3. In addition, the pathways related to retrograde endocannabinoid signalling, GABAergic synapse, long-term potentiation and depression were found to be enriched in KEGG.

4.3.2 Bioinformatic analysis at D11

Genes modulated in the CCI-model at D11

DAVID GO functional enrichment analysis of DEGs negatively modulated in neuropathic pain state (CCI+Saline group) at D11 following peripheral nerve injury compared to normal non-operated mice (Naïve group) revealed functions related to cation transport, cell junction, gated channel activity, neurogenesis, regulation of synaptic transmission, NMDA receptor and cellular ion homeostasis (Table 3). Positively modulated genes were mostly linked to collagen alpha chain, plexin/semaphorin/integrin and positive regulation of cell adhesion (Table 4).

Table 3. DAVID GO analysis of genes downregulated in neuropathic pain condition at D11.

GO-ID	GO term	Enrichment score	P value	FDR	Count of genes
GO:0006811	ion transport	14.9	2.97E-14	4.9E-11	124
GO:0030054	cell junction	13	1.39E-12	1.9E-09	92
GO:0022836	gated channel activity	12.83	2.13E-13	2.82E-10	66
GO:0022008	neurogenesis	10.12	2.36E-11	3.98E-08	94
GO:0007268	synaptic transmission	9.1	9.32E-10	1.57E-06	43
GO:0006812	cation transport	9.09	2.08E-09	3.51E-06	86
IPR003598	Immunoglobulin subtype 2	8.62	6.62E-12	1.12E-08	48
IPR001508	NMDA receptor	8.6	1.49E-09	2.53E-06	13

Table 4. DAVID GO analysis of genes upregulated in neuropathic pain condition at D11.

GO-ID	GO term	Enrichment score	P value	FDR	Count of genes
PTHR10499	collagen alpha chain	6.88	1.37E-07	0.00021	23
IPR003659	plexin/semaphorin/integrin	4.46	1.16E-05	0.02	15
GO:0045785	positive regulation of cell adhesion	4.23	1.83E-05	0.03	14

Among the KEGG and REACTOME pathways (Supplementary table 2) highlighted glutamatergic and GABAergic synapse, nicotine and morphine addiction, circadian entrainment, synaptic vesicle cycle, activation and trafficking of AMPARs, SLC-mediated transmembrane transport, protein-protein interactions at synapses, GPCR ligand binding,

astrocytic glutamate-glutamine uptake and metabolism, acetylcholine neurotransmitter release cycle and potassium transport channels.

Genes modulated in the CCI-model after MNAC13 treatment at D11

Results of the GO enrichment analysis for genes downregulated and upregulated by the MNAC13 in the CCI-model at D11 are shown in Tables 5 and 6, respectively. Collagen alpha chain, von Willebrand factor and positive regulation of immune response were among the most downregulated functional categories, whereas terms linked to gated channel activity, cation transport, synaptic transmission, cell junction, NMDA receptor, cellular ion homeostasis and neurogenesis were found to be significantly upregulated by MNAC13. Surprisingly, I found also terms associated with myofibril assembly, striated muscle cell development and sarcoplasmic reticulum. These findings will be consulted in the section of Discussion.

Table 5. DAVID GO analysis of genes downregulated after MNAC13 treatment in the CCI model at D11.

GO-ID	GO term	Enrichment score	P value	FDR	Count of genes
PTHR10499	collagen alpha chain	10.48	3.34E-12	4.54E-09	19
IPR001007	von Willebrand factor, type C	4.64	1.81E-05	0.03	9
GO:0050778	positive regulation of immune response	4.39	2.41E-05	0.04	15

Table 6. DAVID GO analysis of genes upregulated after MNAC13 treatment in the CCI model at D11.

GO-ID	GO term	Enrichment score	P value	FDR	Count of genes
GO:0030016	myofibril	13.31	3.25E-15	4.22E-12	27
GO:0022836	gated channel activity	12.39	2.16E-12	2.65E-09	41
GO:0006812	cation transport	9.77	1.29E-10	2.06E-07	53
GO:0007268	synaptic transmission	9.02	8.65E-10	1.38E-06	28
GO:0030054	cell junction	8.08	1.18E-08	1.5E-05	49
IPR001508	NMDA receptor	8.07	7.23E-09	1.15E-05	10
IPR003598	immunoglobulin subtype 2	5.7	8.04E-08	0.000128	26
GO:0022008	neurogenesis	5.58	6.45E-07	0.00103	46

The most significantly enriched KEGG and REACTOME pathway categories altered by MNAC13 at D11 (Supplementary table 3) include GABAergic and glutamatergic synapse, calcium and cAMP signalling pathway, striated muscle contraction, collagen biosynthesis and degradation, extracellular matrix organization.

Genes modulated in the CCI-model after αD11 treatment at D11

Significant GO terms for genes modulated in the neuropathic pain model after αD11 treatment at D11, together with their enrichment score and statistical significance are shown in Tables 7 and 8. The GO terms found to be significant in the group of downregulated genes comprise somatodendritic compartment, secretion and exocytosis, ion channel complex, gated channel activity, PKC-like, Pleckstrin homology domain, C2 calcium-dependent membrane targeting, GTP-ase activator activity and voltage-gated potassium channel complex. On the other hand, cell motility, cardiovascular system development, regulation of phosphate metabolic processes and MAPK cascade were some of the GO terms enriched within the group of upregulated genes. Among them, muscle cell differentiation, myofilament and myofibril were detected by DAVID GO analysis, as well.

Table 7. DAVID GO analysis of genes downregulated in the CCI model at D11 following αD11 treatment.

GO-ID	GO term	Enrichment score	P value	FDR	Count of genes
GO:0036477	somatodendritic compartment	12.57	8.01E-15	1.13E-11	84
GO:0046903	secretion	12.48	3.27E-13	5.75E-10	89
GO:0006887	exocytosis	10.29	2.64E-11	4.65E-08	39
GO:0034702	ion channel complex	9.44	3.78E-11	5.33E-08	36
IPR002219	protein kinase C-like, phorbol ester/ diacylglycerol binding	8.36	6.66E-10	1.08E-06	17
GO:0099536	synaptic signaling	8.13	6.34E-09	1.12E-05	51
GO:0022836	gated channel activity	8.04	4.51E-09	6.04E-06	35
GO:0097060	synaptic membrane	6.99	4.18E-09	5.90E-06	35
IPR001849	pleckstrin homology domain	6.47	1.53E-07	2.47E-04	29
GO:0022008	neurogenesis	6.16	8.97E-07	0.00164	98
IPR000008	C2 calcium-dependent membrane targeting	6.04	2.50E-08	4.03E-05	23
GO:0005096	GTPase activator activity	5.96	9.96E-07	0.00133	26
GO:0008076	voltage-gated potassium channel complex	5.69	1.70E-07	2.39E-04	16
GO:0034765	regulation of ion transmembrane transport	5.63	4.38E-06	0.0077	34

Table 8. DAVID GO analysis of genes upregulated in the CCI model at D11 following αD11 treatment.

GO-ID	GO term	Enrichment score	P value	FDR	Count of genes
GO:0030016	myofibril	16.41	3.79E-17	5.52E-14	43
GO:0048870	cell motility	9.55	2.13E-09	3.78E-06	96
GO:0019220	regulation of phosphate metabolic process	8.59	2.20E-10	4.06E-07	113
GO:0043408	regulation of MAPK cascade	7.33	1.05E-08	1.93E-05	58
GO:0072358	cardiovascular system development	6.96	1.03E-07	1.90E-04	76

Based on KEGG and REACTOME analysis (Supplementary table 4), the pathways most significantly modulated by αD11 in the CCI-model at D11 included MAPK signalling, calcium and Rap1 signalling pathways, axon guidance, focal adhesion, cardiomyopathy and cancer-related pathways, signalling by RHO GTPases, striated muscle contraction, voltage gated potassium channels and others.

4.3.3 Bioinformatic analysis at D24

Genes modulated in the CCI-model at D24

Table 9 shows functional categories enriched in genes significantly downregulated at D24 after sciatic nerve injury, while table 10 depicts GO terms associated to genes positively modulated in the neuropathic pain condition at D24. The first includes pathways related to cation transport, gated channel activity, cell junction, neurogenesis, regulation of synaptic transmission and NMDARs, whereas the later comprises categories such as collagen alpha chain, vasculature development, gated channel activity and regulation of cell-substrate adhesion.

Table 9. DAVID GO analysis of genes downregulated in neuropathic pain condition at D24.

GO-ID	GO term	Enrichment score	P value	FDR	Count of genes
GO:0006811	ion transport	13.8	1.31E-13	2.16E-10	121
GO:0022836	gated channel activity	11.76	4.30E-11	5.72E-08	61
GO:0030054	cell junction	10.37	2.45E-10	3.33E-07	84
GO:0006812	cation transport	8.2	1.74E-08	2.94E-05	82
GO:0022008	neurogenesis	6.42	2.27E-07	0.000383	81
GO:0007268	synaptic transmission	6.11	8.11E-07	0.001338	37
IPR001508	NMDA receptor	5.11	5.30E-06	0.008969	10

Table 10. DAVID GO analysis of genes upregulated in neuropathic pain condition at D24.

GO-ID	GO term	Enrichment score	P value	FDR	Count of genes
PTHR10499	Collagen alpha chain	7.98	2.31E-08	3.44E-05	21
GO:0001944	vasculature development	5.1	4.40E-06	0.007358	35

Some of the KEGG and REACTOME pathways worth mentioning are glutamatergic, cholinergic and GABAergic synapse, calcium signalling, axon guidance, potassium channels, ECM organization, ion transport by P-type ATPases, SLC-mediated transmembrane transport, PLCβ-mediated events, RET signalling, semaphorin interactions, neurexins and neuroligins (Supplementary table 5).

Genes modulated in the CCI-model after MNAC13 treatment at D24

The functional enrichment analysis of genes modulated by MNAC13 at D24 after sciatic nerve injury revealed gated channel activity and potassium channels as significantly enriched GO terms within the subset of downregulated genes, and immune system development, Src homology-3 domain, chemotaxis and chemokine activity within the subset of upregulated genes (Table 11).

Table 11. DAVID GO analysis of genes upregulated in the CCI model at D24 following MNAC13 treatment.

GO-ID	GO term	Enrichment score	P value	FDR	Count of genes
GO:0006935	chemotaxis	5.74	1.42E-06	0.002417	26
IPR001452	Src homology-3 domain	5.22	5.73E-07	0.000965	40
GO:0002520	immune system development	5.05	3.87E-06	0.00644	49

Among significantly enriched KEGG and REACTOME pathways (Supplementary table 6) stand out glutamatergic and GABAergic synapse, voltage gated potassium channels, SLC-mediated transmembrane transport, phagosome, leukocyte trans-endothelial migration, Rho GTPase cycle, GPVI-mediated activation cascade, Hippo, Rap1 and TGFbeta signalling pathways.

Genes modulated in the CCI-model after αD11 treatment at D24

At D24 after sciatic nerve injury, the treatment with αD11 induced a massive upregulation of genes involved in synaptic signalling, learning or memory, neuron differentiation, ion transmembrane transport, cell motility, Src homology-3 domain, fibronectin type III, membrane raft and many others, as shown in Table 13, whereas downregulated genes were classified into rather more general terms, such as neurogenesis, somatodendritic compartment and cytoplasm (Table 12).

Table 12. DAVID GO analysis of genes downregulated in the CCI model at D24 following αD11 treatment.

GO-ID	GO term	Enrichment score	P value	FDR	Count of genes
GO:0022008	neurogenesis	6.88	2.79E-07	5.03E-04	89
GO:0036477	somatodendritic compartment	6.09	2.07E-07	2.92E-04	59
GO:0005737	cytoplasm	5.65	4.33E-10	6.11E-07	394
GO:0070062	extracellular exosome	5.34	2.35E-06	0.003319	124

Table 13. DAVID GO analysis of genes upregulated in the CCI model at D24 following αD11 treatment.

GO-ID	GO term	Enrichment score	P value	FDR	Count of genes
GO:0099536	synaptic signalling	17.07	8.43E-18	1.59E-14	99
GO:0036477	somatodendritic compartment	15.51	2.52E-17	3.66E-14	136
GO:0007611	learning or memory	10.09	3.34E-10	6.32E-07	50
GO:0030182	neuron differentiation	9.74	1.11E-14	2.10E-11	171
GO:0034702	ion channel complex	9.55	1.05E-10	1.52E-07	51
GO:0051046	regulation of secretion	9.13	1.78E-09	3.36E-06	97
GO:0034220	ion transmembrane transport	8.75	7.61E-11	1.38E-07	95
GO:0048870	cell motility	8.66	5.09E-11	9.23E-08	156
GO:0050769	positive regulation of neurogenesis	8.18	9.45E-08	1.71E-04	67
GO:0097060	synaptic membrane	7.74	6.11E-08	8.87E-05	49
GO:0008328	ionotropic glutamate receptor complex	7.58	2.05E-08	2.97E-05	18
GO:0043197	dendritic spine	7.40	1.85E-08	2.68E-05	33
GO:0005216	ion channel activity	6.69	2.48E-07	3.52E-04	57
IPR001452	Src homology-3 domain	6.55	5.45E-08	9.22E-05	38
GO:0014069	postsynaptic density	6.43	1.89E-07	2.75E-04	41
GO:0048858	cell projection morphogenesis	6.22	2.51E-07	4.74E-04	97
GO:0045121	membrane raft	6.16	4.24E-07	6.15E-04	51
IPR003961	Fibronectin, type III	5.87	4.41E-07	7.46E-04	36
GO:0045937	positive regulation of phosphate metabolic process	5.76	3.25E-07	6.13E-04	116

As shown in the Supplementary table 7, the most representative KEGG and REACTOME pathways and categories included glutamatergic, GABAergic, dopaminergic and cholinergic synapse, circadian entrainment, axon guidance, calcium signalling pathway, morphine and nicotine addiction, apelin and Rap1 signalling pathways, retrograde endocannabinoid signalling, chemokine signalling pathway, inwardly rectifying potassium channels, opioid signalling, muscle contraction, phase 1–inactivation of fast Na^+ channels, semaphorin interactions, G alpha signalling events, Rho GTPase cycle.

4.3.4 Bioinformatic analysis at D90

Genes modulated in the CCI model at D90

DAVID GO analysis of genes modulated at D90 following sciatic nerve injury are depicted in the table 14 and 15. Compared to the genes upregulated in the CCI model at D90, the genes that were downregulated exhibited a higher degree of clustering into more specific categories, such as cell junction, gated channel activity, NMDA receptor, voltage-dependent potassium channel and cellular ion homeostasis (table 14).

Table 14. DAVID GO analysis of genes downregulated in the CCI model at D90.

GO-ID	GO term	Enrichment score	P value	FDR	Count of genes
GO:0030054	cell junction	9.35	3.56E-09	4.57E-06	62
GO:0022836	gated channel activity	9.14	1.33E-10	1.7E-07	46
GO:0006812	cation transport	8.85	2.79E-09	4.62E-06	63
IPR001508	NMDA receptor	6.62	1.44E-07	0.000236	10
GO:0031226	intrinsic to plasma membrane	6.11	5.51E-07	0.000708	63

Table 15. DAVID GO analysis of genes upregulated in the CCI model at D90.

GO-ID	GO term	Enrichment score	P value	FDR	Count of genes
GO:0022008	neurogenesis	5.79	1.03E-06	0.001645	30

After performing KEGG and REACTOME analysis (Supplementary table 8), we found the following significant pathways enriched in neuropathic pain condition at D90 post-surgery: neuroactive ligand-receptor interaction, glutamatergic, GABAergic and cholinergic synapse, circadian entrainment, cGMP-PKG signalling pathway, long-term depression and potentiation, calcium signalling pathway, axon guidance and axonal growth inhibition (RHOA activation), voltage gated potassium channels, cardiac conduction, GPCR ligand binding, SLC-mediated transmembrane transport, MET activates PTK2 signalling, activation of NMDA receptors and postsynaptic events.

Genes modulated in the CCI model after MNAC13 treatment at D90

Using the DAVID GO tool, no significant GO terms were found for genes downregulated by MNAC13 in the CCI-induced model at D90. On the other hand, GO analysis of genes upregulated by MNAC13 in the CCI mice revealed several categories, including gated channel activity, cell junction, cation transport, symporter activity, NMDA receptor, synaptic transmission and cellular ion homeostasis (table 16).

Table 16. DAVID GO analysis of genes upregulated in the CCI model at D90 following MNAC13 treatment.

GO-ID	GO term	Enrichment score	P value	FDR	Count of genes
GO:0022836	gated channel activity	10.12	1.74E-09	2.19E-06	45
GO:0030054	cell junction	9.96	9.59E-10	1.25E-06	64
GO:0006812	cation transport	6.97	2.64E-07	0.000433	59
GO:0015293	symporter activity	6.78	3.77E-08	4.76E-05	27
IPR001508	NMDA receptor	6.52	1.89E-07	0.00031	10
GO:0007268	synaptic transmission	5.6	2.15E-06	0.00352	28

Among KEGG and REACTOME categories significantly enriched after MNAC13 treatment in CCI-induced mice at D90 post-operatively highlight glutamatergic, GABAergic, dopaminergic and cholinergic synapse, circadian entrainment, morphine and nicotine addiction, cAMP signalling, retrograde endocannabinoid signalling, long-term depression, neuroactive ligand-receptor interaction, SLC-mediated transmembrane transport, opioid signalling, muscle contraction, potassium channels, neurotransmitter release cycle, NMDA and GABA receptor activation, PLC beta and G-protein mediated events (Suppl. table 9).

Genes modulated in the CCI-model after αD11 treatment at D90

Within the group of genes downregulated by αD11 in the CCI-model at D90 after surgery, we found no significantly enriched GO terms. On the other hand, DAVID GO analysis of genes upregulated by αD11 at D90 revealed statistically significant GO terms related to regulation of transmembrane transporter activity, somatodendritic compartment, synaptic signalling, cation transmembrane transport and gated channel activity, which was not surprising. However, to our surprise, finding other GO terms linked to myofibril and myofilament, muscle cell development, sarcoplasm and Z disc was not expected (table 17).

Table 17. DAVID GO analysis of genes upregulated in the CCI model at D90 following αD11 treatment.

GO-ID	GO term	Enrichment score	P value	FDR	Count of genes
GO:0030016	myofibril	18.90	2.05E-20	2.97E-17	49
GO:0006753	nucleoside phosphate metabolic process	8.89	2.72E-10	4.78E-07	60
GO:0036477	somatodendritic compartment	8.29	1.58E-09	2.26E-06	78
GO:0099536	synaptic signaling	8.27	4.24E-09	7.46E-06	55
GO:0098655	cation transmembrane transport	8.15	7.25E-08	1.33E-04	50
GO:0022898	regulation of transmembrane transporter activity	7.27	2.40E-08	4.23E-05	28
GO:0034702	ion channel complex	5.63	1.68E-06	0.00239	30
GO:0005977	glycogen metabolic process	5.42	8.50E-07	0.00149	15
GO:0022836	gated channel activity	5.24	1.25E-05	0.01712	31

Finally, KEGG and REACTOME categories enriched in genes induced by αD11 in the neuropathic pain model comprised circadian rhythm, glutamatergic and GABAergic synapse, calcium signalling pathway, amphetamine and cocaine addiction, MAPK signalling, cAMP and cGMP-PKG signalling, muscle contraction, transmission across chemical synapses, neurotransmitter release cycle, axon guidance, L1CAM interactions, Phase 0 - rapid depolarisation (Supplementary table 10).

4.3.5 Comparative bioinformatic analysis of anti-TrkA and anti-NGF transcriptomic data from DRGs

I performed a comparative bioinformatic analysis of anti-TrkA and anti-NGF transcriptomic data from DRGs in different time points, with a detailed focus on the effects induced by each antibody in the neuropathic pain model in order to identify specific gene targets for both treatments. Firstly, I used Venn diagrams to find common and specific features between both treatments with respect to neuropathic pain condition. Next, I conducted functional enrichment analysis by DAVID tool done separately for upregulated and downregulated genes in each time point. In addition to Gene Ontology, I used g:Profiler toolset for finding the top significantly enriched KEGG and REACTOME pathways that were sorted by P-value.

I used Venn diagrams as a strategy for the identification of specific target genes that were induced by peripheral nerve injury and reversed by anti-TrkA and anti-NGF treatment. Therefore, the analysis was performed separately for downregulated and upregulated genes. With this purpose, I compared genes whose gene expression after analgesic drugs treatment behaved in the opposite way than the one in the neuropathic pain state. In other words, I was interested in genes that were downregulated after sciatic nerve injury and, at the same time, upregulated by both treatments in a specific time point and vice-versa. I referred to this subset of DEGs as “cured” genes.

The following Venn diagrams are representing a group of neuropathic pain-related genes (in orange), together with a group of genes that are specific for each treatment, with genes induced by MNAC13 illustrated in green and genes induced by αD11 illustrated in blue. Upper Venn diagrams depict genes downregulated after sciatic nerve ligature and upregulated by each treatment, while lower Venn diagrams indicate genes upregulated in CCI-induced mice and downregulated by analgesic drug treatment (Fig. 14 – 16).

At D11 after nerve injury (Figure 14), I found 253 genes in total (the sum of both total intersections 140+113), whose expression was modulated in neuropathic pain and, at the same time, reversed by both treatments. The number of “cured” genes at D11 specific for each treatment was as follows: 799 (606+193) for MNAC13 and 386 (192+194) for αD11.

Next, I identified a subset of 878 (693+185) genes “cured” commonly by both treatments at D24 following CCI procedure (Figure 15). In addition, 337 genes (277+60) were healed specifically by MNAC13, whereas 1105 genes (709+396) were inverted by αD11 treatment only.

At D90 post-surgery (Figure 16), there were 302 downregulated and 20 upregulated genes (322 in total) induced by nerve injury whose expression appeared inverted upon the treatment by either MNAC13 or αD11. Furthermore, the total number of neuropathic pain-related genes inverted at D90 specifically by one treatment only was: 523 (495+28) for MNAC13 and 130 (73+57) for αD11.

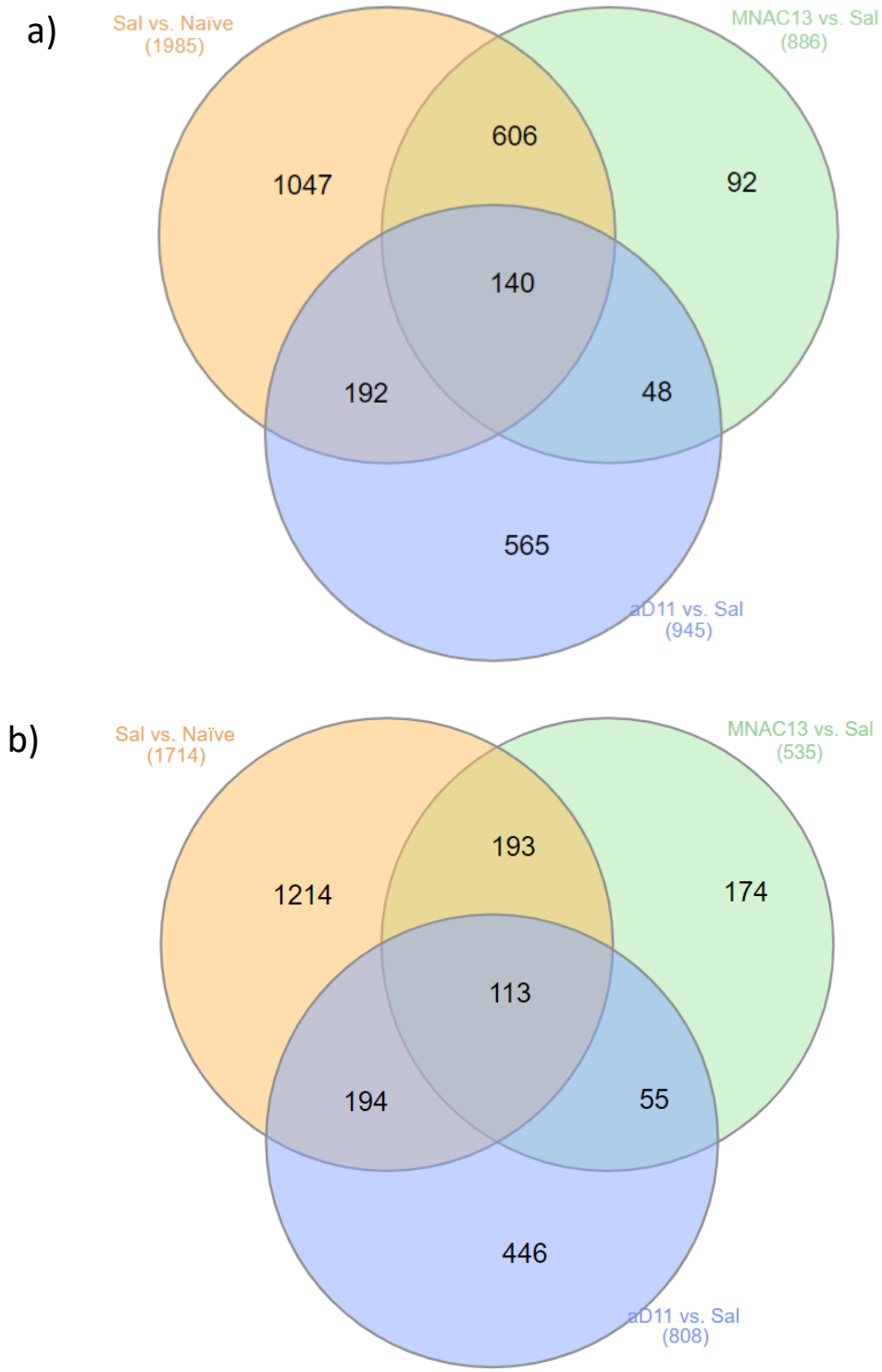

Figure 14. Venn diagrams of DEGs in the DRG at D11.

Venn diagrams depicting the total number of dysregulated genes modulated by the CCI procedure (orange) or by the treatment with either MNAC13 (green) or αD11 (blue) at D11 following peripheral nerve injury. The central overlapping section in Venn diagram identifies "cured" genes that are:

a) downregulated in neuropathic pain condition and upregulated by each treatment;
b) upregulated in neuropathic pain condition and reversed by both MNAC13 and αD11.

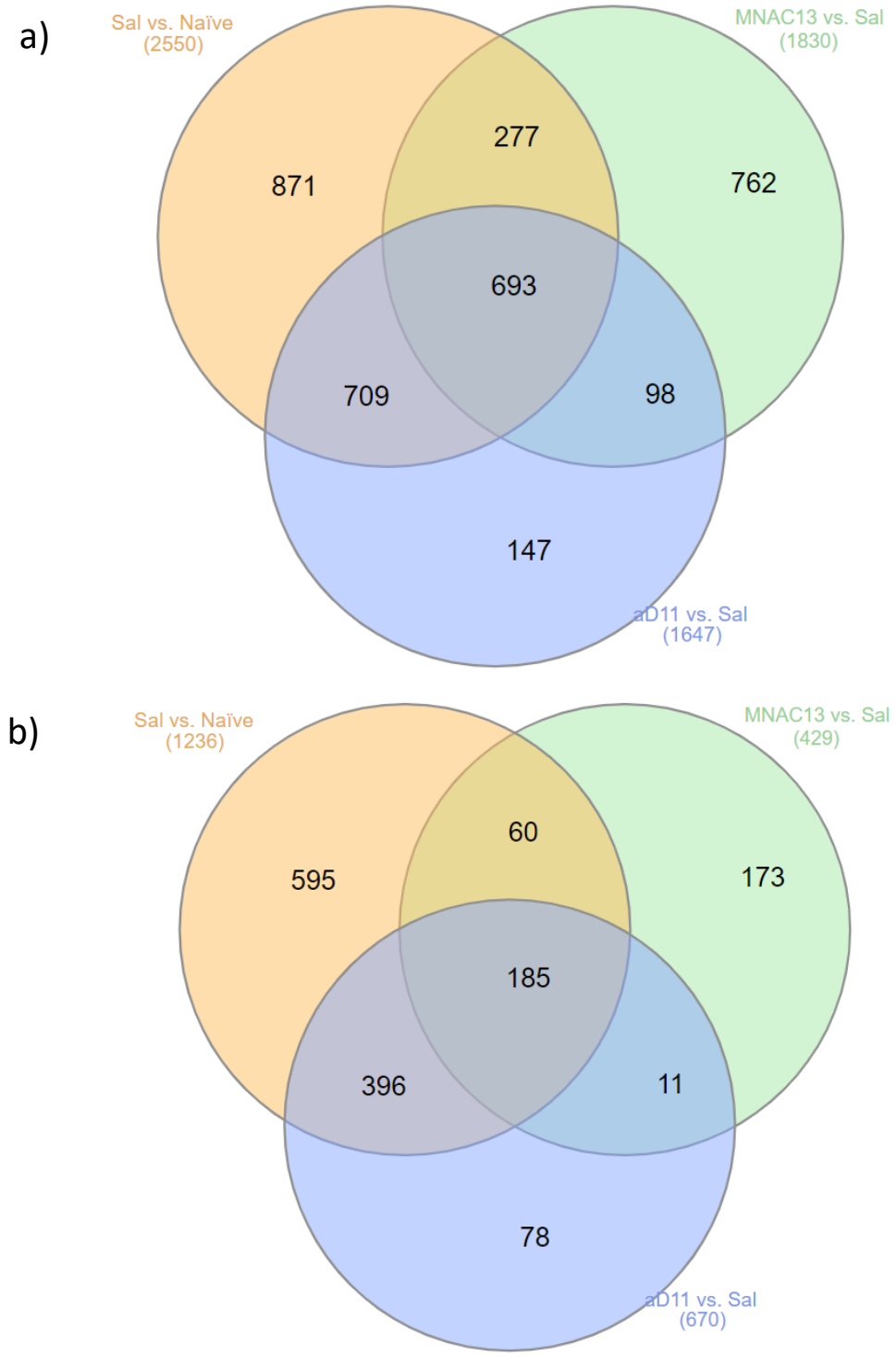

Figure 15. Venn diagrams of DEGs in the DRG at D24.

Venn diagrams showing the total number of dysregulated genes modulated by the CCI procedure (orange) or by the treatment with either MNAC13 (green) or αD11 (blue) at D24 post-surgery. The total intersection of DEGs represents "cured" genes that are:

a) downregulated in neuropathic pain condition and upregulated by each treatment;
b) upregulated in neuropathic pain condition and downregulated by both treatments.

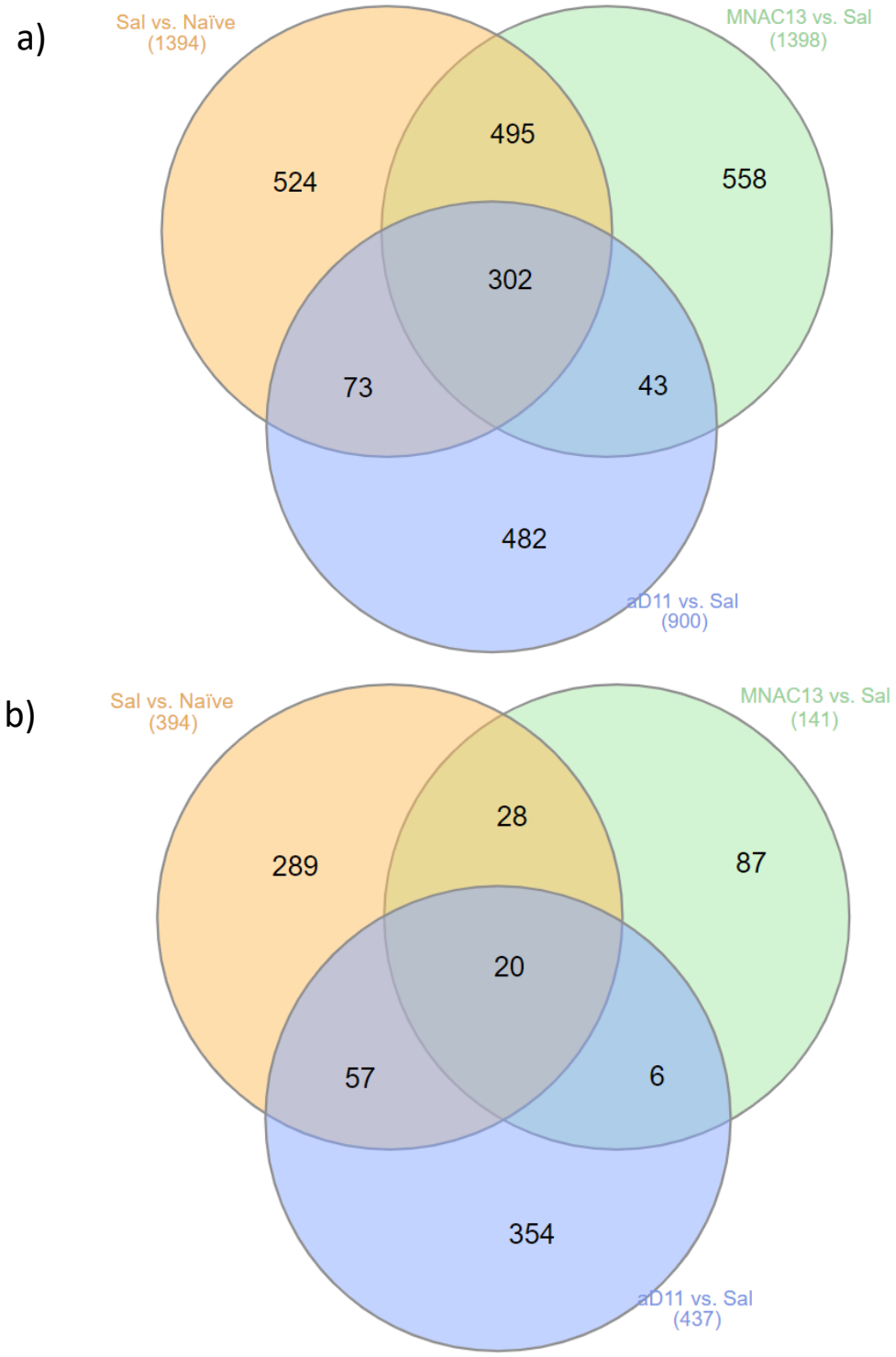

Figure 16. Venn diagrams of DEGs in the DRG at D90.

Venn diagrams depict the total number of dysregulated genes modulated by the CCI procedure (orange) or by the treatment with either MNAC13 (green) or αD11 (blue) at D90 after CCI. The central overlapping section identifies "cured" genes that are:

a) downregulated in the CCI model in comparison with Naïve mice and upregulated by each treatment in comparison with Saline-injected group;
b) upregulated in the CCI model and reversed by both treatments.

Commonalities between MNAC13 and αD11 treatment in the neuropathic pain model

In the next step, I was interested in studying the common effects of MNAC13 and αD11 treatment in the neuropathic pain condition by clustering the genes that were found to be reversed by both treatments in the CCI model. I used DAVID GO tool in order to perform the gene set enrichment analysis. At D11, I detected significantly enriched GO terms only in the group of DEGs downregulated in neuropathic pain condition and upregulated by both analgesic treatments. Both analgesic drugs were able to reverse the expression of genes linked to sarcomere, synaptic signalling and regulation of synaptic plasticity which were dysregulated in the early phase of neuropathic pain (Table 18). No significantly enriched KEGG nor Reactome pathways were found to be inverted by both treatments in the neuropathic pain condition at D11.

Table 18. DAVID GO analysis of DEGs downregulated in the CCI model and upregulated by both MNAC13 and αD11 treatment at D11.

GO-ID	GO term	Enrichment score	P value	FDR	Count of genes
GO:0030017	sarcomere	10.99	6.76E-13	8.45E-10	16
GO:0099536	synaptic signalling	6.77	1.58E-07	2.56E-04	17
GO:0048167	regulation of synaptic plasticity	5.79	6.64E-07	1.08E-03	10

The major reversal of gene expression induced by both antibodies, however, was observed at D24. In contrast to D11, I found a massive antibodies effect on the dynamic transcriptome changes occurring at D24 with a high number of functionally clustered genes. Genes linked to somatodendritic compartment and cation transmembrane transport were at the core of the functional comparison between the group of genes upregulated in the neuropathic pain model and the subset of genes downregulated by both analgesic drugs (Table 19).

Table 19. DAVID GO analysis of DEGs upregulated in the CCI model and downregulated by both MNAC13 and αD11 treatment at D24.

GO-ID	GO term	Enrichment score	P value	FDR	Count of genes
GO:0036477	somatodendritic compartment	7.33	1.28E-08	1.67E-05	28
GO:0098655	cation transmembrane transport	4.45	2.83E-06	0.0048	18

The DAVID GO analysis revealed that most of the genes downregulated in the CCI model and reversed independently by both antibodies at D24 were functionally related to cell motility, regulation of leukocyte differentiation, symporter activity, cellular chemical homeostasis, synaptic signalling, leukocyte cell-cell adhesion, positive regulation of MAPK cascade, regulation of actin cytoskeleton organization, learning, positive regulation of hematopoiesis, Src homology-3 domain, secretion by cell (Table 20).

Table 20. DAVID GO analysis of DEGs downregulated in the CCI model and upregulated by both MNAC13 and αD11 treatment at D24.

GO-ID	GO term	Enrichment score	P value	FDR	Count of genes
GO:0048870	cell motility	8.27	6.05E-10	1.06E-06	81
GO:0002521	leukocyte differentiation	6.57	2.92E-09	5.33E-06	44
GO:0015293	symporter activity	6.18	2.27E-07	3.03E-04	19
GO:0031226	intrinsic component of plasma membrane	6.17	1.37E-07	1.93E-04	77
GO:0099536	synaptic signalling	5.32	4.72E-06	8.62E-03	38
GO:0045937	positive regulation of phosphate metabolic process	5.14	1.96E-07	3.58E-04	62

DAVID GO analysis did not yield functional gene categories enriched in genes upregulated in the CCI-induced mice whose expression was reversed by both antibodies at D90 post-surgery. However, the biological categories enriched in genes downregulated by the CCI procedure at D90 following peripheral nerve injury and inverted in the antibody-treated CCI mice were as following: somatodendritic compartment, synaptic signalling, intrinsic component of plasma membrane, neuron differentiation and development, ion channel complex and potassium ion transmembrane transport, learning, symporter activity (Table 21).

Table 21. DAVID GO analysis of DEGs downregulated in the CCI model and upregulated by both MNAC13 and αD11 treatment at D90.

GO-ID	GO term	Enrichment score	P value	FDR	Count of genes
GO:0036477	somatodendritic compartment	13.12	1.64E-15	2.22E-12	48
GO:0099536	synaptic signaling	12.31	4.73E-13	8.19E-10	34
GO:0031226	intrinsic component of plasma membrane	6.77	1.53E-08	2.03E-05	47
GO:0030182	neuron differentiation	5.97	3.98E-07	6.90E-04	42
GO:0015267	channel activity	5.90	8.70E-08	1.07E-04	23
GO:0044306	neuron projection terminus	5.89	6.17E-07	8.22E-04	15
GO:0034702	ion channel complex	5.75	3.40E-06	0.004535	16
GO:0034220	ion transmembrane transport	5.58	3.25E-06	0.005637	26

The KEGG and REACTOME pathways induced by the CCI procedure at D90 and regulated by both antibodies back to “normal state” include neuroactive ligand-receptor interaction, glutamatergic, GABAergic, cholinergic and dopaminergic synapse, mineral absorption, morphine and nicotine addiction, transmission across chemical synapses, SLC-mediated transmembrane transport, GPCR ligand binding, neurotransmitter release cycle, G

alpha (i) signalling events, potassium channels, gap junction assembly and trafficking, neurotransmitter uptake and metabolism in glial cells, class A/1 (rhodopsin-like receptors), as shown in the Supplementary table 12.

In all studied experimental time points, I observed a strong effect of both antibodies in the reversal of neuropathic pain features, with the most effective inversion of gene expression observed at D24 and D90. Both antibodies were able to induce transcriptome changes which might consequently play an important role in counteracting the effects of neuropathic pain processing pathways. MNAC13 and αD11 independently modulated the gene expression of a considerable amount of genes in the same direction and, at the same time, opposed the expression of some of the pain-related genes, providing strong evidence for their role in the attenuation of neuropathic pain.

Next, I focused my interest on genes that were present in the total intersection of DEGs common for each experimental group (CCI+Saline, CCI+MNAC13, CCI+αD11) at all studied time points (D11, D24, D90). The aim of this analysis was to investigate which proportion of these DEGs in common would be reversed by the drug treatment (CCI+MNAC13, CCI+αD11) with respect to the neuropathic pain state (CCI+Saline). Strikingly, I found that most, if not all, DEGs in the antibody-treated groups have shown an opposite expression with respect to the Saline-treated group. This means that they have been "cured" by both antibodies at almost all time points (only αD11 at early time point shows some exceptions to this), suggesting a role for both antibodies in the healing process. Thus, I decided to search Pubmed in order to find relevant information about possible involvement of these genes in nociception signalling. A brief synthesis of information about these genes is provided in the Appendix.

The list of "cured" genes (e.g. genes that were differentially expressed in neuropathic pain and whose expression was reversed after the antibody treatment) that were in common between MNAC13 and αD11 treatments, are listed in the Table 22. From this list, N6AMT1 came out as an interesting candidate gene that I found most relevant for further studies, for reasons that are explained below.

Table 22. The list of "cured" genes in common between MNAC13 and αD11 treatments.

The vast majority of the DEGs in common for all experimental groups (CCI+Saline, CCI+MNAC13, CCI+αD11) and all experimental time points (D11, D24, D90) are reversed by both antibody treatments (e.g. they are "cured").

		Sal vs Nai			MNAC13 vs Sal			aD11 vs Sal		
GeneSym	GeneName	D11	D24	D90	D11	D24	D90	D11	D24	D90
		logFC	logFC	logFC	logFC	logFC	logFC	logFC	logFC	logFC
Ajap1	adherens junction associated protein 1	-5.68	-5.56	-2.39	3.85	1.86	3.23	2.33	5.24	1.81
Cdh22	cadherin 22	-5.50	-5.77	-3.08	4.57	3.70	3.61	1.22	4.67	2.54
Gfap	glial fibrillary acidic protein	-5.45	-5.89	-2.21	4.08	2.97	2.72	1.31	4.68	2.79
Ajap1	adherens junction associated protein 1	-5.42	-5.71	-2.97	3.22	2.13	3.76	2.35	4.70	2.12
Gfap	glial fibrillary acidic protein	-5.11	-7.17	-2.25	4.33	4.89	3.58	1.37	6.48	3.06
Prr18	proline rich 18	-5.10	-6.70	-1.87	4.47	4.75	4.48	-1.35	5.29	2.94
Ptpn5	protein tyrosine phosphatase, non-receptor type 5	-4.80	-4.66	-1.18	3.30	1.54	2.86	1.33	3.77	1.29
Rnd1	Rho family GTPase 1	-4.76	-4.91	-1.17	3.25	2.13	2.19	2.20	4.16	1.30
Apln	apelin	-4.55	-5.00	-2.24	3.49	3.05	3.29	-1.13	3.93	2.65
Tmem91	transmembrane protein 91	-4.48	-6.05	-4.58	2.64	2.11	4.78	-1.05	6.26	3.44
		-4.44	-3.69	-2.05	3.39	1.18	2.38	1.22	3.11	2.03
Usp29	ubiquitin specific peptidase 29	-4.37	-4.80	-2.64	3.05	1.65	3.92	-1.33	4.43	2.28
Ankrd34b	ankyrin repeat domain 34B	-4.06	-3.54	-1.86	3.69	1.62	3.41	-1.23	2.62	1.45
Scrg1	scrapie responsive gene 1	-4.03	-5.12	-1.83	3.48	3.18	3.10	-1.57	3.74	2.55
Syt13	synaptotagmin XIII	-3.94	-4.91	-2.69	2.84	1.59	4.71	-1.88	4.24	2.51
Car14	carbonic anhydrase 14	-3.89	-3.45	-1.30	2.67	1.52	1.11	1.03	2.49	2.17
Chat	choline acetyltransferase	-3.80	-3.84	-1.69	1.49	2.18	2.68	1.33	2.03	1.26
		-3.62	-2.59	-1.68	3.04	1.14	2.39	1.25	2.37	4.03
Sst	somatostatin	-3.59	-3.23	-2.46	1.57	-1.27	3.15	-1.98	3.19	1.93
Kndc1	kinase non-catalytic C-lobe domain (KIND) containing 1	-3.46	-3.60	-2.31	2.78	1.41	2.69	-1.77	2.72	1.85
Grin2b	glutamate receptor, ionotropic, NMDA2B (epsilon 2)	-3.44	-3.81	-2.26	2.49	1.97	2.39	1.96	3.14	1.24
Ptprd	protein tyrosine phosphatase, receptor type, D	-3.41	-3.39	-1.56	2.01	1.07	2.23	-1.02	2.64	2.12
Ppp1r1b	protein phosphatase 1, regulatory (inhibitor) subunit 1B	-3.36	-3.04	-1.29	2.37	1.41	1.28	1.15	1.86	1.00
Nfatc2	nuclear factor of activated T cells, cytoplasmic, calcineurin dependent 2	-3.15	-3.05	-2.31	2.63	1.33	2.24	1.45	2.47	1.69
Dixdc1	DIX domain containing 1	-3.05	-3.85	-2.41	1.80	2.47	2.79	1.26	2.81	1.35
Glb6	gap junction protein, beta 6	-3.04	-3.68	-1.85	2.50	2.91	2.77	-1.20	2.90	1.52
Cacna1g	calcium channel, voltage-dependent, T type, alpha 1G subunit	-3.02	-4.37	-2.17	1.11	2.32	2.93	-1.51	4.08	2.01
Arc	activity regulated cytoskeletal-associated protein	-2.98	-3.13	-1.50	2.12	1.02	1.09	1.90	2.37	1.01
Slc14a1	solute carrier family 14 (urea transporter), member 1	-2.46	-3.49	-1.02	1.72	2.10	1.90	-1.07	3.09	1.32
N6amt1	N-6 adenine-specific DNA methyltransferase 1 (putative)	2.89	2.43	1.54	-1.83	-1.16	-1.43	-2.73	-1.74	-1.27

4.4 N6amt1 as a potential therapeutic target in neuropathic pain

Following the bioinformatics analysis, I selected the N6amt1 (N-6 Adenine-Specific DNA Methyltransferase 1) as a candidate gene for further analysis in this study, for several reasons. First, there is a total gap in the knowledge about the function of the protein encoded by this gene and, even more so, about its role in neuropathic pain. Second, the expression profile of N6amt1 reflects, interestingly, an opposite behaviour to the transcriptome changes induced by anti-NGF and anti-TrkA in the CCI model, with respect to the other TOP 30 DEGs listed in the Table 22. Third, and most important, N6-Adenine methylation is an emerging epigenetic modification of both DNA and RNA in prokaryotes and eukaryotes (Ji, Wang et al. 2018), but whether N6amt1 is the *bona fide* N6-adenine DNA MTase in mammals is still in debate. As outlined below, N6amt1 might also target proteins for its methyltransferase activity.

The experiments that I described above, demonstrating the long-term analgesia and the extensive transcriptional changes triggered by the anti-NGF and anti-TrkA antibodies, suggest that epigenetic mechanisms might underlie these findings. For this reason, the identification of N6amt1 as being modulated both by anti-NGF and anti-TrkA appeared to me particularly intriguing, as a possible target for further investigation. In the next lines, a brief introduction regarding the function and biological properties of N6amt1 reported in the literature will be provided, followed by my preliminary results.

4.4.1 What is known about N6amt1: general background

The N6AMT1 gene was initially identified in a genetic screen designed to discover genes causing defects in heme metabolism in *E. coli* (Nakayashiki, Nishimura et al. 1995) and annotated as HEMK2, a putative protoporphyrinogen oxidase required for heme biogenesis. However, subsequent biochemical and genetic studies have demonstrated no apparent involvement of the HemK enzyme in the heme biosynthesis (Le Guen, Santos et al. 1999). Biochemical and structural studies revealed, instead, that this enzyme functions as N5-glutamine methyltransferase which catalyses the methylation of the glutamine residue at the conserved tripeptide GGQ motif of eukaryotic release factor 1 (eRF1), one of the ribosomal translation termination factors (Figaro, Scrima et al. 2008). This novel glutamine-specific MTase activity led to renaming of HEMK2 to PrmC (protein methyltransferase C). Glutamine methylation of the mammalian eRF1 is known to trigger the hydrolysis of the peptidyl-tRNA in the ribosomal P-site, which causes the release of the nascent polypeptide chain and ensures efficient termination of translation (Heurgue-Hamard, Champ et al. 2002, Nakahigashi, Kubo et al. 2002). Later, additional protein substrates with glutamine residues, apart from the polypeptide release factor, were found to be methylated by PrmC, such as CHD5 (chromodomain helicase DNA-binding protein 5), NUT (nuclear protein in testis), ANKRD34A (Ankyrin Repeat Domain 34A) and ABCA2 (ATP Binding Cassette Subfamily A Member 2) (Kusevic, Kudithipudi et al. 2016). Interestingly, it was later found that PrmC, in complex with its cofactor TRMT112 (referred to as lysine methyltransferase 9, KMT9), can methylate not only glutamine residue, but also lysine residue in the position 12 of histone H4 substrate (H4K12) (Metzger, Wang et al. 2019). In the following years, the HEMK2/PrmC protein adopted the name N6AMT1 (N6-adenine–specific DNA methyltransferase 1), because of the presence of the (D/N)PPY amino acid sequence motif in the methyltransferase domain,

which is characteristic for bacterial SAM-dependent/AdoMet-dependent N6-adenine and N4-cytosine-specific DNA methyltransferases (Yang, Shipman et al. 2004). However, its involvement in N6-adenine DNA methylation in mammals remained dubious for many years (Ratel, Ravanat et al. 2006) until just recently, when Xiao et al. showed that N6-methyladenine modification was present in the human genomic DNA and N6amt1 was suggested to function as a N6-adenine DNA methyltransferase (MTase) in human cells (Xiao, Zhu et al. 2018).

Two different isoforms of both human and mouse N6AMT1 have been identified, reflecting long and short transcription variants. The main human isoform, represented by a long form N6AMT1iso1, contains six exons, including the NPPY motif essential for binding the planar amide side chain of Gln. The alternatively spliced short isoform, N6AMT1iso2, is lacking exon IV encoding for the substrate binding motif NPPY (Leetsi, Ounap et al. 2019). Human N6AMT1iso1 shares 34% identity with the yeast homolog Mtq2p, while mouse equivalent of N6AMT1iso1 (PRED28 alpha) shares 33% identity with Mtq2p. In mice, however, the short form PRED28 beta, resulting from exon V deletion, still contains the NPPY motif. Both transcripts are present in all tissues examined in mice, although to different relative levels according to the stage of development (Figaro, Scrima et al. 2008). While N6amt1 (HEMK2) is present in the cytosol, its homolog HEMK1 (HMPrmc) is localised in mitochondria, with the former being responsible for the methylation of the eRF1 as mentioned above, and the latter methylating the corresponding site in the mitochondrial release factor, regulating this way the mitochondrial translational activity (Figaro, Scrima et al. 2008). N6AMT1 forms a heterodimeric complex with TRMT112 (named after tRNA methylation protein tRNA Methyltransferase Subunit 11-2), which is necessary for its catalytic MTase activity and stability/solubility. TRMT112 is a small evolutionarily conserved zinc finger protein that acts as a subunit for several methyltransferases involved in rRNA, tRNA, DNA and protein methylation, such as rRNA methyltransferase BUD23 (also known as WBSCR22, MERM1 and RNMT2) and tRNA methyltransferases ALKBH8 (AlkB Homolog 8, also known as TRM9) and TRMT11 (TRNA Methyltransferase 11 Homolog) (Leetsi, Ounap et al. 2019). Human Trm112 and mouse homolog share 30% and 33% identity with yeast Trm112p, respectively. However, both of them lack three of the four Cys residues coordinating the Zn atom (Figaro, Scrima et al. 2008). Based on the crystal structure of the Trm112-MTase complexes, a beta-zipper interaction is formed between the beta-strands of both TRMT112 and its interacting partner, resulting in a continuous large eleven-stranded beta-sheet, which generates a hydrophobic interface in the complex. (Leetsi, Ounap et al. 2019).

Interestingly, the expression of TRMT112 in the model of neuropathic pain remained largely unchanged, except for the D3 post-surgery, as shown in Table 23. Therefore, the ratio between N6AMT1 and TRMT112 changes in the neuropathic pain model and is re-established by both anti-NGF and anti-TrkA antibodies.

N6amt1 is an unusual enzyme with a dual function capable of methylating two structurally different substrates, acting on both proteins and DNA. Strikingly, this MTase is capable of targeting two different amino acids in protein substrates, namely glutamine and lysine. Thus, the N6AMT1 protein has been documented to function as a DNA adenine-N6 MTase, a histone H4 lysine-12 and eukaryotic release factor eRF1 glutamine MTase (Figaro, Scrima et al. 2008, Xiao, Zhu et al. 2018, Metzger, Wang et al. 2019). The common feature of the three potential substrates is the amino group (NH2) of adenine, lysine, and glutamine,

respectively. The NPPY motif plays a role in the recognition of planar nitrogen either in nucleic acid bases or in Gln (peptidic) side chains (Figaro, Scrima et al. 2008). These interesting findings of a rare multiple functionality of N6AMT1 in both epigenetic and post-translational modifications deserve more attention.

4.4.2 Preliminary results

Since I have performed a global gene expression analysis, I looked at the genes that have been reported in the literature as potential targets for epigenetic modifications mediated by N6amt1 and evaluated their transcription profile based on our data.

Xiao *et al*. detected the presence of N6-adenine DNA methylation (m6dA) in the human genome and identified N6amt1 as being responsible for this modification. They found a higher deposition of m6dA in exon regions of genes linked to G protein-coupled receptor molecules (Xiao, Zhu et al. 2018). One year later, Li and his colleagues identified the same epigenetic modification in the adult brain in response to extinction learning, with neuronal activity-related genes exhibiting an increased m6dA deposition (Li, Zhao et al. 2019). In both cases, N6amt1-mediated accumulation of m6dA positively correlated with increased gene expression of the target genes, considering m6dA as an epigenetic mark of transcriptional activation. N6amt1 can control the gene expression in different ways, not only through N6-adenine DNA methylation, but also via histone H4 methylation (Metzger, Wang et al. 2019). Methylation mark on lysine 12 of histone H4 (H4K12me1) represents an activation mark, since the MTase activity of N6AMT1 positively regulated the expression of genes related to cell cycle progression, such as BIRC5, CDK1, OSGIN2, PHGDH, RTKN2, ODF2, STIL and VRK1 in prostate cancer cell line. Among neuronal activity-induced genes, especially BDNF exon IV mRNA expression was increased by the deposition of m6dA at BDNF P4 promoter. In this study, however, BDNF mRNA expression in the DRGs remained mostly unchanged, except for D11, when it was found to be upregulated in the neuropathic pain condition (Table 23). The expression of neither GPCR-related genes nor cell cycle-related genes did not match entirely with the data already published in the literature. Since the expression of genes is tissue-specific and can vary over time and the authors have employed study models different from the neuropathic pain model, there might be diverse factors involved in the regulation of expression of the above mentioned genes in the DRGs of CCI-induced mice. Moreover, gene expression changes induced by peripheral nerve injury and by the anti-TrkA or anti-NGF antibody treatment may differ a lot from the changes occurring in tumours.

In the present study, I examined the N6AMT1 gene expression changes in the DRG tissue measured by microarray technique. The neuropathic pain condition significantly induced the expression of N6AMT1, while the administration of each of the antibodies strongly attenuated its expression (Table 23). As a crucial prerequisite for further analysis of the N6AMT1 gene and proteins, I performed a validation of the microarray expression results by qRT-PCR. Microarray results were validated by qRT-PCR, confirming an upregulation of N6AMT1 in the DRG taken from a mouse undergoing a neuropathic pain protocol and a downregulation of the N6AMT1 after the antibody treatment of mice, as shown in Figure 17.

Before undertaking analysis of the DRG and, in order to set up the conditions for the analysis of the N6AMT1 expression, I decided to verify the expression of N6AMT1 in the human neuroblastoma cell line SH-SY5Y. SH-SY5Y cells represent a suitable cellular model

to investigate the signalling and the actions of NGF, as these cells are expressing both NGF receptors. The expression of N6AMT1 appears to be responsive to NGF signaling, since it has been modulated by anti-NGF and anti-TrkA antibodies in DRG. Therefore, I considered that SH-SY5Y cells might be a good system to analyse both N6AMT1 expression and its regulation by NGF. I was interested whether the activation of NGF signalling pathway could affect the expression of N6amt1 and Trmt112 at mRNA and protein level in SH-SY5Y cells. Thus, I treated SH-SY5Y cells with hNGF-WT at different time points (15 min, 30 min, 1 hour, 2 hours for qRT-PCR and 30 min, 1 hour, 2 hours for WB analysis) in order to evaluate the expression of N6amt1 and Trmt112 by qRT-PCR and WB. I prepared samples for qRT-PCR analysis and tried to optimize different antibodies for WB analysis (anti-Trmt112 ORB240172, anti-N6amt1 ORB341253). Out of several antibodies that I tested, from different commercial sources, I could not find an antibody giving a specific and convincing signal. Therefore, I could not set up the conditions for the Western blot analysis of N6AMT1 expression at the protein level in SH-SY5Y cells or in DRGs. This analysis will require better antibodies to be available or be developed.

In addition, I planned to perform experiments aimed to overexpress N6amt1 and Trmt112 proteins fused with GFP in SH-SY5Y cell line. Transfection of the human neuroblastoma cell line with Trmt112-GFP plasmid (OriGene) using the Lipofectamine protocol resulted efficient with a subset of positively transfected cells expressing Trmt112-GFP, while transfection of SH-SY5Y cells with N6amt1-GFP plasmid (RG217745, OriGene) using the same protocol failed due to a defective plasmid. Since the commercial N6amt1-GFP plasmid was unexpectedly missing a big portion of the backbone vector, GFP region included, I decided to subclone the intact N6amt1 gene into a GFP-containing backbone plasmid available in our laboratory. After a successful subcloning, I performed the multiplication of the new N6amt1-GFP plasmid in *E. coli* with subsequent extraction of the plasmid. Obtaining a functional plasmid is the first step before proceeding with overexpression studies that are planned as part of future goals.

In conclusion, following microarray analysis, N6AMT1 gene was selected as an interesting target for future studies, since I had observed changes in its expression profile at all studied time points. Interestingly, the expression of this gene behaved quite the opposite way from the other differentially expressed genes listed in the Table 22, with N6AMT1 being upregulated in the DRGs in the neuropathic pain condition and downregulated after the analgesic treatment. The microarray results were subsequently confirmed via qRT-PCR method. Given its multiple function as an epigenetic modifier, N6AMT1 can potentially represent an interesting target in pain therapies. Further studies will be needed in order to deepen the knowledge about the cellular function of N6AMT1, its role in neuropathic pain and its possible use as a therapeutic target. These studies should include the evaluation of protein expression and functional activity of N6AMT1 in the mouse DRGs and the elucidation of molecular mechanisms in neuropathic pain model.

Table 23. Expression profile of N6amt1, its binding partner TRMT112 and some potential N6amt1 targets in the DRG tissue of CCI-induced mice treated either with Saline, MNAC13 or αD11.

			Sal vs Naïve			MNAC13 vs Saline			αD11 vs Saline		
Gene symbol	Gene name	Gene ID	D3	D11	D24	D90	D11	D24	D90	D11	D24	D90
N6amt1	N-6 adenine-specific DNA methyltransferase 1	A_55_P2043762		2.89	2.43	1.54	-1.83	-1.16	-1.43	-2.73	-1.74	-1.27
Trmt112	tRNA methyltransferase 11-2	A_66_P127118	1.21									
Bdnf *	brain derived neurotrophic factor	A_55_P2036303		1.17								
Birc5 **	baculoviral IAP repeat-containing 5	A_55_P1983773	3.48	1.08				1.48		-1.47		
		A_55_P1983768	3.93	1.07			-1.17	1.76		-1.29		
Odf2 **	outer dense fiber of sperm tails 2	A_55_P1952414	-1.44									
Stil **	Scl/Tal1 interrupting locus	A_55_P1972792				-1.01		1.39				
Gpr160 ***	G protein-coupled receptor 160	A_55_P1956627	1.97	1.45						-1.09		
Pf4 ***	platelet factor 4	A_51_P441426	3.39					1.19				
Gpr68 ***	G protein-coupled receptor 68	A_55_P1956083	-1.57	-1.70	-1.94		1.19					1.43
Gpr179 ***	G protein-coupled receptor 179	A_55_P1962851	3.06	1.14				-1.35		-2.58		
Sstr5 ***	somatostatin receptor 5	A_66_P120347	-1.12									

The table depicts expression profile of N6amt1, Trmt112 and other genes, which have been reported in the literature as potential N6amt1 targets, analysed by Agilent microarray technique in our model of neuropathic pain and after the analgesic drug treatment. The N6amt1-mediated modifications, that regulate the expression of these genes, were reported/described as following:

* N6-adenine DNA methylation (m6dA) of neuronal activity-related genes, especially Bdnf P4 promoter, within infralimbic prefrontal cortex in the adult brain (Li, Zhao et al. 2019)

** histone H4 methylation on lysine 12 (H4K12me1) of genes encoding molecules involved in the cell cycle in PC-3M prostate cancer cells (Metzger, Wang et al. 2019)

*** N6-adenine DNA methylation (m6dA) of G protein-coupled receptor (GPCR)-related genes in human blood-derived DNA samples (Xiao, Zhu et al. 2018)

Figure 17. N6amt1 mRNA expression level quantified by qRT-PCR in DRGs at D90.

qRT-PCR analysis of N6amt1 expression from the DRG tissue of mice sacrificed at D90 post-surgery representing three different conditions: CCI-induced mice treated with Saline relative to the naïve (non-operated) control group; mice that underwent CCI procedure and were treated either with MNAC13 or αD11 relative to the Saline-treated group. N6amt1 mRNA expression was normalised against the expression of the housekeeper PPIA. The values of the relative N6amt1 expression were calculated using delta delta Ct method and expressed as a Log2 fold change. Data are presented as the means ± SD (n = 4). Symbol (**) indicates statistical differences ($p \leq 0.01$) observed between groups of mice treated with different substances.

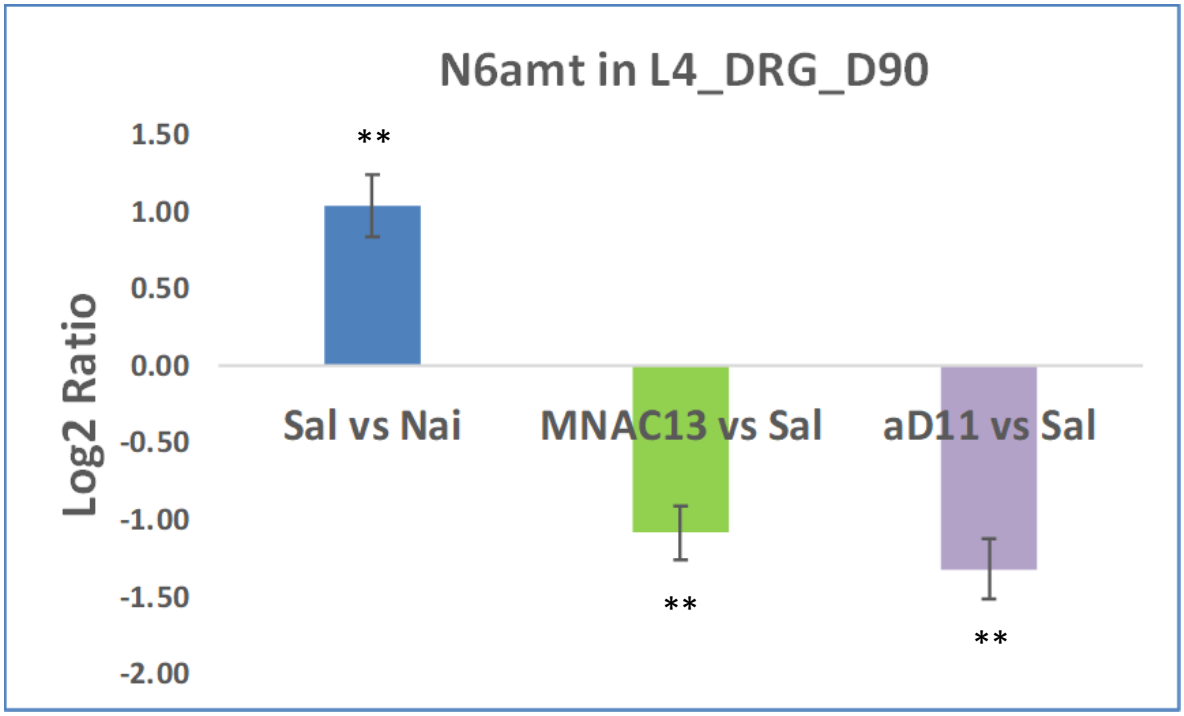

5 DISCUSSION

5.1 Need for novel analgesic drugs in pain therapies

Neuropathic pain is a debilitating condition with a negative impact on society and patients' life. Even though improvements have been made in the last decades in alleviating chronic pain symptoms, a satisfactory treatment of chronic pain states still remains a big therapeutic challenge in contrast to the beneficial outcome obtained in the successful treatment of acute pain. Considering the complex nature of neuropathic pain, it is of essential importance to identify molecular signals involved in the pain transduction pathway and to understand the molecular and cellular mechanisms that favour the onset and maintenance of the chronic stage in order to discover new pain relevant targets. One of the molecules known to be implicated in pain signalling is NGF. Besides acting as a nerve growth and differentiation factor during embryonic development, NGF plays an important role in modulation of nociception and regeneration from nerve injury.

Analgesic therapeutics currently used for treating chronic pain states are mostly inadequate and of limited use, with potential complications and considerable side effects. In some cases, they are poorly tolerated and might cause dependence. Therefore, there is an increasing need for the discovery of new painkillers with the purpose of developing new therapeutic strategies that would be more effective and accurate and do not present side effects common for the drugs currently employed in pain therapies. Anti-NGF directed therapy could satisfy these needs, since humanized monoclonal antibodies targeting NGF, such as tanezumab, fulranumab and fasinumab, have already shown promising results in preclinical studies and/or clinical trials, but are not without problems. Therefore, the development of new NGF-directed monoclonal antibodies represents a prospective approach in chronic pain therapy, even if several safety issues should be still resolved or optimized. For this reason, there is a high interest in the NGF signalling pathways, downstream of NGF itself. One of the therapeutic advantages of using monoclonal antibodies as pain modulators is that, due to their size, they do not cross the blood-brain barrier, hence they can be used for a more precise targeting of neural lesions and nociception in the PNS without having a direct effect on the CNS. This feature suggests that they might be acting more accurately on their peripheral targets, exhibiting less side effects when compared to small therapeutic molecules able to cross the BBB.

The monoclonal antibodies that have been developed in our laboratory, MNAC13 and αD11, are designed to block the TrkA receptor and sequester free NGF, respectively (Ugolini, Marinelli et al. 2007, Covaceuszach, Marinelli et al. 2012). Both monoclonal antibodies are targeting the NGF-signalling pathway, a pathway known to be involved in pain processing and nociception signalling. While MNAC13 is acting exclusively on the TrkA receptor, inhibiting its function and activation, αD11 has broader implications affecting not only TrkA-mediated signalling, but also p75 signalling by neutralizing their ligand NGF. Even though the mechanism of action of both antibodies is different, they have been proven to effectively reduce both acute and chronic pain in diverse animal models, therefore they might represent efficient therapeutic candidates with future applications in chronic pain therapies.

No study has investigated anti-NGF and anti-TrkA in a head-to-head comparison in preclinical chronic pain models. The study performed in this thesis is the first head-to-head comparison of this sort.

5.2 Evaluation of the anti-NGF and anti-TrkA induced analgesia in a murine model of neuropathic pain

There exist different animal models, such as chronic sciatic nerve constriction (loose sciatic ligation), partial sciatic nerve ligation (Seltzer's model), spinal roots ligation (SNL), spared nerve injury (SNL), for evaluating different neuropathic pain etiologies and manifestations, producing sensory deficits, such as allodynia, hyperalgesia and spontaneous pain. Some of these models study peripheral neuropathic pain mechanisms, while others focus more on central mechanisms. In my PhD study, I used the CCI model, consisting of the sciatic nerve ligature of mouse hind limb (Figure 2), which resembles closely human sciatica and thus, represents a suitable tool for studying peripheral nerve injury. Since previous reports about the analgesic effects of αD11 and MNAC13 (Ugolini, Marinelli et al. 2007, Covaceuszach, Marinelli et al. 2012) have not addressed the question of the duration of anti-hyperalgesia, but hinted at the possibility of a long lasting analgesic effect, I decided to expand the behavioural experiments for observing antibody-induced analgesia in order to assess how long the analgesic effect would last.

In the present study, I analysed the time course of analgesia of the two monoclonal antibodies, MNAC13 (anti TrkA) and αD11 (anti NGF), in the CCI model of neuropathic pain, and performed a head-to-head comparison of their efficacy. Interestingly, I observed that a repeated administration of a higher dose of MNAC13 and αD11 (100 µg/mouse/day, injected i. p. from D3 to D10), but not of a lower dose, induced a long-lasting analgesia, which, in case of MNAC13, persisted up to D130 post-CCI (Fig. 4 and Fig. 5). Results from the ELISA assay have shown that the residual antibody levels detected in the blood at D46 were below the threshold of pharmacological activity (Figure 8), estimated from the results at the lower dose experiments, yet the anti-hyperalgesia was still significant from D46 until D130 in the antibody-treated mice that underwent the CCI surgery, as demonstrated by behavioural studies (Fig. 5). Moreover, antibody-induced changes did not alter tissue integrity of the DRGs, which showed no damage to neurons and no change in microglia in the tissue, according to the immunohistochemical evaluation of DRGs in the antibody-treated CCI mice (Figure 9). To put it another way, neither antibody affected negatively the health status of DRGs, which, in turn, could have resulted in less sensitivity to pain stimuli.

In conclusion, the long-lasting phase of the analgesic effect observed after D46 in the CCI-induced mice treated with anti-TrkA or anti-NGF appears not to be due to the direct pharmacological effect of each antibody, nor due to a damage or loss of neurons in the DRG tissue.

All these observations raised the question about the mechanism of the antibody-induced analgesia in the neuropathic pain mouse model. Thus, I hypothesized that there might be a shift from the pharmacologically produced early analgesia to the non-pharmacologically produced late phase of the analgesia. Early analgesia might be caused by the pharmacological effect of both antibodies which are still present in the blood above the effective levels and contribute to a direct blocking of NGF-signalling. On the other hand, late analgesia might be a consequence of a non-pharmacological effect, when the concentration of the two antibodies in the blood is below the effective threshold, however, the two antibodies might have already triggered the activation of downstream signalling pathways which might lead to a new transcriptional program responsible for the long-lasting anti-hyperalgesic effect, possibly involving epigenetic alterations that maintain those transcriptional changes. This would be very important for the establishment of chronic pain.

5.3 Transcriptome profiling of pain-relevant areas of the nervous system

Since neuropathic pain and its pathogenic mechanisms are associated with gene expression changes, I investigated gene expression profile and analysed these changes by bioinformatics methods. I have used Agilent microarray technology and a subsequent bioinformatics analysis to identify differentially expressed genes (DEGs) and activated signalling pathways in association with CCI-induced chronic neuropathic pain and antibody treatment. In this study, I reported for the first time the transcriptome changes related to antibodies targeting the NGF signalling axis in the CCI-mice at different stages of neuropathic pain condition. The transcriptome profiling of tissues relevant to pain processing pathways, namely DRGs, SC and ACC, was assessed at different time points. The results of transcriptome analysis revealed that, in general, the induction of neuropathic pain leads mostly to downregulation of genes with respect to healthy non-operated mice, while the treatment with the antibodies induces an upregulation of genes in the operated mice at all studied time points. Not surprisingly, the DRG tissue presented the greatest number of DEGs, among all studied tissues, most likely because of the expression and direct availability of NGF receptors, TrkA and p75, in the DRGs. Hence, I decided to analyse more in detail the effects of both analgesic drugs on the peripheral nervous system. Three days after the CCI procedure, I identified a massive modulation of genes, with more than 8000 differentially expressed probes with a fold change greater than 2. At D11 post-surgery, a total of 5658; 2102 and 2841 DEGs in the Saline, MNAC13- and αD11-treated group, respectively, were screened. At D24 following the CCI, 6164 probes in the neuropathic pain model, 3526 probes in the MNAC13-treated group and 3318 probes in the αD11-treated group were found to be differentially modulated. Finally, at D90 post-operatively, I found 3086 DEGs in the Saline-treated group, 2648 and 2211 DEGs in the MNAC13- and αD11-treated mice, respectively.

A sink effect between the peripheral and the central pools of NGF?

Both antibodies, when injected i.p. in the mice (100 µg/mouse/day), do not pass across the BBB (Figure 11) and were not detected in the brain tissue at the time point when the antibody concentration in the serum reached its highest peak (D11) (Figure 8). Although MNAC13 and αD11 should not be able to act on the CNS directly, due to the BBB, the transcriptome analysis revealed significant changes in the gene expression present also in the CNS. Interestingly, I observed a lesser impact of the MNAC13 on the gene expression in the CNS in comparison with αD11. The central effect of αD11 antibody on the transcriptomic changes might be due to a *sink effect*. The basis of the sink effect is as following: if NGF exists in an equilibrium between a brain pool and a peripheral pool, it is possible that neutralising the peripheral pool with the anti-NGF antibody triggers the passage of NGF from the brain to the peripheral blood, thus depleting the brain pool. This phenomenon could be tested in future experiments. Investigating the presence of a sink effect leading to a reduction of central NGF levels upon peripheral sequestration of NGF by anti-NGF antibody administration, would be very important in light of the forthcoming approval of tanezumab by the FDA.

Are long-lasting effects on pain pathways intrinsic to the NGF signalling pathways in sensory neurons?

When studying the effects of NGF on nociceptive behaviour in the rat, Lewin *et al*. discovered that a single systemic injection of NGF (1mg/kg body weight) led to a profound heat and mechanical hyperalgesia, which persisted for several days. While heat hyperalgesia appeared within minutes, mechanical hyperalgesia became first apparent around 7 h after the

injection, becoming maximal and sustained at 24 h (Lewin, Ritter et al. 1993). Thus, the NGF-dependent mechanisms that underlie heat hyperalgesia seem to be different from those that underlie the mechanical hyperalgesia. However, transient elevation of NGF by a single systemic or local injection is unlikely to produce sustained TrkA activation, since this neurotrophin would be rapidly degraded by extracellular proteases, or washed away and diluted after injection. Therefore, transiently increased NGF levels might be sufficient to initiate a complex series of molecular events, some of which are local and fast, while others are global and long-lasting. All these diverse molecular changes initiated by NGF serve to promote hyperalgesia, lasting often for days or even weeks (Lewin, Lechner et al. 2014). There exist several hypotheses about the mechanisms underlying the NGF-induced long-lasting sensitization. Lindsay and Harmar postulated that NGF can induce long-lasting changes in gene expression in adult sensory neurons, and substance P and CGRP were among the first genes shown to be controlled by NGF (Lindsay 1988). Lewin and his colleagues argued that signalling endosomes and transduction complexes, the so-called transducosomes, play an important role in sustaining the long-lasting sensitization initiated by NGF, via the transport of novel, perhaps modulatory, proteins involved in the regulation of transduction at the peripheral endings of sensory neurons (Lewin, Lechner et al. 2014). Moreover, it has been well documented that epigenetic alterations produced after nerve injury, including histone modifications, DNA methylation, non-coding RNAs, and alteration of chromatin modifiers, have been shown to contribute to the generation and maintenance of neuropathic pain (Penas and Navarro 2018). Thus, one might speculate that the mechanisms through which NGF is producing long-lasting sensitization might include changes in gene expression, epigenetic modifications and other long-lasting cell-signalling alterations and that, these may be the same mechanisms that are targeted by MNAC13 and αD11 antibodies, responsible for long-lasting analgesia in our neuropathic pain model. These observations further validate the hypothesis that long-lasting transcription modulation mechanisms are an intrinsic part of NGF signalling and that these might be exploited in the analgesic action of anti-NGF and anti-TrkA and might subserve the mechanism of the effect described in the thesis. This hypothesis will provide the basis for future experiments.

5.4 Transcriptomic changes in the DRGs following CCI

In the current study, I investigated the mechanisms underlying the initiation and maintenance of neuropathic pain via transcriptome analysis of DRGs from mice that underwent the CCI surgery. To characterize important roles of DEGs in the neuropathic pain condition and to elucidate their regulatory networks in relation to chronic pain state, I performed bioinformatics analysis using Venn diagrams, g:Profiler toolset and functional enrichment analysis by DAVID GO tool.

I first identified a subset of mRNAs that were differentially expressed in the NP model with respect to healthy mice. The results suggest that these DEGs might play a role in the establishment of chronic pain. As demonstrated by DAVID GO analysis, the gene families or groups found to be downregulated in the CCI-mice during diverse stages of neuropathic pain progression were involved in cell junction, regulation of synaptic transmission, cation transport, ion/gated channel activity, NMDA receptor and neurogenesis, whereas the genes upregulated in the NP were related mostly to collagen alpha chain and vasculature development. Among the genes upregulated specifically at early stages of NP development (D3) highlight those involved in the regulation of the immune system and cholesterol biosynthetic process. Using KEGG and REACTOME, I further mapped the functional gene pathways whose transcription was altered and identified specific clusters involved in

glutamatergic and GABAergic synapse, calcium signalling pathway, transmission across chemical synapses, activation of NMDA, AMPA and GABA receptors, neurexins and neuroligins and axon guidance.

Collagen has been described to play an important role in nerve regeneration and peripheral nerve repair (Koopmans, Hasse et al. 2009). PNI (peripheral nerve injury) increases the proliferation rate of Schwann cells and macrophages and both cell types produce TGFβ, principle growth factor responsible for fibroblast recruitment and collagen formation after peripheral nerve injury. TGFβ regulates scar formation in the PNS in response to severe trauma to the nerve, by recruiting fibroblasts to the site of damage which, next to Schwann cells, contribute to the production of collagen. During the process of nerve regeneration there is long lasting gene expression of collagen types I, III and IV in the basal lamina of the proximal nerve stump. Collagen type I and III are believed to provide mechanical support for axonal growth and regeneration. The gene expression of collagen type-V on the contrary seems to be enhanced if axonal reinnervation is allowed (Koopmans, Hasse et al. 2009).

As reported by Lim *et al*. (Lim, Shi et al. 2014), blood-borne cells and molecules may play a role in the development of neuropathic chronic pain. Nerve injury triggers a long-lasting disruption of the blood-nerve barrier (BNB), a selectively permeable barrier that creates an immunologically and biochemically privileged space for peripheral axons and supporting cells. Activated macrophages and denervated Schwann cells secrete matrix metalloproteases that attack the basal lamina of endoneurial blood vessels, producing a disruption of the blood-nerve barrier. Injured axons cause hyperemia and swelling by releasing vasoactive mediators, such as CGRP, substance P, bradykinin and nitric oxide (Scholz and Woolf 2007). The breakdown of the BNB in neuropathic conditions permits access of blood-borne cells and molecules to the endoneurium, which in turn, take part in the local inflammatory cascade. Following nerve injury, VEGF is expressed by resident macrophages and fibrinogen, a clotting plasma protein, deposits in the nerve. Interestingly, nerve injury-triggered opening of the BNB allows the entry of analgesic molecules that typically cannot pass the BNB, including MNAC13 and αD11, which could have selective access to injured nerves over healthy tissues.

I also observed in the NP model an upregulation of genes encoding enzymes involved in the synthesis of cholesterol, steroids and other lipids, including CYB5R1 (Cytochrome B5 Reductase 1), CYB5R3 (Cytochrome B5 Reductase 3), CYP39A1 (Cytochrome P450 Family 39 Subfamily A Member 1), MVK (Mevalonate Kinase), MVD (Mevalonate Diphosphate Decarboxylase), enzymes catalysing ketogenesis, such as HMGCS1 (3-Hydroxy-3-Methylglutaryl-CoA Synthase 1) and HMGCS2 (3-Hydroxy-3-Methylglutaryl-CoA Synthase 2), together with SOAT2 (Sterol O-Acyltransferase 2), an enzyme involved in the production of cholesterol esters which are then stored as cytoplasmic lipid droplets inside the cell. Many of these enzymes are membrane-bound proteins localized in the endoplasmic reticulum. Cholesterol is a major lipid constituent of cell membranes in animals that modulates physical properties of these membranes. Changes in the membrane properties may affect the function of several membrane proteins, such as receptors and transporters, some of which might also play a role in the pathogenesis of neuropathic pain. Cholesterol also serves as an important precursor for the biosynthesis of steroid hormones, including sex hormones. Sex-dependent differences in pain both in humans and in animal models, are well established. Recently, estradiol, an important estrogen steroid hormone in both women and men, has been shown to reduce allodynia in female mice subjected to sciatic nerve ligature to similar extent as in male mice (Vacca, Marinelli et al. 2016).

Local immune and inflammatory processes also contribute to the initiation of chronic pain. Following primary sensory afferent injury, activated nociceptors and non-neural

inflammatory cells (macrophages, neutrophils, and lymphocytes) that reside within or infiltrate into the injured DRG release multiple inflammatory mediators, collectively referred to as the "inflammatory soup". They include a variety of signalling molecules, such as neurotransmitters, peptides (substance P, CGRP, bradykinin), eicosanoids and related lipids (prostaglandins, thromboxanes, leukotrienes, endocannabinoids), neurotrophins, cytokines, and chemokines, as well as extracellular proteases and protons. In particular, cytokines and chemokines, as part of the immune and inflammatory response, play an important role in the pathogenesis of pain. These factors can induce changes in neuronal gene expression, which lead to the abnormal electrical activity. TNFα is released by activated microglia and macrophages in the DRGs, interleukins are produced by leukocytes and ATP, a ligand for the P2X family of purino-receptors, is expressed in DRG nociceptive neurons.

Other clusters found to be significantly enriched in NP model were synaptic transmission, cation transport, gated/ion channel activity, NMDAR, AMPAR and GABA receptors. In neuropathic pain, there is a shift in ion channel composition in sensory afferents, leading to alterations in membrane excitation threshold. Transduction of stimuli at peripheral ends of sensory afferents is carried out by transient receptor potential channels, Na^+ channels, and ATP-sensitive receptors (Guha and Shamji 2016). Conduction of the signal through axons is maintained by voltage-gated sodium channels (Na_v), which are typically excitatory, and voltage-gated potassium channels (K_v). Neuronal hyperexcitability after peripheral afferent injury is promoted by K_v dysfunction and Na_v upregulation/overexpression and enhanced function. Resurgent Na^+ currents, which contribute to action potential propagation, are potentiated by inflammatory mediators, whereas K^+ currents, which restore membrane polarization, are mostly attenuated by these inflammatory compounds (Guha and Shamji 2016). Interestingly, glutamate contributes to peripheral sensitization and hyperexcitability by binding in a non-synaptic manner to AMPA and NMDA receptors, which mediate peripheral cell-cell interactions (e.g. upon release from immune cells) or autocrine regulation (upon release from sensory endings following TRPV1-mediated Ca^{2+} influx) (Gangadharan and Kuner 2013). Synaptic transmission between DRG nociceptors and spinal neurons is regulated and implemented by voltage-gated Ca^{2+} channels and postsynaptic glutamate receptors. Nerve injury is associated with an increase in presynaptic neurotransmitter release from nociceptors (Inquimbert, 2012). Increased presynaptic release of neurotransmitters and potentiation of neurotransmitter signalling in postsynaptic neurons lead to spinal LTP (Gangadharan and Kuner 2013).

In summary, CCI-associated transcriptomic changes in the DRGs appeared to be particularly relevant to several features associated with peripheral nerve injury, such as regulation of synaptic transmission, cation transport, ion/gated channel activity, NMDA receptor, calcium signalling pathway, regulation of immune system. These differentially expressed gene clusters include transcripts that have been clearly implicated in the pathology associated with neuropathic pain. Considering the identified molecular pathways, induction of neuropathic pain may alter the expression of genes that may mediate the above described alterations in biological functions.

5.5 Transcriptomic changes in the DRGs following anti-NGF and anti-TrkA treatment

Next, I analysed the effects of MNAC13 and αD11 mAb and the functional role that they might be playing in the response to peripheral nerve injury, since both antibodies induced transcriptome changes in the DRGs that could be detected long after the initial injury, suggesting that further bioinformatics analysis might help to elucidate transcriptional

mechanisms of the long-term analgesic effect of both antibodies associated to chronic pain alleviation.

Overall, MNAC13 induced a strong upregulation of genes relevant to myofibril, cell junction, regulation of synaptic transmission, cation transport, gated channel activity, NMDA receptor, neurogenesis at D11 and D90 as demonstrated by DAVID GO analysis, with slightly different group of genes upregulated at D24, namely immune system development, chemotaxis and chemokine activity. Interestingly, the functional enrichment analysis revealed that most of the gene clusters that were upregulated in the MNAC13-treated group appeared to be downregulated in the DRGs of CCI-mice. In general, GABAergic synapse, glutamatergic synapse and calcium signalling pathway were among the most frequently modulated pathways according to KEGG and REACTOME.

Regarding gene clusters modulated specifically at a certain experimental time point, DAVID GO analysis uncovered a significant downregulation of collagen alpha chain related genes at D11 in the MNAC13-treated CCI mice, reflecting the fact that excessive collagen formation can act as mechanical barrier after peripheral nerve injury (PNI), since scar formation delays and limits nerve regeneration. The KEGG/REACTOME analysis confirmed these findings, with assembly of collagen fibrils, collagen chain trimerization, collagen biosynthesis and degradation of ECM being among the most prominent pathways. Interestingly, the same Collagen alpha chain DAVID GO term was found to be upregulated in the NP model.

As shown by KEGG and REACTOME analysis of DRG transcriptome from CCI-mice treated with MNAC13, at D24, immune system-related pathways were dominant (neutrophil degranulation and B cell receptor signalling pathway) together with signalling by Rho GTPases (RHO GTPases activate NADPH oxidases); platelet homeostasis and platelet activation; leukocyte transendothelial migration; phagosomes and ROS and RNS production in phagocytes; whereas at D90, the pathways related to SLC-mediated transmembrane transport and inwardly rectifying K^+ channels were highlighted.

The following general observations were made after performing the bioinformatics analysis of the CCI-induced mice treated with αD11. Downregulated gene clusters were found mostly at D11 and D24, with the following significantly enriched GO terms: somatodendritic compartment, secretion and exocytosis, extracellular exosomes, neurogenesis. GO terms related to downregulated genes specifically enriched at D11 include PKC-like, phorbol ester/diacylglycerol binding, Pleckstrin homology domain, GTPase activator activity, voltage-gated potassium channel complex, C2 calcium-dependent membrane targeting, regulation of ion transmembrane transport and those related to upregulated genes include myofibril, cell motility, regulation of phosphate metabolic process, and regulation of MAPK cascade.

At D24 and D90, I found among upregulated gene clusters partially overlapping GO terms in the αD11-treated group, including synaptic signalling, somatodendritic compartment, ion/gated channel activity, ion channel complex, regulation of phosphate metabolic process, whereas some GO terms were specific for D24, such as learning or memory, regulation of secretion, cell motility, positive regulation of neurogenesis, synaptic membrane, dendritic spine, postsynaptic density; and other GO terms were found to be specific for D90, such as cation transmembrane transport and myofibril.

Myofibrils are made of long proteins including actin, myosin, and titin, and other proteins organized into thick and thin filaments called myofilaments, constituting muscle fibres. However, the proteins the myofibrils are composed of might be involved in the process of peripheral nerve repair and regeneration. For instance, actin cytoskeleton has been

associated with the extension and directional elongation of axon within the axonal growth cone (Wang, Shan et al. 2018). In addition, extracellular application of myosin II or skeletal muscle extract to neurons resulted in a robust increase in the number of axons initiated by each neuron or the number of survival neurons (Valmier, Mallie et al. 1993, Silver and Gallo 2005).

KEGG and REACTOME analysis mainly confirmed previous results obtained by DAVID GO functional enrichment analysis, with calcium signalling pathway, MAPK signalling pathway, signalling by Rho GTPases, cytokine signalling in immune system, muscle contraction, axon guidance and potassium channels significantly enriched at D11; axon guidance, glutamatergic and GABAergic synapse, transmission across chemical synapses, potassium channels, platelet activation and hemostasis predominant at D24 and lastly, transmission across chemical synapses, neurotransmitter release cycle, muscle contraction, glycogen metabolism, glutamatergic and GABAergic synapse, calcium signalling pathway and MAPK signalling pathway prevailing at D90.

The above mentioned DAVID GO functional enrichment analysis revealed that several GO terms are in common in the group of CCI-induced mice and the antibody-treated group and, moreover, these GO terms were regulated in the opposite direction in these two groups, suggesting that the antibody treatment might be targeting the same molecular pathways that are involved in the NP establishment. Thus, I postulated a hypothesis that the changes in the gene expression induced by the chronic pain state might be, at least in part, reversed upon the antibody treatment. To answer the question whether the gene expression dysregulated in neuropathic pain might be reversed by the treatment with both painkillers, I conducted a systemic comparative analysis of the transcriptomic data between CCI-induced mice and MNAC13 and αD11-treated groups across different stages of neuropathic pain progression. I found that up to 30-50% of genes found to be dysregulated in neuropathic pain appeared to be reversed by antibody treatment. The bioinformatics analysis revealed that these functional gene clusters were involved in sarcomere, synaptic signalling and regulation of synaptic plasticity, somatodendritic compartment, cation transmembrane transport, cell motility, regulation of leukocyte differentiation, symporter activity, cellular chemical homeostasis, leukocyte cell-cell adhesion, positive regulation of MAPK cascade, regulation of actin cytoskeleton organization, learning, positive regulation of hemopoiesis, Src homology-3 domain, secretion by cell.

5.6 N6amt1 emerges as a new potential pharmacological target in pain therapies

Analysing genes whose expression is regulated by analgesic drugs might be useful for the screening of new candidate therapeutic targets for the treatment of NP. Thus, I decided to focus on the DEGs that were shown to be dysregulated in all experimental time points in neuropathic pain state and whose expression profile appeared to be reversed by the treatment with both antibodies. Many of the genes fulfilling these criteria (see extended table 22 in the Appendix) have been already reported to be associated with neuropathic pain. There were some genes, however, not clearly implicated in the development of NP, one of them being N6amt1. For this reason, I have selected N6amt1 as a candidate gene for future studies (Table 22). N6amt1 represents an interesting protein to study which deserves more attention, given its multiple role in regulating diverse cellular and molecular processes, as reported in the literature.

Figaro *et al*. demonstrated that human N6AMT1 interacts with TRMT112 forming a stable heterodimeric complex which methylates the eRF1 translation factor substrate on the glutamine residue in the GGQ motif (Figaro, Scrima et al. 2008). Glutamine methylation is a very subtle post-translational modification, which only slightly affects substrates chemical properties. N5-Gln methylation of eRF1 changes the properties of the catalytic pocket. eRF1

is known to catalyse polypeptide release from the ribosome during the translation termination and the lack of eRF1 methylation might diminish stop codon read-through, affecting the accuracy/efficiency of translation termination. N6AMT1 alone was unable to methylate eRF1 and its association with TRMT112 not only increased methylation activity of N6AMT1 but was also essential for its solubilisation (Figaro, Scrima et al. 2008). Interestingly, N6AMT1, together with fibrillarin, are the only two proteins with a glutamine-specific protein methyltransferase activity described in the human proteome so far (Kusevic, Kudithipudi et al. 2016).

Several years later, the spectrum of N6AMT1/Trmt112 targets for glutamine-specific protein methylation was broadened thanks to the study led by Kusevic *et al*. (Kusevic, Kudithipudi et al. 2016). The study was based on the use of protein arrays and the authors initially identified 138 putative novel N6AMT1 substrates in the human proteome (Kusevic, Kudithipudi et al. 2016). Methylation mediated by N6AMT1 was subsequently tested *in vitro* on peptide arrays containing synthesized peptides with the target glutamine in the center. They found 49 methylated peptide substrates with an activity comparable with eRF1, and 76 of the putative substrates showed a reduced but clearly detectable activity. Most of the highly methylated peptide substrates harboured an Arg at the +7 position, and an Ser, Arg, or Gly at the +1 position. *In vitro* methylation of 11 out of the 20 tested protein domains was confirmed also at the protein level. Four of them displayed a strong methylation comparable with eRF1 (CHD5, NUT, ANKRD34A, ABCA2) and seven protein domains were methylated to a lower extent (GHDC, ZSCAN10, RPP1, ASH1L, ARGEF10, TGFB3, AMPD2). Methylation status of two of these proteins, CHD5 and NUT, was validated *in vivo* in HEK293 cells using methyl-glutamine specific antibody (Kusevic, Kudithipudi et al. 2016).

Another interesting N6AMT1/TRMT112 protein target, histone H4, came out from research conducted by Metzger *et al*., studying the methylation of different histones in human prostate cancer cells (Metzger, Wang et al. 2019). Among all histones tested, N6AMT1-TRMT112 heterodimer monomethylated exclusively histone H4 at lysine 12 both *in vitro* and *in vivo*. Interestingly, siRNA-mediated knockdown of N6AMT1 significantly reduced the proliferation of human prostate tumour cell lines, without affecting the proliferation of non-cancer cell lines (HEK293 or C2C12) nor of several non-prostate human tumour cell lines (HepG2, NGP, HCT116$^{-/-}$), indicating that the control of tumour cell proliferation was cell type specific. Upon N6AMT1 depletion, the authors detected not only a decrease in H4K12me1 levels at promoters of direct target genes, but also an increase in levels of the repressive H4K20me3 at transcription start sites (TSSs). Furthermore, ChIP-seq analysis revealed a significant enrichment of N6AMT1-TRMT112 collocations at gene promoters in PC-3M cells, suggesting their role in transcriptional regulation. Subsequent gene enrichment analysis of RNA-seq data uncovered genes encoding proteins involved in cell cycle regulation, such as BIRC5 (baculoviral IAP repeat–containing 5), CDK1 (cyclin-dependent kinase 1), ODF2 (outer dense fiber of sperm tails 2), OSGIN2 (oxidative stress–induced growth inhibitor family member 2), PHGDH (phosphoglycerate dehydrogenase), RTKN2 (rhotekin 2), STIL (centriolar assembly protein), and VRK1 (vaccinia-related kinase 1) (Metzger, Wang et al. 2019).

Interestingly, N6AMT1 modulates gene expression not only through the methylation of histone H4 at Lys12, but also via direct methylation of DNA at the deoxyadenosine. So far, only two papers led by Li and Xiao have focused on the role of N6AMT1 in the N6-adenine DNA methylation. The former studied the function of N6AMT1 in 6mA modification during fear extinction learning, whereas the later studied the 6mA distribution in blood lymphocytes and cancer cells

Li *et al*. observed a significant increase in m6dA deposition and in N6AMT1 mRNA and protein levels both in primary cortical neurons in response to KCl-induced depolarization and in the adult brain (infralimbic prefrontal cortex) following fear extinction learning, indicating that N6AMT1 expression was activity-dependent (Li, Zhao et al. 2019). m6dA deposition in response to fear extinction learning was significantly increased within the promoter (at a site +1bp downstream of the TSS and +4bp from the start codon), 5´ UTR (untranslated region) and coding regions (CDS) and was mostly enriched at sites containing GATC motif. Moreover, the authors found a positive correlation between m6dA deposition and gene expression in neurons selectively activated by fear extinction learning, suggesting that dynamic G(m6dA)TC site modification might play an important role in the epigenetic regulation of experience-dependent gene expression in the adult brain. Interestingly, the overexpression of N6amt1 led to a global increase in m6dA within primary cortical neurons, whereas knockdown of N6amt1 caused a reduction in the accumulation of m6dA. A gene ontology analysis revealed significant extinction learning-induced gene clusters, with synapse being the most significant cluster, including genes such as Bdnf, Homer2, Gabrr3, Gabrd and Rab3a. Extinction training led to an increase of m6dA accumulation at a GATC site immediately downstream of the TSS of the Bdnf P4 promoter and an increase in N6amt1 occupancy adjacent to this GATC site, where N6amt1 binding site is located. Bdnf exon IV is known to be highly activity-dependent and is directly involved in the formation of fear extinction memory. The proximal promoter region of another plasticity-related gene, Rab3a, also exhibited a pattern of epigenetic modification similar to that of Bdnf P4 locus (Li, Zhao et al. 2019).

In another study, Xiao *et al*. have observed that DNA 6mA modification was extensively present in the human blood-derived DNA samples, as detected by single-molecule real-time (SMRT) sequencing (Xiao, Zhu et al. 2018). SMRT sequencing identified a broad 6mA genomic distribution, with a higher density of the 6mA modification sites (6mA/A) in the mitochondria genome and across autosomal chromosomes. [G/C]AGG[C/T] has been identified as the most prevalent motif sequence being associated with 6mA modification sites in human genome DNA. 6mA modification sites were highly enriched in the coding regions, around the exon regions from TSS to TTS, especially around TTSs. 6mA abundance positively correlated with RNA expression level, as measured by 6mA-IP-seq, indicating that 6mA sites mark actively transcribed genes in human cells. N6AMT1 was identified as the methyltransferase responsible for DNA 6mA modification in the human genome, with the conserved NPPY motif being important for its catalytic function. In an *in vitro* methylation assay, the recombinant N6AMT1-Flag was able directly and efficiently methylate four synthetic DNA oligonucleotide substrates. In addition, in an *in vivo* experiment, silencing of N6AMT1 in MHCC-LM3 cells decreased the DNA 6mA modification level, while overexpression of N6AMT1 increased the DNA 6mA modification level in a dose-dependent manner, without affecting RNA m6A levels. Thus, N6AMT1 methyltransferase mediated the addition of 6mA in human genomic DNA, but not in RNA. Functional enrichment analysis on genes with the highest 6mA density in transcribed regions revealed GPCR family as a significantly enriched GO category (Xiao, Zhu et al. 2018).

Finally, Woodcock *et al*. (2019) conducted a comparative study regarding *in vitro* MTase activities of N6AMT1 on the three potential substrates, analysing changes in DNA adenine, histone H4 lysine and eRF1 glutamine methylation (Woodcock, Yu et al. 2019). For this purpose, they used a purified recombinant human N6AMT1-TRMT112 heterodimer complex and potential enzyme substrates: short DNA double-stranded oligos containing N6AMT1 recognition sequence, peptide derived from eRF1 (residues 179-193) or histone H4 (residues 1-20). They observed a MTase activity of N6AMT1-TRMT112 complex on eRF1-

derived peptide and a more reduced activity on histone H4 at the condition of pH8. Mass spectrometry analysis confirmed full methylation of glutamine-containing eRF1 peptides and a residual methylation of H4 peptide substrates. After increasing the pH to 10.5, since most histone lysine MTases have optimal *in vitro* activity at approximately pH10, a significant increase in lysine H4 peptide methylation was observed, indicating that the deprotonation of the target nitrogen in the lysine residue by high pH is preferred for methylation to occur. However, at the high pH, the MTase activity of N6AMT1-TRMT112 complex on glutamine-containing eRF1 peptide was significantly reduced. Interestingly, Woodcock et al. was not able to detect adenine methylation on the DNA oligo substrates *in vitro* in the presence of N6AMT1-TRMT112 heterodimer (Woodcock, Yu et al. 2019). It is worth to mention that the authors did not investigate whether the DNA adenine methylation might occur in the absence of Trmt112, with N6AMT1 only, since it has been previously reported that N6AMT1 alone was sufficient to methylate the adenine in DNA *in vitro* (Xiao, Zhu et al. 2018). These findings raise the possibility that N6AMT1 protein alone and in complex with its partner TRMT112 recognize different substrates and, depending on whether the heterodimer complex is formed or not, N6amt1 may possess protein or DNA methyltransferase activities, respectively (Leetsi, Ounap et al. 2019).

In the current study, N6amt1 was found to be upregulated in the DRGs of the CCI-induced mice and downregulated after the analgesic drugs treatment, indicating that this gene might be involved in pain modulation and, in addition, it may represent a target for antibody-mediated events leading to analgesia. I validated the expression of N6amt1 mRNA in the DRGs in the murine NP model using qRT-PCR method (Figure 17). Further studies will help to elucidate the role that N6amt1 plays in neuropathic pain. The follow-up experiments should characterize N6amt1 expression at protein level by WB and its subcellular localisation in the DRGs by IF. The immunofluorescence technique can also be used to investigate whether N6amt1 colocalises with any of the previously reported protein targets, e.g. eRF1 at translational sites (not only in the somata of the sensory neurons, but also at sites of local translation at the central synapses and at peripheral nerve endings in the skin) or histone H4 in the nucleus. It could be useful to confirm the above-mentioned protein interactions by Co-IP assays. Not only N6amt1 interactions with its known targets, but the identification of new protein targets utilising protein microarrays and identification of protein interactions via peptide SPOT arrays could also be investigated. Evaluating the interaction with its cofactor Trmt112 is of high importance as well, since N6amt1 is capable of acting as either DNA or protein methyl-transferase depending on the N6amt1-Trmt112 complex formation. N6amt1 alone is able to methylate the adenine in DNA, whereas it can methylate proteins only when being in complex with Trmt112. Hence, determining by WB and Co-IP assays the proportion of unbound N6amt1 and heterodimer N6amt1-Trmt112 complex to the total amount of N6amt1 present in different cellular compartments could shed more light into the diversified function of N6amt1.

In vivo experiments should include behavioural testing of mechanical allodynia in the CCI-mice, whose DRGs were injected with shRNA against N6amt1. Because I observed in this study a downregulation of N6amt1 in the MNAC13- and αD11-treated group, I would expect that shRNA-mediated N6amt1 silencing would induce pain relief in the CCI-mice. Measuring changes in the DNA and/or protein methylation status in the DRGs in the neuropathic pain model, after MNAC13 and αD11 treatment and after the injection of shRNA-N6amt1 is of high interest. 6mA-IP-seq could be employed to identify in the DRGs new N6-adenine DNA methylation sites relevant for neuropathic pain signalling. The results obtained by m6A-IP-seq could be validated by 6mA-IP qPCR and DNA dot blotting using anti-6mA antibody. Apart from the DNA methylation, the protein methylation status of eRF1, H4 and other putative

targets in the NP model could also be evaluated via peptide methylation assays using radioactively labeled [methyl-3H]AdoMet.

Next step would consist of functional studies *in vitro* in order to better understand the molecular mechanism and function of N6amt1. For this purpose, I could employ dissociated sensory neurons culture from DRGs isolated from CCI-mice, cell line with permanently deleted gene (CRISPR-Cas9 mediated KO) and cell lines with either stable N6amt1 overexpression (transfected plasmid with recombinant N6amt1-GFP) or transient N6amt1 silencing (siRNA directed against N6amt1). As described for *in vivo* experiments, the methylation status could be evaluated in these cell lines as well. Finally, since N6amt1 might also participate in the regulation of translation via eRF1 methylation, I could utilise a global analysis of cellular protein translation by pSILAC (pulsed stable isotope labeling by amino acids in cell culture) which directly provides information about translation rates on a proteome-wide scale (Schwanhausser, Gossen et al. 2009). This method could potentially identify proteins that might be translationally regulated by N6amt1 activity.

Figure 18. The scheme of future experiments designed for studying N6amt1 function.

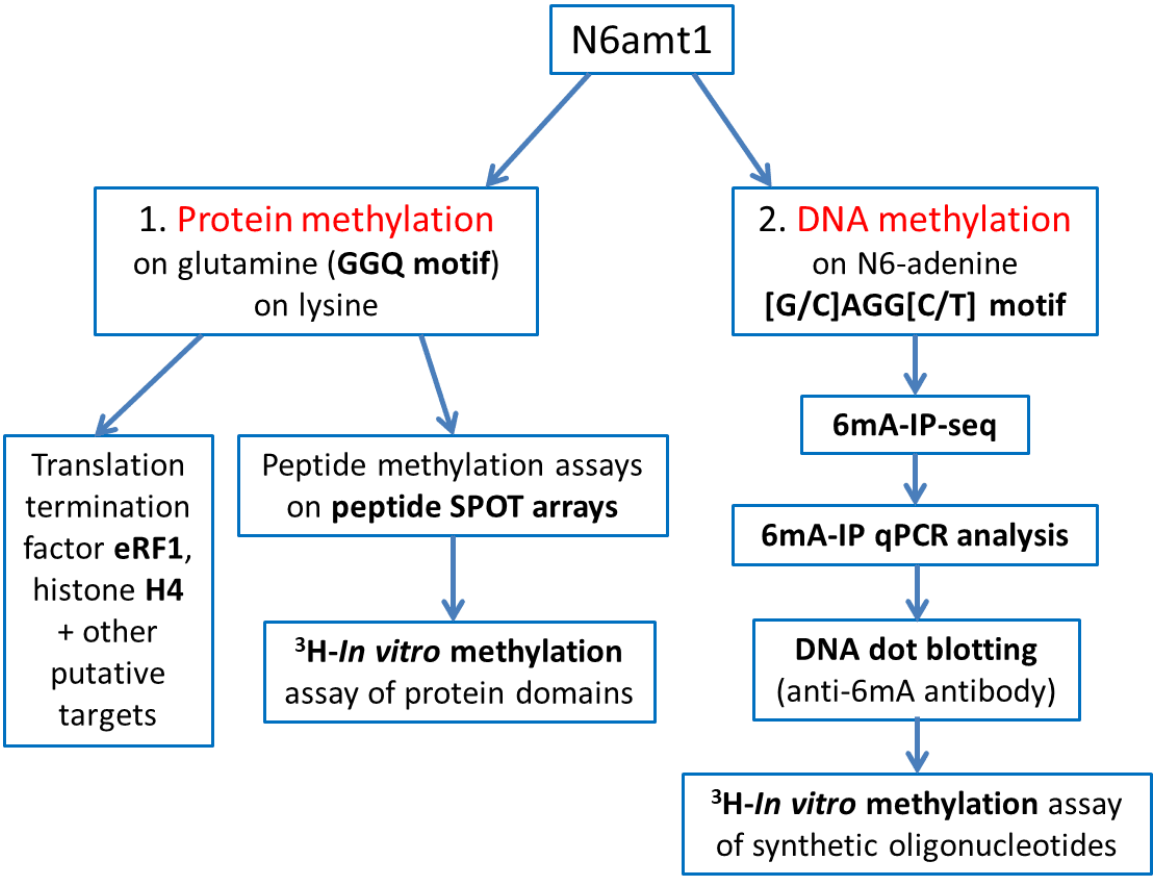

6 SUMMARY

- As demonstrated by behavioural studies, the treatment with either αD11 or MNAC13 (100 µg/mouse/day injected i.p. from D3 to D10) significantly attenuated mechanical hypersensitivity in the CCI mice with a surprisingly long-lasting analgesic effect which, in case of MNAC13, persisted up to D130 post-operatively.

- The pharmacokinetics profile of the antibodies measured by ELISA assay has shown that after reaching its peak at D11, the antibody levels in the serum have gradually decreased, with the concentration at D46 being lower than the pharmacologically active dose. Curiously, the behavioural tests performed at D46 and in the late chronic phase clearly demonstrated the presence of anti-hyperalgesia in the antibody-treated CCI mice. Of note, the antibody-induced analgesia did not alter the health status of DRGs which presented no apparent damage nor disconnection of neurons in the tissue.

- Both pain-specific and antibody-specific gene expression fingerprinting in the murine NP model have been identified and described in the CNS (ACC and SC) and PNS (DRGs). Transcriptome profiling of tissues relevant to the pain transduction pathway has revealed that both antibodies induced massive gene expression changes in the PNS. The two antibodies modulated different genes peripherally in the DRGs, showing only a partial overlap. MNAC13 had a lesser impact on the modulation of genes in the CNS in comparison to αD11.

- Both antibody treatments were able to reverse 30-50% of the DEGs in the DRG, with the major inversion observed at D24 and D90, providing evidence for their role in the attenuation of neuropathic pain. These “cured” genes were mainly associated with synaptic signaling, regulation of synaptic plasticity, somatodendritic compartment, ion/cation transmembrane transport, ion channel complex and channel activity.

- Following microarray analysis, N6AMT1 has been selected as an interesting candidate gene, since I observed changes in its expression profile throughout the study, with the gene being upregulated in the DRGs in the neuropathic pain condition and downregulated after the analgesic treatment. The expression of N6AMT1 has been validated by qRT-PCR. Given its multiple functions as an epigenetic modifier, N6AMT1 could potentially represent a novel target in pain therapies.

- The long-lasting analgesic effect induced in the CCI mice by anti-TrkA and anti-NGF led me to speculate about the possible molecular mechanisms behind the late analgesia, which might be a consequence of the activation of downstream signalling pathways by the two antibodies leading to a new transcriptional program responsible for the long-lasting anti-hyperalgesic effect, probably mediated by epigenetic modifications.

7 FUTURE PERSPECTIVES

The aim of future studies will be to evaluate the possible role of epigenetic mechanisms in mediating the long-lasting analgesia induced by both anti-NGF and anti-TrkA treatments in the CCI mice. The epigenetic alterations, including histone modifications (histone acetylation and methylation), DNA methylation, diverse non-coding RNAs and chromatin re-modelling (alteration of chromatin modifiers) have been implicated in the induction and maintenance of neuropathic pain. An eventual contribution of these epigenetic processes to the anti-NGF and anti-TrkA mediated long-term analgesia in the DRGs should also be addressed by following these steps:

- To examine changes in the DNA methylation, histone lysine methylation, global histone acetylation and alterations of other chromatin modifiers both in CCI mice and in antibody-treated mice through DNA methylation-seq and ChIP-seq.

- To investigate whether these epigenetic alterations correlate with the transcriptomic changes occurring in our experimental model. Intersection of epigenomic and transcriptomic data might reveal an association between the gene expression fingerprinting specific for each antibody and the corresponding changes in the epigenomics.

- To identify the so-called “cured” genomic regions, which represent regions within the genome that have been epigenetically altered by nerve injury and, concurrently, whose epigenetic status has been reversed following the analgesic drugs treatment.

- To employ epigenetic drugs and other small molecule inhibitors interfering with epigenetic modifiers, in order to see how they affect the pathogenesis of chronic pain and the analgesic effect of both anti-NGF and anti-TrkA.

All these experiments might provide a valuable insight into understanding epigenetic mechanisms in chronic pain. Furthermore, they might help to identify new epigenetically relevant targets that are regulated by anti-NGF and anti-TrkA and, that could be proposed in the future as new pharmacological targets.

8 APPENDIX

Supplementary table 1. KEGG and REACTOME pathways significantly enriched in CCI-induced mice at D3 post-surgery.

The colors for log scale:

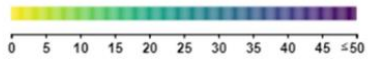

KEGG		stats	
Term name	Term ID	p_{adj}	$-\log_{10}(p_{adj})$ 0 ≤16
Glutamatergic synapse	KEGG:04724	7.100×10^{-8}	
Nicotine addiction	KEGG:05033	2.559×10^{-5}	
Morphine addiction	KEGG:05032	3.591×10^{-5}	
Circadian entrainment	KEGG:04713	3.881×10^{-5}	
Amphetamine addiction	KEGG:05031	9.394×10^{-5}	
GABAergic synapse	KEGG:04727	9.910×10^{-5}	
Retrograde endocannabinoid signaling	KEGG:04723	2.511×10^{-4}	
Long-term potentiation	KEGG:04720	3.248×10^{-4}	
Neuroactive ligand-receptor interaction	KEGG:04080	7.750×10^{-4}	
Cocaine addiction	KEGG:05030	1.583×10^{-3}	
Dopaminergic synapse	KEGG:04728	2.525×10^{-3}	
Calcium signaling pathway	KEGG:04020	6.917×10^{-3}	
Long-term depression	KEGG:04730	9.722×10^{-3}	
Amyotrophic lateral sclerosis (ALS)	KEGG:05014	1.853×10^{-2}	
Synaptic vesicle cycle	KEGG:04721	2.336×10^{-2}	
Insulin secretion	KEGG:04911	2.547×10^{-2}	

REAC		stats	
Term name	Term ID	p_{adj}	$-\log_{10}(p_{adj})$ 0 ≤16
Neuronal System	REAC:R-MMU-112316	2.027×10^{-13}	
Transmission across Chemical Synapses	REAC:R-MMU-112315	4.610×10^{-9}	
Neurotransmitter receptors and postsynaptic signal transmission	REAC:R-MMU-112314	2.366×10^{-8}	
Protein-protein interactions at synapses	REAC:R-MMU-6794362	7.961×10^{-8}	
Neurexins and neuroligins	REAC:R-MMU-6794361	1.739×10^{-6}	
Activation of NMDA receptors and postsynaptic events	REAC:R-MMU-442755	9.179×10^{-4}	
Unblocking of NMDA receptors, glutamate binding and activation	REAC:R-MMU-438066	1.419×10^{-3}	
GABA receptor activation	REAC:R-MMU-977443	3.128×10^{-3}	
Transport of inorganic cations/anions and amino acids/oligopeptides	REAC:R-MMU-425393	3.592×10^{-3}	
Activation of AMPA receptors	REAC:R-MMU-399710	4.143×10^{-3}	
Activation of Ca-permeable Kainate Receptor	REAC:R-MMU-451308	6.701×10^{-3}	
Ionotropic activity of kainate receptors	REAC:R-MMU-451306	6.701×10^{-3}	
Opioid Signalling	REAC:R-MMU-111885	6.986×10^{-3}	
Synaptic adhesion-like molecules	REAC:R-MMU-8849932	1.114×10^{-2}	
EPH-Ephrin signaling	REAC:R-MMU-2682334	1.184×10^{-2}	
Neurotransmitter release cycle	REAC:R-MMU-112310	1.184×10^{-2}	
Neurotransmitter uptake and metabolism In glial cells	REAC:R-MMU-112313	1.246×10^{-2}	
Astrocytic Glutamate-Glutamine Uptake And Metabolism	REAC:R-MMU-210455	1.246×10^{-2}	
Activation of kainate receptors upon glutamate binding	REAC:R-MMU-451326	1.246×10^{-2}	
Glutamate binding, activation of AMPA receptors and synaptic plasticity	REAC:R-MMU-399721	1.687×10^{-2}	
Trafficking of AMPA receptors	REAC:R-MMU-399719	1.687×10^{-2}	
Glutamate Neurotransmitter Release Cycle	REAC:R-MMU-210500	1.838×10^{-2}	
Cysteine formation from homocysteine	REAC:R-MMU-1614603	1.838×10^{-2}	
Ca-dependent events	REAC:R-MMU-111996	4.484×10^{-2}	
Bicarbonate transporters	REAC:R-MMU-425381	4.837×10^{-2}	

Supplementary table 2. KEGG and REACTOME pathways significantly enriched in CCI-induced mice at D11 post-surgery.

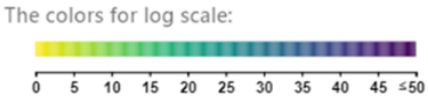

KEGG		stats	
Term name	Term ID	p_{adj}	$-\log_{10}(p_{adj})$ 0 ≤16
Glutamatergic synapse	KEGG:04724	5.472×10^{-3}	
GABAergic synapse	KEGG:04727	6.596×10^{-3}	
Nicotine addiction	KEGG:05033	6.596×10^{-3}	
Circadian entrainment	KEGG:04713	6.596×10^{-3}	
Synaptic vesicle cycle	KEGG:04721	6.596×10^{-3}	
Amphetamine addiction	KEGG:05031	7.169×10^{-3}	
Morphine addiction	KEGG:05032	2.602×10^{-2}	
Proximal tubule bicarbonate reclamation	KEGG:04964	2.602×10^{-2}	
Neuroactive ligand-receptor interaction	KEGG:04080	3.215×10^{-2}	
Cocaine addiction	KEGG:05030	3.928×10^{-2}	

REAC		stats	
Term name	Term ID	p_{adj}	$-\log_{10}(p_{adj})$ 0 ≤16
Neuronal System	REAC:R-MMU-112316	1.237×10^{-5}	
Transmission across Chemical Synapses	REAC:R-MMU-112315	1.403×10^{-4}	
Neurotransmitter release cycle	REAC:R-MMU-112310	1.403×10^{-4}	
Activation of AMPA receptors	REAC:R-MMU-399710	8.616×10^{-4}	
Neurotransmitter receptors and postsynaptic signal transmission	REAC:R-MMU-112314	3.071×10^{-3}	
Trafficking of AMPA receptors	REAC:R-MMU-399719	6.826×10^{-3}	
Glutamate binding, activation of AMPA receptors and synaptic plasticity	REAC:R-MMU-399721	6.826×10^{-3}	
Astrocytic Glutamate-Glutamine Uptake And Metabolism	REAC:R-MMU-210455	6.826×10^{-3}	
SLC-mediated transmembrane transport	REAC:R-MMU-425407	6.826×10^{-3}	
Transport of inorganic cations/anions and amino acids/oligopeptides	REAC:R-MMU-425393	6.826×10^{-3}	
Neurotransmitter uptake and metabolism In glial cells	REAC:R-MMU-112313	6.826×10^{-3}	
Cysteine formation from homocysteine	REAC:R-MMU-1614603	1.601×10^{-2}	
Protein-protein interactions at synapses	REAC:R-MMU-6794362	2.059×10^{-2}	
Peptide ligand-binding receptors	REAC:R-MMU-375276	2.146×10^{-2}	
Trafficking of GluR2-containing AMPA receptors	REAC:R-MMU-416993	2.728×10^{-2}	
GPCR ligand binding	REAC:R-MMU-500792	3.156×10^{-2}	
Acetylcholine Neurotransmitter Release Cycle	REAC:R-MMU-264642	3.823×10^{-2}	
Ion homeostasis	REAC:R-MMU-5578775	3.823×10^{-2}	
Potassium transport channels	REAC:R-MMU-1296067	3.823×10^{-2}	
Axonal growth inhibition (RHOA activation)	REAC:R-MMU-193634	4.961×10^{-2}	

Supplementary table 3. KEGG and REACTOME pathways significantly enriched after MNAC13 treatment in CCI-induced mice at D11 post-surgery.

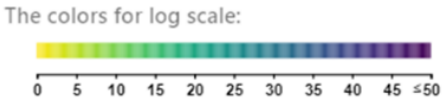

KEGG		stats	
Term name	Term ID	p_{adj}	$-\log_{10}(p_{adj})$ 0 ≤16
Cardiac muscle contraction	KEGG:04260	7.410×10^{-5}	
Protein digestion and absorption	KEGG:04974	8.724×10^{-5}	
GABAergic synapse	KEGG:04727	1.376×10^{-4}	
Nicotine addiction	KEGG:05033	7.397×10^{-4}	
Calcium signaling pathway	KEGG:04020	1.647×10^{-3}	
Dilated cardiomyopathy (DCM)	KEGG:05414	1.647×10^{-3}	
Glutamatergic synapse	KEGG:04724	2.634×10^{-3}	
Hypertrophic cardiomyopathy (HCM)	KEGG:05410	2.684×10^{-3}	
Adrenergic signaling in cardiomyocytes	KEGG:04261	2.684×10^{-3}	
cAMP signaling pathway	KEGG:04024	3.035×10^{-3}	
Proximal tubule bicarbonate reclamation	KEGG:04964	7.648×10^{-3}	
Circadian entrainment	KEGG:04713	7.648×10^{-3}	
Neuroactive ligand-receptor interaction	KEGG:04080	8.243×10^{-3}	
Amphetamine addiction	KEGG:05031	8.569×10^{-3}	
Morphine addiction	KEGG:05032	1.712×10^{-2}	
Glycine, serine and threonine metabolism	KEGG:00260	3.848×10^{-2}	
cGMP-PKG signaling pathway	KEGG:04022	3.848×10^{-2}	
Mineral absorption	KEGG:04978	3.938×10^{-2}	

REAC		stats	
Term name	Term ID	p_{adj}	$-\log_{10}(p_{adj})$ 0 ≤16
Striated Muscle Contraction	REAC:R-MMU-390522	1.052×10^{-9}	
Muscle contraction	REAC:R-MMU-397014	4.153×10^{-9}	
Collagen chain trimerization	REAC:R-MMU-8948216	8.449×10^{-7}	
Degradation of the extracellular matrix	REAC:R-MMU-1474228	4.155×10^{-6}	
Neuronal System	REAC:R-MMU-112316	1.374×10^{-5}	
Collagen biosynthesis and modifying enzymes	REAC:R-MMU-1650814	5.629×10^{-5}	
Assembly of collagen fibrils and other multimeric structures	REAC:R-MMU-2022090	7.975×10^{-5}	
Transmission across Chemical Synapses	REAC:R-MMU-112315	1.287×10^{-4}	
Transport of small molecules	REAC:R-MMU-382551	1.465×10^{-4}	
Extracellular matrix organization	REAC:R-MMU-1474244	2.161×10^{-4}	
Collagen degradation	REAC:R-MMU-1442490	2.338×10^{-4}	
ECM proteoglycans	REAC:R-MMU-3000178	2.578×10^{-4}	
Collagen formation	REAC:R-MMU-1474290	3.755×10^{-4}	
Ion homeostasis	REAC:R-MMU-5578775	5.049×10^{-4}	
Integrin cell surface interactions	REAC:R-MMU-216083	2.742×10^{-3}	
Neurotransmitter receptors and postsynaptic signal transmission	REAC:R-MMU-112314	2.941×10^{-3}	
NCAM1 interactions	REAC:R-MMU-419037	2.941×10^{-3}	
SLC-mediated transmembrane transport	REAC:R-MMU-425407	3.390×10^{-3}	
Cardiac conduction	REAC:R-MMU-5576891	3.471×10^{-3}	
G alpha (i) signalling events	REAC:R-MMU-418594	4.402×10^{-3}	
Non-integrin membrane-ECM interactions	REAC:R-MMU-3000171	6.773×10^{-3}	
Transport of inorganic cations/anions and amino acids/oligopeptides	REAC:R-MMU-425393	7.697×10^{-3}	
Platelet calcium homeostasis	REAC:R-MMU-418360	1.621×10^{-2}	
Regulation of Insulin-like Growth Factor (IGF) transport and uptake by Insulin-like Growth Factor Binding Proteins (IGFBPs)	REAC:R-MMU-381426	1.621×10^{-2}	
Platelet homeostasis	REAC:R-MMU-418346	2.144×10^{-2}	
Post-translational protein phosphorylation	REAC:R-MMU-8957275	2.301×10^{-2}	
Erythrocytes take up oxygen and release carbon dioxide	REAC:R-MMU-1247673	2.523×10^{-2}	
Bicarbonate transporters	REAC:R-MMU-425381	2.523×10^{-2}	

Supplementary table 4. KEGG and REACTOME pathways significantly enriched after αD11 treatment in CCI-induced mice at D11 post-operatively.

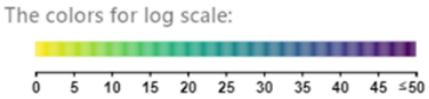

KEGG		stats	
Term name	Term ID	p_{adj}	$-\log_{10}(p_{adj})$ 0 ≤16
MAPK signaling pathway	KEGG:04010	5.248×10^{-4}	
Calcium signaling pathway	KEGG:04020	5.248×10^{-4}	
Rap1 signaling pathway	KEGG:04015	1.844×10^{-3}	
Hypertrophic cardiomyopathy (HCM)	KEGG:05410	2.333×10^{-3}	
Arrhythmogenic right ventricular cardiomyopathy (ARVC)	KEGG:05412	2.333×10^{-3}	
Dilated cardiomyopathy (DCM)	KEGG:05414	2.727×10^{-3}	
Axon guidance	KEGG:04360	3.122×10^{-3}	
Colorectal cancer	KEGG:05210	3.138×10^{-3}	
Focal adhesion	KEGG:04510	3.138×10^{-3}	
Cardiac muscle contraction	KEGG:04260	3.486×10^{-3}	
Glioma	KEGG:05214	6.713×10^{-3}	
Cushing syndrome	KEGG:04934	6.713×10^{-3}	
Hepatocellular carcinoma	KEGG:05225	1.427×10^{-2}	
Breast cancer	KEGG:05224	1.476×10^{-2}	
Neuroactive ligand-receptor interaction	KEGG:04080	1.476×10^{-2}	
B cell receptor signaling pathway	KEGG:04662	1.476×10^{-2}	
Non-small cell lung cancer	KEGG:05223	2.054×10^{-2}	
Endometrial cancer	KEGG:05213	2.054×10^{-2}	
GnRH secretion	KEGG:04929	2.054×10^{-2}	
Cortisol synthesis and secretion	KEGG:04927	2.146×10^{-2}	
Cell cycle	KEGG:04110	3.114×10^{-2}	
Fc gamma R-mediated phagocytosis	KEGG:04666	3.114×10^{-2}	
p53 signaling pathway	KEGG:04115	3.350×10^{-2}	
Aldosterone synthesis and secretion	KEGG:04925	3.812×10^{-2}	
Proteoglycans in cancer	KEGG:05205	3.812×10^{-2}	
Nicotine addiction	KEGG:05033	3.852×10^{-2}	
Gap junction	KEGG:04540	3.852×10^{-2}	
Pancreatic cancer	KEGG:05212	4.669×10^{-2}	

The colors for log scale:

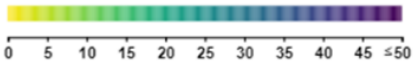

REAC		stats	
Term name	Term ID	p_{adj}	$-\log_{10}(p_{adj})$ 0 ≤16
Axon guidance	REAC:R-MMU-422475	2.159×10^{-5}	
Signaling by Rho GTPases	REAC:R-MMU-194315	8.539×10^{-4}	
Muscle contraction	REAC:R-MMU-397014	1.540×10^{-3}	
RHO GTPases Activate Formins	REAC:R-MMU-5663220	1.667×10^{-3}	
Cytokine Signaling in Immune system	REAC:R-MMU-1280215	1.667×10^{-3}	
Neuronal System	REAC:R-MMU-112316	1.667×10^{-3}	
Striated Muscle Contraction	REAC:R-MMU-390522	5.342×10^{-3}	
RHO GTPase Effectors	REAC:R-MMU-195258	1.054×10^{-2}	
Resolution of Sister Chromatid Cohesion	REAC:R-MMU-2500257	1.054×10^{-2}	
Potassium Channels	REAC:R-MMU-1296071	1.054×10^{-2}	
Voltage gated Potassium channels	REAC:R-MMU-1296072	1.054×10^{-2}	
Mitotic Prometaphase	REAC:R-MMU-68877	1.441×10^{-2}	
Platelet activation, signaling and aggregation	REAC:R-MMU-76002	1.463×10^{-2}	
Other interleukin signaling	REAC:R-MMU-449836	1.684×10^{-2}	
RHO GTPases Activate NADPH Oxidases	REAC:R-MMU-5668599	2.153×10^{-2}	
Rho GTPase cycle	REAC:R-MMU-194840	2.153×10^{-2}	
Effects of PIP2 hydrolysis	REAC:R-MMU-114508	2.680×10^{-2}	
Kinesins	REAC:R-MMU-983189	3.738×10^{-2}	
Signaling by Interleukins	REAC:R-MMU-449147	3.882×10^{-2}	

Supplementary table 5. KEGG and REACTOME pathways significantly enriched in CCI-induced mice at D24 post-surgery.

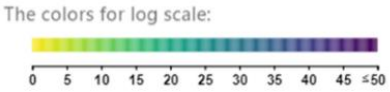

KEGG		stats	
Term name	Term ID	p_{adj}	$-\log_{10}(p_{adj})$
Glutamatergic synapse	KEGG:04724	5.363×10^{-11}	
Axon guidance	KEGG:04360	2.269×10^{-8}	
Circadian entrainment	KEGG:04713	2.966×10^{-7}	
Proximal tubule bicarbonate reclamation	KEGG:04964	2.169×10^{-6}	
Salivary secretion	KEGG:04970	5.783×10^{-6}	
Calcium signaling pathway	KEGG:04020	1.592×10^{-5}	
Insulin secretion	KEGG:04911	1.892×10^{-5}	
Cholinergic synapse	KEGG:04725	2.089×10^{-5}	
GABAergic synapse	KEGG:04727	2.753×10^{-5}	
Protein digestion and absorption	KEGG:04974	6.367×10^{-5}	
Aldosterone synthesis and secretion	KEGG:04925	8.112×10^{-5}	
Pancreatic secretion	KEGG:04972	8.112×10^{-5}	
Morphine addiction	KEGG:05032	1.860×10^{-4}	
Rap1 signaling pathway	KEGG:04015	2.287×10^{-4}	
Long-term depression	KEGG:04730	2.473×10^{-4}	
cGMP-PKG signaling pathway	KEGG:04022	2.661×10^{-4}	
cAMP signaling pathway	KEGG:04024	2.944×10^{-4}	
Oxytocin signaling pathway	KEGG:04921	4.787×10^{-4}	
Arrhythmogenic right ventricular cardiomyopathy (ARVC)	KEGG:05412	4.787×10^{-4}	
Nicotine addiction	KEGG:05033	4.787×10^{-4}	
Apelin signaling pathway	KEGG:04371	4.787×10^{-4}	
Gastric acid secretion	KEGG:04971	4.787×10^{-4}	
Endocrine and other factor-regulated calcium reabsorption	KEGG:04961	7.729×10^{-4}	
Neuroactive ligand-receptor interaction	KEGG:04080	8.052×10^{-4}	
GnRH secretion	KEGG:04929	8.808×10^{-4}	
Platelet activation	KEGG:04611	1.042×10^{-3}	
Bile secretion	KEGG:04976	1.042×10^{-3}	
Serotonergic synapse	KEGG:04726	1.383×10^{-3}	
Long-term potentiation	KEGG:04720	1.531×10^{-3}	
Mineral absorption	KEGG:04978	1.559×10^{-3}	
Adrenergic signaling in cardiomyocytes	KEGG:04261	1.898×10^{-3}	
Dopaminergic synapse	KEGG:04728	1.898×10^{-3}	
Fc gamma R-mediated phagocytosis	KEGG:04666	1.970×10^{-3}	
Proteoglycans in cancer	KEGG:05205	2.407×10^{-3}	
Pathways in cancer	KEGG:05200	2.707×10^{-3}	
Aldosterone-regulated sodium reabsorption	KEGG:04960	5.204×10^{-3}	
Dilated cardiomyopathy (DCM)	KEGG:05414	5.296×10^{-3}	
ECM-receptor interaction	KEGG:04512	5.317×10^{-3}	
Amphetamine addiction	KEGG:05031	5.518×10^{-3}	
Hypertrophic cardiomyopathy (HCM)	KEGG:05410	7.633×10^{-3}	
Retrograde endocannabinoid signaling	KEGG:04723	7.939×10^{-3}	
Melanogenesis	KEGG:04916	1.024×10^{-2}	
Carbohydrate digestion and absorption	KEGG:04973	1.240×10^{-2}	
Spinocerebellar ataxia	KEGG:05017	1.299×10^{-2}	
Cushing syndrome	KEGG:04934	1.299×10^{-2}	
Phosphatidylinositol signaling system	KEGG:04070	1.346×10^{-2}	
Vascular smooth muscle contraction	KEGG:04270	1.460×10^{-2}	
Gap junction	KEGG:04540	1.590×10^{-2}	
Growth hormone synthesis, secretion and action	KEGG:04935	1.724×10^{-2}	
Thyroid hormone signaling pathway	KEGG:04919	1.838×10^{-2}	
Cortisol synthesis and secretion	KEGG:04927	2.648×10^{-2}	
Cell adhesion molecules (CAMs)	KEGG:04514	2.781×10^{-2}	
Renin secretion	KEGG:04924	2.810×10^{-2}	
Hepatocellular carcinoma	KEGG:05225	3.043×10^{-2}	
Inositol phosphate metabolism	KEGG:00562	3.250×10^{-2}	
Relaxin signaling pathway	KEGG:04926	3.374×10^{-2}	
AGE-RAGE signaling pathway in diabetic complications	KEGG:04933	3.659×10^{-2}	
Wnt signaling pathway	KEGG:04310	3.897×10^{-2}	
Focal adhesion	KEGG:04510	4.034×10^{-2}	
Natural killer cell mediated cytotoxicity	KEGG:04650	4.034×10^{-2}	
Thyroid hormone synthesis	KEGG:04918	4.645×10^{-2}	
Ras signaling pathway	KEGG:04014	4.645×10^{-2}	

The colors for log scale:

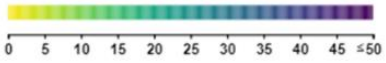

REAC		stats	
Term name	Term ID	p_{adj}	$-\log_{10}(p_{adj})$ 0 ≤16
Neuronal System	REAC:R-MMU-112316	8.546×10^{-16}	
Cardiac conduction	REAC:R-MMU-5576891	1.069×10^{-8}	
Transmission across Chemical Synapses	REAC:R-MMU-112315	5.642×10^{-8}	
Ion homeostasis	REAC:R-MMU-5578775	3.306×10^{-7}	
Axon guidance	REAC:R-MMU-422475	3.083×10^{-6}	
Muscle contraction	REAC:R-MMU-397014	3.083×10^{-6}	
Neurotransmitter receptors and postsynaptic signal transmission	REAC:R-MMU-112314	3.083×10^{-6}	
Potassium Channels	REAC:R-MMU-1296071	4.300×10^{-6}	
Platelet activation, signaling and aggregation	REAC:R-MMU-76002	3.111×10^{-5}	
Extracellular matrix organization	REAC:R-MMU-1474244	1.627×10^{-4}	
Hemostasis	REAC:R-MMU-109582	1.967×10^{-4}	
Transport of inorganic cations/anions and amino acids/oligopeptides	REAC:R-MMU-425393	2.389×10^{-4}	
Platelet homeostasis	REAC:R-MMU-418346	2.608×10^{-4}	
Protein-protein interactions at synapses	REAC:R-MMU-6794362	7.342×10^{-4}	
Activation of NMDA receptors and postsynaptic events	REAC:R-MMU-442755	7.755×10^{-4}	
Regulation of insulin secretion	REAC:R-MMU-422356	1.001×10^{-3}	
Opioid Signalling	REAC:R-MMU-111885	1.126×10^{-3}	
Platelet calcium homeostasis	REAC:R-MMU-418360	1.695×10^{-3}	
Integrin cell surface interactions	REAC:R-MMU-216083	1.784×10^{-3}	
Ion transport by P-type ATPases	REAC:R-MMU-936837	1.877×10^{-3}	
Assembly of collagen fibrils and other multimeric structures	REAC:R-MMU-2022090	3.485×10^{-3}	
RET signaling	REAC:R-MMU-8853659	3.850×10^{-3}	
Transport of small molecules	REAC:R-MMU-382551	5.504×10^{-3}	
SLC-mediated transmembrane transport	REAC:R-MMU-425407	5.841×10^{-3}	
Integration of energy metabolism	REAC:R-MMU-163685	8.911×10^{-3}	
Synthesis of IP3 and IP4 in the cytosol	REAC:R-MMU-1855204	9.252×10^{-3}	
Voltage gated Potassium channels	REAC:R-MMU-1296072	1.277×10^{-2}	
Developmental Biology	REAC:R-MMU-1266738	1.370×10^{-2}	
Semaphorin interactions	REAC:R-MMU-373755	1.448×10^{-2}	
MET activates PTK2 signaling	REAC:R-MMU-8874081	1.523×10^{-2}	
Synaptic adhesion-like molecules	REAC:R-MMU-8849932	2.092×10^{-2}	
Collagen chain trimerization	REAC:R-MMU-8948216	2.102×10^{-2}	
G-protein mediated events	REAC:R-MMU-112040	2.102×10^{-2}	
cGMP effects	REAC:R-MMU-418457	2.107×10^{-2}	
Other semaphorin interactions	REAC:R-MMU-416700	2.138×10^{-2}	
Nitric oxide stimulates guanylate cyclase	REAC:R-MMU-392154	2.138×10^{-2}	
Glucagon-like Peptide-1 (GLP1) regulates insulin secretion	REAC:R-MMU-381676	2.215×10^{-2}	
Effects of PIP2 hydrolysis	REAC:R-MMU-114508	2.269×10^{-2}	
Glucagon-type ligand receptors	REAC:R-MMU-420092	2.802×10^{-2}	
Trafficking of AMPA receptors	REAC:R-MMU-399719	2.948×10^{-2}	
Glutamate binding, activation of AMPA receptors and synaptic plasticity	REAC:R-MMU-399721	2.948×10^{-2}	
ECM proteoglycans	REAC:R-MMU-3000178	2.948×10^{-2}	
Inwardly rectifying K+ channels	REAC:R-MMU-1296065	3.314×10^{-2}	
Unblocking of NMDA receptors, glutamate binding and activation	REAC:R-MMU-438066	3.456×10^{-2}	
Signaling by MET	REAC:R-MMU-6806834	3.456×10^{-2}	
PLC beta mediated events	REAC:R-MMU-112043	3.457×10^{-2}	
Collagen formation	REAC:R-MMU-1474290	3.457×10^{-2}	
Class B/2 (Secretin family receptors)	REAC:R-MMU-373080	4.117×10^{-2}	
Non-integrin membrane-ECM interactions	REAC:R-MMU-3000171	4.313×10^{-2}	
Neurexins and neuroligins	REAC:R-MMU-6794361	4.313×10^{-2}	
Phase 1 - inactivation of fast Na+ channels	REAC:R-MMU-5576894	4.401×10^{-2}	
Collagen biosynthesis and modifying enzymes	REAC:R-MMU-1650814	4.483×10^{-2}	
Basigin interactions	REAC:R-MMU-210991	4.483×10^{-2}	
Rho GTPase cycle	REAC:R-MMU-194840	4.536×10^{-2}	
G alpha (12/13) signalling events	REAC:R-MMU-416482	4.584×10^{-2}	
Reduction of cytosolic Ca++ levels	REAC:R-MMU-418359	4.666×10^{-2}	
GABA receptor activation	REAC:R-MMU-977443	4.674×10^{-2}	
Inositol phosphate metabolism	REAC:R-MMU-1483249	4.737×10^{-2}	
Signaling by Receptor Tyrosine Kinases	REAC:R-MMU-9006934	4.737×10^{-2}	
Activation of kainate receptors upon glutamate binding	REAC:R-MMU-451326	4.792×10^{-2}	
Ion channel transport	REAC:R-MMU-983712	4.792×10^{-2}	

Supplementary table 6. KEGG and REACTOME pathways significantly enriched after MNAC13 treatment in CCI-induced mice at D24 post-operatively.

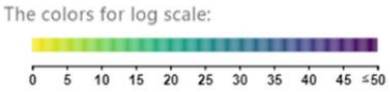

KEGG		stats	
Term name	Term ID	p_{adj}	$-\log_{10}(p_{adj})$ 0 ≤16
Leishmaniasis	KEGG:05140	1.515×10^{-4}	
GABAergic synapse	KEGG:04727	3.880×10^{-3}	
Glutamatergic synapse	KEGG:04724	3.880×10^{-3}	
Cell adhesion molecules (CAMs)	KEGG:04514	3.880×10^{-3}	
Platelet activation	KEGG:04611	3.880×10^{-3}	
Viral myocarditis	KEGG:05416	8.545×10^{-3}	
B cell receptor signaling pathway	KEGG:04662	8.545×10^{-3}	
Osteoclast differentiation	KEGG:04380	8.545×10^{-3}	
Phagosome	KEGG:04145	1.180×10^{-2}	
Leukocyte transendothelial migration	KEGG:04670	1.180×10^{-2}	
Hippo signaling pathway	KEGG:04390	1.622×10^{-2}	
Hematopoietic cell lineage	KEGG:04640	1.789×10^{-2}	
Rap1 signaling pathway	KEGG:04015	2.077×10^{-2}	
Axon guidance	KEGG:04360	2.077×10^{-2}	
Toxoplasmosis	KEGG:05145	2.382×10^{-2}	
Neuroactive ligand-receptor interaction	KEGG:04080	3.116×10^{-2}	
Cholinergic synapse	KEGG:04725	3.116×10^{-2}	
Circadian entrainment	KEGG:04713	3.434×10^{-2}	
TGF-beta signaling pathway	KEGG:04350	3.490×10^{-2}	
Antigen processing and presentation	KEGG:04612	4.805×10^{-2}	

REAC		stats	
Term name	Term ID	p_{adj}	$-\log_{10}(p_{adj})$ 0 ≤16
Platelet activation, signaling and aggregation	REAC:R-MMU-76002	9.244×10^{-5}	
Hemostasis	REAC:R-MMU-109582	9.244×10^{-5}	
Neutrophil degranulation	REAC:R-MMU-6798695	3.729×10^{-4}	
Neuronal System	REAC:R-MMU-112316	3.729×10^{-4}	
RHO GTPases Activate NADPH Oxidases	REAC:R-MMU-5668599	1.076×10^{-3}	
Immune System	REAC:R-MMU-168256	3.755×10^{-3}	
Erythrocytes take up oxygen and release carbon dioxide	REAC:R-MMU-1247673	4.149×10^{-3}	
Innate Immune System	REAC:R-MMU-168249	1.334×10^{-2}	
GPVI-mediated activation cascade	REAC:R-MMU-114604	1.566×10^{-2}	
Voltage gated Potassium channels	REAC:R-MMU-1296072	1.566×10^{-2}	
Transport of small molecules	REAC:R-MMU-382551	1.816×10^{-2}	
Rho GTPase cycle	REAC:R-MMU-194840	1.816×10^{-2}	
Other semaphorin interactions	REAC:R-MMU-416700	1.816×10^{-2}	
Transmission across Chemical Synapses	REAC:R-MMU-112315	1.897×10^{-2}	
SLC-mediated transmembrane transport	REAC:R-MMU-425407	1.897×10^{-2}	
Transport of inorganic cations/anions and amino acids/oligopeptides	REAC:R-MMU-425393	2.523×10^{-2}	
Signaling by Rho GTPases	REAC:R-MMU-194315	2.523×10^{-2}	
Platelet homeostasis	REAC:R-MMU-418346	2.523×10^{-2}	
Opioid Signalling	REAC:R-MMU-111885	2.523×10^{-2}	
O2/CO2 exchange in erythrocytes	REAC:R-MMU-1480926	3.192×10^{-2}	
Erythrocytes take up carbon dioxide and release oxygen	REAC:R-MMU-1237044	3.192×10^{-2}	
Molecules associated with elastic fibres	REAC:R-MMU-2129379	3.476×10^{-2}	
ROS and RNS production in phagocytes	REAC:R-MMU-1222556	3.925×10^{-2}	
G-protein mediated events	REAC:R-MMU-112040	4.819×10^{-2}	

Supplementary table 7. KEGG and REACTOME pathways significantly enriched after αD11 treatment in CCI-induced mice at D24 post-operatively.

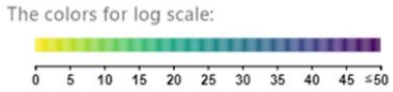

KEGG		stats	
Term name	Term ID	p_{adj}	$-\log_{10}(p_{adj})$ 0 ≤16
Glutamatergic synapse	KEGG:04724	1.698×10^{-10}	
Circadian entrainment	KEGG:04713	3.955×10^{-8}	
GABAergic synapse	KEGG:04727	2.568×10^{-6}	
Morphine addiction	KEGG:05032	3.091×10^{-5}	
Neuroactive ligand-receptor interaction	KEGG:04080	7.403×10^{-5}	
Nicotine addiction	KEGG:05033	1.136×10^{-4}	
Axon guidance	KEGG:04360	2.239×10^{-4}	
Pancreatic secretion	KEGG:04972	2.682×10^{-4}	
cAMP signaling pathway	KEGG:04024	2.833×10^{-4}	
Salivary secretion	KEGG:04970	2.987×10^{-4}	
Dopaminergic synapse	KEGG:04728	3.097×10^{-4}	
Calcium signaling pathway	KEGG:04020	3.097×10^{-4}	
Amphetamine addiction	KEGG:05031	3.097×10^{-4}	
Cholinergic synapse	KEGG:04725	3.097×10^{-4}	
Proximal tubule bicarbonate reclamation	KEGG:04964	4.758×10^{-4}	
Insulin secretion	KEGG:04911	4.843×10^{-4}	
Retrograde endocannabinoid signaling	KEGG:04723	1.291×10^{-3}	
Fc gamma R-mediated phagocytosis	KEGG:04666	1.540×10^{-3}	
Pathways in cancer	KEGG:05200	2.703×10^{-3}	
Endocrine and other factor-regulated calcium reabsorption	KEGG:04961	2.706×10^{-3}	
Aldosterone synthesis and secretion	KEGG:04925	3.504×10^{-3}	
Adrenergic signaling in cardiomyocytes	KEGG:04261	3.705×10^{-3}	
Mineral absorption	KEGG:04978	4.066×10^{-3}	
Apelin signaling pathway	KEGG:04371	4.066×10^{-3}	
Rap1 signaling pathway	KEGG:04015	4.503×10^{-3}	
Bile secretion	KEGG:04976	4.503×10^{-3}	
Platelet activation	KEGG:04611	5.067×10^{-3}	
Natural killer cell mediated cytotoxicity	KEGG:04650	5.067×10^{-3}	
Serotonergic synapse	KEGG:04726	7.952×10^{-3}	
Cushing syndrome	KEGG:04934	9.285×10^{-3}	
Cocaine addiction	KEGG:05030	9.285×10^{-3}	
Spinocerebellar ataxia	KEGG:05017	9.677×10^{-3}	
Melanogenesis	KEGG:04916	1.091×10^{-2}	
B cell receptor signaling pathway	KEGG:04662	1.235×10^{-2}	
Long-term depression	KEGG:04730	1.271×10^{-2}	
Chemokine signaling pathway	KEGG:04062	1.338×10^{-2}	
Basal cell carcinoma	KEGG:05217	1.454×10^{-2}	
Gastric acid secretion	KEGG:04971	1.787×10^{-2}	
Long-term potentiation	KEGG:04720	2.360×10^{-2}	
Relaxin signaling pathway	KEGG:04926	2.596×10^{-2}	
cGMP-PKG signaling pathway	KEGG:04022	3.085×10^{-2}	
Alcoholism	KEGG:05034	3.191×10^{-2}	
Leukocyte transendothelial migration	KEGG:04670	3.374×10^{-2}	
Adherens junction	KEGG:04520	3.374×10^{-2}	
Vascular smooth muscle contraction	KEGG:04270	3.644×10^{-2}	
Ras signaling pathway	KEGG:04014	3.644×10^{-2}	
Leishmaniasis	KEGG:05140	3.729×10^{-2}	
Wnt signaling pathway	KEGG:04310	4.495×10^{-2}	

The colors for log scale:

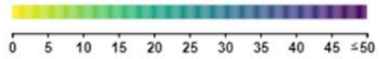

REAC		stats	
Term name	Term ID	p_{adj}	$-\log_{10}(p_{adj})$ 0 ≤16
Neuronal System	REAC:R-MMU-112316	2.816×10^{-12}	
Transmission across Chemical Synapses	REAC:R-MMU-112315	6.842×10^{-7}	
Neurotransmitter receptors and postsynaptic signal transmission	REAC:R-MMU-112314	5.321×10^{-6}	
Potassium Channels	REAC:R-MMU-1296071	2.660×10^{-4}	
Platelet activation, signaling and aggregation	REAC:R-MMU-76002	8.122×10^{-4}	
Hemostasis	REAC:R-MMU-109582	8.122×10^{-4}	
Opioid Signalling	REAC:R-MMU-111885	8.122×10^{-4}	
Muscle contraction	REAC:R-MMU-397014	8.122×10^{-4}	
Cardiac conduction	REAC:R-MMU-5576891	8.122×10^{-4}	
G alpha (q) signalling events	REAC:R-MMU-416476	8.202×10^{-4}	
Phase 1 - inactivation of fast Na+ channels	REAC:R-MMU-5576894	9.181×10^{-4}	
Platelet homeostasis	REAC:R-MMU-418346	1.872×10^{-3}	
Class B/2 (Secretin family receptors)	REAC:R-MMU-373080	2.022×10^{-3}	
Other semaphorin interactions	REAC:R-MMU-416700	2.074×10^{-3}	
Activation of NMDA receptors and postsynaptic events	REAC:R-MMU-442755	2.270×10^{-3}	
Glucagon-like Peptide-1 (GLP1) regulates insulin secretion	REAC:R-MMU-381676	2.676×10^{-3}	
Integration of energy metabolism	REAC:R-MMU-163685	3.263×10^{-3}	
Regulation of insulin secretion	REAC:R-MMU-422356	3.263×10^{-3}	
Glucagon-type ligand receptors	REAC:R-MMU-420092	3.263×10^{-3}	
Axon guidance	REAC:R-MMU-422475	4.813×10^{-3}	
G alpha (z) signalling events	REAC:R-MMU-418597	5.378×10^{-3}	
Neutrophil degranulation	REAC:R-MMU-6798695	5.662×10^{-3}	
GPCR ligand binding	REAC:R-MMU-500792	5.662×10^{-3}	
G-protein beta:gamma signalling	REAC:R-MMU-397795	5.982×10^{-3}	
Transport of small molecules	REAC:R-MMU-382551	8.840×10^{-3}	
G beta:gamma signalling through BTK	REAC:R-MMU-8964315	9.922×10^{-3}	
RHO GTPases Activate NADPH Oxidases	REAC:R-MMU-5668599	1.250×10^{-2}	
G alpha (i) signalling events	REAC:R-MMU-418594	1.411×10^{-2}	
Prostacyclin signalling through prostacyclin receptor	REAC:R-MMU-392851	1.411×10^{-2}	
Protein-protein interactions at synapses	REAC:R-MMU-6794362	1.526×10^{-2}	
Ion homeostasis	REAC:R-MMU-5578775	1.601×10^{-2}	
Inwardly rectifying K+ channels	REAC:R-MMU-1296065	1.653×10^{-2}	
Ca2+ pathway	REAC:R-MMU-4086398	1.723×10^{-2}	
G beta:gamma signalling through PLC beta	REAC:R-MMU-418217	1.799×10^{-2}	
GABA receptor activation	REAC:R-MMU-977443	1.799×10^{-2}	
Transport of inorganic cations/anions and amino acids/oligopeptides	REAC:R-MMU-425393	1.873×10^{-2}	
Vasopressin regulates renal water homeostasis via Aquaporins	REAC:R-MMU-432040	1.874×10^{-2}	
G beta:gamma signalling through PI3Kgamma	REAC:R-MMU-392451	1.874×10^{-2}	
ADP signalling through P2Y purinoceptor 1	REAC:R-MMU-418592	1.874×10^{-2}	
GPVI-mediated activation cascade	REAC:R-MMU-114604	2.281×10^{-2}	
Presynaptic function of Kainate receptors	REAC:R-MMU-500657	2.281×10^{-2}	
Rho GTPase cycle	REAC:R-MMU-194840	2.291×10^{-2}	
Activation of kainate receptors upon glutamate binding	REAC:R-MMU-451326	2.291×10^{-2}	
Unblocking of NMDA receptors, glutamate binding and activation	REAC:R-MMU-438066	2.867×10^{-2}	
Signal amplification	REAC:R-MMU-392518	2.867×10^{-2}	
ADP signalling through P2Y purinoceptor 12	REAC:R-MMU-392170	2.867×10^{-2}	
G beta:gamma signalling through CDC42	REAC:R-MMU-8964616	3.634×10^{-2}	
Thromboxane signalling through TP receptor	REAC:R-MMU-428930	3.842×10^{-2}	
Cooperation of PDCL (PhLP1) and TRiC/CCT in G-protein beta folding	REAC:R-MMU-6814122	4.825×10^{-2}	

Supplementary table 8. KEGG and REACTOME pathways significantly enriched in CCI-induced mice at D90 post-surgery.

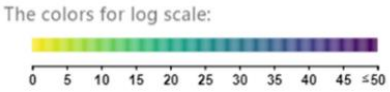

KEGG		stats	
Term name	Term ID	p_{adj}	$-\log_{10}(p_{adj})$ 0 ≤16
Neuroactive ligand-receptor interaction	KEGG:04080	1.482×10^{-6}	
Glutamatergic synapse	KEGG:04724	7.807×10^{-6}	
Circadian entrainment	KEGG:04713	7.742×10^{-5}	
cGMP-PKG signaling pathway	KEGG:04022	1.292×10^{-3}	
Long-term depression	KEGG:04730	1.292×10^{-3}	
Mineral absorption	KEGG:04978	1.292×10^{-3}	
Salivary secretion	KEGG:04970	1.514×10^{-3}	
Calcium signaling pathway	KEGG:04020	1.550×10^{-3}	
Endocrine and other factor-regulated calcium reabsorption	KEGG:04961	4.440×10^{-3}	
Nicotine addiction	KEGG:05033	4.735×10^{-3}	
Amphetamine addiction	KEGG:05031	6.772×10^{-3}	
Spinocerebellar ataxia	KEGG:05017	6.772×10^{-3}	
cAMP signaling pathway	KEGG:04024	6.772×10^{-3}	
Aldosterone synthesis and secretion	KEGG:04925	6.772×10^{-3}	
GABAergic synapse	KEGG:04727	6.772×10^{-3}	
Protein digestion and absorption	KEGG:04974	8.484×10^{-3}	
Cushing syndrome	KEGG:04934	8.484×10^{-3}	
Proximal tubule bicarbonate reclamation	KEGG:04964	1.007×10^{-2}	
Axon guidance	KEGG:04360	2.268×10^{-2}	
Pancreatic secretion	KEGG:04972	2.268×10^{-2}	
Cocaine addiction	KEGG:05030	2.807×10^{-2}	
Morphine addiction	KEGG:05032	3.524×10^{-2}	
Long-term potentiation	KEGG:04720	3.524×10^{-2}	
Cholinergic synapse	KEGG:04725	4.995×10^{-2}	

REAC		stats	
Term name	Term ID	p_{adj}	$-\log_{10}(p_{adj})$ 0 ≤16
Neuronal System	REAC:R-MMU-112316	5.214×10^{-9}	
Transmission across Chemical Synapses	REAC:R-MMU-112315	8.745×10^{-5}	
Potassium Channels	REAC:R-MMU-1296071	6.021×10^{-4}	
Neurotransmitter receptors and postsynaptic signal transmission	REAC:R-MMU-112314	6.577×10^{-4}	
Cardiac conduction	REAC:R-MMU-5576891	4.989×10^{-3}	
Voltage gated Potassium channels	REAC:R-MMU-1296072	5.504×10^{-3}	
Transport of inorganic cations/anions and amino acids/oligopeptides	REAC:R-MMU-425393	1.900×10^{-2}	
GPCR ligand binding	REAC:R-MMU-500792	2.305×10^{-2}	
Ion homeostasis	REAC:R-MMU-5578775	2.305×10^{-2}	
SLC-mediated transmembrane transport	REAC:R-MMU-425407	2.330×10^{-2}	
Platelet homeostasis	REAC:R-MMU-418346	2.639×10^{-2}	
Hemostasis	REAC:R-MMU-109582	2.727×10^{-2}	
MET activates PTK2 signaling	REAC:R-MMU-8874081	2.928×10^{-2}	
Axon guidance	REAC:R-MMU-422475	3.166×10^{-2}	
Signal Transduction	REAC:R-MMU-162582	4.117×10^{-2}	
Axonal growth inhibition (RHOA activation)	REAC:R-MMU-193634	4.441×10^{-2}	
Activation of NMDA receptors and postsynaptic events	REAC:R-MMU-442755	4.441×10^{-2}	
Transport of small molecules	REAC:R-MMU-382551	4.441×10^{-2}	
Extracellular matrix organization	REAC:R-MMU-1474244	4.441×10^{-2}	
MET promotes cell motility	REAC:R-MMU-8875878	4.502×10^{-2}	

Supplementary table 9. KEGG and REACTOME pathways significantly enriched after MNAC13 treatment in CCI-induced mice at D90 post-operatively.

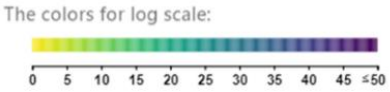

KEGG		stats	
Term name	Term ID	p_{adj}	$-\log_{10}(p_{adj})$ 0 ≤16
Glutamatergic synapse	KEGG:04724	4.284×10^{-9}	
GABAergic synapse	KEGG:04727	9.472×10^{-7}	
Circadian entrainment	KEGG:04713	9.909×10^{-5}	
Morphine addiction	KEGG:05032	2.420×10^{-4}	
Calcium signaling pathway	KEGG:04020	3.414×10^{-4}	
Dopaminergic synapse	KEGG:04728	3.920×10^{-4}	
Spinocerebellar ataxia	KEGG:05017	4.703×10^{-4}	
Neuroactive ligand-receptor interaction	KEGG:04080	1.279×10^{-3}	
Nicotine addiction	KEGG:05033	1.279×10^{-3}	
Adrenergic signaling in cardiomyocytes	KEGG:04261	1.279×10^{-3}	
cAMP signaling pathway	KEGG:04024	1.359×10^{-3}	
Retrograde endocannabinoid signaling	KEGG:04723	2.197×10^{-3}	
Pancreatic secretion	KEGG:04972	5.434×10^{-3}	
Cholinergic synapse	KEGG:04725	5.434×10^{-3}	
Amphetamine addiction	KEGG:05031	5.434×10^{-3}	
Salivary secretion	KEGG:04970	5.767×10^{-3}	
Long-term depression	KEGG:04730	6.740×10^{-3}	
Mineral absorption	KEGG:04978	7.141×10^{-3}	
Endocrine and other factor-regulated calcium reabsorption	KEGG:04961	7.141×10^{-3}	
Aldosterone synthesis and secretion	KEGG:04925	7.567×10^{-3}	
Insulin secretion	KEGG:04911	7.845×10^{-3}	
Cushing syndrome	KEGG:04934	1.214×10^{-2}	
GnRH secretion	KEGG:04929	1.363×10^{-2}	
Synaptic vesicle cycle	KEGG:04721	1.698×10^{-2}	
Proximal tubule bicarbonate reclamation	KEGG:04964	2.013×10^{-2}	
Dilated cardiomyopathy (DCM)	KEGG:05414	2.490×10^{-2}	
Cocaine addiction	KEGG:05030	2.677×10^{-2}	
Protein digestion and absorption	KEGG:04974	2.677×10^{-2}	
cGMP-PKG signaling pathway	KEGG:04022	2.786×10^{-2}	
Gastric acid secretion	KEGG:04971	2.786×10^{-2}	
Arrhythmogenic right ventricular cardiomyopathy (ARVC)	KEGG:05412	2.786×10^{-2}	

The colors for log scale:

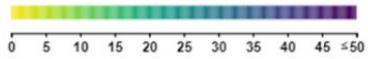

REAC		stats	
Term name	Term ID	p_{adj}	$-\log_{10}(p_{adj})$ 0 ≤16
Neuronal System	REAC:R-MMU-112316	9.721×10^{-16}	
Transmission across Chemical Synapses	REAC:R-MMU-112315	1.221×10^{-10}	
Neurotransmitter receptors and postsynaptic signal transmission	REAC:R-MMU-112314	1.240×10^{-6}	
Transport of small molecules	REAC:R-MMU-382551	6.315×10^{-5}	
SLC-mediated transmembrane transport	REAC:R-MMU-425407	1.515×10^{-4}	
Transport of inorganic cations/anions and amino acids/oligopeptides	REAC:R-MMU-425393	4.341×10^{-4}	
Protein-protein interactions at synapses	REAC:R-MMU-6794362	1.126×10^{-3}	
Opioid Signalling	REAC:R-MMU-111885	1.251×10^{-3}	
Cardiac conduction	REAC:R-MMU-5576891	4.815×10^{-3}	
Muscle contraction	REAC:R-MMU-397014	6.263×10^{-3}	
Neurotransmitter release cycle	REAC:R-MMU-112310	6.304×10^{-3}	
Potassium Channels	REAC:R-MMU-1296071	9.239×10^{-3}	
Ion homeostasis	REAC:R-MMU-5578775	9.923×10^{-3}	
Activation of NMDA receptors and postsynaptic events	REAC:R-MMU-442755	1.040×10^{-2}	
GABA receptor activation	REAC:R-MMU-977443	1.056×10^{-2}	
PLC beta mediated events	REAC:R-MMU-112043	1.383×10^{-2}	
Glutamate Neurotransmitter Release Cycle	REAC:R-MMU-210500	1.422×10^{-2}	
G-protein mediated events	REAC:R-MMU-112040	1.553×10^{-2}	
Glutamate binding, activation of AMPA receptors and synaptic plasticity	REAC:R-MMU-399721	2.089×10^{-2}	
Trafficking of AMPA receptors	REAC:R-MMU-399719	2.089×10^{-2}	
Regulation of insulin secretion	REAC:R-MMU-422356	2.089×10^{-2}	
Reduction of cytosolic Ca++ levels	REAC:R-MMU-418359	2.580×10^{-2}	
Bicarbonate transporters	REAC:R-MMU-425381	2.766×10^{-2}	
Ion transport by P-type ATPases	REAC:R-MMU-936837	3.379×10^{-2}	
G alpha (i) signalling events	REAC:R-MMU-418594	3.575×10^{-2}	
Inwardly rectifying K+ channels	REAC:R-MMU-1296065	4.389×10^{-2}	
Post-translational modification: synthesis of GPI-anchored proteins	REAC:R-MMU-163125	4.389×10^{-2}	
Integration of energy metabolism	REAC:R-MMU-163685	4.581×10^{-2}	
Unblocking of NMDA receptors, glutamate binding and activation	REAC:R-MMU-438066	4.581×10^{-2}	

Supplementary table 10. KEGG and REACTOME pathways significantly enriched after αD11 treatment in CCI-induced mice at D90 post-operatively.

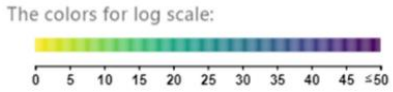

KEGG		stats	
Term name	Term ID	p_{adj}	$-\log_{10}(p_{adj})$ 0 ≤16
Circadian rhythm	KEGG:04710	5.839×10^{-3}	
Glutamatergic synapse	KEGG:04724	6.108×10^{-3}	
Calcium signaling pathway	KEGG:04020	7.369×10^{-3}	
Carbon metabolism	KEGG:01200	7.369×10^{-3}	
Amphetamine addiction	KEGG:05031	7.369×10^{-3}	
Cocaine addiction	KEGG:05030	7.369×10^{-3}	
Circadian entrainment	KEGG:04713	8.841×10^{-3}	
Proximal tubule bicarbonate reclamation	KEGG:04964	9.562×10^{-3}	
MAPK signaling pathway	KEGG:04010	1.344×10^{-2}	
Insulin secretion	KEGG:04911	1.725×10^{-2}	
GABAergic synapse	KEGG:04727	1.725×10^{-2}	
cAMP signaling pathway	KEGG:04024	1.944×10^{-2}	
Central carbon metabolism in cancer	KEGG:05230	2.007×10^{-2}	
Glucagon signaling pathway	KEGG:04922	2.007×10^{-2}	
Insulin signaling pathway	KEGG:04910	2.154×10^{-2}	
Biosynthesis of amino acids	KEGG:01230	2.158×10^{-2}	
cGMP-PKG signaling pathway	KEGG:04022	2.505×10^{-2}	
Citrate cycle (TCA cycle)	KEGG:00020	2.507×10^{-2}	
Hypertrophic cardiomyopathy (HCM)	KEGG:05410	2.849×10^{-2}	
Morphine addiction	KEGG:05032	2.849×10^{-2}	
Cardiac muscle contraction	KEGG:04260	3.103×10^{-2}	
Dilated cardiomyopathy (DCM)	KEGG:05414	3.143×10^{-2}	
Cushing syndrome	KEGG:04934	3.143×10^{-2}	

REAC		stats	
Term name	Term ID	p_{adj}	$-\log_{10}(p_{adj})$ 0 ≤16
Muscle contraction	REAC:R-MMU-397014	2.329×10^{-7}	
Neuronal System	REAC:R-MMU-112316	7.054×10^{-6}	
Striated Muscle Contraction	REAC:R-MMU-390522	7.054×10^{-6}	
Transmission across Chemical Synapses	REAC:R-MMU-112315	9.276×10^{-4}	
Pyruvate metabolism and Citric Acid (TCA) cycle	REAC:R-MMU-71406	9.276×10^{-4}	
Metabolism	REAC:R-MMU-1430728	1.518×10^{-3}	
Glycogen metabolism	REAC:R-MMU-8982491	2.749×10^{-3}	
Neurotransmitter release cycle	REAC:R-MMU-112310	7.964×10^{-3}	
Citric acid cycle (TCA cycle)	REAC:R-MMU-71403	1.270×10^{-2}	
Cardiac conduction	REAC:R-MMU-5576891	1.270×10^{-2}	
Metabolism of carbohydrates	REAC:R-MMU-71387	1.989×10^{-2}	
L1CAM interactions	REAC:R-MMU-373760	1.989×10^{-2}	
Phase 0 - rapid depolarisation	REAC:R-MMU-5576892	3.147×10^{-2}	
Axon guidance	REAC:R-MMU-422475	3.813×10^{-2}	
HSP90 chaperone cycle for steroid hormone receptors (SHR)	REAC:R-MMU-3371497	4.339×10^{-2}	

Supplementary tab1e 11. The common KEGG and REACTOME pathways inverted by both antibodies in the CCI model at D24.

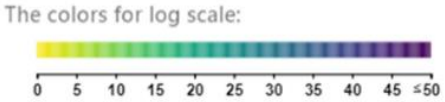

KEGG		stats	
Term name	Term ID	p_{adj}	$-\log_{10}(p_{adj})$ 0 ≤16
B cell receptor signaling pathway	KEGG:04662	1.362×10^{-3}	
Fc gamma R-mediated phagocytosis	KEGG:04666	1.362×10^{-3}	
Platelet activation	KEGG:04611	3.182×10^{-3}	
Axon guidance	KEGG:04360	7.757×10^{-3}	
Glutamatergic synapse	KEGG:04724	1.124×10^{-2}	
Proximal tubule bicarbonate reclamation	KEGG:04964	1.229×10^{-2}	
Cholinergic synapse	KEGG:04725	2.194×10^{-2}	
Fc epsilon RI signaling pathway	KEGG:04664	2.223×10^{-2}	
Natural killer cell mediated cytotoxicity	KEGG:04650	2.223×10^{-2}	
GABAergic synapse	KEGG:04727	2.223×10^{-2}	
Neuroactive ligand-receptor interaction	KEGG:04080	2.324×10^{-2}	
Calcium signaling pathway	KEGG:04020	3.092×10^{-2}	
Osteoclast differentiation	KEGG:04380	3.168×10^{-2}	
Circadian entrainment	KEGG:04713	3.609×10^{-2}	
cAMP signaling pathway	KEGG:04024	3.752×10^{-2}	

REAC		stats	
Term name	Term ID	p_{adj}	$-\log_{10}(p_{adj})$ 0 ≤16
Innate Immune System	REAC:R-MMU-168249	7.888×10^{-4}	
Neutrophil degranulation	REAC:R-MMU-6798695	7.888×10^{-4}	
Hemostasis	REAC:R-MMU-109582	7.912×10^{-4}	
Platelet activation, signaling and aggregation	REAC:R-MMU-76002	1.804×10^{-3}	
Immune System	REAC:R-MMU-168256	1.804×10^{-3}	
Neuronal System	REAC:R-MMU-112316	3.733×10^{-3}	
Phase 1 - inactivation of fast Na+ channels	REAC:R-MMU-5576894	1.206×10^{-2}	
GPVI-mediated activation cascade	REAC:R-MMU-114604	1.206×10^{-2}	
Transport of inorganic cations/anions and amino acids/oligopeptides	REAC:R-MMU-425393	1.255×10^{-2}	
G-protein mediated events	REAC:R-MMU-112040	1.255×10^{-2}	
SLC-mediated transmembrane transport	REAC:R-MMU-425407	1.255×10^{-2}	
Opioid Signalling	REAC:R-MMU-111885	1.255×10^{-2}	
Transport of small molecules	REAC:R-MMU-382551	3.899×10^{-2}	
Synthesis of Lipoxins (LX)	REAC:R-MMU-2142700	4.175×10^{-2}	
Transmission across Chemical Synapses	REAC:R-MMU-112315	4.175×10^{-2}	
ROS and RNS production in phagocytes	REAC:R-MMU-1222556	4.313×10^{-2}	
PLC beta mediated events	REAC:R-MMU-112043	4.313×10^{-2}	

Supplementary table 12. The common KEGG and REACTOME pathways inverted by both antibodies in the CCI model at D90.

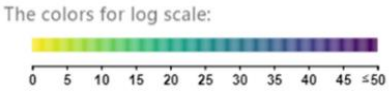

KEGG		stats	
Term name	Term ID	p_{adj}	$-\log_{10}(p_{adj})$ 0 ≤16
Neuroactive ligand-receptor interaction	KEGG:04080	7.400×10^{-5}	
Glutamatergic synapse	KEGG:04724	7.400×10^{-5}	
Proximal tubule bicarbonate reclamation	KEGG:04964	1.382×10^{-3}	
GABAergic synapse	KEGG:04727	1.382×10^{-3}	
Circadian entrainment	KEGG:04713	2.473×10^{-3}	
Amphetamine addiction	KEGG:05031	5.108×10^{-3}	
Morphine addiction	KEGG:05032	5.108×10^{-3}	
Mineral absorption	KEGG:04978	7.727×10^{-3}	
Insulin secretion	KEGG:04911	1.147×10^{-2}	
Nicotine addiction	KEGG:05033	1.444×10^{-2}	
Cholinergic synapse	KEGG:04725	1.458×10^{-2}	
Cocaine addiction	KEGG:05030	2.103×10^{-2}	
cAMP signaling pathway	KEGG:04024	2.360×10^{-2}	
Dopaminergic synapse	KEGG:04728	2.988×10^{-2}	
Metabolism of xenobiotics by cytochrome P450	KEGG:00980	2.997×10^{-2}	
Synaptic vesicle cycle	KEGG:04721	3.103×10^{-2}	

REAC		stats	
Term name	Term ID	p_{adj}	$-\log_{10}(p_{adj})$ 0 ≤16
Neuronal System	REAC:R-MMU-112316	1.144×10^{-7}	
Transmission across Chemical Synapses	REAC:R-MMU-112315	1.702×10^{-5}	
SLC-mediated transmembrane transport	REAC:R-MMU-425407	2.673×10^{-4}	
GPCR ligand binding	REAC:R-MMU-500792	1.828×10^{-3}	
Transport of small molecules	REAC:R-MMU-382551	1.828×10^{-3}	
Neurotransmitter release cycle	REAC:R-MMU-112310	3.148×10^{-3}	
G alpha (i) signalling events	REAC:R-MMU-418594	5.863×10^{-3}	
Potassium Channels	REAC:R-MMU-1296071	8.720×10^{-3}	
Cysteine formation from homocysteine	REAC:R-MMU-1614603	8.967×10^{-3}	
Transport of inorganic cations/anions and amino acids/oligopeptides	REAC:R-MMU-425393	1.404×10^{-2}	
Neurotransmitter receptors and postsynaptic signal transmission	REAC:R-MMU-112314	1.960×10^{-2}	
Inwardly rectifying K+ channels	REAC:R-MMU-1296065	2.134×10^{-2}	
Transport of bile salts and organic acids, metal ions and amine compounds	REAC:R-MMU-425366	2.134×10^{-2}	
Neurotransmitter uptake and metabolism In glial cells	REAC:R-MMU-112313	2.641×10^{-2}	
Class A/1 (Rhodopsin-like receptors)	REAC:R-MMU-373076	2.641×10^{-2}	
Gap junction assembly	REAC:R-MMU-190861	2.641×10^{-2}	
Astrocytic Glutamate-Glutamine Uptake And Metabolism	REAC:R-MMU-210455	2.641×10^{-2}	
ATP sensitive Potassium channels	REAC:R-MMU-1296025	2.641×10^{-2}	
Peptide ligand-binding receptors	REAC:R-MMU-375276	3.133×10^{-2}	
Gap junction trafficking	REAC:R-MMU-190828	4.310×10^{-2}	
Gap junction trafficking and regulation	REAC:R-MMU-157858	4.946×10^{-2}	

Table 19 (extended). DAVID GO analysis of DEGs upregulated in the CCI model and downregulated by both MNAC13 and αD11 treatment at D24 (the list of genes included).

GO-ID	GO term	Enrichment score	P value	FDR	Count of genes	Genes
GO:0036477	somatodendritic compartment	7.33	1.28E-08	1.67E-05	28	COBL, SNCG, CADM1, GRIK1, TH, ASAP1, ARFGEF2, SHH, KCNIP4, RGS10, PRKAR2B, PDE1C, P2RY1, AGRP, HTR1F, RET, MYO1A, KCND3, GNAO1, KCNB1, DGKI, MAPK1, KCNJ4, CTSL, PPP1R2, AGTR1A, P2RX3, P2RX2
GO:0098655	cation transmembrane transport	4.45	2.83E-06	0.0048	18	KCND3, TRPC3, TRPC6, PANX1, KCNB1, FGF12, KCNIP2, PRKG1, FKBP1B, KCNIP4, KCNJ4, SLC4A11, CCDC109B, STAC, P2RX3, P2RX2, NEDD4L, HTR1F

Table 20 (extended). DAVID GO analysis of DEGs downregulated in the CCI model and upregulated by both MNAC13 and αD11 treatment at D24 (the list of genes included).
(see next page)

GO-ID	GO term	Enrichment score	P value	FDR	Count of genes	Genes
GO:0048870	cell motility	8.2652124	6.05E-10	1.06E-06	81	FERMT3, FAM110C, WWC1, TLR2, GJA1, VTN, FGF13, IL17RA, CITED2, GATA2, WNT4, ATP2B4, S1PR1, SPINT2, ATOH8, DEPDC1B, SYK, MATK, EGR1, ARC, C5AR2, ELANE, VANGL2, ARTN, LEF1, DNAIC1, WAS, TRPM2, TNFAIP6, SMO, PODXL2, MADCAM1, BIN2, ALOX12, CCK, WNT5B, IFITM1, SOX1, ENPP2, CATSPERD, ABI3, ITGB2, CX3CL1, SOX9, CCL5, MDK, SOX8, TRF, DCHS1, DNAH6, VCAM1, RAC2, AGT, PYCARD, ACAN, FCER1G, NFATC2, SELPLG, PLTP, CSF1R, ARHGDIB, PTPRC, SELP, DIXDC1, MYO1G, NCKAP1L, CCL19, MYO1F, SMAD3, TBX1, PRR5L, VAV1, NKX6-1, ADGRG3, CCL17, HDAC4, LRP1, CXCL14, EPHA8, JAK3, ARAP3
GO:0002521	leukocyte differentiation	6.5659786	2.92E-09	5.33E-06	44	FGFR3, PRTN3, EFNA2, CCL5, C1QC, TRF, BTK, CITED2, BATF, TAL1, GATA2, FOS, WNT4, GFI1B, PDE1B, LYL1, BCL11A, FCER1G, INPP5D, ACIN1, CAR2, CSF1R, TYROBP, RHOH, SYK, EGR1, FZD9, PTPRC, DTX1, HCLS1, NCKAP1L, CCL19, LEF1, NFAM1, VAV1, TRPM2, ADGRG3, CD83, PLCG2, INPP4B, JAK3, ZFPM1, TREM2, SASH3
GO:0015293	symporter activity	6.1813969	2.27E-07	3.03E-04	19	SLC38A3, SLC12A8, SLC13A5, SLC6A1, SLC15A2, SLC16A11, SLC12A5, SLC32A1, SLC1A2, SLC17A5, SLC4A10, SLC6A9, GM5868, SLC38A1, SLC5A7, SLC4A4, SLC15A3, SLC1A1, SLC25A18
GO:0031226	intrinsic component of plasma membrane	6.1730397	1.37E-07	1.93E-04	77	KCNE1L, KCNJ16, KCNC1, GPR84, KCNC3, SLC13A5, SLC6A1, SLC15A2, ATP1B2, TACR2, SLC16A11, GABRB1, TLR2, AQP4, KCNJ10, TSPAN9, HVCN1, IL17RA, SLC1A2, ATP2B4, S1PR1, GRIN2B, SLCO1C1, HHIP, SLC4A4, PILRA, C5AR2, KCND2, NCF1, RXFP3, NCF4, GRM1, TRPM2, GRM5, CD37, CHRM2, SSTR1, SLC38A1, CAR4, SLC38A5, ITGAL, SLC38A3, FGFR3, ENPP2, ITGB2, CNTFR, CLDN11, SLC32A1, SLCO1A4, LAPTM5, IL12RB1, TSPAN33, RASAL3, FCER1G, GM5868, OLFM3, SCNN1A, SNAP25, PTPRC, SLC12A5, GRIA3, ATP1A2, SHANK1, ATP13A5, ADGRG3, TENM4, LAT, SLC4A10, SLC6A9, LRP1, LTB4R1, EPHA8, ADRA1B, SYT13, SLC18A3, SLC5A7, SLC14A1
GO:1902533	positive regulation of intracellular signal transduction	6.1365242	2.17E-06	0.0039619	53	SEPT4, FAM110C, WWC1, TLR2, GJA1, GSTM7, UNC5B, SYK, PIK3CG, C5AR2, VANGL2, FGF23, GRM1, NTSR2, HCST, GRM5, DNAJC27, RASGRF1, HIPK2, TREM2, FGD2, ITGAL, FGFR3, LMNB1, ADCYAP1R1, CX3CL1, CCL5, SOX9, GPRC5B, TRF, C1QTNF3, CHIL1, RASGRP4, AGT, PYCARD, TNFRSF19, PIK3R5, SKIL, HAP1, CSF1R, SELP, DIXDC1, PTPRC, HCLS1, CCL19, TBX1, TPD52L1, PRR5L, CCL17, FZD10, EPHA8, ADRA1B, EPOR
GO:0055082	cellular chemical homeostasis	5.5515746	9.99E-07	0.0017580	48	ATP1B2, ADCYAP1R1, GJA1, AQP4, CCL5, SESN2, PAX2, TRF, GSTM7, VCAM1, GATA2, ATP2B4, S1PR1, C1QTNF3, HK3, AGT, MT1, SLC4A4, HAP1, CAR2, PIK3CG, PTPRC, C5AR2, TBXAS1, RXFP3, PTPRN2, SLC12A5, FGF23, CCL19, ALMS1, SMAD3, CFTR, GJB6, ATP1A2, GRM1, TRPM2, ATP13A5, TRPM1, LCN2, SLC4A10, PLCG2, CACNA1G, ADRA1B, EPOR, HEPH, INPP4B, JAK3, SLC40A1
GO:1902105	regulation of leukocyte differentiation	5.5235315	1.57E-06	0.0027578	25	FGFR3, CCL5, C1QC, GATA2, TAL1, FOS, GFI1B, INPP5D, ACIN1, CAR2, CSF1R, TYROBP, SYK, PTPRC, DTX1, HCLS1, CCL19, NCKAP1L, LEF1, NFAM1, CD83, INPP4B, JAK3, ZFPM1, SASH3
GO:0099536	synaptic signaling	5.3248013	4.72E-06	0.0086244	38	CPLX3, GFAP, KCNC3, SNCAIP, SLC6A1, TACR2, KCNJ10, CX3CL1, GRIN2B, AGT, CAMK2B, SNAP23, SNAP25, CHAT, HAP1, CAR2, EGR1, ARC, MYO6, GABRA3, PTPRN2, PTPN5, SLC12A5, NPAS4, SHANK1, GRM1, GRM5, SLC6A9, DOC2A, PENK, CHRM2, RASGRF1, SSTR1, OTOF, CACNA1G, SYT13, SLC18A3, SLC5A7

GO-ID	GO term	Enrichment score	P value	FDR	Count of genes	Genes
GO:0002761	regulation of myeloid leukocyte differentiation	5.2110287	1.89E-06	0.0034514	16	FGFR3, HCLS1, LEF1, CCL5, C1QC, GATA2, TAL1, FOS, GFI1B, INPP4B, INPP5D, ZFPM1, ACIN1, CAR2, CSF1R, TYROBP
GO:0007159	leukocyte cell-cell adhesion	5.155708351	3.21E-07	5.66E-04	38	ITGAL, FERMT3, ITGB2, CCL5, APBB1IP, BATF, VCAM1, WNT4, IL12RB1, RAC2, BCL11A, RASAL3, PYCARD, FCER1G, SELPLG, EBI3, RHOH, SYK, EGR1, PTPRC, SELP, CCDC88B, EFNB3, DTX1, ELANE, FCGR4, CCL19, NCKAP1L, SMAD3, LEF1, WAS, VAV1, CD83, LAT, PODXL2, MADCAM1, JAK3, SASH3
GO:0045937	positive regulation of phosphate metabolic process	5.143609688	1.96E-07	3.58E-04	62	WWC1, TLR2, VTN, SCT, ATP2B4, NOS2, RAMP1, APLN, SYK, PIK3CG, C5AR2, CAMP, VANGL2, FGF23, GRM1, NTSR2, CCNL2, GRM5, DNAJC27, INHBA, HIPK2, TREM2, FGD2, FGFR3, CCK, LMNB1, ENPP2, ADCYAP1R1, APOC2, CX3CL1, GPRC5B, SOX9, CCL5, TRF, RGMA, PPP1R16B, CHIL1, C1QTNF3, AGT, PYCARD, TNFRSF19, PIK3R5, KNDC1, CSF1R, PTPRC, DIXDC1, HCLS1, PTPN5, NCKAP1L, CCL19, SMAD3, TEAD1, TBX1, TPD52L1, PRR5L, CCL17, LAT, FZD10, EPHA8, PLK1, ADRA1B, EPOR
GO:0043410	positive regulation of MAPK cascade	4.882616943	3.30E-07	6.04E-04	36	FGD2, FGFR3, LMNB1, WWC1, TLR2, CX3CL1, CCL5, TRF, C1QTNF3, CHIL1, AGT, PYCARD, TNFRSF19, PIK3R5, CSF1R, SYK, PIK3CG, DIXDC1, PTPRC, C5AR2, VANGL2, FGF23, CCL19, TPD52L1, TBX1, NTSR2, GRM1, CCL17, GRM5, DNAJC27, FZD10, EPHA8, HIPK2, ADRA1B, EPOR, TREM2
GO:0032956	regulation of actin cytoskeleton organization	4.470523685	1.25E-05	0.02201717	25	TRIOBP, FES, ARHGAP6, WNT4, S1PR1, PYCARD, CSF1R, ARHGDIB, MAGEL2, DIXDC1, HCK, HCLS1, VANGL2, MYO1F, ALMS1, NCKAP1L, SMAD3, SHANK1, WAS, TRPM2, FMN2, FZD10, LRP1, GMFG, CIT
GO:0007612	learning	4.40551612	6.58E-06	0.01156953	18	ARC, SLC6A1, TACR2, PTGS1, SLC12A5, FGF13, NPAS4, ATP1A2, SHANK1, GRM5, FOS, SCT, PAK7, GRIN2B, PDE1B, PPP1R1B, ADRA1B, SNAP25
GO:1903708	positive regulation of hemopoiesis	4.39198398	1.07E-05	0.0187554	19	PTPRC, HCLS1, NCKAP1L, CCL19, LEF1, CCL5, FES, FOS, INHBA, CD83, GATA2, TAL1, GFI1B, INPP5D, ACIN1, CAR2, SASH3, CSF1R, SYK
IPR001452	Src homology-3 domain	4.368972358	7.65E-06	0.01204816	20	FYB, GRAP, NCF1, NCF4, HCLS1, HCK, MPP3, ABI3, MYO1F, ARHGEF9, SHANK1, VAV1, BTK, SLA, PRAM1, PLCG2, TJP3, SASH3, ARHGAP9, MATK
GO:0032940	secretion by cell	4.355784808	5.46E-06	0.00998132	53	KCNC3, SNCAIP, TACR2, PTGS1, NELL2, TLR2, GJA1, FES, IL17RA, BTK, EXOC3L4, GATA2, SCT, GRIN2B, NOS2, APLN, SYK, C5AR2, MYO6, PTPRN2, FGF23, CFTR, TRPM2, INHBA, DOC2A, OTOF, PRAM1, TNFAIP2, CPLX3, CCK, CX3CL1, CCL5, RAC2, LY6E, C1QTNF3, CHIL1, AGT, PYCARD, SYBU, FCER1G, SNAP23, SNAP25, HAP1, CSF1R, HCK, MYO1G, MYO1F, CCL19, NKX6-1, LAT, SLC6A9, CACNA1G, SYT13
GO:2000145	regulation of cell motility	4.255163806	2.27E-05	0.04144141	45	WNT5B, IFITM1, ENPP2, FERMT3, FAM110C, ABI3, TLR2, VTN, CX3CL1, CCL5, SOX9, FES, TRF, CITED2, WNT4, S1PR1, RAC2, SPINT2, AGT, ACAN, PYCARD, ATOH8, CSF1R, ARHGDIB, EGR1, PTPRC, SELP, C5AR2, ELANE, MYO1F, NCKAP1L, SMAD3, CCL19, LEF1, PRR5L, WAS, NKX6-1, ADGRG3, HDAC4, TNFAIP6, LRP1, CXCL14, MADCAM1, ARAP3, ALOX12

Table 21 (extended). DAVID GO analysis of DEGs downregulated in the CCI model and upregulated by both MNAC13 and αD11 treatment at D90 (the list of genes included).

GO-ID	GO term	Enrichment score	P value	FDR	Count of genes	Genes
GO:0036477	somatodendritic compartment	13.12113	1.64E-15	2.22E-12	48	KCNC1, ACHE, KCNC3, CCK, GABRB1, NELL2, GNG13, BCAN, KCNJ11, SLC32A1, SLC1A2, DAB1, GRIN2B, PDE1B, PPP1R1B, UNC5A, LMTK3, CAMK2B, BRINP3, KNDC1, CHAT, HAP1, DIXDC1, ARC, KCND2, MYO6, PTPN5, ERMN, SLC12A5, GRIA3, ATP1A2, PDYN, NTSR1, NTSR2, CRHR1, GRM5, SMO, SKOR1, GRIA2, PENK, CHRM2, RASGRF1, MAP2, CACNA1G, NRSN2, BEGAIN, SLC5A7, SST
GO:0099536	synaptic signaling	12.30965	4.73E-13	8.19E-10	34	GFAP, KCNC3, SLC6A1, PNKD, SYT3, KCNJ10, CX3CL1, SHISA8, GRIN2B, HRH3, AGT, CAMK2B, SV2A, CHAT, HAP1, CHRNA2, ARC, MYO6, PTPN5, SLC12A5, NTSR1, PDYN, CRHR1, GRM5, SLC6A9, DOC2A, GRIA2, PENK, CHRM2, RASGRF1, CACNA1G, SYT13, SLC18A3, SLC5A7
GO:0031226	intrinsic component of plasma membrane	6.774969	1.53E-08	2.03E-05	47	KCNC1, IGDCC4, SLC38A3, KCNC3, FGFR3, CALY, SLC6A1, ATP1B2, GABRB1, AQP4, KCNJ10, CLDN11, KCNA7, KCNJ11, KCNJ3, SLC32A1, SLC1A2, SHISA8, S1PR1, SLC2A5, GRIN2B, UNC5A, SLCO1C1, GM5868, OLFM3, CHRNA2, KCND2, SLC12A5, GRIA3, CACNG2, ATP1A2, GAS1, NTSR1, CRHR1, GRM5, SLC6A9, SEMA6B, GRIA2, CHRM2, ADRA1B, SYT13, SLC18A3, SLC38A1, SLC5A7, SLC14A1, CAR4, ABCC8
GO:0030182	neuron differentiation	5.969526	3.98E-07	6.90E-04	42	ACHE, GFAP, FGFR3, CCK, SOX1, GABRB1, SYT3, GJA1, LRRC38, S1PR1, DAB1, UNC5A, CAMK2B, BRINP3, OLFM3, KNDC1, CHAT, HAP1, DIXDC1, CPNE9, NGEF, PTPRD, MYO6, EFNB3, DTX1, CNTN6, PTPN5, SLC12A5, GAS1, NKX6-1, RND2, SMO, SKOR1, SEMA6B, CBLN1, RND1, RASGRF1, MAP2, VEGFA, CNTN4, FAIM2, NTM
GO:0015267	channel activity	5.902575	8.70E-08	1.07E-04	23	KCNC1, KCND2, KCNC3, KCNAB3, GABRB1, ASIC4, CACNA1I, GJA1, AQP4, KCNJ10, GRIA3, CACNG2, GJC2, KCNJ3, KCNA7, KCNJ11, GRIA2, GRIN2B, CACNA1G, DENND5B, SLC14A1, ABCC8, CHRNA2
GO:0044306	neuron projection terminus	5.886846	6.17E-07	8.22E-04	15	DIXDC1, CCK, KCNC3, GRIA3, PDYN, NTSR1, SLC32A1, GRIA2, PENK, GRIN2B, CHRM2, SCRG1, SLC18A3, SV2A, HAP 1
GO:0034702	ion channel complex	5.752655	3.40E-06	0.004535	16	KCNC1, KCND2, KCNC3, GABRB1, CACNA1I, GRIA3, CACNG2, KCNA7, KCNJ11, SHISA8, GRIA2, GRIN2B, CACNA1G, OLFM3, ABCC8, CHRNA2
GO:0034220	ion transmembrane transport	5.577006	3.25E-06	0.005637	26	KCNC1, KCNC3, ATP1B2, GABRB1, AQP4, GJA1, KCNJ10, KCNJ11, KCNJ3, KCNA7, GSTM7, SLC1A2, GM5868, SLC1A1, HAP1, CHRNA2, ARC, KCND2, CACNA1I, SLC12A5, ATP1A2, CACNG2, NTSR1, CRHR1, RASGRF1, CACNA1G
GO:0048666	neuron development	5.095233	5.84E-07	0.001011	36	ACHE, GFAP, FGFR3, CCK, SOX1, GABRB1, SYT3, GJA1, LRRC38, DAB1, UNC5A, CAMK2B, OLFM3, KNDC1, CHAT, HAP1, DIXDC1, CPNE9, NGEF, PTPRD, MYO6, EFNB3, PTPN5, SLC12A5, GAS1, NKX6-1, RND2, SMO, SEMA6B, SKOR1, RND1, RASGRF1, MAP2, VEGFA, CNTN4, NTM
GO:0071805	Potassium ion transmembrane transport	4.904282	9.16E-07	0.001172	11	KCNC1, KCND2, KCNC3, KCNAB3, ATP1B2, SLC12A5, KCNJ10, ATP1A2, KCNJ11, KCNA7, KCNJ3
GO:0034765	regulation of ion transmembrane transport	4.795813	1.19E-05	0.020561	18	KCNC1, ARC, KCND2, KCNC3, KCNAB3, ATP1B2, GJA1, KCNJ10, ATP1A2, CACNG2, NTSR1, KCNJ3, KCNA7, KCNJ11, GSTM7, CRHR1, RASGRF1, HAP1
GO:0007612	learning	4.61371	1.69E-06	0.002828	13	CRHR1, GRM5, ARC, SLC6A1, PDE1B, GRIN2B, CHST10, HRH3, PPP1R1B, SLC12A5, ADRA1B, ATP1A2, NTSR1
GO:0015293	symporter activity	4.087047	2.17E-05	0.026393	11	SLC32A1, SLC38A3, SLC6A9, SLC1A2, SLC6A1, SLC12A5, SLC5A7, GM5868, SLC38A1, SLC1A1, SLC25A18
GO:0051960	regulation of nervous system development	3.938531	2.38E-05	0.041201	29	ACHE, GFAP, FGFR3, SYT3, CX3CL1, TRF, LINGO4, DAB1, CAMK2B, BRINP3, KNDC1, HAP1, ADGRB2, DIXDC1, CPNE9, NGEF, PTPRD, DTX1, PTPN5, NKX6-1, GRM5, RND2, SMO, CBLN1, SEMA6B, MAP2, VEGFA, CNTN4, NTM

Table 22 (extended). The list of "cured" genes in common between MNAC13 and αD11 treatments.

Ajap1 (**Adherens Junctions Associated Protein 1**), a protein highly expressed in the brain (mainly in neurons), ovaries and kidney, plays a role in cell adhesion and cell migration. It acts as a putative tumour suppressor, by supressing epithelial-to-mesenchymal transition in some tumours (Entrez Gene Summary). Interestingly, it was found recently that AJAP1 was tightly associated with the γ-Aminobutyric acid type B receptor subunit 1 (GABABR1) (Schwenk et al., 2016) and GABA-B receptor has anti-hypersensitive effect and its activation promotes nerve regeneration and ameliorates neuropathic pain (Magnaghi et al., 2014; Migita et al., 2018)

Cdh22 (**Cadherin 22**) is a putative calcium-dependent cell adhesion protein, expressed predominantly in the brain. It may be involved in morphogenesis and tissue formation in neural and non-neural cells during development and maintenance of the brain and neuroendocrine organs (Entrez Gene Summary).

Gfap (**Glial Fibrillary Acidic Protein**) encodes a class-III intermediate filament protein in mature astrocytes. It is used as a cell-specific marker to distinguish astrocytes from other glial cells during development. GFAP is also known as a marker for astrocyte activation in different pain models and its upregulation correlates with nerve injury-induced neuropathic pain (W. Wang et al., 2009). GFAP expression is low in the intact adult central nervous system (CNS), but increases after nerve injury in satellite cells of the DRG (Woodham, Anderson, Nadim, & Turmaine, 1989) and in astrocytes of the spinal cord dorsal horn (Garrison, Dougherty, Kajander, & Carlton, 1991).

With respect to the GFAP expression in DRG, one study compared temporal and dynamic changes in GFAP gene expression from injured (ipsilateral) and non-injured (contralateral) L5/6 DRG after spinal nerve ligation (SNL) injury in rats (D. S. Kim et al., 2009). GFAP showed an upregulation of its mRNA in injured DRG at the early stages of tactile allodynia development (at 2-days and 2-weeks), but decreased substantially at 20-weeks post nerve injury. GFAP proteins, mainly detected in DRG non-neuronal cells, were also increased in injured DRG at 2 days and 2 weeks post nerve injury, which at 20 weeks returned to a level close to that observed in non-injured DRG. However, the pattern of increased GFAP protein expression differed from that of GFAP mRNA, suggesting a non-correlative regulation between GFAP mRNA and proteins in DRG following spinal nerve ligation. Furthermore, spinal nerve ligation injury in GFAP knockout mice resulted in neuropathic pain states with similar onset, but a shortened duration of allodynia compared with that in wild-type littermates. Intrathecal GFAP antisense oligonucleotide injection (50 μg/rat/day for four days) in SNL rats starting six weeks after nerve injury, reversed injury-induced allodynia and GFAP upregulation in DRG and spinal cord. However, similar antisense treatment which started two weeks post nerve injury was not effective in allodynia reversal.

Interestingly, our data indicate that GFAP mRNA expression was downregulated in the ipsilateral DRG of CCI-induced mice as compared to that of naïve non-operated mice in all experimental time points. The above mentioned studies used the contralateral side as an internal control, thereby the expression of GFAP was based on the comparison of the contralateral side relative to the ipsilateral side within the same mouse. In the naïve non-operated animals, the astrocytes remain in a resting state, while in the CCI-mice injury-induced activation of astrocytes and the potential migration of astrocytes might play a role in their unequal distribution in the ipsilateral vs. contralateral sides. Thus, our seemingly contradictory results might be explained in part by the use of a different comparison method. Moreover, the changes in GFAP mRNA expression do not often correlate with changes in protein levels as mentioned previously. The unusual GFAP expression pattern observed in DRGs in our animal model remains to be clarified and validated/confirmed by further experimental analysis.

Prr18 (**Proline Rich 18**) is a protein coding gene with unknown function. However, an important paralog of this gene, Reticulon 4 (RTN4), is a potent neurite outgrowth inhibitor, which may play an

important role in blocking the regeneration of the central nervous system in higher vertebrates. Among its related pathways belong p75 NTR receptor-mediated signalling (Entrez Gene Summary).

Ptpn5 (**Protein Tyrosine Phosphatase Non-Receptor Type 5**) encodes the protein STEP (Striatal-Enriched Protein Tyrosine Phosphatase), which is a brain-specific phosphatase that modulates key signalling molecules involved in synaptic plasticity and neuronal function, including MAPKs, Src family kinases and NMDA receptors. STEP dephosphorylates GluN2B and ERK1/2, promoting internalization of GluN2B and inactivation of ERK1/2, two important contributors to central sensitization/pain sensitivity. Both genetic deletion and pharmacological inhibition of STEP induced thermal hyperalgesia and mechanical allodynia in the lumbar spinal cord underscoring its involvement in the modulation of nociception (Azkona et al., 2016). Increasing STEP activity might have therapeutic relevance on inflammatory and neuropathic pain (Goebel-Goody et al., 2012).

Rnd1 (**Rho Family GTPase 1**), member of the Rho GTPase family. It is an atypical Rho GTPase, which has a low affinity for GDP, and constitutively binds GTP. It is found predominantly in an active GTP-bound conformation. RND1 regulates the rearrangements of the actin cytoskeleton in response to extracellular growth factors. It induces the Rac-dependent formation of neuritic processes in part by disruption of the cortical actin filaments. It has been demonstrated that RND1 is involved in oncogenesis and response to cancer therapeutics (Mouly et al., 2019). RND1 represents a direct target of miR-199a-5p, an important regulator of intercellular junctions, which may play a role in the establishment of bladder pain syndrome caused by defects in urothelial integrity (Monastyrskaya et al., 2013).

Apln (**Apelin**) is an endogenous ligand for the apelin receptor (APLNR). It drives internalization of the apelin receptor. The encoded preproprotein is proteolytically cleaved into biologically active C-terminal peptide fragments. These biologically active peptides regulate diverse biological functions including body fluid homeostasis (by influencing vasopressin release), cardiovascular function and development, cytokine production, myocardial contractility and insulin secretion (Entrez Gene Summary). The apelin-APJ system is located in the central CNS (in pain-associated regions such as opioid-rich brain areas, including the arcuate nucleus of the hypothalamus and the spinal trigeminal nucleus, spinal cord) and peripheral nervous systems PNS (dorsal root ganglia). The apelin-APJ system is involved in the modulation of nociception, inflammatory, visceral and neuropathic pain. Apelin may serve a dual function in pain processing.

The supraspinal (intracerebroventricular injection) and spinal (intrathecal) administration of apelin-13 significantly induced antinociception in a mouse visceral pain model, while intraperitoneal injection of apelin-13 had no effect (S. Y. Lv, Qin, Wang, Yang, & Chen, 2012). Similarly, intracerebroventricular apelin-13 administration promoted dose- and time-related antinociception in acute nociceptive models through the mu opioid receptor signalling (Xu, Wang, Fan, & Chen, 2009). In tail-flick test, spinal apelin-13 (intrathecal injection) induced a significant antinociceptive effect via opioid receptor (S. Lv et al., 2013). In the neuropathic pain model, a repeated (1 week) intrathecal administration of [Pyr1] apelin-13 reduced pain symptoms in rats after the spinal cord injury (SCI) (Hajimashhadi, Aboutaleb, & Nasirinezhad, 2017).

However, in another study, spinal (intrathecal) administration of apelin-13 produced hyperalgesia in the late phase of a formalin test, most likely mediated by GABAA receptor. A single intrathecal administration of ML221, an APJ antagonist, attenuated mechanical allodynia and heat hyperalgesia 7 days following CCI, in a dose-dependent manner. Intraspinal delivery of ML221, at the onset of and in fully-established neuropathic pain, persistently alleviated CCI-induced pain hypersensitivity, suggesting the role of the apelin-APJ system in initiating and maintaining pain (Xiong et al., 2017).

Chronic constriction injury (CCI) of the sciatic nerve produced sustained spinal apelin and APJ upregulation in rats (Xiong et al., 2017). Accordingly, in our mouse model, Apelin expression in the spinal cord (SC) was upregulated at D90 after CCI procedure (+1.95) and downregulated after the

treatment with aD11 (-1.51) (results not shown). On the contrary, expression of Apelin in the DRGs was decreased in the CCI-induced mice in all experimental time points, and reversed by the treatment with both antibodies (see Table 1).

Tmem91 (**Transmembrane Protein 91**) is the Interferon-induced transmembrane protein (IFITM) belonging to a family of transmembrane proteins called the dispanins. An important paralog of this gene is SYNDIG1L (Synapse Differentiation Inducing 1 Like) and SYNDIG1. The product of the later gene may regulate AMPA receptor content at nascent synapses, and have a role in postsynaptic development and maturation (UniProtKB/Swiss-Prot Summary).

Usp29 (**Ubiquitin Specific Peptidase 29**) is a deubiquitinase that plays an important role in the regulation of DNA replication by stabilizing the checkpoint adaptor, Claspin. USP29 mediates deubiquitination of Claspin, which is involved in the ATR (ATM and Rad3-related)-Chk1 pathway of the DNA damage checkpoint and is also required for correct DNA replication. USP29-depleted cells show a major defect in the S-phase progression (Y. Martin et al., 2015).

Ankrd34b (**Ankyrin Repeat Domain 34B**) is a cytosolic/dendritic phosphoprotein (58 KDa) whose function is not yet clarified. Recently, it was found to be overexpressed in tumour tissues of patients and could serve as a novel RNA biomarker for prostate cancer (Nikitina et al., 2017).

Scrg1 (**Scrapie-Responsive Gene 1 Protein, Stimulator of Chondrogenesis 1**), a gene with increased cerebral mRNA levels in transmissible spongiform encephalopathies (TSE) such as scrapie, is associated with neurodegenerative processes and autophagy observed in TSE (Dron et al., 2005). SCRG1 together with its receptor, BST1 (bone marrow stromal cell antigen 1), are positive regulators of self-renewal, migration, and osteogenic differentiation in human mesenchymal stem cells during tissue and bone regeneration (Aomatsu et al., 2014). It was described as one of the genes that might be involved in tumour-promoting transformation of neural stem cells induced by glioblastoma extracellular vesicles (J. Wang et al., 2019).

Syt13 (**Synaptotagmin 13**) belongs to a synaptotagmin family of type-I membrane proteins, which function as membrane traffickers in multicellular organisms. SYT13 is an atypical SYT which lacks an N-terminal extracellular domain and is classified as a Ca^{2+}-independent isoform. Since SYT13 is expressed in various tissues outside the brain, it may be involved in constitutive vesicle transport (Fukuda & Mikoshiba, 2001). Human SYT13 plays an important role in the development of tumours possibly through pathways implicated in epithelial to mesenchymal transition (Jahn, Best, & Coleman, 2010). Synaptotagmin 13 has a neuroprotective function across motor neuron diseases, since the overexpression of SYT13 in amyotrophic lateral sclerosis (ALS) and spinal muscular atrophy (SMA) patients motor neurons in vitro improves their survival and increases axon lengths (Nizzardo et al., 2020).

Car14 (**Carbonic Anhydrase 14**) is an extracellular membrane-bound carbonic anhydrase that belongs to a large family of zinc metalloenzymes. These enzymes catalyse the reversible hydration of carbon dioxide to bicarbonate participating in a variety of biosynthetic reactions, including respiration, calcification, bone resorption, pH and CO_2 homeostasis and electrolyte secretion in various organs. The enzyme shows a diversity in tissue distribution and in its subcellular localisation (Entrez Gene Summary for CA14 Gene). Car14 is strongly expressed in brain (on neurons but not glia), and in retina (on glial cells, astrocytes and retinal pigment epithelium but not on neurons) (Nagelhus et al., 2005). In the hippocampus, Car14 regulates pH transients in the perisynaptic microenvironment that impact H^+-sensitive NMDA receptors (NMDARs) modulating this way a short-term postsynaptic potentiation (Makani et al., 2012).

Chat (**Choline O-Acetyltransferase**) is an enzyme which catalyses the biosynthesis of the neurotransmitter acetylcholine (ACh) from acetyl CoA and choline at cholinergic synapses. Polymorphisms in this gene have been associated with Alzheimer's disease and mild cognitive

impairment (Entrez Gene Summary for CHAT Gene). Hippocampal ChAT activity was found to be decreased after formalin-induced pain (Aloisi, Albonetti, Lodi, Lupo, & Carli, 1993). Acetylcholinesterase inhibitors (such as Neostigmine) have been used as an efficient therapeutic treatment for dementia of Alzheimer's disease and chronic pain due to the fact that cholinergic deficit is considered as an early finding in cognitive impairment and persisting pain (Eldufani & Blaise, 2019).

Sst (**Somatostatin**) is an abundant neuropeptide with a wide range of physiological effects on neurotransmission, secretion, regulation of the endocrine system and cell proliferation of both normal and tumorigenic cells. This hormone inhibits the release of numerous secondary hormones by binding to high-affinity G-protein-coupled somatostatin receptors. SST was identified as a biomarker for neuropathic pain that could serve as potential therapeutic target for treating neuropathic pain (Zhu, Liu, Wan, Lu, & Zhao, 2019). Pharmacogenetic activation of cortical somatostatin interneurons reverses mechanical allodynia in a mouse model of neuropathic pain (Cichon, Blanck, Gan, & Yang, 2017). Somatostatin activity inhibits nociceptive signalling pathways via SST2 and SST4 receptor subtypes that are expressed at multiple sites, including peripheral nerve terminals, DRG neurons, the dorsal horn of the spinal cord, and spinal interneurons. A somatostatin receptor type 4 agonists demonstrated to be effective in traditional rodent pain models. J-2156 alleviates mechanical hyperalgesia in a rat model of chronic low back pain (Park et al., 2019). Similarly, orally active novel pyrrolo-pyrimidine molecules (C1-C4) reduced pain sensitivity in a chronic neuropathy model (Kantas et al., 2019).

Kndc1 (**Kinase Non-Catalytic C-Lobe Domain (KIND) Containing 1**) is a brain-specific RAS-Guanine nucleotide exchange factor (GEF) predominantly expressed in cerebellar granule cells. It negatively regulates neuronal dendrite growth by mediating a signalling pathway linking RAS and MAP2 (Hayashi et al., 2017). This gene may be involved in cellular senescence and could potentially be targeted by anti-aging therapies (C. Zhang et al., 2014).

Grin2b (**Glutamate Receptor, Ionotropic, N-Methyl D-Aspartate 2B**), also named as **NR2B**, is a component of the NMDA receptor complexes which are members of the ionotropic class of glutamate receptors. The NMDA receptors are heterotetramers consisting of seven differentially expressed subunits including NR1 (GRIN1), NR2 (GRIN2A, GRIN2B, GRIN2C, or GRIN2D) and NR3 (GRIN3A or GRIN3B). The NR1 are obligatory subunits required for the formation of functional NMDARs, whereas the NR2 and NR3 subunits modify NMDAR channel activity and properties (Traynelis et al., 2010). NR2B-containing receptors show slower activation kinetics, lower open probability, and slower deactivation kinetics than NR2A-containing receptors (Sanz-Clemente, Nicoll, & Roche, 2013).

In the central nervous system (CNS), NR1 subunit is distributed ubiquitously, while NR2 subunits exhibit regional distribution with a predominate expression in forebrain structures (Monyer, Burnashev, Laurie, Sakmann, & Seeburg, 1994). In the spinal cord, NR2B subunit is located prevalently in the superficial dorsal horn (Boyce et al., 1999). In the DRGs, NR1 is expressed in large and small peptidergic and non-peptidergic primary afferent neurons and, NR2B and NR2D are expressed at higher levels than NR2A and NR2C (Marvizon et al., 2002; Willcockson & Valtschanoff, 2008). In the periphery, NR1 subunit is present in approximately 50% of the myelinated and 20-30% of the unmyelinated axons in plantar (mixed motor and sensory) and sural nerves (Coggeshall & Carlton, 1998).

The NMDARs are ligand-gated ion channels with high calcium permeability and voltage-dependent sensitivity to magnesium. Channel activation requires binding of the neurotransmitter glutamate to the epsilon subunit, glycine binding to the zeta subunit, and membrane depolarization to eliminate Mg^{2+} block. The NMDARs play an important role not only in brain development, circuit formation, synaptic plasticity (long-term depression), cellular migration and differentiation, but also in the pain transmission and facilitation. While AMPA and kainate receptors mediate monosynaptic reflexes and acute nociceptive responses, NMDA receptors are implicated in polysynaptic spinal pathways and in chronic

nociceptive responses (Chia-Chih Alex Tseng. Neuropsychiatry (2017): The N-methyl-D-aspartate (NMDA) receptor in skin, dorsal root ganglion and spinal cord: an ideal target gene for RNA interference therapy for pain relief). Thus, NMDA receptors have been targeted for the treatment of neuropathic pain and, NMDA receptor antagonists have been well documented for their analgesic effect in various experimental studies.

Intrathecal administration of NMDA has been shown to induce pain hyperalgesia in mice and the release of substance P in the rat dorsal horn, while the treatment with NR2B-selective blockers relieved pain in various animal models of neuropathic pain. Indeed, intrathecal administration of an NR2B antagonist effectively reduced pain-like behaviour and mechanical pain hypersensitivity following L5- spinal nerve ligation (Qu et al., 2009). Moreover, intrathecal injections of small interfering RNAs (siRNAs) targeting the NR2B reduced formalin-induced nociception and downregulated the expression of NR2B in the spinal cord (Tan, Yang, Shih, Lan, & Cheng, 2005; R. X. Zhang et al., 2013). Hence, according to several studies the mechanism of NR2B antagonists´ action seems to be mediated predominantly at the spinal cord level.

Many NMDARs synthesized in primary sensory neurons are transported from DRGs to their central presynaptic terminals inside the spinal dorsal horn. These presynaptic NMDARs (in contrast to postsynaptic NMDARs) can promote spontaneous neurotransmitter release in the absence of neuronal depolarization (Deng, Chen, & Pan, 2019). Under normal physiological conditions, presynaptic NMDARs in the spinal dorsal horn are not functionally active in regulating neurotransmitter release (they are quiescent) and blocking NMDARs with AP5 at the spinal cord level had no effect on spontaneous or evoked synaptic glutamate release to spinal lamina I or lamina II neurons in normal rats (S. R. Chen, Hu, Chen, & Pan, 2014; Xie, Chen, Chen, Zeng, & Pan, 2016). However, in opioid-induced hyperalgesia and chronic neuropathic pain conditions, presynaptic NMDARs in the spinal dorsal horn became tonically active and could be stimulated by endogenous glutamate even without relief of the Mg^{2+} block to potentiate glutamate release from nociceptive primary afferent terminals in neuropathic pain (Deng et al., 2019).

However, bath application of exogenous NMDA was shown to attenuate synaptic glutamate release evoked from primary afferent nerve stimulation (Bardoni, Torsney, Tong, Prandini, & MacDermott, 2004), most likely by inhibiting voltage-gated Ca^{2+} channels through activation of calcineurin induced by calcium influx (Z. Z. Wu, Chen, & Pan, 2006). Moreover, conditional knockout of NR1 subunit (NR1-cKO) in DRG neurons (but not in spinal cord neurons) lead to mechanical and thermal hypersensitivity. This increased neuronal (hyper)excitability in NR1-deficient DRG neurons was shown to be due to the impairment of Ca^{2+}-activated slow conductance K^+ channels in NR1 conditional knockout (NR1-cKO) mice (Pagadala et al., 2013). Other study has shown that conditional knockout of NR1 subunit in DRG neurons in mice does not affect normal nociception (McRoberts et al., 2011). The reports about the involvement of presynaptic NMDARs in pain processing show a lot of discrepancy and need to be validated independently.

At the spinal cord level, the activation of spinal NMDARs plays an essential role in the development of central sensitization and pain hypersensitivity after nerve injury since the majority of neurons in spinal lamina II are glutamatergic excitatory interneurons involved in nociceptive transmission (Santos, Rebelo, Derkach, & Safronov, 2007). However, at the level of DRGs, the role of peripheral (presynaptic) NMDARs expressed by primary afferent neurons in regulating intrinsic neuronal excitability and pain sensitivity remains controversial.

In one study, the authors evaluated the expression and distribution of different NR subunits within rat DRG at Day 23 and Day 86 following peripheral nerve injuries in two different models: sural-SNI (spared nerve injury) model with strong hypersensitivity in both regions and tibial-SNI animals with milder neuropathic pain (Norcini et al., 2016). They found no significant differences in the intensity of NR2B labeling in L3-DRG between either tibial-SNI or sural-SNI relative to the control group at Day

23 post-surgery. In contrast, at Day 86 post-surgery, tibial-SNI displayed an increase in NR2B protein within the perinuclear region of the neuronal somata and satellite glia cells. In both SNIs, microglia/macrophages showed a transient increase in NR2B protein detected at Day 23 but not at Day 86. Among all NMDA receptor subunits, only NR2B mRNA expression was up-regulated in the ipsilateral L4-DRG of sural-SNI at Day 86 post-surgery, other transcripts (NR1, NR2A, NR2D, NR2C) showed no significant changes in their expression. Interestingly, the mRNA expression encoding different NMDAR subunits at Day 23 following SNI was not evaluated. It was demonstrated that the primary sensory neurons and their surrounding satellite glia cells express functional NMDAR (Castillo et al., 2013). In addition, somata of DRG neurons within the sensory ganglia (Brumovsky, Watanabe, & Hokfelt, 2007) (Gu et al., 2010) and peripheral Schwann cells (Parpura, Liu, Jeftinija, Haydon, & Jeftinija, 1995) can store and release glutamate, contributing this way to the excitability of peripheral sensory neurons.

Ptprd (**Protein Tyrosine Phosphatase Receptor Type D**) is a member of the protein tyrosine phosphatase (PTP) family, signalling molecules controlling a variety of cellular processes, such as cell growth, differentiation, mitotic cycle, and oncogenic transformation. It represents a receptor-type PTP with an extracellular region composed of three Ig-like and eight fibronectin type III-like domains, a single transmembrane segment and two tandem intracytoplasmic catalytic domains (Entrez gene summary). In spinal cord, a dense PTPRD mRNA expression in moto-neurons and significant expression in scattered dorsal horn neurons was observed (Uhl & Martinez, 2019). PTPRD is involved in dephosphorylation of phosphotyrosine residues in the transcription factor STAT3 (M. Kim, Morales, Jang, Cho, & Kim, 2018), and most likely in FYN and SRC. Loss of PTPRD causes aberrant neurogenesis in neural precursor cells, mediated by the hyperactivation of TrkB and PDGFRβ and their downstream MEK-ERK signalling pathway. Thus, PTPRD regulates the neuronal development through the dephosphorylation of receptor tyrosine kinases, including TrkB and PDGFRβ (Tomita et al., 2020).

Ppp1r1b (**Protein Phosphatase 1 Regulatory Inhibitor Subunit 1B**) also known as DARPP (Dopamine and cAMP Regulated Phosphoprotein) is a bifunctional signal transduction molecule. Multiple transcript variants encoding different isoforms have been found for this gene (Entrez gene summary). The dual function of DARPP-32 consists in modulation of protein phosphatase and kinase activities. It functions either as an inhibitor of protein-phosphatase 1(PP1) when phosphorylated at Thr-34 by PKA or, as an inhibitor of protein kinase PKA when phosphorylated at Thr-75 (Belkhiri, Zhu, & El-Rifai, 2016). It plays a role in many biochemical processes, such as cancer and neurotransmission controlled by dopamine. DARPP-32 and its truncated form t-DARPP are frequently overexpressed in several types of cancer, such as adenocarcinomas of the breast, prostate, colon, stomach, oesophagus and lung. t-DARPP/DARPP-32 overexpression causes drug resistance to the trastuzumab (Herceptin) in an aggressive form of breast cancer, likely through AKT activation, which leads to cell survival and inhibition of apoptosis (Avanes, Lenz, & Momand, 2019). It has been also associated with schizophrenia, Alzheimer's disease and bipolar disorder, thus it may serve as a therapeutic target for neurologic and psychiatric disorders.

Nfatc2 (**Nuclear Factor of Activated T-Cells, Cytoplasmic, Calcineurin-Dependent 2**) is a member of the nuclear factor of activated T cells (NFAT) family that comprises five isoforms termed NFATc1-c4 (regulated by calcineurin, a Ca^{2+}/CaM-dependent serine/threonine phosphatase, also termed as PP2B), and NFAT5. NFAT proteins are transcription factors normally present in the cytoplasm in a hyperphosphorylated (inactive) state which translocate to the nucleus upon dephosphorylation by calcineurin triggered by T cell receptor (TCR) stimulation, where it becomes a member of the nuclear factors of activated T cells transcription complex. This complex plays a central role in the inducible expression of cytokine genes in T-cells during the immune response, especially in the induction of the IL-2, IL-3, IL-4, IL-5, IL-13, IL-8, TNF-α, GM-CSF, FOXP3, Igκ, IFNγ, CD5, CD25, CD28, CD40, Fas ligand, MIP-1α, Syk, COX-2. NFATs may also regulate gene expression of signalling molecules, such as Ca^{2+} regulators (IP3R, RCAN1), growth factors (VEGF, neurotrophins), myelination genes (P0

and Krox-20), glucose regulation genes (insulin, HNF1, PDX, and GLUT2), cell cycle and death regulator/activators (CDK4, Bcl-2 and cyclins A2, D1, and D2), oncogenes (Wnt, β-catenin), microRNAs (miR-21, miR-23, miR-24, miR-27, miR-125, miR-195, miR-199, and miR-224), and surfactants (sftpa, sftpb, sftpc, and abca3) (Kipanyula, Kimaro, & Seke Etet, 2016). Previous studies have linked the calcineurin/NFAT pathway to the induction and development of chronic pain. Most of these studies focused on the NFATc4 and its pronociceptive effects, however the role of NFATc2 in mechanisms of pain induction and maintenance remains largely unknown.

Chronic pain may lead to neuronal CCR2 chemokine receptor upregulation via activation of the NFAT pathway in DRG neurons (Jung & Miller, 2008). Under normal physiological conditions, CCR2 is not expressed by DRG neurons but it was found to be upregulated in several animal models of neuropathic pain where it plays an important role in the development and maintenance of neuropathic pain. Activation of the NFAT pathway in the DRG neuronal cell line F11 increased CCR2 promoter activity and induced CCR2 transcription.

Bradykinin, produced at sites of tissue injury and inflammation, elicits acute pain and alters the sensitivity of nociceptive neurons to subsequent stimuli, which, in turn, can enact long-lasting changes in nociceptor function by activating members of the NFAT family of transcription factors (Jackson, Usachev, & Thayer, 2007). In neurons, a 2-min exposure to bradykinin induced the translocation of GFP-NFAT4 fusion protein from the cytoplasm to the nucleus, which could be effectively blocked by calcineurin inhibition. Moreover, bradykinin triggered a concentration-dependent increase in NFAT-mediated transcription of a luciferase gene reporter via B2 receptor and PLC activation, and inositol triphosphate-mediated Ca2+ release.

In other study, NGF induced gene expression of pro-nociceptive genes (including BDNF) in cultured DRG cells via activation of NFATc4 in a calcineurin-dependent manner. Interestingly, BDNF stimulation within cultured spinal neurons increased the expression of the pro-nociceptive genes through both NFAT-dependent and NFAT-independent transcriptional mechanisms (Groth, Coicou, Mermelstein, & Seybold, 2007).

In the DRG and spinal cord, Calcineurin-NFATc mediate the expression of several pronociceptive and proinflammatory genes, including cyclooxygenase-2, NGF, interleukin-1, and chemokine receptor CCR2 (Flockhart, Diffey, Farr, Lloyd, & Reynolds, 2008; Groth et al., 2007; Marchand, Perretti, & McMahon, 2005). Peripheral nerve injury induced time-dependent changes in NFATc1–c4 expression in the DRG in a rat model of neuropathic pain. NFATc1–c4 mRNA levels in the spinal cord were not altered significantly by nerve injury, however, nerve injury persistently increased only NFATc4 mRNA levels in the DRG, while transiently elevated NFATc1–c3 mRNA levels, with NFATc2 mRNA levels being increased only at D7 after nerve injury when compared with sham. Nerve injury also significantly increased the protein level of dephosphorylated NFATc4 in the DRG. In addition, treatment with specific NFATc inhibitor 11R-VIVIT significantly attenuated the development of tactile allodynia early after peripheral nerve injury, suggesting the role of NFATc activation in the development of neuropathic pain (Cai, Chen, & Pan, 2013).

Experimental evidence has shown that a loss of calcineurin (protein phosphatase 3) activity and protein content of its Aα isoform in the ipsilateral post-synaptic density (PSD) of spinal dorsal horn neurons was associated with pain behaviour after chronic constriction injury (CCI) of the rat sciatic nerve. The treatment with a single intrathecal administration/injection of exogenous calcineurin provided prolonged pain relief in CCI animals for four days by restoring the phosphatase's activity and Aα content in the PSD. Conversely, an intrathecal application of the calcineurin inhibitor FK-506 elicited pain behaviour in control uninjured animals and significantly reduced calcineurin activity in the PSD (Miletic, Lippitt, Sullivan, & Miletic, 2013). Moreover, increases in spinal NMDA receptor activity were described as a result of calcineurin inhibitor induced pain syndrome (CIPS). It was shown that treatment with calcineurin inhibitor, FK506, increased drastically the amplitude of excitatory

postsynaptic currents mediated by NMDA receptor in dorsal horn neurons (S. R. Chen et al., 2014; Miletic, Hermes, Bosscher, Meier, & Miletic, 2015).

Dixdc1 (**DIX Domain Containing 1**) is a positive regulator of the Wnt signalling pathway, it activates WNT3A signalling via DVL2 and regulates JNK activation by AXIN1 and DVL2. Dixdc1 promotes cell proliferation in several types of cancer, such as acute myeloid leukaemia, colon cancer, Non-Hodgkin's lymphomas, pancreatic ductal adenocarcinoma (J. Chen et al., 2017; Li et al., 2016; Xin, Li, & Wang, 2018) and participates in psychiatric pathogenesis (P. M. Martin et al., 2018).

A time-dependent up-regulation of Dixdc1 protein expression was detected in rat astrocytes and neurons after acute traumatic brain injury (TBI) in the ipsilateral cortex. In addition, knockdown of Dixdc1 expression in primary astrocytes with Dixdc1-specific siRNA transfection induced G0/G1 arrest of cell cycle and significantly decreased cell proliferation, suggesting that Dixdc1 is potentially involved in CNS injury and repair via astrocyte proliferation after traumatic brain injury in adult rats (Lu et al., 2017).

In the peripheral nervous system (PNS), Dixdc1 expression, distribution and functions in the lesion and regeneration were examined in the sciatic nerves from 6 hours up to 4 weeks after rat sciatic nerve crush (SNC) injury. SNC induced an increase in Dixdc1 protein levels in Schwann cells from day 1 after crush, with a noticeable peak at one week and then gradual decrease to the normal level. After sciatic nerve crush, Dixdc1 might promote Schwann cell proliferation by targeting CyclinD1 and p21 partially through the activation of PI3K/AKT pathway (W. Wu, Liu, Liu, Yu, & Wang, 2016).

Other research group studying DNA methylation differences in Schwann cells (SCs) isolated from sciatic nerve before and after peripheral nerve system (PNS) injury (at 7 days) found that Dixdc1 was among the 433 newly discovered hypermethylated genes as detected by high-throughput MeDIP-Seq (Methylated DNA Immunoprecipitation Sequencing) analysis. In addition, Dixdc1 mRNA expression, confirmed by qRT-PCR, was downregulated in activated Schwann cells (ASCs) compared with normal Schwann cells (NSCs) (Zhou et al., 2017).

Gjb6 (**Gap Junction Protein, Beta 6**) encodes **Connexin 30** (**Cx30**). Connexin proteins assemble into gap channels. Gap junctions are specialized cell-cell contacts that allow the transport of molecules up to 1kDa, including nutrients, metabolites (glucose), ions (K^+, Ca^{2+}) and second messengers (IP3, cAMP) between the cytoplasm of adjacent cells. Gap junctions interconnect the cytoplasm of neighbouring cells via docking of two connexons expressed in each of the adjacent membranes. Undocked connexons, made up of six connexin proteins assembled in groups and referred to as hemichannels, may open and connect the cytoplasm with the extracellular fluid. The specific permeability of the gap junction is determined by a specific connexin composition of the hemichannel (Entrez gene summary). Connexin 30 was shown to be linked to neuronal development and adult neurogenesis (Swayne & Bennett, 2016), depressive-like behaviours (Huang et al., 2019), cancer (Arun, Vanisree, & Ravisankar, 2016) and hereditary deafness (Wingard & Zhao, 2015). It is also involved in basic cognitive processes through shaping synaptic and network activities. Neuronal activity increased hippocampal Cx30 protein levels in perisynaptic processes via a posttranslational mechanism regulating lysosomal degradation (Ghezali et al., 2019). Cx30 deficiency was shown to increase ramified microglia in the CNS in the naïve state and improve chronic experimental autoimmune encephalomyelitis through redirecting microglia toward an anti-inflammatory phenotype, suggesting a role of astrocytic Cx30 in regulating microglial number and functional state (Fang et al., 2018).

In the central nervous system (CNS), Cx30 and Cx43 are expressed by astrocytes which form networks interconnected by gap junctions. Interestingly, connexin 30 is an unusually stable, long-lived connexin that exhibits a long half-life (>12 h) when assembled into gap junctions (Kelly, Shao, Jagger, & Laird, 2015). Astrocytic connexins can also act as hemichannels to control the release of small molecules such as ATP and glutamate into the extracellular space (Xing, Yang, Cui, & Chen, 2019). Transgenic mice

with only Cx30 deletion or with deletions of both Cx43 and Cx30 were used in a study evaluating the role of Cx43 in the development and maintenance of central neuropathic pain following spinal cord injury (SCI) (M. J. Chen et al., 2012). Interestingly, SCI-induced heat hyperalgesia and mechanical allodynia fully developed in transgenic mice with Cx30 deletion only, while transgenic mice with deletions of both Cx43 and Cx30 exhibited improved pain scores after SCI, as compared to controls. In other study, the expression of Cx43 in astrocytes following traumatic SCI was found to be upregulated (Theriault, Frankenstein, Hertzberg, & Nagy, 1997) and blocking the expression of Cx43 attenuated inflammation and improved functional recovery following SCI (Cronin, Anderson, Cook, Green, & Becker, 2008). All these findings support an important role of Cx43 in the development and maintenance of chronic pain following spinal cord injury, the exact role of Cx30 in this process, however, remains to be elucidated.

Cacna1g (**Calcium Channel, Voltage-Dependent, T Type, Alpha 1G Subunit**). Voltage-sensitive calcium channels (VSCC) mediate calcium influx into excitable cells in response to depolarization. They regulate a variety of calcium-dependent processes, including muscle contraction, hormone secretion, neurotransmission, gene expression, cell motility, cell division, and cell death (Entrez Gene Summary). The T-type channels are 'low-voltage activated (LVA)' calcium channels that generate currents that are both transient, owing to fast inactivation, and tiny, owing to small conductance. T-type channels seem to be involved in pacemaker activity in both central neurons and cardiac nodal cells and they also support calcium signalling in secretory cells and vascular smooth muscle. They may be relevant in the modulation of firing patterns of neurons which is important for information processing. T-type calcium channels are robustly expressed in small and medium sized DRG neurons corresponding to the majority of nociceptors, and in neurons of the dorsal horn from the superficial laminae. Interestingly, T-type calcium channels appear to modulate nociceptive signalling both in DRGs and at the spinal level and hence, can serve as potential pharmacological targets for treating pain (Bourinet & Zamponi, 2005). Several inhibitors of T-type calcium channels, including ethosuximide (Flatters & Bennett, 2004) or mibefradil (Dogrul et al., 2003), dihydropyridines (DHPs) and its derivatives (Kumar et al., 2002) and 3,4-dihydroquinazoline KYS-05090S (Kang et al., 2012; M'Dahoma et al., 2016) exhibit potent analgesic and anti-nociceptive properties.

Three different types of T-type channels have been described, Cav3.1 (α1G isoform), Cav3.2 (α1H) and Cav3.3 (α1I), with different biophysical and pharmacological characteristics, suggesting that they may mediate distinct cellular functions (Bourinet & Zamponi, 2005). Further experiments will be needed in order to distinguish the selective role of these channels in the transmission and processing of nociceptive information. Different T-type channel isoforms show high degree of sequence homology which makes the design of selective inhibitors challenging. Lack of selective T-type calcium channel blockers hinder unravelling the specific role of each isoform in the pain mechanism.

In one study, the role of Cav3.1 calcium channels was addressed in thalamocortical oscillations between Cav3.1 KO mice and control animals both subjected to trigeminal neuropathic pain (TNP) (Choi, Yu, Hwang, & Llinas, 2016). While both groups developed mechanical hypersensitivity after TNP insult, the Cav3.1 KO-TNP mice exhibited a lower degree of mechanical hypersensitivity compared with control-TNP animals. The reduced peak low-frequency oscillations in the primary somatosensory cortical and thalamic brain regions detected in TNP-induced control mice were not found in the Cav3.1 KO-TNP strain, as recorded by EEG.

Another study revealed an increased perception of visceral pain in Cav3.1 deficient mice. Moreover, thalamic infusion of a T-type calcium channel blocker induced similar hyperalgesia (to visceral pain) in wild-type mice. In response to visceral pain, the ventroposterolateral thalamic neurons revealed a persisting single-spike pattern in the Cav3.1 knockout mice, whereas neurons from wild type mice displayed burst activity (D. Kim et al., 2003). Hence, the activation of Cav3.1 T-type channels in the thalamus appears to mediate an inhibition of visceral hypersensitivity, thus underlying an

antinociceptive role of Cav3.1 operating in the thalamus. However, it is important to note that somatic nociception and visceral sensitivity are very different in nature and, in many cases, involve distinct pathways and mediators (Bourinet & Zamponi, 2005). Indeed, another study reported that mice lacking CaV3.1 (alpha1G(-/-)) T-type Ca^{2+} channels have reduced spontaneous pain and attenuated mechanical and thermal hyperalgesia after L5 spinal nerve ligation, suggesting a pro-nociceptive role of alpha(1G) T-type Ca^{2+} channels in the development of neuropathic pain (Na, Choi, Kim, Park, & Shin, 2008).

Out of all CaV3 isoforms (Cav3.1, Cav3.2 and Cav3.3 calcium channels) selectively and locally depleted by antisense oligonucleotides injection, only antisense knockdown of Cav3.2 resulted in a robust analgesia and antiallodynia. This study has demonstrated a pronociceptive role of Cav3.2 in primary afferent sensory neurons in acute and chronic pain states (Bourinet et al., 2005) making peripheral CaV3.2 channels an interesting pharmacological target in analgesic drug development.

The above mentioned experiments show that Cav3.2 calcium channels and possibly Cav3.3 are implicated in pain signalling, with Cav3.2 having likely pro-nociceptive function. However, the possible involvement of Cav3.1 channels in the induction and/or maintenance of neuropathic pain states has yet to be identified.

Slc14a1 (**Solute Carrier Family 14 (Urea Transporter), Member 1 (Kidd Blood Group**) is a urea channel that mediates the transport of urea, the main nitrogenous breakdown product of protein catabolism, across cell membranes. The rate of urea conduction is increased by hypotonic stress. UT-A (SLC14A2) and UT-B (SLC14A1), facilitative urea transporters from the SLC14A family, both having a similar basic structure, play an important role in two major physiological processes - urea nitrogen salvaging and maintenance of urea concentration which prevents water loss in collecting ducts of renal medulla (Stewart, 2011). UT-A transporters, mainly found in the kidney, are highly specific for urea with relatively lower transport rates. They are highly regulated at both gene expression and cellular localization levels. In contrast, UT-B transporters are more widespread in diverse tissues, transport both urea and water, having a relatively high transport rate. They appear to be less acutely regulated. UT-B membrane transporters are important in several cellular functions, including urea nitrogen salvaging in the colon, nitric oxide pathway modulation in the hippocampus, bone metabolism, male reproductive function, blood pressure and the normal cardiac conduction system. In addition, genomic linkage studies have revealed potential additional roles for SLC14A1 and SLC14A2 in hypertension and bladder carcinogenesis (Shayakul, Clemencon, & Hediger, 2013). UT-B helps to maintain urea concentrations at physiological levels in the CNS where, unlike in the liver, the urea cycle is incomplete (Yu et al., 2019). In the CNS, UT-B is expressed in the olfactory bulb, cortex, caudate nucleus, hippocampus, and hypothalamus of mice. In the brain, UT-B is also expressed by astrocytes where it co-localizes with GFAP. However, there is no evidence of UT-B expression in oligodendrocytes, microglia, and vascular endothelial cells. Its deficiency and dysfunction contribute to the pathogenesis of many diseases. UT-B deficiency increases the sensitivity of bladder epithelial cells to apoptosis and UT-B-null mice develop II-III atrioventricular block and depressive-like behaviours, most likely due to UT-B deficiency-increased urea contents in the cerebral cortex and hypothalamus and reduced NO in the hippocampus of mice (Yu et al., 2019).

Arc (**Activity-regulated Cytoskeleton-associated Protein**) also known as Arg3.1, is an immediate early gene which plays a crucial role in activity-dependent synaptic plasticity in the telencephalic brain regions, such as hippocampus and cortex (Bramham, Worley, Moore, & Guzowski, 2008). It is required in processes essential for synaptic structural rearrangement such as long-term potentiation (LTP) and depression (LTD) and for the formation of long-term memory. Arc is involved in homeostatic synaptic scaling of AMPA receptors (AMPARs) by promoting endocytosis of AMPARs in response to synaptic activity which regulates the levels of surface AMPARs in response to chronic changes in neuronal activity (Shepherd et al., 2006). Arc self-assembles into virion-like capsids that encapsulate RNAs and mediate intercellular ARC mRNA transfer in the nervous system via extracellular vesicles. In the new

target cells, ARC capsids are endocytosed and ARC mRNA can undergo activity-dependent translation. ARC-containing virion-like capsids may be required to eliminate synaptic material (Entrez Gene Summary). Arc mediates activity-dependent synapse elimination in the developing cerebellum, and spinal processing. In addition to its role in synapses, it is also essential in the regulation of the immune system, including fast dendritic cell migration and T-cell activation. Dysfunctional forms of activity-dependent plasticity, such as LTP and LTD that lead to persistent changes in neuronal sensitivity, may underlie chronic pain disorders (Hossaini, Jongen, Biesheuvel, Kuhl, & Holstege, 2010).

In pain processing, long term synaptic changes play an important role, especially during chronic pain. The role of Arc in nociceptive processing in the spinal cord was investigated by evaluating expression of Arc in the rat spinal cord following pain stimuli (Hossaini et al., 2010). Interestingly, Arc was not expressed at detectable levels in naïve spinal cord. However, after peripheral nociceptive stimulation, Arc was found to be *de novo* expressed predominantly in spinal enkephalinergic interneurons in the superficial dorsal horn (located in the laminae I and II) and its expression was stimulus intensity dependent. Interestingly, Arc expression was present only in the acute phase of chronic inflammatory and neuropathic pain. In a model of acute pain, the number of Arc mRNA expressing neurons increased over time, reached a peak at 4 hours and then declined. In the CFA-induced chronic pain model, temporal expression of Arc mRNA was highest at 1.5 hrs post injection and then gradually declined, no expression of Arc mRNA was found from 10 hrs to 60 hrs post injection. In the spared nerve injury (SNI) model for neuropathic pain, expression of Arc mRNA was only observed at two hours after the operation. Arc mRNA was not expressed 1 week or 2 weeks after the operation when the neuropathic pain symptoms had developed. Moreover, the pain behaviour in Arc knockout (KO) mice after nociceptive stimuli was not significantly different from their wild type (WT) littermates. All these evidence suggest that Arc-dependent long-term synaptic changes in spinal pain transmission are a feature of anti-nociceptive, i.e. enkephalinergic, rather than pro-nociceptive neurons.

Another study aimed to explore the role of Arc in the PNS-induced analgesic effect on bone cancer pain in a rat model (Sun et al., 2018). Many electrical nerve stimulation methods have anti-nociceptive effects, among them peripheral nerve stimulation (PNS) was shown to be effective in relieving neuropathic pain, diabetic pain, and chronic headache (Huntoon & Burgher, 2009; Lee, Horazeck, Nahm, & Huh, 2015; Thakral et al., 2013). Furthermore, Arc transcription and translation can be induced by high frequency (>100 Hz) currents PNS (Waung, Pfeiffer, Nosyreva, Ronesi, & Huber, 2008). Indeed, PNS at 60 Hz and 120 Hz for 20 min upregulated Arc expression in the spinal cord, increased thermal pain thresholds in naïve rats, and relieved bone-cancer-induced allodynia and hyperalgesia. In addition, high frequency PNS also reduced the expression of GluA1, but not pGluNR2B, in the spinal cord dorsal horn. Finally, the pain relief and GluA1 downregulation induced by PNS were inhibited by intrathecal administration of Arc shRNA. Thus, the authors hypothesized that PNS-induced Arc expression in the spinal cord subsequently reduced the density of AMPAR on dendrites membrane by promoting AMPAR internalization and/or by decreasing global AMPAR expression, which together resulted in pain relief.

9 REFERENCES

Abdiche, Y. N., et al. (2008). "Probing the binding mechanism and affinity of tanezumab, a recombinant humanized anti-NGF monoclonal antibody, using a repertoire of biosensors." Protein Sci **17**(8): 1326-1335.

Aloe, L. (2004). "Rita Levi-Montalcini: the discovery of nerve growth factor and modern neurobiology." Trends Cell Biol **14**(7): 395-399.

Aloe, L., et al. (2012). "Nerve growth factor: from the early discoveries to the potential clinical use." J Transl Med **10**: 239.

Andreev, N., et al. (1995). "Peripheral administration of nerve growth factor in the adult rat produces a thermal hyperalgesia that requires the presence of sympathetic post-ganglionic neurones." Pain **63**(1): 109-115.

Apfel, S. C., et al. (1998). "Recombinant human nerve growth factor in the treatment of diabetic polyneuropathy. NGF Study Group." Neurology **51**(3): 695-702.

Apfel, S. C., et al. (2000). "Efficacy and safety of recombinant human nerve growth factor in patients with diabetic polyneuropathy: A randomized controlled trial. rhNGF Clinical Investigator Group." JAMA **284**(17): 2215-2221.

Austin, P. J., et al. (2012). "Chronic constriction of the sciatic nerve and pain hypersensitivity testing in rats." J Vis Exp(61).

Balanescu, A. R., et al. (2014). "Efficacy and safety of tanezumab added on to diclofenac sustained release in patients with knee or hip osteoarthritis: a double-blind, placebo-controlled, parallel-group, multicentre phase III randomised clinical trial." Ann Rheum Dis **73**(9): 1665-1672.

Bannwarth, B. and M. Kostine (2014). "Targeting nerve growth factor (NGF) for pain management: what does the future hold for NGF antagonists?" Drugs **74**(6): 619-626.

Basbaum, A. I., et al. (2009). "Cellular and molecular mechanisms of pain." Cell **139**(2): 267-284.

Belanger, P., et al. (2017). "From the Cover: Evaluation of the Effects of Tanezumab, a Monoclonal Antibody Against Nerve Growth Factor, on the Sympathetic Nervous System in Adult Cynomolgus Monkeys (Macaca fascicularis): A Stereologic, Histomorphologic, and Cardiofunctional Assessment." Toxicol Sci **158**(2): 319-333.

Belanger, P., et al. (2018). "Development of pain therapies targeting nerve growth factor signal transduction and the strategies used to resolve safety issues." J Toxicol Sci **43**(1): 1-10.

Bennett, D. L. (2001). "Neurotrophic factors: important regulators of nociceptive function." Neuroscientist **7**(1): 13-17.

Bennett, D. L., et al. (1998). "Endogenous nerve growth factor regulates the sensitivity of nociceptors in the adult rat." Eur J Neurosci **10**(4): 1282-1291.

Bennett, G. J. and Y. K. Xie (1988). "A peripheral mononeuropathy in rat that produces disorders of pain sensation like those seen in man." Pain **33**(1): 87-107.

Berardi, N., et al. (1994). "Monoclonal antibodies to nerve growth factor affect the postnatal development of the visual system." Proc Natl Acad Sci U S A **91**(2): 684-688.

Berenbaum, F., Blanco, F. J., Guermazi, A., Miki, K., Yamabe, T., Viktrup, L., Junor, R., Carey, W., Brown, M. T., West, C. R., & Verburg, K. M. (2020). Subcutaneous tanezumab for osteoarthritis of the hip or knee: efficacy and safety results from a 24-week randomised phase III study with a 24-week follow-up period. *Annals of the rheumatic diseases*, *79*(6), 800–810.

Berkemeier, L. R., et al. (1991). "Neurotrophin-5: a novel neurotrophic factor that activates trk and trkB." Neuron **7**(5): 857-866.

Bhangare, K. P., et al. (2017). "An Analysis of New Approaches and Drug Formulations for Treatment of Chronic Low Back Pain." Anesthesiol Clin **35**(2): 341-350.

Bjordal, J. M., et al. (2004). "Non-steroidal anti-inflammatory drugs, including cyclo-oxygenase-2 inhibitors, in osteoarthritic knee pain: meta-analysis of randomised placebo controlled trials." BMJ **329**(7478): 1317.

Bowler, K. E., et al. (2011). "The effect of a monoclonal antibody to calcitonin-gene related peptide (CGRP) on injury-induced ectopic discharge following lingual nerve injury." Neurosci Lett **505**(2): 146-149.

Brown, M. T., et al. (2012). "Tanezumab reduces osteoarthritic knee pain: results of a randomized, double-blind, placebo-controlled phase III trial." J Pain **13**(8): 790-798.

Brown, M. T., et al. (2013). "Tanezumab reduces osteoarthritic hip pain: results of a randomized, double-blind, placebo-controlled phase III trial." Arthritis Rheum **65**(7): 1795-1803.

Bueker, E. D. (1948). "Implantation of tumors in the hind limb field of the embryonic chick and the developmental response of the lumbosacral nervous system." Anat Rec **102**(3): 369-389.

Butt, M., et al. (2014). "Morphologic, stereologic, and morphometric evaluation of the nervous system in young cynomolgus monkeys (Macaca fascicularis) following maternal administration of tanezumab, a monoclonal antibody to nerve growth factor." Toxicol Sci **142**(2): 463-476.

Capsoni, S., et al. (2010). "Dissecting the involvement of tropomyosin-related kinase A and p75 neurotrophin receptor signaling in NGF deficit-induced neurodegeneration." Proc Natl Acad Sci U S A **107**(27): 12299-12304.

Cattaneo A. (2013). Immunosympathectomy as the first phenotypic knockout with antibodies. *Proceedings of the National Academy of Sciences of the United States of America*, *110*(13), 4877–4885. https://doi.org/10.1073/pnas.1217586110.

Cattaneo, A., et al. (1999). "Functional blockade of tyrosine kinase A in the rat basal forebrain by a novel antagonistic anti-receptor monoclonal antibody." J Neurosci **19**(22): 9687-9697.

Cattaneo, A., et al. (1988). "Three distinct types of monoclonal antibodies after long-term immunization of rats with mouse nerve growth factor." J Neurochem **50**(4): 1003-1010.

Chang, D. S., et al. (2016). "Anti-nerve growth factor in pain management: current evidence." J Pain Res **9**: 373-383.

Chao, M. V. and B. L. Hempstead (1995). "p75 and Trk: a two-receptor system." Trends Neurosci **18**(7): 321-326.

Chao M. V. (2019). Stoichiometry counts. Proceedings of the National Academy of Sciences of the United States of America, 116(43), 21343–21345. https://doi.org/10.1073/pnas.1914583116

Chao M. V. (2003). Neurotrophins and their receptors: a convergence point for many signalling pathways. Nature reviews. Neuroscience, **4**(4), 299–309. https://doi.org/10.1038/nrn1078

Chen, B., et al. (2014). "Syntaxin 8 modulates the post-synthetic trafficking of the TrkA receptor and inflammatory pain transmission." J Biol Chem **289**(28): 19556-19569.

Chou, R., et al. (2017). "Systemic Pharmacologic Therapies for Low Back Pain: A Systematic Review for an American College of Physicians Clinical Practice Guideline." Ann Intern Med **166**(7): 480-492.

Chou, R., et al. (2007). "Medications for acute and chronic low back pain: a review of the evidence for an American Pain Society/American College of Physicians clinical practice guideline." Ann Intern Med **147**(7): 505-514.

Clary, D. O. and L. F. Reichardt (1994). "An alternatively spliced form of the nerve growth factor receptor TrkA confers an enhanced response to neurotrophin 3." Proc Natl Acad Sci U S A **91**(23): 11133-11137.

Cohen, S. P. and J. Mao (2014). "Neuropathic pain: mechanisms and their clinical implications." BMJ **348**: f7656.

Covaceuszach, S., et al. (2004). "Purification, crystallization, X-ray diffraction analysis and phasing of a Fab fragment of monoclonal neuroantibody alphaD11 against nerve growth factor." Acta Crystallogr D Biol Crystallogr **60**(Pt 7): 1323-1327.

Covaceuszach, S., et al. (2008). "Dissecting NGF interactions with TrkA and p75 receptors by structural and functional studies of an anti-NGF neutralizing antibody." J Mol Biol **381**(4): 881-896.

Covaceuszach, S., et al. (2001). "Purification, crystallization and preliminary X-ray analysis of the Fab fragment from MNAC13, a novel antagonistic anti-tyrosine kinase A receptor monoclonal antibody." Acta Crystallogr D Biol Crystallogr **57**(Pt 9): 1307-1309.

Covaceuszach, S., et al. (2005). "Neutralization of NGF-TrkA receptor interaction by the novel antagonistic anti-TrkA monoclonal antibody MNAC13: a structural insight." Proteins **58**(3): 717-727.

Covaceuszach, S., et al. (2015). "The conundrum of the high-affinity NGF binding site formation unveiled?" Biophys J **108**(3): 687-697.

Covaceuszach, S., et al. (2012). "Single cycle structure-based humanization of an anti-nerve growth factor therapeutic antibody." PLoS One **7**(3): e32212.

Davies, A. M., et al. (1995). "Developmental changes in NT3 signalling via TrkA and TrkB in embryonic neurons." EMBO J **14**(18): 4482-4489.

Dawbarn, D., et al. (2006). "NGF receptor TrkAd5: therapeutic agent and drug design target." Biochem Soc Trans **34**(Pt 4): 587-590.

Delcroix, J. D., et al. (2003). "NGF signaling in sensory neurons: evidence that early endosomes carry NGF retrograde signals." Neuron **39**(1): 69-84.

Dyck, P. J., et al. (1997). "Intradermal recombinant human nerve growth factor induces pressure allodynia and lowered heat-pain threshold in humans." Neurology **48**(2): 501-505.

Ekman, E. F., et al. (2014). "Efficacy and safety of intravenous tanezumab for the symptomatic treatment of osteoarthritis: 2 randomized controlled trials versus naproxen." J Rheumatol **41**(11): 2249-2259.

Ernfors, P., et al. (1990). "Molecular cloning and neurotrophic activities of a protein with structural similarities to nerve growth factor: developmental and topographical expression in the brain." Proc Natl Acad Sci U S A **87**(14): 5454-5458.

Esposito, D., et al. (2001). "The cytoplasmic and transmembrane domains of the p75 and Trk A receptors regulate high affinity binding to nerve growth factor." J Biol Chem **276**(35): 32687-32695.

Ferrell, W. R. and N. J. Russell (1986). "Extravasation in the knee induced by antidromic stimulation of articular C fibre afferents of the anaesthetized cat." J Physiol **379**: 407-416.

Figaro, S., et al. (2008). "HemK2 protein, encoded on human chromosome 21, methylates translation termination factor eRF1." FEBS Lett **582**(16): 2352-2356.

Frade, J. M. and Y. A. Barde (1998). "Nerve growth factor: two receptors, multiple functions." Bioessays **20**(2): 137-145.

Friedly, J., et al. (2010). "Epidemiology of spine care: the back pain dilemma." Phys Med Rehabil Clin N Am **21**(4): 659-677.

Gangadharan, V. and R. Kuner (2013). "Pain hypersensitivity mechanisms at a glance." Dis Model Mech **6**(4): 889-895.

Garaci, E., et al. (2003). "Anti-nerve growth factor Ab abrogates macrophage-mediated HIV-1 infection and depletion of CD4+ T lymphocytes in hu-SCID mice." Proc Natl Acad Sci U S A **100**(15): 8927-8932.

Garry, M. G. and K. M. Hargreaves (1992). "Enhanced release of immunoreactive CGRP and substance P from spinal dorsal horn slices occurs during carrageenan inflammation." Brain Res **582**(1): 139-142.

Gee, A. P., et al. (1983). "Nerve growth factor: stimulation of polymorphonuclear leukocyte chemotaxis in vitro." Proc Natl Acad Sci U S A **80**(23): 7215-7218.

Gimbel, J. S., et al. (2014). "Long-term safety and effectiveness of tanezumab as treatment for chronic low back pain." Pain **155**(9): 1793-1801.

Gold, B. G., et al. (1991). "Regulation of axonal caliber, neurofilament content, and nuclear localization in mature sensory neurons by nerve growth factor." J Neurosci **11**(4): 943-955.

Gorin, P. D. and E. M. Johnson (1979). "Experimental autoimmune model of nerve growth factor deprivation: effects on developing peripheral sympathetic and sensory neurons." Proc Natl Acad Sci U S A **76**(10): 5382-5386.

Guha, D. and M. F. Shamji (2016). "The Dorsal Root Ganglion in the Pathogenesis of Chronic Neuropathic Pain." Neurosurgery **63 Suppl 1**: 118-126.

Hallbook, F., et al. (1991). "Evolutionary studies of the nerve growth factor family reveal a novel member abundantly expressed in Xenopus ovary." Neuron **6**(5): 845-858.

Hefti F. (1986). Nerve growth factor promotes survival of septal cholinergic neurons after fimbrial transections. *The Journal of neuroscience: the official journal of the Society for Neuroscience*, *6*(8), 2155–2162. https://doi.org/10.1523/JNEUROSCI.06-08-02155.1986

Hefti, F. F., et al. (2006). "Novel class of pain drugs based on antagonism of NGF." Trends Pharmacol Sci **27**(2): 85-91.

Hempstead, B. L., et al. (1991). "High-affinity NGF binding requires coexpression of the trk proto-oncogene and the low-affinity NGF receptor." Nature **350**(6320): 678-683.

Heurgue-Hamard, V., et al. (2002). "The hemK gene in Escherichia coli encodes the N(5)-glutamine methyltransferase that modifies peptide release factors." EMBO J **21**(4): 769-778.

Hochberg, M. C. (2015). "Serious joint-related adverse events in randomized controlled trials of anti-nerve growth factor monoclonal antibodies." Osteoarthritis Cartilage **23 Suppl 1**: S18-21.

Hochberg, M. C., et al. (2016). "When Is Osteonecrosis Not Osteonecrosis?: Adjudication of Reported Serious Adverse Joint Events in the Tanezumab Clinical Development Program." Arthritis Rheumatol **68**(2): 382-391.

Horton, A., et al. (1997). "NGF binding to p75 enhances the sensitivity of sensory and sympathetic neurons to NGF at different stages of development." Mol Cell Neurosci **10**(3-4): 162-172.

Ji, P., Wang, X., Xie, N., & Li, Y. (2018). N6-Methyladenosine in RNA and DNA: An Epitranscriptomic and Epigenetic Player Implicated in Determination of Stem Cell Fate. *Stem cells international*, *2018*, 3256524. https://doi.org/10.1155/2018/3256524

Kalso, E., et al. (2013). "Drugs for neuropathic pain." BMJ **347**: f7339.

Katz, N., et al. (2011). "Efficacy and safety of tanezumab in the treatment of chronic low back pain." Pain **152**(10): 2248-2258.

Kendall, G., et al. (1995). "Nerve growth factor induces the Oct-2 transcription factor in sensory neurons with the kinetics of an immediate-early gene." J Neurosci Res **40**(2): 169-176.

Kissin, I. (2015). "Scientometrics of drug discovery efforts: pain-related molecular targets." Drug Des Devel Ther **9**: 3393-3404.

Kivitz, A. J., et al. (2013). "Efficacy and safety of tanezumab versus naproxen in the treatment of chronic low back pain." Pain **154**(7): 1009-1021.

Kojima, M., et al. (1995). "Role of nerve growth factor in the expression of trkA mRNA in cultured embryonic rat basal forebrain cholinergic neurons." J Neurosci Res **42**(6): 775-783.

Koopmans, G., et al. (2009). "Chapter 19: The role of collagen in peripheral nerve repair." Int Rev Neurobiol **87**: 363-379.

Kusevic, D., et al. (2016). "Substrate Specificity of the HEMK2 Protein Glutamine Methyltransferase and Identification of Novel Substrates." J Biol Chem **291**(12): 6124-6133.

Lane, N. E., et al. (2010). "Tanezumab for the treatment of pain from osteoarthritis of the knee." N Engl J Med **363**(16): 1521-1531.

Lang, U. E., et al. (2003). "Nerve growth factor serum concentrations in healthy human volunteers: physiological variance and stability." Neurosci Lett **344**(1): 13-16.

Le Guen, L., et al. (1999). "Functional analysis of the hemK gene product involvement in protoporphyrinogen oxidase activity in yeast." FEMS Microbiol Lett **173**(1): 175-182.

Lee, J. H., et al. (2014). "A monoclonal antibody that targets a NaV1.7 channel voltage sensor for pain and itch relief." Cell **157**(6): 1393-1404.

Lee, K. F., et al. (1994). "p75-deficient embryonic dorsal root sensory and neonatal sympathetic neurons display a decreased sensitivity to NGF." Development **120**(4): 1027-1033.

Leetsi, L., et al. (2019). "The Common Partner of Several Methyltransferases TRMT112 Regulates the Expression of N6AMT1 Isoforms in Mammalian Cells." Biomolecules **9**(9).

Leibrock, J., et al. (1989). "Molecular cloning and expression of brain-derived neurotrophic factor." Nature **341**(6238): 149-152.

Levi-Montalcini, R. and P. U. Angeletti (1968). "Nerve growth factor." Physiol Rev **48**(3): 534-569.

Levi-Montalcini, R. and B. Booker (1960). "Destruction of the Sympathetic Ganglia in Mammals by an Antiserum to a Nerve-Growth Protein." Proc Natl Acad Sci U S A **46**(3): 384-391.

Levi-Montalcini R. (1987). The nerve growth factor 35 years later. *Science (New York, N.Y.)*, *237*(4819), 1154–1162. https://doi.org/10.1126/science.3306916

Lewin, G. R., et al. (2014). "Nerve growth factor and nociception: from experimental embryology to new analgesic therapy." Handb Exp Pharmacol **220**: 251-282.

Lewin, G. R., et al. (1993). "Nerve growth factor-induced hyperalgesia in the neonatal and adult rat." J Neurosci **13**(5): 2136-2148.

Lewin, G. R., et al. (1994). "Peripheral and central mechanisms of NGF-induced hyperalgesia." Eur J Neurosci **6**(12): 1903-1912.

Li, X., et al. (2019). "The DNA modification N6-methyl-2'-deoxyadenosine (m6dA) drives activity-induced gene expression and is required for fear extinction." Nat Neurosci **22**(4): 534-544.

Lim, T. K., et al. (2014). "Blood-nerve barrier dysfunction contributes to the generation of neuropathic pain and allows targeting of injured nerves for pain relief." Pain **155**(5): 954-967.

Lindsay, R. M. (1988). "Nerve growth factors (NGF, BDNF) enhance axonal regeneration but are not required for survival of adult sensory neurons." J Neurosci **8**(7): 2394-2405.

Lindsay, R. M. and A. J. Harmar (1989). "Nerve growth factor regulates expression of neuropeptide genes in adult sensory neurons." Nature **337**(6205): 362-364.

Luvisetto, S., et al. (2006). "Pain sensitivity in mice lacking the Ca(v)2.1alpha1 subunit of P/Q-type Ca2+ channels." Neuroscience **142**(3): 823-832.

Maisonpierre, P. C., et al. (1990). "Neurotrophin-3: a neurotrophic factor related to NGF and BDNF." Science **247**(4949 Pt 1): 1446-1451.

Mantyh, P. W., et al. (2011). "Antagonism of nerve growth factor-TrkA signaling and the relief of pain." Anesthesiology **115**(1): 189-204.

Mantyh, W. G., et al. (2010). "Blockade of nerve sprouting and neuroma formation markedly attenuates the development of late stage cancer pain." Neuroscience **171**(2): 588-598.

Marchetti, L., Bonsignore, F., Gobbo, F., Amodeo, R., Calvello, M., Jacob, A., Signore, G., Schirripa Spagnolo, C., Porciani, D., Mainardi, M., Beltram, F., Luin, S., & Cattaneo, A. (2019). Fast-diffusing $p75^{NTR}$ monomers support apoptosis and growth cone collapse by neurotrophin ligands. *Proceedings of the National Academy of Sciences of the United States of America*, *116*(43), 21563–21572.

Mayorga, A. J., et al. (2016). "Efficacy and safety of fulranumab as monotherapy in patients with moderate to severe, chronic knee pain of primary osteoarthritis: a randomised, placebo- and active-controlled trial." Int J Clin Pract **70**(6): 493-505.

McArthur, J. C., et al. (2000). "A phase II trial of nerve growth factor for sensory neuropathy associated with HIV infection. AIDS Clinical Trials Group Team 291." Neurology **54**(5): 1080-1088.

McKelvey, L., et al. (2013). "Nerve growth factor-mediated regulation of pain signalling and proposed new intervention strategies in clinical pain management." J Neurochem **124**(3): 276-289.

McMahon, S. B. (1996). "NGF as a mediator of inflammatory pain." Philos Trans R Soc Lond B Biol Sci **351**(1338): 431-440.

McNamee, K. E., et al. (2010). "Treatment of murine osteoarthritis with TrkAd5 reveals a pivotal role for nerve growth factor in non-inflammatory joint pain." Pain **149**(2): 386-392.

Mendell, L. M. (2002). "Does NGF binding to p75 and trkA receptors activate independent signalling pathways to sensitize nociceptors?" J Physiol **544**(Pt 2): 333.

Mendell, L. M., et al. (1999). "Neurotrophins, nociceptors, and pain." Microsc Res Tech **45**(4-5): 252-261.

Metzger, E., et al. (2019). "KMT9 monomethylates histone H4 lysine 12 and controls proliferation of prostate cancer cells." Nat Struct Mol Biol **26**(5): 361-371.

Miller, C. G., et al. (2015). "The current status of imaging in anti-NGF clinical trials." Osteoarthritis Cartilage **23 Suppl 1**: S3-7.

Miller, F. D. and D. R. Kaplan (2001). "On Trk for retrograde signaling." Neuron **32**(5): 767-770.

Molnar, M., et al. (1997). "A critical period in the sensitivity of basal forebrain cholinergic neurones to NGF deprivation." Neuroreport **8**(2): 575-579.

Molnar, M., et al. (1998). "The effects of anti-nerve growth factor monoclonal antibodies on developing basal forebrain neurons are transient and reversible." Eur J Neurosci **10**(10): 3127-3140.

Nakahigashi, K., et al. (2002). "HemK, a class of protein methyl transferase with similarity to DNA methyl transferases, methylates polypeptide chain release factors, and hemK knockout induces defects in translational termination." Proc Natl Acad Sci U S A **99**(3): 1473-1478.

Nakayashiki, T., et al. (1995). "Cloning and sequencing of a previously unidentified gene that is involved in the biosynthesis of heme in Escherichia coli." Gene **153**(1): 67-70.

Nickel, J. C., et al. (2012). "Preliminary assessment of safety and efficacy in proof-of-concept, randomized clinical trial of tanezumab for chronic prostatitis/chronic pelvic pain syndrome." Urology **80**(5): 1105-1110.

Norman, B. H. and J. S. McDermott (2017). "Targeting the Nerve Growth Factor (NGF) Pathway in Drug Discovery. Potential Applications to New Therapies for Chronic Pain." J Med Chem **60**(1): 66-88.

Otten, U., et al. (1984). "Nerve growth factor induces plasma extravasation in rat skin." Eur J Pharmacol **106**(1): 199-201.

Owolabi, J. B., et al. (1999). "Characterization of antiallodynic actions of ALE-0540, a novel nerve growth factor receptor antagonist, in the rat." J Pharmacol Exp Ther **289**(3): 1271-1276.

Paoletti, F., et al. (2009). "Intrinsic structural disorder of mouse proNGF." Proteins **75**(4): 990-1009.

Patel, M. K., et al. (2018). "Tanezumab: Therapy targeting nerve growth factor in pain pathogenesis." J Anaesthesiol Clin Pharmacol **34**(1): 111-116.

Penas, C. and X. Navarro (2018). "Epigenetic Modifications Associated to Neuroinflammation and Neuropathic Pain After Neural Trauma." Front Cell Neurosci **12**: 158.

Pesavento, E., et al. (2000). "Blocking the NGF-TrkA interaction rescues the developmental loss of LTP in the rat visual cortex: role of the cholinergic system." Neuron **25**(1): 165-175.

Petty, B. G., et al. (1994). "The effect of systemically administered recombinant human nerve growth factor in healthy human subjects." Ann Neurol **36**(2): 244-246.

Pezet, S. and S. B. McMahon (2006). "Neurotrophins: mediators and modulators of pain." Annu Rev Neurosci **29**: 507-538.

Porro, C. A. and M. Cavazzuti (1993). "Spatial and temporal aspects of spinal cord and brainstem activation in the formalin pain model." Prog Neurobiol **41**(5): 565-607.

Ratel, D., et al. (2006). "Undetectable levels of N6-methyl adenine in mouse DNA: Cloning and analysis of PRED28, a gene coding for a putative mammalian DNA adenine methyltransferase." FEBS Lett **580**(13): 3179-3184.

Ruberti, F., et al. (1993). "Cloning and expression of an anti-nerve growth factor (NGF) antibody for studies using the neuroantibody approach." Cell Mol Neurobiol **13**(5): 559-568.

Sanga, P., et al. (2013). "Efficacy, safety, and tolerability of fulranumab, an anti-nerve growth factor antibody, in the treatment of patients with moderate to severe osteoarthritis pain." Pain **154**(10): 1910-1919.

Sawada, J., et al. (2000). "Nerve growth factor functions as a chemoattractant for mast cells through both mitogen-activated protein kinase and phosphatidylinositol 3-kinase signaling pathways." Blood **95**(6): 2052-2058.

Schaible, H. G. (2015). Pain control. New York, NY, Springer Berlin Heidelberg.

Schifitto, G., et al. (2001). "Long-term treatment with recombinant nerve growth factor for HIV-associated sensory neuropathy." Neurology **57**(7): 1313-1316.

Schnitzer, T. J., et al. (2015). "Efficacy and safety of tanezumab monotherapy or combined with non-steroidal anti-inflammatory drugs in the treatment of knee or hip osteoarthritis pain." Ann Rheum Dis **74**(6): 1202-1211.

Scholz, J. and C. J. Woolf (2007). "The neuropathic pain triad: neurons, immune cells and glia." Nat Neurosci **10**(11): 1361-1368.

Schwanhausser, B., et al. (2009). "Global analysis of cellular protein translation by pulsed SILAC." Proteomics **9**(1): 205-209.

Seidel, M. F., et al. (2010). "Nerve growth factor in rheumatic diseases." Semin Arthritis Rheum **40**(2): 109-126.

Seidel, M. F., et al. (2013). "Nerve growth factor: an update on the science and therapy." Osteoarthritis Cartilage **21**(9): 1223-1228.

Silver, L. and G. Gallo (2005). "Extracellular Muscle Myosin II Promotes Sensory Axon Formation." DNA Cell Biol **24**(7): 438-445.

Skaper, S. D. (2001). "Nerve growth factor: a neurokine orchestrating neuroimmune-endocrine functions." Mol Neurobiol **24**(1-3): 183-199.

Sleigh, J. N., et al. (2016). "A simple, step-by-step dissection protocol for the rapid isolation of mouse dorsal root ganglia." BMC Res Notes **9**: 82.

Sofroniew, M. V., et al. (2001). "Nerve growth factor signaling, neuroprotection, and neural repair." Annu Rev Neurosci **24**: 1217-1281.

Spierings, E. L., et al. (2013). "A phase III placebo- and oxycodone-controlled study of tanezumab in adults with osteoarthritis pain of the hip or knee." Pain **154**(9): 1603-1612.

Svensson, P., et al. (2003). "Injection of nerve growth factor into human masseter muscle evokes long-lasting mechanical allodynia and hyperalgesia." Pain **104**(1-2): 241-247.

Tanga, F. Y., et al. (2005). "The CNS role of Toll-like receptor 4 in innate neuroimmunity and painful neuropathy." Proc Natl Acad Sci U S A **102**(16): 5856-5861.

Thoenen, H. and Y. A. Barde (1980). "Physiology of nerve growth factor." Physiol Rev **60**(4): 1284-1335.

Tiseo, P. J., et al. (2014). "Fasinumab (REGN475), an antibody against nerve growth factor for the treatment of pain: results from a double-blind, placebo-controlled exploratory study in osteoarthritis of the knee." Pain **155**(7): 1245-1252.

Tive, L., Bello, A. E., Radin, D., Schnitzer, T. J., Nguyen, H., Brown, M. T., & West, C. R. (2019). Pooled analysis of tanezumab efficacy and safety with subgroup analyses of phase III clinical trials in patients with osteoarthritis pain of the knee or hip. *Journal of pain research*, *12*, 975–995. https://doi.org/10.2147/JPR.S191297

Toni, T., et al. (2014). "Systems Pharmacology of the NGF Signaling Through p75 and TrkA Receptors." CPT Pharmacometrics Syst Pharmacol **3**: e150.

Turk, D. C., et al. (2011). "Treatment of chronic non-cancer pain." Lancet **377**(9784): 2226-2235.

Ugolini, G., et al. (2007). "The function neutralizing anti-TrkA antibody MNAC13 reduces inflammatory and neuropathic pain." Proc Natl Acad Sci U S A **104**(8): 2985-2990.

Vacca, V., et al. (2016). "17beta-estradiol counteracts neuropathic pain: a behavioural, immunohistochemical, and proteomic investigation on sex-related differences in mice." Sci Rep **6**: 18980.

Vadivelu, N., et al. (2015). "Ketorolac tromethamine - routes and clinical implications." Pain Pract **15**(2): 175-193.

Valmier, J., et al. (1993). "Skeletal muscle extract and nerve growth factor have developmentally regulated survival promoting effects on distinct populations of mammalian sensory neurons." Muscle Nerve **16**(4): 397-403.

Van der Zee, C. E., et al. (1996). "Survival of cholinergic forebrain neurons in developing p75NGFR-deficient mice." Science **274**(5293): 1729-1732.

Wall, P. D., et al. (2006). Wall and Melzack's textbook of pain. Philadelphia, Elsevier/Churchill Livingstone.

Wang, Y., et al. (2018). "Actin Cytoskeleton Affects Schwann Cell Migration and Peripheral Nerve Regeneration." Front Physiol **9**: 23.

Watson, J. J., et al. (2008). "Targeting nerve growth factor in pain: what is the therapeutic potential?" BioDrugs **22**(6): 349-359.

Wild, K. D., et al. (2007). "Antibodies to nerve growth factor reverse established tactile allodynia in rodent models of neuropathic pain without tolerance." J Pharmacol Exp Ther **322**(1): 282-287.

Winston, J. H., et al. (2003). "Acute pancreatitis results in referred mechanical hypersensitivity and neuropeptide up-regulation that can be suppressed by the protein kinase inhibitor k252a." J Pain **4**(6): 329-337.

Woodcock, C. B., et al. (2019). "Human HemK2/KMT9/N6AMT1 is an active protein methyltransferase, but does not act on DNA in vitro, in the presence of Trm112." Cell Discov **5**: 50.

Woolf, C. J. (1996). "Phenotypic modification of primary sensory neurons: the role of nerve growth factor in the production of persistent pain." Philos Trans R Soc Lond B Biol Sci **351**(1338): 441-448.

Woolf, C. J. and M. B. Max (2001). "Mechanism-based pain diagnosis: issues for analgesic drug development." Anesthesiology **95**(1): 241-249.

Wyatt, S., et al. (1997). "Sympathetic neuron survival and TrkA expression in NT3-deficient mouse embryos." EMBO J **16**(11): 3115-3123.

Xiao, C. L., et al. (2018). "N(6)-Methyladenine DNA Modification in the Human Genome." Mol Cell **71**(2): 306-318 e307.

Yang, Z., et al. (2004). "Structural characterization and comparative phylogenetic analysis of Escherichia coli HemK, a protein (N5)-glutamine methyltransferase." J Mol Biol **340**(4): 695-706.

Yoon, S. O., et al. (1998). "Competitive signaling between TrkA and p75 nerve growth factor receptors determines cell survival." J Neurosci **18**(9): 3273-3281.

Yuen, E. C., et al. (1996). "Nerve growth factor and the neurotrophic factor hypothesis." Brain Dev **18**(5): 362-368.

Zahn, P. K., et al. (2004). "Effect of blockade of nerve growth factor and tumor necrosis factor on pain behaviors after plantar incision." J Pain **5**(3): 157-163.

Zhi, M. J., et al. (2017). "Application of the chronic constriction injury of the partial sciatic nerve model to assess acupuncture analgesia." J Pain Res **10**: 2271-228